Development and Optimisation of Mass Spectrometric Techniques for the Analysis of Antimalarial Pharmaceuticals

DISSERTATION

zur Erlangung des Grades eines Doktors

der Naturwissenschaften

vorgelegt von

Derick Nzogoa Ateacha

geb. in Muyuka, Kamerun

eingereicht bei der Naturwissenschaftlich-Technischen Fakultät

der Universität Siegen

Siegen 2018

„gedruckt auf alterungsbeständigem holz- und säurefreiem Papier“

Betreuer und erster Gutachter

Prof. Dr. Carsten Engelhard

Universität Siegen, Analytische Chemie

Zweiter Gutachter

Prof. Dr. Ulrich Jonas

Universität Siegen, Makromolekulare Chemie

Mietglieder der Promotionskommission

Prof. Dr. Holger Schönherr

Universität Siegen, Physikalische Chemie I

Prof. Dr. Xin Jiang

Universität Siegen, Lehrstuhl für Oberflächen- und Werkstofftechnologie

Tag der mündlichen Prüfung

10.07.2018

Die vorliegende Arbeit wurde im Zeitraum von Oktober 2013 bis Mai 2018 im Arbeitskreis von Prof. Dr. Carsten Engelhard im Department Chemie und Biologie der Naturwissenschaftlich-Technischen Fakultät der Universität Siegen durchgeführt.

Abstract

Antimalarials are drugs used against malaria, an infectious disease caused by a parasite that belongs to the genius *plasmodium*. Drug therapy to eradicate this disease is increasingly hindered by resistance of the parasite to drugs currently in use. The drug resistance has been partly attributed to the presence of drugs with wrong or low active pharmaceutical ingredients. Thus, there is an increasing need for analytical procedures to investigate the quality of antimalarial-based pharmaceuticals. Amongst the analytical techniques, the most used to date is high performance liquid chromatography (HPLC) in the reversed-phase (RP) mode coupled to mass spectrometry (MS). However, RP-HPLC is characterised by a relatively long analysis time and a consumption of a large amount of organic solvents. In a quest to develop a fast and efficient analytical method, different mass spectrometric-based techniques are developed and optimised in this thesis. In the first section, high-temperature HPLC mass spectrometry (HT-HPLC-MS)-based technique tailored for the analysis of antimalarials is developed and optimised. HPLC at high temperature permits faster separation compared to standard conditions with a reduction in chemical waste, better chromatographic selectivity and an enhanced desolvation in the MS ionisation source. Prior to HT-HPLC-MS method development, a HT-HPLC heating system was optimised for best performance and successfully coupled to a triple quadrupole mass spectrometer via electrospray ionisation (ESI) and atmospheric pressure chemical ionisation (APCI) sources. Because of the antimalarial properties of *Cinchona* alkaloids, a HT-HPLC-MS method with an XBridge C_{18} column and ESI source was developed and optimised for their analysis. The optimised method permits the separation and detection of the four major chiral alkaloids: cinchonine, cinchonidine, quinine, and quinidine and their dihydro-derivatives: dihydrocinchonine, dihydrocinchonidine, dihydroquinine, and dihydroquinidine with reduction in analysis time and organic solvents, better chromatographic selectivity and enhanced MS ionisation efficiency. Limits of detection (LOD) in the μg L^{-1} range were obtained. The method was shown to be suitable in the separation and detection of *Cinchona* alkaloids present in a commercial sample. Also, because of the antimalarial properties of artemisinin (ART) and some of its derivatives (artesunate (AS), dihydroartemisinin (DHA), and artemether (AM)), another HT-HPLC-MS strategy with a zirconia-polybutadiene (ZrO_2-PBD) column, was developed and optimised for their analysis. After optimisation, DHA, ART, and AM were detected as their ammonium adducts ($[M + NH_4]^+$) at *m/z* 302, 300, and 316, while AS was

detected as a characteristic fragment ion at *m/z* 272. From evaluation of ESI and APCI sources during HT-HPLC-MS analysis, best detection sensitivity for ART and derivatives is obtained with ESI compared to APCI. LODs in the μg mL^{-1} range were obtained with HT-HPLC-ESI-MS. The optimised HT-HPLC-ESI-MS and HT-HPLC-ESI-MS/MS method were successfully applied in the screening of AM in commercial Coartem drug tablets.

In the second section, direct MS-based methods, which use minimal sample preparation procedures and relatively small sample amounts were developed and optimised for fast screening of antimalarials. In the first part of this section, a time-of-flight secondary ion mass spectrometry (ToF-SIMS) method was optimised to screen for *Cinchona* alkaloids including quinine (Qn). ToF-SIMS analysis of Qn provided significant fingerprint SIMS fragments, which were later used in the fast qualitative screening of Qn and related compounds in small amounts of *Cinchona* bark and extract. The results demonstrate for the first time the ability of ToF-SIMS to perform direct analysis and fast qualitative screening (less than 10 minutes analysis time) of *Cinchona* alkaloids. In the second part of this section, an analytical method involving low-temperature plasma ambient desorption/ionisation mass spectrometry (LTP-ADI-MS) was developed and optimised for rapid qualitative screening of active antimalarial pharmaceutical ingredients. The method was shown to be capable of detecting the active ingredient in antimalarial drug tablets (Coartem and Malarone) as their protonated molecular ions and other characteristic ions in less than three minutes and with minimal sample preparation. Characteristic fragment ions of target molecules were used for structural identification even in the presence of a tablet matrix.

Kurzfassung

Malariamittel sind Medikamente gegen Malaria, einer ansteckenden Erkrankung, verursacht durch Parasiten die zur Gattung *Plasmodium* gehörten. Eine medikamentöse Therapie zur Ausrottung dieser Krankheit wird zunehmend durch die Resistenz des Parasiten gegenüber derzeit verwendeten Medikamenten behindert. Die Arzneimittelresistenz wurde teilweise dem Verbrauch von Arzneimitteln mit falschen oder zu niedrig dosierten pharmazeutischen Wirkstoffen zugeschrieben. Daher besteht ein zunehmender Bedarf an analytischen Verfahren zur Untersuchung der Qualität von Medikamenten auf Antimalaria-Basis. Unter den analytischen Techniken ist die Hochleistungsflüssigkeitschromatographie (HPLC) im Umkehrphasenmodus (RP), gekoppelt an die Massenspektrometrie (MS), am häufigsten verwendet worden. Die RP-HPLC ist jedoch durch eine relativ lange Analysezeit und der Verbrauch einer großen Menge an organischen Lösungsmitteln gekennzeichnet. Auf der Suche nach einer schnelleren und effizienteren Methode, wurden in dieser verschiedene Massenspektrometrie-Techniken eingesetzt. Im ersten Abschnitt wurden die Hochtemperatur-HPLC-Massenspektrometrie (HT-HPLC-MS) für die Analyse von Antimalariamitteln entwickelt und optimiert. Die HPLC bei hohen Temperaturen im Vergleich zu Standardbedingungen ermöglicht eine schnellere Trennung mit weniger chemischem Abfall, besserer chromatographischer Selektivität und verbesserter Ionisierungseffizienz. Vor der Entwicklung der HT-HPLC-MS-Methode wurde ein HT-HPLC-Heizsystem für optimale Leistung optimiert und erfolgreich mit einem Triple-Quadrupol-Massenspektrometer über Elektrospray-Ionisations-(ESI) und Chemische Ionisation bei Atmosphärendruck (APCI) gekoppelt worden. Aufgrund der Antimalaria-Eigenschaften von *Cinchona*-Alkaloiden wurde eine HT-HPLC-MS-Methode mit einer XBridge C_{18}-Säule und ESI-Quelle entwickelt und für ihre Analyse optimiert. Die optimierte Methode erlaubt die Trennung und den Nachweis der vier wichtigsten chiralen Alkaloide: Cinchonin, Cinchonidin, Chinin, und Chinidin und ihre Dihydro-Derivate: Dihydrocinchonin, Dihydrocinchonidin, Dihydrochinin und Dihydrochinidin mit Verringerung der Analysezeit und organischer Lösungsmittel, bessere chromatographische Selektivität und verbesserte MS-Ionisierungseffizienz. Eine Nachweisgrenze (LOD) im $\mu g\ L^{-1}$ Bereich wurde mit der Methode erreicht. Es wurde gezeigt, dass das Verfahren zur Trennung und zum Nachweis von *Cinchona*-Alkaloiden geeignet ist, die in kommerziellen Proben vorliegen.

Aufgrund der Antimalaria-Eigenschaften von Artemisinin (ART) und einigen seiner Derivate (Artesunat (AS), Dihydroartemisinin (DHA) und Artemether (AM)) wurde eine weitere HT-HPLC-MS-Strategie mit einer Zirkonoxid-Polybutadien (ZrO_2-PB) Säulen für ihre Analyse entwickelt und optimiert. Nach der Optimierung wurden DHA, ART, und AM als ihre Ammoniumaddukte ($[M + NH_4]^+$) bei *m/z* 302, 300 und 316 nachgewiesen, sowie AS als charakteristisches Fragmention bei *m/z* 272. Der Vergleich von ESI- und APCI-Quellen während der HT-HPLC-MS-Analyse, ergab die beste Nachweisempfindlichkeit für ART und Derivate mit ESI. Ein Nachweisgrenze im μg mL^{-1}-Bereich wird mit HT-HPLC-ESI-MS erhalten. Die optimierte HT-HPLC-ESI-MS- und HT-HPLC-ESI-MS/MS-Methode wurde erfolgreich im Screening von AM in kommerziellen Coartem-Arzneimitteltabletten eingesetzt.

Im zweiten Abschnitt wurden direkte massenspektrometrische Methoden entwickelt und optimiert, die minimale Probenvorbereitung und eine relativ kleine Probenmenge für ein schnelles Screening von Antimalariamitteln verwenden. Im ersten Teil dieses Abschnitts wurde die Time-of-Flight-Sekundärionen-Massenspektrometrie (ToF-SIMS) für das Screening auf *Cinchona*-Alkaloide einschließlich Chinin (Qn) optimiert. Die ToF-SIMS-Analyse von Qn lieferte signifikante Fingerabdruck-SIMS-Fragmente, die später beim schnellen qualitativen Screening von Qn und verwandten Verbindungen in kleinen Mengen von *Cinchona*-Rinde und -Extrakten verwendet wurden. Die Ergebnisse zeigen zum ersten Mal die Fähigkeit von ToF-SIMS, eine direkte Analyse und ein schnelles qualitatives Screening (weniger als 10 Minuten Analysezeit) von *Cinchona*-Alkaloiden durchzuführen. Im zweiten Teil dieses Abschnitts wurde eine analytische Methode mit Niedertemperaturplasma-Desorptions/Ionisations-Massenspektrometrie (LTP-ADI-MS) entwickelt und für das schnelle qualitative Screening aktiver Arzneimittel gegen Malaria optimiert. Es wurde gezeigt, dass das Verfahren in der Lage ist, den Wirkstoff in Antimalariamittel-Tabletten (Coartem und Malarone) als deren protonierte Molekülionen und andere charakteristische Ionen in weniger als drei Minuten und mit minimaler Probenvorbereitung zu detektieren. Charakteristische Fragment-Ionen von Zielmolekülen wurden zur strukturellen Identifizierung sogar in Gegenwart der Tablettenmatrix verwendet.

Table of Content

Abstract i

Kurzfassung iii

Table of Content v

Chapter 1 Introduction and Scope of the Thesis 1

1.1 Background 2

1.2 Scope of the thesis 6

1.3 State-of-the-art in mass spectrometric-based methods for antimalarial analysis 8

1.3.1 Atmospheric pressure ionisation mass spectrometry (API-MS) 8

1.3.2 Ambient desorption ionisation mass spectrometry (ADI-MS) 10

1.3.3 Matrix-assisted laser desorption ionisation mass spectrometry (MALDI-MS) 11

1.3.4 Time-of-flight secondary ion mass spectrometry (ToF-SIMS) 11

Chapter 2 Fundamental Study on High-Temperature High Performance Liquid Chromatography Mass Spectrometry for Pharmaceutical Analysis ..13

2.1 Introduction 14

2.2 Experimental 16

2.2.1 Chemicals and materials 16

2.2.2 HT-HPLC heating system instrumentation and optimisation 16

2.2.3 HT-HPLC-MS analysis 17

2.2.4 Data acquisition and processing 18

2.3 Results and Discussion 19

2.3.1 HT-HPLC heating system evaluation 19

2.3.2 HT-HPLC-MS analysis 20

2.4 Conclusion 24

Appendix for Chapter 2 25

Chapter 3 Optimisation and Application of High-Temperature High Performance Liquid Chromatography Mass Spectrometry for the Analysis of *Cinchona* Alkaloids 26

3.2 Introduction 27

3.3 Experimental 31

3.3.1 Chemicals and materials 31

3.3.2 HT-HPLC-MS instrumentation and analysis 31

3.3.3 Sample preparation 32

3.3.4 Data acquisition and processing 33

3.4 Results and Discussion 33

3.4.1 Mobile phase optimisation 33

3.4.2 Effect of temperature on separation and chromatographic parameters 35

3.4.3 Effect of temperature on MS detection 39

3.4.4 Application of HT-HPLC-MS to commercial *Cinchona* extract 43

3.5 Conclusion 46

Appendix for Chapter 3 47

Chapter 4 Analysis of Artemisinin-Based Antimalarial Pharmaceuticals by High-Temperature High Performance Liquid Chromatography Mass Spectrometry 51

4.1 Introduction 52

4.2 Experimental 55

4.2.1 Chemicals and materials 55

4.2.2 HT-HPLC-MS instrumentation and analysis 55

4.2.3 Sample preparation 56

4.2.4 Data acquisition and processing 57

4.3 Results and Discussion 58

4.3.1 Optimisation of HT-HPLC-MS method for analysis of ART-based antimalarials 58

4.3.2 ESI optimisation....59
4.3.3 HT-HPLC-ESI-MS of ART and derivatives....61
4.3.4 HT-HPLC-ESI-MS quantitative analysis....63
4.3.5 HT-HPLC-ESI-MS/MS optimisation and analysis of ART and derivatives....64
4.3.6 HT-HPLC-APCI-MS optimisation and analysis of ART and derivatives....66
4.3.7 HT-HPLC-ESI- vs -APCI-MS of ART and derivatives....69
4.3.8 Applications to the analysis of AM in Coartem drug tablet....70
4.4 Conclusion....72
Appendix for Chapter 4....73
Chapter 5 Direct Analysis of Alkaloids in Natural *Cinchona* Bark and Commercial Extracts using Time-of-Flight Secondary Ion Mass Spectrometry....94
5.1 Introduction....95
5.2 Experimental Section....97
5.2.1 Chemicals and reagents....97
5.2.2 Standard and sample preparation....97
5.2.3 High-performance liquid chromatography mass spectrometry....98
5.2.4 ToF-SIMS measurements....98
5.2.5 Laser Microscopy....98
5.3 Results and Discussion....99
5.3.1 Ionisation and fragmentation of Qn standard....99
5.3.2 Characterisation of *Cinchona* bark....103
5.3.3 Characterisation of *Cinchona* extract....108
5.3.4 Detectability of quinine from bark vs. extract....111
5.4 Conclusion and Future Perspectives....113
Appendix for Chapter 5....114

Chapter 6 Rapid Qualitative Screening of Antimalarials Using Low-Temperature Plasma Desorption/Ionisation Orbitrap Mass Spectrometry 119

6.1 Introduction 120

6.2 Experimental Section 122

6.2.1 Chemicals and Sample 122

6.2.2 Standard and sample preparation 122

6.2.3 LTP-MS analysis 122

6.2.4 LC-MS reference method analysis 123

6.3 Results and Discussions 125

6.3.1 Ambient ionisation mass spectrometry 125

6.3.2 Analysis of real drug sample 128

6.3.3 LC-QQQ-MS screening 133

6.4 Conclusion 136

Appendix for Chapter 6 137

Chapter 7 Concluding Remarks and Future Perspectives 145

7.1 Summary and Conclusions 146

7.2 Future Perspectives 148

References 150

List of Figures 170

List of Tables 178

List of Abbreviations and Symbols 180

Acknowledgements 183

Curriculum Vitae 184

List of Publications 185

Chapter 1

Introduction and Scope of the Thesis

1.1 Background

Antimalarial agents are drugs used against malaria, an infectious disease caused by the parasite belonging to the genus *plasmodium* [1]. The five species belonging to the genus plasmodium are; *P. falciparum*, *P. vivax P. ovale, P. malariae*, and *P. knowlesi* of which *P. falciparum* and *P. vivax* are responsible for more than 95 % of the deaths caused by malaria, with *P. falciparum* accounting for most deaths every year [1,2]. Though the disease is transmitted primarily through a bite from an infected female anopheles mosquito, transmission via an infected blood is also possible [3]. The occurrence of malaria is prevalence around the tropical areas, such as sub-Saharan Africa, Southeast Asia, Middle East and Central and South Americas [4,5]. Malaria is one of the most deadly diseases in human history. According to World Health Organization (WHO) 2015 report on malaria, there were approximately 214 million recorded cases globally with 438000 leading to death.

The main strategies to minimise and solve this enormous public health problem can be divided into three categories: (1) the vector control, (2) vaccination, (3) chemotherapy [6,7]. The vector control aims at reducing the transmission of the parasite from human to mosquito and vice versa. This has been achieved largely with insecticide-treated mosquito nets (ITNs) or indoor residual spraying (IRS) and long lasting insecticidal nets (LLIN). Vaccination, which for most infectious disease is an ultimate weapon, involves prevention of transmission and thus elimination of the disease. Despite efforts in the development of vaccine, there is still no commercial vaccine with direct effect on the parasitic infection. Chemotherapy strategy, which aims at suppressing the blood-stage infection in humans, is the main strategy using drugs that belongs to either the quinoline or the antifolate groups [1,7]. The above explained strategies have been characterised by drug resistance in one way or another. Details of the resistance by the parasite in the different strategies is beyond the scope of this work but some details are stated in the publication by Biot *et al.* [7].

Quinoline-based drugs remain the most widely used in the fight against malaria. Structurally, they can be subcategorised into classes of 4-aminoquinolines, 8-aminoquinolines and aryl amino alcohols [8]. Quinine and quinidine (*Cinchona* alkaloids) belong to the aryl amino alcohols class and are known to be the first drugs used in the treatment of malaria parasites. In this class also belongs halofantrine, which is structurally similar to quinine and also effective against the drug resistant *P. falciparum*. Chloroquine and amodiaquine are 4-

aminoquinoline, used in the prevention and treatment of all types of malaria. Primaquine, an 8-aminoquinoline, is known to be used in the treatment of *P. vivax*.

An increase in the resistance toward quinoline-based drugs paved the way for a peroxide-based antimalarial treatment referred to as artemisinin (ART)-based therapies (ACTs). Drugs belonging to this group are ART, isolated from *Artemisia annua,* a Chinese herb, and its derivatives: artemether (AM), artesunate (AS), dihydroartemisinin (DHA), arteether and arteclinic acid. ART-based therapies are presently the WHO first line of drugs against the resistant strain *P. falciparum* and have led to a 60% reduction in malaria-related death from 2000 to 2015 [9,10].

Another relevant class of antimalarials are antifolates, which interfere with folate metabolism, a pathway necessary to the survival of the malaria parasite. One of the most widely used antifolate combinations are pyrimethamine, chloroquanide or dapsone as a dihydrofolate reductase (DHFR) inhibitor combined with sulfalene or sulfadoxine as dihydropteroate synthase (DHPS) inhibitor [7,11]. The drug combination, proguanil and atovaquone (Malarone) also belong to the antifolate class. In Figure 1.1, the chemical structures of some current drugs used in the treatment of malaria are shown.

Recently, there is increasing research in the use of metallopharmaceutical compounds in the treatment of malaria. This has mostly been driven by limited availability of efficient antimalarial agents and resistance of the current line of drugs used in the treatment of patients. Different template metal-chloroquine complexes have been synthesized and tested for their potency against malaria parasite. The main objective of the complexes was to increase the biological activities of the drugs currently in use and to avoid resistance of the parasite. Based on the activity of the synthesized complex, gold-chloroquine complexes, ferroquine and ruthenium-chloroquine are amongst those with greatest biological activity of the drugs. Although ferroquine is the only one being developed at industrial level, the concept has widen the scope for further drug design [7].

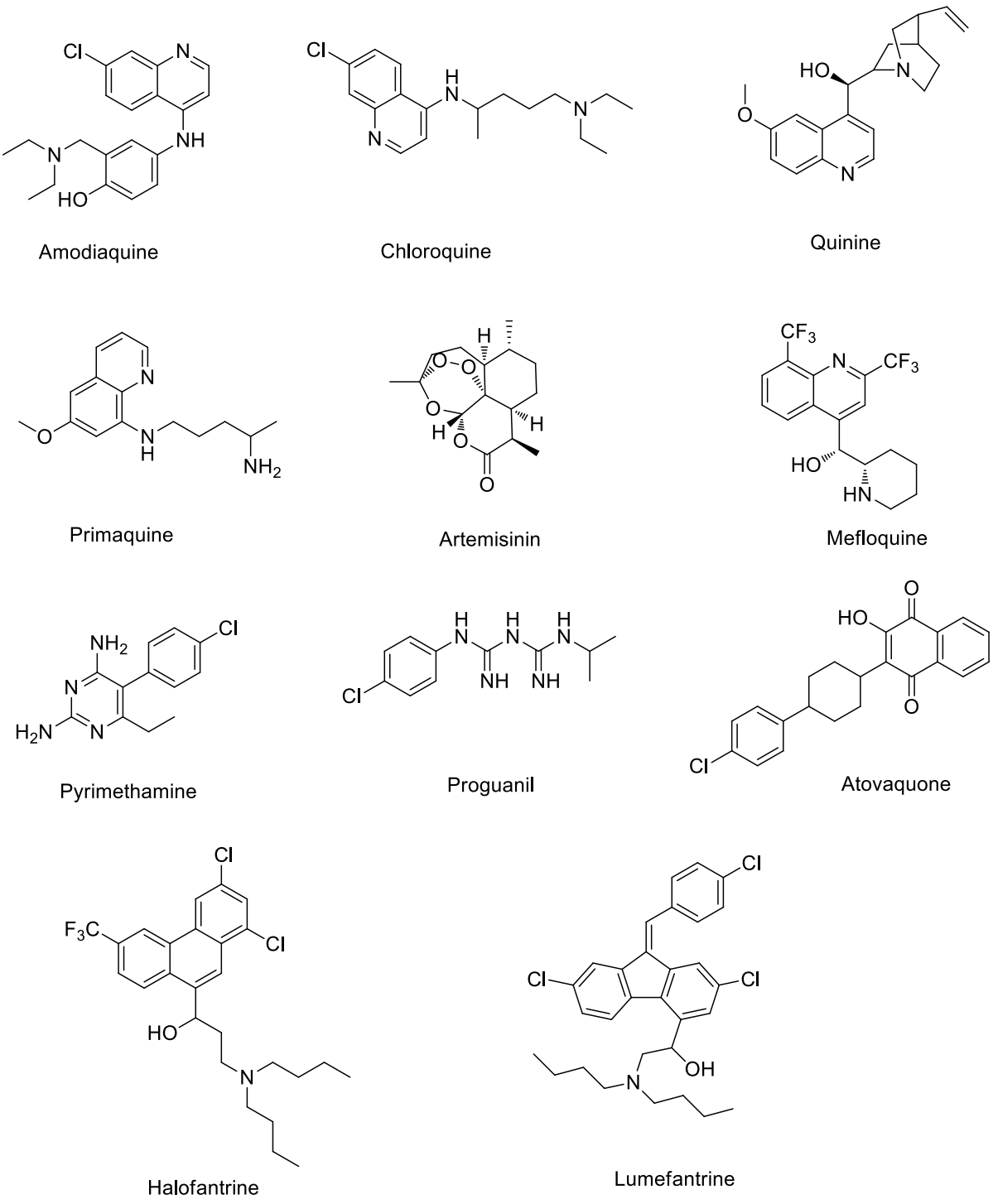

Figure 1.1: Chemical structures and names of current antimalarial drugs.

The aforementioned progress made by the use of ACTs is being threatened by an increasing resistance of the parasite to ACTs. This leads to ineffective treatment especially in malaria prone areas. This current increase in resistance is attributed to an increasing presence of counterfeited ACTs drugs [12-15]. Per WHO definition, counterfeited drugs are those that are

"deliberately and fraudulently mislabelled with respect to the identity and/or source". As with other counterfeited pharmaceutical drugs, counterfeited antimalarials may contain products with wrong ingredient(s), without active ingredient(s), or with an insufficient amount of active ingredient(s) [16]. For instance, on a study of the quality of medicine carried between 2003 and 2013, the highest proportion of failure was among antimalarials [17].

Different analytical methods such as combine handheld spectroscopic device (Raman and near infrared) [18-21] with colorimetric assays [22-24] and thin-layer chromatography (TLC) [25] have been employed to check the quality of antimalarial agents via detecting and quantifying one or a few active ingredients. Though these methods have been effective and cheap, they run short of providing a complete picture of the chemical composition of the active ingredients as well as the non-active ingredients or toxic ingredients.

The capacity of mass spectrometry (MS) to provide information on the molecular weight and chemical structure, which in combination gives the fingerprint of analyte in a complex mixture, makes it an indispensable analytical method for getting chemical information on counterfeited antimalarials. In a publication by Raquel *et al.* [26], the contribution of MS in the study of antimalarial agents was discussed in terms of the compounds quality, stability, screening of impurities and pharmacokinetic studies. In Chapter 1.3, an overview in the state-of-the-art in MS-based method in analysis of antimalarial agents is provided. Special attention is given to the different ionisation process preceding the MS detection. Recent applications within the last decade are discussed and new directions are suggested.

1.2 Scope of the thesis

The aim of this thesis was to develop new and optimised mass spectrometry based techniques for the analysis of pharmaceuticals including antimalarial agents. In Chapter 1, a general introduction into antimalarials and malaria is given. Also, the state-of-the-art in MS-based methods in the analysis of antimalarials is critically discussed. Based on the MS-based approach of analysis, an outline for the thesis is presented below.

High-temperature high performance liquid chromatography mass spectrometry-based approach

Chapter 2 centres on fundamental studies of coupling a high-temperature high performance liquid chromatography (HT-HPLC) to triple quadrupole MS and the exploration of the advantages of the system in the analysis of pharmaceuticals. Since an integral part of HT-PLC is an efficient heating system, this chapter focuses on optimisation of the heating system and application of the system in HT-HPLC-MS analysis to investigate the influence of eluent temperatures on separation and MS response. This chapter paves the way for Chapters 3 and 4, which the optimised heating system is applied for HT-HPLC-MS analysis of antimalarials.

In Chapter 3, the optimised HT-HPLC coupled to triple quadrupole MS via atmospheric pressure chemical ionisation (APCI) and electrospray ionisation (ESI) sources is applied in the HT-HPLC-MS method development and optimisation for the analysis of *Cinchona* alkaloids. In addition to the effect of column temperature on separation, the effect of the eluent temperature on MS ionisation is evaluated. The developed method is later applied in the analysis of aqueous commercial *Cinchona* alkaloids.

Chapter 4 presents studies on the analysis of artemisinin-based antimalarial pharmaceuticals using HT-HPLC-MS with a Zirconia-based polybutadiene (Zr-PBD) column. APCI and ESI ionisation sources parameters are optimised for the detection of ammonium adducts ($[M + NH_4]^+$) of artemisinin and derivatives. The optimised HT-HPLC-MS and –MS/MS method is successfully applied to screen commercial Coartem drug tablets for the presence of artemether, a derivative of artemisinin.

Direct mass spectrometry-based approach

In Chapter 5, the potential of ToF-SIMS is exploited for the first time to screen for *Cinchona* alkaloids including quinine. The method centres on establishing fingerprint fragments of quinine, which can be applied for ToF-SIMS analysis of *Cinchona* bark and commercial

Cinchona extract. Results are presented for TOF-SIMS analysis of quinine in *Cinchona* bark. In addition, results from 3D laser microscopy and HT-HPLC-MS analysis are shown to support the ToF-SIMS findings.

The potentials of LTP-MS, an ADI-MS technique in the fast screening of antimalarials with minimal sample preparation, is presented in Chapter 6. A home-built LTP probe is coupled to an Orbitrap mass spectrometer and used to produce characteristic mass fragments from aqueous standard antimalarial compounds. The technique is applied in the rapid screening of active pharmaceutical ingredients in commercial drug samples.

In Chapter 7, a summary of the results obtained from the different developed and optimised mass spectrometry-based techniques used in the thesis is presented. An evaluation of the different techniques with respect to quality control of antimalarials is given. Based on the results and discussions shown in the different chapters, a possible direction for future work is outlined.

1.3 State-of-the-art in mass spectrometric-based methods for antimalarial analysis

MS-based methods are increasingly being used to get information on the pharmacokinetics, stability, quality, and impurity of antimalarials. This is due to the capacity of MS to provide information on molecular weight and structural details for ionisable compounds such as antimalarials. In principle, MS analysis involves converting the analyte molecules into a charged (ionised) state, with subsequent analysis of the ions and any resulting fragments from the ionisation process on the basis of their mass-to-charge ratio (*m/z*) [27]. In view of the ionisation process, different ionisation techniques such as electron impact ionisation (EI) [28,29], laser desorption ionisation (LDI) [30-32], atmospheric pressure ionisation (API) [33-38], ambient desorption ionisation (ADI) [39-42], and matrix assisted laser desorption ionisation (MALDI) [43,44] have been used in combination with MS detectors for either the analysis of antimalarials or diagnosis of malaria. This section discusses some details on the capabilities of API, ADI and MALDI coupled to mass spectrometry for the analysis of antimalarials. In addition, time-of-flight- secondary ion mass spectrometry (ToF-SIMS) shall be introduced in view of its application in the study carried out in Chapter 4.

1.3.1 Atmospheric pressure ionisation mass spectrometry (API-MS)

From literature survey, API sources are the most used amongst the different ionisation sources that have been coupled to MS for the analysis of antimalarial agents. This has been primarily due to the ease of coupling an API source to high performance liquid chromatography (HPLC). There are three main API-based techniques including electrospray ionisation (ESI) [45-48], atmospheric pressure chemical ionisation (APCI) [48,49], and atmospheric pressure photoionisation (APPI) [50,51].

Detailed discussions on the instrumentation, development and principle of ionisation of the different API sources shall not be discussed in this thesis. However, Figure 1.2 shows a representation of the different API sources and their ionisation mechanism. In either of the API sources, the molecules of interest are usually ionised with possible fragmentations. The ionised molecules are detected as positive and negative molecular ions or adducts for positive and negative mode of detection, respectively.

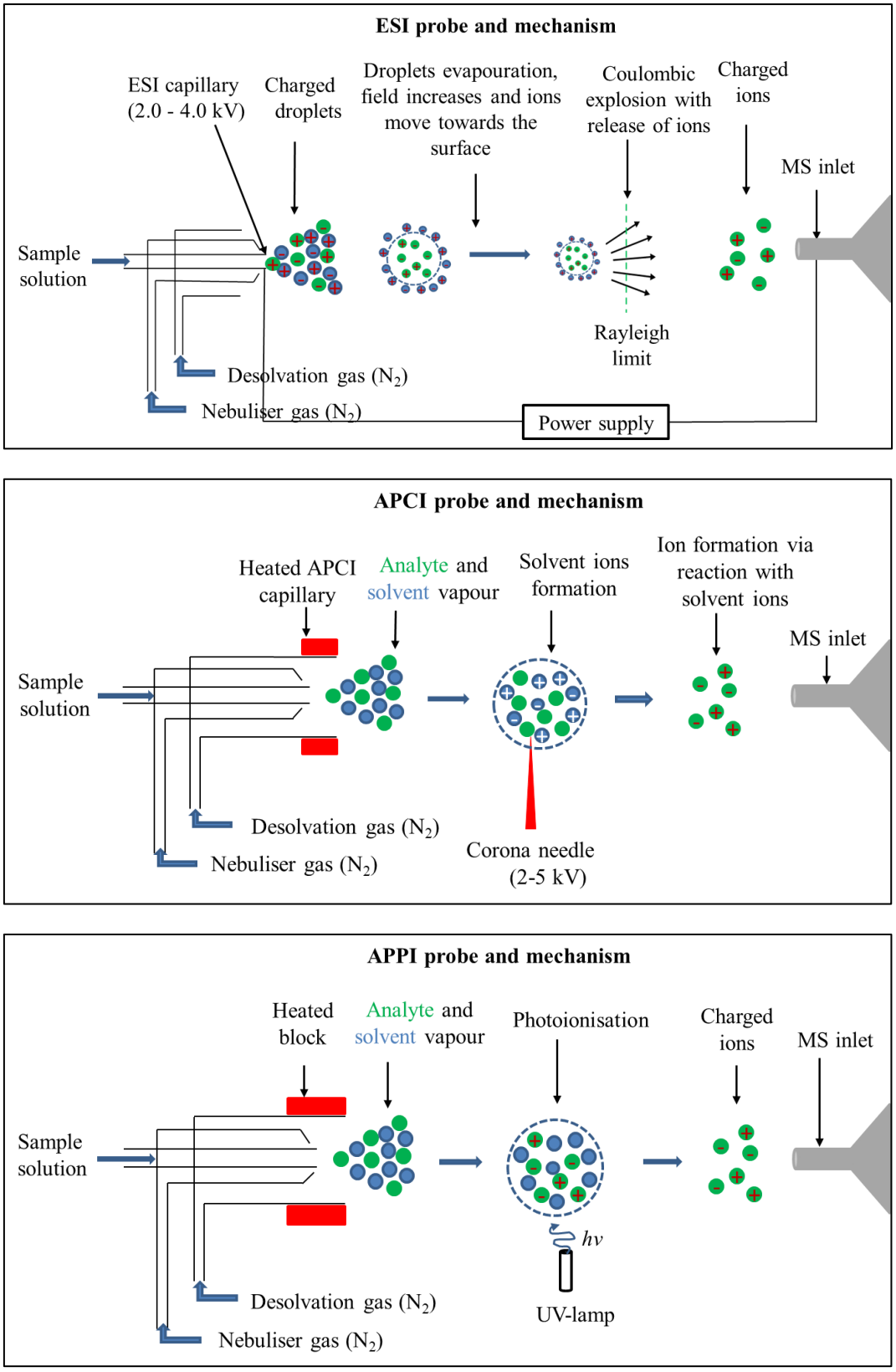

Figure 1.1: Schematic of different API probes and their ionisation mechanism.

Louw *et al.*, [33] demonstrated the potentials of the main API sources including ESI, APCI, and APPI coupled to MS for the analysis of ART-based antimalarials and their metabolites produced from human liver microsome (HLM) incubations. In the study, the mobile phase from a reversed-phase high performance liquid chromatography (RP-HPLC) on a Kinetex C_{18} column was coupled to triple quadrupole linear ion trap (LIT) MS system. For each of the ionisation sources, the method was developed and optimised for the detection of the ammonium adduct ($[M + NH_4]^+$) of DHA, ART, AM and AS. To achieve $[M + NH_4]^+$) as the base peak in the mass spectra, a moderate source temperature (100-200 °C) was applied. The ESI and APCI sources produced comparable results with less in-source fragmentation compared to APPI sources. In addition, while ESI gave the highest signal intensity for the metabolite, APPI was found to be advantageous due to its high signal-to-noise ratio (S/N) especially when operated in the selective ion scan mode.

Another API-MS based technique by Hodel *et al.* [52], showed the use of LC-MS/MS to improve understanding of 14 antimalarial drugs (artemether, artesunate, dihydroartemisinin, amodiaquine, N-desethyl-amodiaquine, lumefantrine, desbutyl-lumefantrine, piperaquine, pyronaridine, mefloquine, chloroquine, quinine, pyrimethamine and sulfadoxine) pharmacokinetics, efficacy and toxicity. The LC method (reversed-phase) made use of gradient elution of 20 mM ammonium formate (AF) and acetonitrile (ACN) both containing 0.5 % formic acid (FA). The LC was coupled to triple quadrupole mass analyser via an ESI interface operated in the positive ion mode.

1.3.2 Ambient desorption ionisation mass spectrometry (ADI-MS)

The growing area of ADI-MS is characterised by the ability to perform analysis in ambient environment with minimal or no sample preparation. In principle, for ADI-MS, samples are desorbed/ionized in open air and transferred via an inlet capillary into the MS. Fundamentals and mechanistic approach of ADI are beyond the scope of this writing but can be obtained in the review by Monge *et al.* [53]. The two original ADI techniques, direct analysis in real time (DART) [54,55] and desorption electrospray ionisation (DESI) [19,40] coupled to MS have been used in screening of antimalarial agents. Both techniques have demonstrated their usefulness in the direct screening of widely counterfeited antimalarial drug containing AS. In a recent publication by Bernier *et al.* [42], a portable DART-single quadrupole (QDa) mass analyser was used efficiently for rapid fingerprinting of a set of ACTs antimalarial tablets. The instrument used, though not handheld, was capable of sorting falsified antimalarial drugs

and identify wrong ingredients with potential health implications. Another class of ADI-MS technique capable of direct analysis of gaseous, liquid and/or solid samples are the plasma-based ADI-MS techniques. These techniques are known to be well suited for analysing compounds with atomic masses less than 1000 Da and as a result have found great application in fast screening analysis of small organic molecules in samples such as agrochemicals, pharmaceuticals, illicit drugs and herbal medicine [56]. Details on the different plasma-based ionisation sources and the mechanism of ionisation can be found in the review by Albert *et al.* [56]. In Chapter 6 the potential of low-temperature plasma-mass spectrometry (LTP-MS), a plasma-based ADI-MS technique, is used in combination with high-resolution Orbitrap MS for rapid screening of antimalarials.

1.3.3 Matrix-assisted laser desorption ionisation mass spectrometry (MALDI-MS)

MALDI-MS is one of the most widely used and rapidly growing soft ionisation MS based methods, which has also been used in the analysis of antimalarials. In principle, a sample is primarily co-crystallised with large molar excess of a matrix compound that is usually an ultraviolet-absorbing weak organic acid. The sample-matrix mixture absorbs laser energy, which is later converted to heat. A small segment of the matrix rapidly heats up and vaporises with the sample. The matrix does not only aid in the vaporisation but also functions as proton donor and acceptor, making it possible for the analyte to be desorbed and ionised in both positive and negative ion mode [57-59]. The resulting mass spectrum shows the protonated molecular ion $[M + H]^+$ in the positive ion mode and deprotonated molecular ion $[M - H]^-$ in the negative ion mode. In the publication by Shrivas *et al.* [43], a variant of MALDI-MS, referred to as atmospheric pressure-MALDI (AP-MALDI) was successfully applied to the bioanalysis of quinine (Qn) using human urine and plasma samples. Based on the experimental procedures, Qn was detected as the protonated molecular ion ($[M + H]^+$) at *m/z* 325.4 with limits of detection (LOD) of 0.18 and 0.24 μM in urine and plasma, respectively.

1.3.4 Time-of-flight secondary ion mass spectrometry (ToF-SIMS)

Contrary to MALDI, ToF-SIMS is a matrix free approach involving the use of a high energetic primary ion beam to bombard and eject “secondary” ions, which are detected by a mass spectrometer, typically a time-of-flight mass analyser (ToF-SIMS) [60,61]. In principle, after primary ion bombardment, the emitted species from the sample surface are electrons, neutral atoms, molecular species as well as atomic and clusters ions. Only the secondary ions are detected by the mass spectrometer. The mass spectrum provides information on the

chemical composition of the sample surface. Organic molecules are detected as positive or negative molecular adducts but the technique suffers from severe fragmentation (compared to MALDI). In addition, clusters of molecular ions can also be detected. A detailed background on the instrumental design, ionisation principle, and secondary ion characteristics is beyond the scope of this thesis but a schematic of SIMS source and mechanism is shown in Figure 1.3. So far ToF-SIMS was not used in the analysis of antimalarial agents. In Chapter 5, ToF-SIMS method is developed and applied for analysing *Cinchona* alkaloid antimalarial-based compounds.

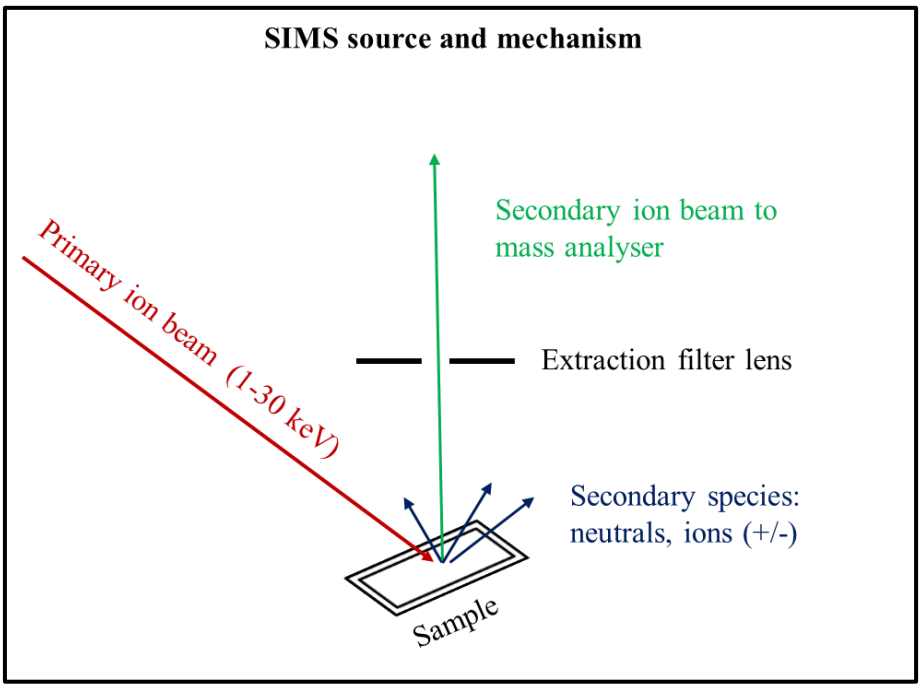

Figure 1.2: Schematic of SIMS source and mechanism.

Chapter 2

Fundamental Study on High-Temperature High Performance Liquid Chromatography Mass Spectrometry for Pharmaceutical Analysis

Abstract

High temperature high performance liquid chromatography coupled to mass spectrometry (HT-HPLC-MS) via atmospheric pressure ionisation (API) sources could possess some advantages over standard LC operated at ambient temperature. However, such advantages can only be exploited if an efficient HTLC heating system is coupled successfully to the ionisation source of the MS. A prototype LC heating system developed by the Germany Institute of Food Technologies (DIL) has been optimised and evaluated with respect to chromatographic parameters including peak retention time (t_R), height, area and asymmetry (A_s). The repeatability in peak t_R, height, area and A_s characterised by small %RSD of 0.39-0.54, 0.78-0.90, 0.82-1.05 and 1.37-2.07 respectively, for benzene demonstrated the efficiency of the heating system. The successful coupling of the system to a Quattro LC mass analyser via an API source and application for HT-HPLC-MS analysis of caffeine paves the way for the system to be used in HT-HPLC-MS analysis of pharmaceuticals.

2.1 Introduction

High performance liquid chromatography (HPLC) at high temperatures (up to 250 °C) is known to have some advantages over HPLC at ambient temperature [62-66]. The advantages are drawn from the physicochemical properties of pure solvents and binary solvent mixtures at elevated temperatures. These physicochemical properties including decreased static permittivity and lower eluent viscosity have been broadly studied by Teutenberg *et al.* [67-69]. For instance it has been suggested that at 150 °C (at a pressure of 50 bar), the static permittivity of water is almost the same as that of about 70% methanol or acetonitrile /water mixtures [70]. As a result, the elution strength of pure mobile aqueous phases in RPLC at elevated temperatures matches that of solvent/water mixtures used in RP-HPLC. The decreased viscosity simultaneously leads to reduced backpressure and improved diffusivity of the analyte. As a result, higher flow rates can be used to decrease the total analysis time. The reduced backpressure makes it possible to replace methanol and acetonitrile by ethanol. The nontoxic nature of ethanol and water makes their use in analysis to be considered as "green chromatography". Furthermore, at higher temperature, the Van Deemter plot flattens out and high flow rates can be used with slight effect on the column efficiency. In addition, the reduced backpressure enables the use of smaller particles to further increase the efficiency [71-73]. Selectivity changes that occur with varying column temperatures have also been exploited for baseline separation and changes in the elution order [74].

Mass spectrometry (MS) has become an indispensable and most specific analytical technique that provides information not only about the molecular weight but also on structural details, which in combination gives the fingerprint of an analyte in a complex mixture. The sensitivity, selectivity and specificity of MS coupled with the separation power of LC have made it an important analytical tool especially in the pharmaceutical and biochemical analysis.

The aforementioned advantages of HT-HPLC coupled to MS would lead to a characteristic decrease in analysis time and as well could affect the MS ionisation efficiency in a way different from LC at lower temperatures. For instance it is known that coupling of HT-HPLC to MS entails that a hot eluent is entering the ionisation source of the MS, which can enhance the MS evapouration process (desolvation) an eluent of lower temperatures entering the ionisation source [75]. The enhancement in desolvation is because of the lower vapour pressure of hot eluent compared to eluent of low temperatures. HT-HPLC-MS, exists more

than two decades, but with the advancement in column and instrumental development, the technique is still exploited in recent times to solve some analytical problems and give response to some unanswered questions. The coupling of HT-HPLC to MS has mostly been achieved via electrospray ionisation (ESI) with interesting results. One of such results obtained by Albert *et al.* [75], showed a positive effect of temperature on ESI-MS sensitivity for basic pharmaceutical compounds. Another interesting result by de Boer *et al.*, involved the coupling of HT-HPLC with continuous-flow enzyme-substrate reaction where the reaction products were detected by ESI-MS. In addition to ESI interfaces, HT-HPLC has also been coupled with MS via plasma-based interfaces such as inductively coupled plasma (ICP). De Vlieger *et al.* [76] showed the coupling of HT-HPLC simultaneously to ESI and ICP-MS for characterisation of halogen containing drug metabolites. Apart from ESI and ICP based interfaces, HT-HPLC has been coupled to MS using the isotope ratio mass spectrometry (IRMS) method. The most important consideration before the use of the IRMS method is the fact that mobile phase had to free of carbon or any carbon containing buffers. This is because any carbon-containing compound in the mobile phase would also be fully converted to carbon dioxide and thus gives an incorrect measurement of the isotopic composition of the analyte of interest. In this regard, HT-HPLC with just water as mobile phase is a pre-requisite. Zhang *et al.* [77,78] have studied details of this technique.

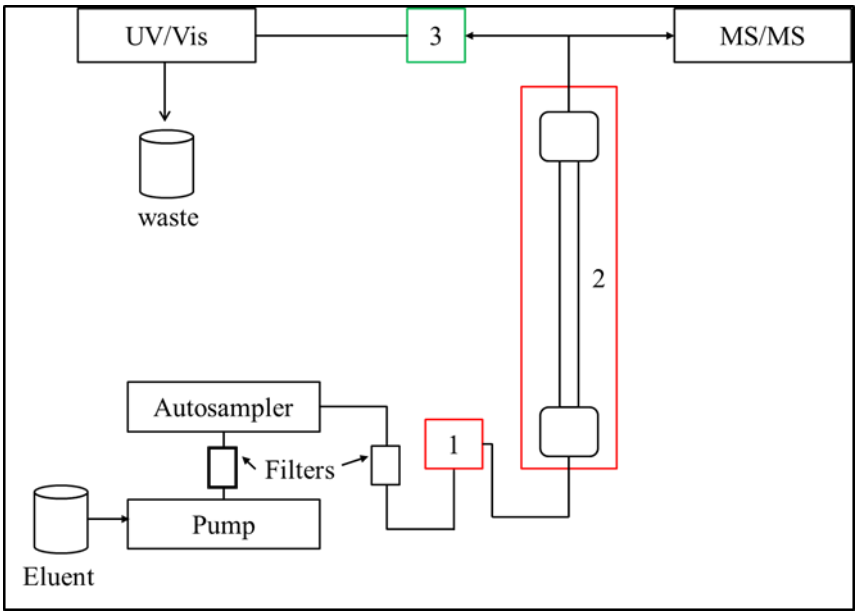

Figure 2.1: Schematic of HT-HPLC system coupled simultaneously to MS and UV/Vis detectors. 1) Eluent preheater, 2) column heater, 3) post-column cooler.

Since one of the pre-requisite of HT-HPLC is to have an efficient heating system that does not suffer from any axial and radial temperature gradient within the LC column, this fundamental study involves a primary optimisation of the heating system to be used for HT-HPLC-MS study in the next Chapters. The heating system have been optimised by evaluating resulting chromatographic parameters such as retention time (t_R), peak area, height, and asymmetry (A_s). Furthermore, the optimised system is coupled to Quattro LC mass spectrometer operated in the selected ion recording (SIR) and MS scan ion mode (SIR-scan mode). Additional optimisation of the HT-HPLC-MS system is achieved by evaluating the influences of changing column temperature on MS detector response. Caffeine is used as test substance to check the applicability of the system in pharmaceutical analysis. A schematic for the HT-HPLC-MS system that shall be used in this study and those in the next two chapters is shown in Figure 2.1.

2.2 Experimental

2.2.1 Chemicals and materials

Analytical grade caffeine (99.0%, Sigma-Aldrich, Steinheim, Germany) was used to make standard for LC-MS study. Analytical grade benzene (99.7%, Merck, Darmstadt, Germany,) and ethylbenzene (99.8%, Fluka Chemie GmbH, Buchs, Switzerland) were used to prepare a standard solution applied for optimisation of the heating system. MS grade ammonium formate (AF) (≥ 99.0%, Fluka, Steinheim, Germany) and formic acid (FA) (≥ 99.0%, Th.Geyer GmbH & Co.KG, Renningen, Germany) were applied as mobile phase additives. HPLC grade methanol (MeOH) and acetonitrile (ACN) were from Fisher Scientific (Loughborough, UK). Bi-distilled deionized water was prepared using a distillation apparatus from Heraeus-Quarzschmelze GmbH (Hanau, Germany). A Whatmann polyamide membrane filter, 0.22 µm pore size (Sigma-Aldrich Chemie GmbH, Schnelldorf, Germany), was employed to filter the aqueous solvent. Calibrated WTW pH meter (Weilheim, Germany) was applied in pH measurement of the aqueous solvent.

2.2.2 HT-HPLC heating system instrumentation and optimisation

For this experiment, an Acela HPLC system (Thermo Fisher Scientific, Bremen, Germany) consisting of a quaternary pump with built-in solvent degassing system and an autosampler with a 25-µL sample loop was used. Mobile phase from the HPLC system was transferred to an external heating system via an inline filter with pore size of 0.2 µm (VICI Valco

Instruments Co. Inc., Schenkon, Switzerland). The heating system was a prototype developed by German Institute of Food Technologies (DIL) (Quakenbrück, Germany). The system was comprised of an eluent preheater, a column heater and a post-column cooler, which can be independently temperature-programmed. Each unit was constructed from an aluminium block to provide efficient heat transfer. For the column heater unit, an additional aluminium column jacket, adapted to the dimensions of the column, was used. The setup ensures that the temperature of the mobile phase entering the column matches with the temperature of the stationary phase and, thus, eliminates a temperature mismatch issue.

Prior to applying the HT-HPLC heating system for HT-HPLC-MS analysis, it was optimised and tested. A test mixture of benzene and ethylbenzene (0.01 mol L^{-1} each), a 150 x 4.6 mm NUCLEODUR C_{18} Gravity column (Macherey-Nagel, Düren, Germany, particle size, 3.0 µm, pore size, 110 Å), scanning spectra UV/Vis detector (Spectra-Physics Analytical, Santa Clara, CA, USA) (λ = 240 nm) and mobile phase comprising of MeOH/water (30/70) were used in this optimisation step. The chromatographic parameters: peak retention times, asymmetries, areas and heights were measured to observe the efficiency of the heating system. For the system evaluation, an eluent preheater temperature of 90 and 95 °C were applied while the column heater unit was maintained at 90 °C throughout the optimisation process. Since a UV/Vis detector was used in the process, the post-column cooler was maintained at 25 °C. The temperature of the solvent coming out of the column outlet was measured to ascertain this fact.

2.2.3 HT-HPLC-MS analysis

For the HT-HPLC-MS fundamental study, a 150 x 4.6 mm Zirconia-based polybutadiene column (Discover Zr-PBD, SUPELCO, Bellefonte, PA, USA particle size, 3.0 µm, pore size, 300 Å was used. For a 150 x 4.6 mm column used in this chapter and the next two chapters, mobile phase relative flow rate of 1.0 mL min^{-1} was found to be greater than the nebuliser capacity of the ESI source of the mass spectrometer. As a result, post-column splitting of the mobile phase, adapted to the ESI nebuliser preceded the HT-HPLC-MS analysis. The post-column splitting was achieved via a zero dead-volume stainless steel T-piece (0.25 mm bore, VICI Valco Instruments Co. Inc.). The split mobile phase was sent either simultaneously to the inlet of the MS and UV/Vis detectors or to MS inlet and waste as shown in Figure 2.1. For this chapter, the latter was used. The capillary used to connect the autosampler injector to the eluent preheater and post-column cooler to the T-piece was a stainless steel capillary with

a 0.25 mm inner diameter. The split ratio for the T-piece was approximated by manually measuring the solvent volume from both the UV/Vis detector outlet and the solvent volume just before the MS inlet probe. For the split ratio measurement, a mobile phase consisting of MeOH/water (50/50) and set flow rate 500 μL min^{-1} were used. In this case, the desired split ratio of 1:1 was obtained with a relative standard deviation (RSD) of 0.6%. The polyether ether ketone (PEEK) capillary from the T-piece to the MS source was maintained at 15 cm in order to minimize post-column cooling effect and thus benefit from potential advantages of hot solvent entering ionisation sources. For the HT-HPLC-MS analysis, 5 μg mL^{-1} (25.7 μmol L^{-1}) of caffeine in series with Zr-PBD column and a Quattro LC mass analyser operated in the SIR-scan ion mode was used. A mobile phase was used consisting of ACN/water (30/70) with 0.1% FA in the water.

2.2.4 Data acquisition and processing

The ChromQuest software (version ChromQuest 5.0, Thermo Scientific) was used to control the Accela LC system and the UV/Vis detector while MassLynx 3.5 (Micromass, UK) was used for mass spectrometer instrumental control. Data acquisition and processing for UV/Vis and MS detector was done with the ChromQuest and MassLynx software respectively. Further data analysis was performed with OriginLab 2015 (OriginLab, Northampton, MU, USA).

2.3 Results and Discussion

2.3.1 HT-HPLC heating system evaluation

As stated in the introductory section, HT-HPLC has some advantages over HPLC at ambient temperature. However, these advantages can only be exploited when an efficient heating system is in place. The instrumental design of an efficient heating system should be able to avoid the occurrence of axial and radial temperature gradient within the column which could be responsible for extra intra-column band broadening [62,75,79]. Such effect, also known as "thermal mismatch" occurs when an eluent flows into an already heated column. To avoid this effect, the eluent has to be preheated to minimize the temperature gradient. As a result, before using a coupled system as shown in Figure 2.1, the eluent preheater and the column heater had to be evaluated. For the evaluation, an eluent preheater temperature of 90 and 95 °C were applied while the column heater unit was maintained at 90 °C throughout. Chromatographic parameters such as the t_R, peak area, height and A_s, which are affected by thermal mismatch, were measured to evaluate the efficiency of the heating system. As shown in Table 2.1, there is an overall good repeatability of peak t_R, area, height, and A_s. This can be seen in the %RSD shown in the table. Apart from the A_s of benzene, an overall improvement in the repeatability of the chromatographic parameters was observed while the eluent preheater section was set at five degrees higher than the column heater. The reason for this can be attributed to the minimized eluent temperature gradient in the column accompanying cold eluent entering a heated column. Some detailed study on the effect of preheating temperature can be found in the review by Teutenberg *et al.* [73]. The poor symmetry for benzene was attributed to possible tailing effect. From the data in Table 2.1 below, it can be postulated that, when the capillary between the pre-column heater and the column heater compartment is relatively short (approx. 7 cm in this work), the pre-column heater temperature and the column heater temperature setting can be the same with minimal temperature gradient effect on the chromatographic parameters.

Table 2.1: HT-HPLC chromatographic parameters of benzene (B) and ethylbenzene (EB) used to evaluate the efficiency of the HTLC heating system.

	t_R (min)		**Peak height (mAU)**		**Peak area (mAU)**		**Asymmetry factor**	
	B	EB	B	EB	B	EB	B	EB
Chromatographic parameters at pre-column heater temperature of 90 °C								
	3.8	5.97	14048	11393	302724	326390	1.86	1.23
	3.84	5.99	14197	11511	306654	329019	1.87	1.22
	3.83	6.01	14353	11619	310139	335232	1.91	1.16
	3.8	5.99	14259	11562	308755	336326	1.91	1.19
Mean	3.82	5.99	14214	11521	307068	331741	1.89	1.2
SD	0.021	0.016	128.05	96.21	3231.03	4804.57	0.03	0.03
%RSD	0.54	0.27	0.90	0.84	1.05	1.45	1.37	2.57
Chromatographic parameters at pre-column heater temperature of 95 °C								
	3.82	5.98	14213	11854	309939	336497	1.7	1.17
	3.8	5.99	14275	11866	310339	337283	1.77	1.17
	3.8	6.01	14101	11917	305572	345900	1.74	1.2
	3.83	6.01	14030	11940	305985	341959	1.77	1.18
Mean	3.81	6.00	14155	11894	307959	340410	1.75	1.18
SD	0.02	0.01	110.01	40.94	2529	4382.89	0.04	0.01
%RSD	0.39	0.25	0.78	0.34	0.82	1.29	2.09	1.16

t_R = peak retention time, RSD = relative standard deviation, A_s= asymmetry measured at 10% peak height, flow rate =500 µL min^{-1}

2.3.2 HT-HPLC-MS analysis

In contrast to UV/Vis detector where hot eluent for HT-HPLC system has to be cooled before entering the detector, MS detection can instead be enhanced by hot eluent. As mentioned before, the enhancement in detection is based on the MS detection principle in which eluent is converted from the liquid state to the gaseous, a process best enhanced by hot eluent. The

coupling process here takes into consideration that other HTLC parameters such as eluent buffers are volatile enough for the LC-MS interface. Though the coupling of HT-HPLC to MS is straightforward, challenges arise when using a 150 x 4.6 mm column for which a set flow rate of 1.0 mL min^{-1} is good for the HTLC column but not for the ESI interface that suffers from spray and signal instability. In addition, the characteristic use of limited percentage of organic modifier in HT-HPLC measurements could be problematic when coupling to MS via ESI interface. This is because ESI interface is not only sensitive to the LC flow rate, eluent additives, but also the percentage of organic modifier in the eluent where higher percentage organic modifier results to better signal intensity relative to eluent with lower percentage organic modifier. Contrary to ESI interface, atmospheric pressure chemical ionisation (APCI) interface, based on its design and ionisation principle, can be operated with 100% organic or 100% aqueous mobile phases at flow rates up to 2 mL min^{-1}. Therefore, for this fundamental study, the focus was on the HT-HPLC-ESI taking into consideration the use of 150 x 4.6 mm column, limited organic modifier, and flow rate of 1.0 mL min^{-1}. In view of the challenge posed by high flow rate, the effluent from the heated column was split via a zero dead-volume T-piece (1:1 split ratio in this case). In addition, to adapt the ionisation source to the limited organic solvent used in the HT-HPLC process, the source block temperature, nebuliser and desolvation gas had to be optimised according to the instrumental requirements. Other strategy used to solve the limited organic solvent effect on the ESI ionisation process includes the post-column addition of organic solvent to enhance the ESI signal. This was not done here because the signal response especially from the SIR scan function was significant. However, such can be encouraged when HT-HPLC-MS is applied in the analysis of traces for which organic solvent may help enhance the signal intensity. A test solution containing caffeine (25.7 µmol L^{-1}) was used to evaluate the coupling of HT-HPLC to MS. With an injection volume of 5.0 µL and 1:1 post-column splitting, an effective concentration of 25.7 x 10^{-12} moles (5.0 ng on column) of caffeine was used for the evaluation.

ESI and APCI signal response (peak area and height) is known to increase with increase in eluent temperature to a maximum and then decreases [79]. Figure 2.2 shows the extracted ion mass chromatogram (XIC) of caffeine at different column temperatures. The traditional decrease in t_R with increase in column temperature was not very vigilant. Though this was not the aim of this study, it could be attributed to the low hydrophobicity for the Zr-PBD column and the fast flow rate, which led to the low retention of caffeine. The aim of this was to apply

the optimised HT-HPLC system in evaluating the effect of temperature on the signal intensity.

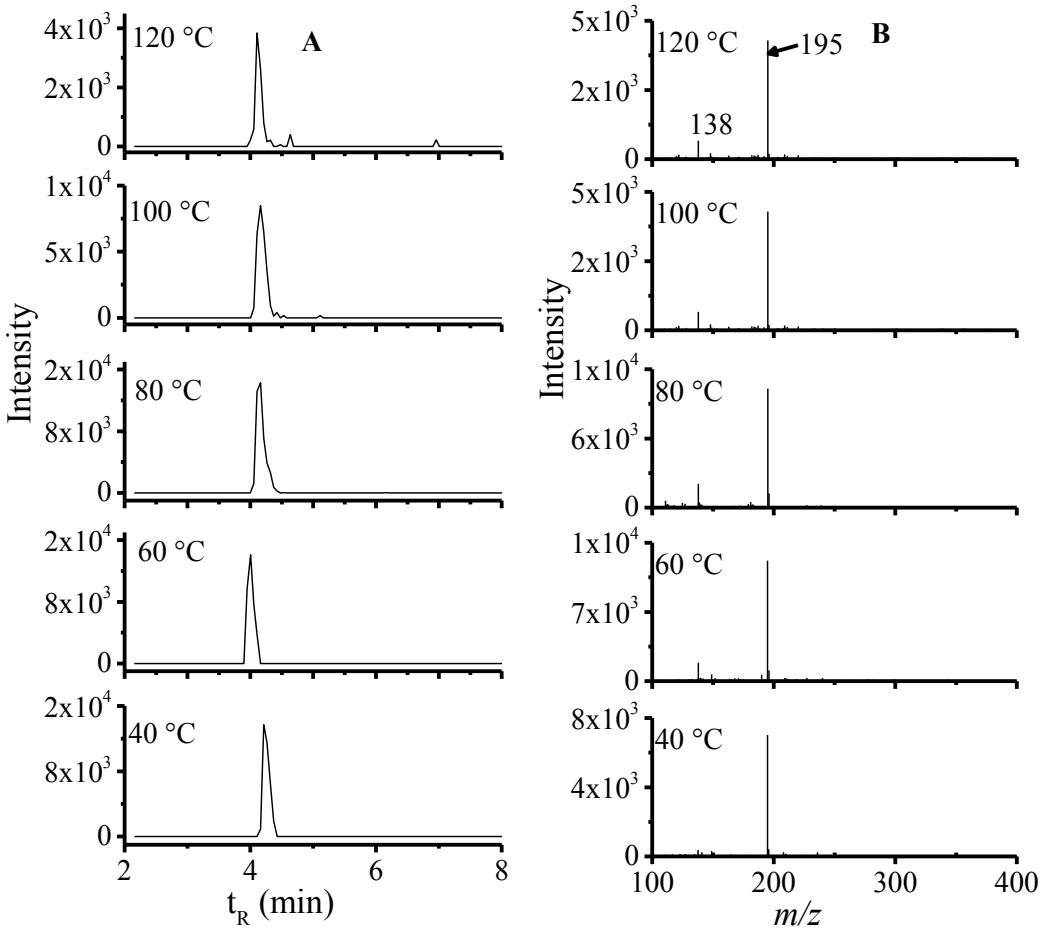

Figure 2.2: Effect of eluent temperature on positive ESI-MS response. A) Extracted ion mass chromatogram (XIC) of *m/z* 195 ($C_8H_{11}N_4O_2^+$), B) mass spectra of caffeine at the respective column temperatures.

From Table 2.2 and Figure 2.3, the results from SIR and scan ion mode show that the MS response (peak area) increases from T 40 to 60 °C and then decreases. The response from the scan ion mode suffers from large standard deviation, which is probably from problems associated with the peak integration.

Generally, when the peak width and t_R decreases with increasing temperature, the MS response may also reduce but this was not the case here since the change in t_R from T 40 °C (t_R 4.1 ± 0.1) to 120 °C (t_R 4.1 ± 0.0) was insignificant.

Table 2.2: Effect of eluent temperature on MS response (peak area) for caffeine using HT-HPLC-MS.

	[a] SIR response		[b] Scan response	
T (°C)	Avg. (n = 3)	%RSD	Avg. (n = 3)	%RSD
40	22263	0.4	2297	35.0
60	42964	0.2	5810	4.3
80	31651	7.8	3495	4.5
100	16415	8.5	3179	20.0
120	8346	2.2	1290	30.0

[a] MS response from selected ion recording (SIR) mode [b] MS response from scan mode

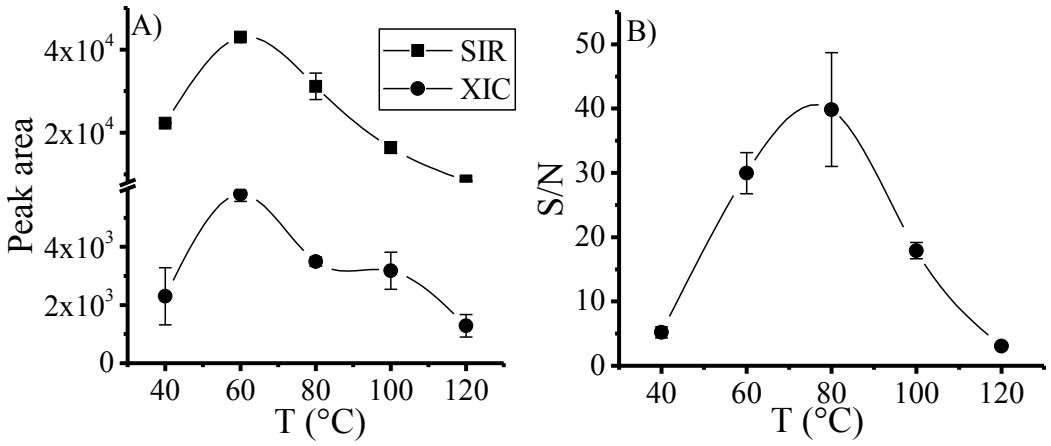

Figure 2.3: Effect of eluent temperature on peak area (A) and S/N (B). The areas were calculated using the SIR mass chromatogram of *m/z* 195 and extracted ion chromatogram (XIC) of caffeine (scan range, *m/z* 195 - 196).

This can be because at the tested temperatures, the caffeine molecule spends all the time in the mobile phase than in the stationary phase. The repeatability of the mass spectra for caffeine shows the stability of the compound in the tested temperature range. The higher S/N for SIR mode compared to XIC for caffeine is attributed to the greater "dwell time" (one second) on the *m/z* 195 compared to one second scan duration for the entire scan range (*m/z* 100 - 400) from which XIC of *m/z* 195 was extracted from. From Figure 2.3B, the S/N increases from T 40 °C to a maxima at around 80 °C and decreases as the temperature was increased further to T 120 °C.

2.4 Conclusion

In this chapter, a prototype HT-HPLC heating system has been optimised and evaluated with respect to chromatographic parameters including peak retention time, height, area and asymmetry. The repeatability of the chromatographic parameters validates the efficiency of the HT-HPLC heating system. The efficient heating system has been coupled successfully to Quattro LC mass analyser via ESI source operated in a positive ion mode and the combined system effectively applied for HT-HPLC-MS analysis of caffeine, a basic pharmaceutical. With the system, the temperature of the eluent was found to influence not only the chromatographic parameters but also the MS ionisation process. This fundamental study shows that by coupling such an efficient HT-HPLC heating system to MS detector, one can benefit simultaneously from the advantages of HT-HPLC such as reduced retention time, limited organic solvent and also potential positive effect of hot eluent on the ionisation process. The HT-HPLC-MS system shall be applied in the next two Chapters for HT-HPLC-MS analysis of antimalarial pharmaceuticals.

Appendix for Chapter 2

Table A 2.1: Mass spectrometric parameters used in fundamental HT-HPLC-MS of caffeine.

Scan Parameters	
Mass range (scan mode)	100 - 400
Scan duration (sec)	1.0
Inter scan delay (sec)	0.10
SIR channel mass	194 & 195
SIR dwell time (sec)	1
Ionisation mode	ESI+
Data type	Compressed centroid
ESI Source	
Capillary voltage (kV)	3.5
Cone voltage (V)	53
Extractor voltage (V)	5.0
RF lens voltage (V)	0.0
Source temp. (°C)	145
Desolvation temp (°C)	400
Analyser vacuum (mBar)	1.1×10^{-5}
Gas cell vacuum (mBar)	2.0×10^{-5}
Nebuliser gas flow (L h^{-1})	62
Drying gas flow (L h^{-1})	555

Chapter 3

Optimisation and Application of High-Temperature High Performance Liquid Chromatography Mass Spectrometry for the Analysis of *Cinchona* Alkaloids

Abstract

Cinchona alkaloids are known to be of pharmaceutical and stereochemical relevance. In this chapter, a method based on high-temperature high performance liquid chromatography (HT-HPLC) on XBridge C_{18} column coupled to triple quadrupole mass spectrometer (MS) via electrospray ionisation (ESI) is developed and optimised for the analysis Cinchona alkaloids. The use of an elevated temperature (25-90 °C), 10% organic modifier, formate buffer, and MS in the scan and selected ion recording (SIR) modes (SIR-scan mode) permits the separation and detection of the four major chiral alkaloids: cinchonine (Cn), cinchonidine (Cdn), quinine (Qn) and quinidine (Qdn) and their dihydro-derivatives: dihydrocinchonine (DCn), dihydrocinchonidine (DCdn), dihydroquinine (DQn) and dihydroquinidine (DQdn) with reduction in analysis time and chemical waste, better chromatographic selectivity and enhanced desolvation process in the MS ionisation source. Limits of detection (LOD) of 15.1, 15.6, 38.3 and 35.4 $\mu g\ L^{-1}$ for Cn, Cdn, Qdn and Qn, respectively were obtained. The developed method was successfully applied for the analysis of major Cinchona alkaloids and derivatives in commercial Cinchona extract.

Based on: D.N. Ateacha, C. Engelhard, submitted for publication.

3.2 Introduction

The separation power of high performance liquid chromatography (HPLC) coupled to the high sensitivity, selectivity and specificity of mass spectrometry (MS) has made it an indispensable analytical technique in the analysis of pharmaceuticals including *Cinchona alkaloids* [1]. Though *Cinchona* alkaloids contain about 35 basic compounds, analytical procedures have centred on the four major chiral alkaloids: cinchonine (Cn), cinchonidine (Cdn), quinine (Qn) and quinidine (Qdn) and their dihydro-derivatives: dihydrocinchonine (DCn), dihydrocinchonidine (DCdn), dihydroquinine (DQn) and dihydroquinidine (DQdn) (*cf* Figure 3.1) [2]. This is because of their pharmaceutical and stereochemical relevance [3-5]. For instance, Qn, a major *Cinchona* alkaloid functions as an antimalarial pharmaceutical drug used against malaria disease and as a muscle relaxant while its pseudo enantiomer, Qdn, is a cardiac depressant (antiarrhythmic) [6]. In addition, they have been used in organic synthesis as co-catalyst in enantioselective reduction of ketones [7]. Due to their relevance, a good number of analytical procedures ranging from thin layer chromatography (TLC), gas chromatography (GC), capillary electrophoresis/capillary electrochromatography and HPLC have been developed and applied in the analysis of *Cinchona* alkaloids [2, 8-11]. Amongst the analytical procedures, reversed-phase (RP) HPLC based on octadecylsilyl (ODS) columns (C_{18}) has been the most commonly used until date. The C_{18} RP-HPLC has been used in synergy with a variety of detectors such as UV/Vis, fluorescence, and MS for the analysis of *Cinchona* alkaloids [6]. Although RP-HPLC has been used for decades as the prime analytical technique for *Cinchona* alkaloids, the analysis is still challenging with the separation procedure marked by separation selectivity (α) problems coming from their similarity in chemical structure. In addition to the separation selectivity problems, resultant peaks are generally characterized by peak tailing and broadening. Tailing are detrimental especially in the analysis of complex mixture because of loss of separation baseline resolution (R_s) and potential effects on quantitative analysis. These problems are reflected in the few number of publications showing the successful separation of these major alkaloids [3, 6, 12]. The tailing and broadening have been attributed to two main sources. Firstly, C_{18} RP columns including new generation columns tend to have heterogenous surfaces with no less than two distinct adsorption sites: the hydrophobic interaction sites of the alkyl-ligands characterized by a fast adsorption-desorption kinetics and cation exchange sites derived from residual silanols with usually slow kinetics. Secondly, overloading of the low density and cation-exchange sites leads to heterogenous thermodynamic and consequently peak tailing

[13]. Numerous analytical strategies ranging from modification of the surface chemistry of the silanol group to mobile phase optimisation have been applied to minimise these effects [2, 3, 10, 14]. Surface modification strategy such as the use of octylsilyl column (C_8) relative to C_{18} have been used to obtain better peak shape and separation selectivity in the separation of *Cinchona* alkaloids [15]. In a similar strategy, strong cation exchange (SCX) and chiral-SCX (cSCX) type stationary phase have been designed and used against the commonly used C_{18} RP stationary phase [3, 12]. Mobile phase strategy to overcome the aforementioned challenge has centred on pH optimisation and the use of mobile phase additives such as amines. Details on these strategies with respect to *Cinchona* alkaloids is beyond the scope of this work but can be found in the review by McCalley *et al.* [6] and publication by Hoffmann *et al.* [3, 12].

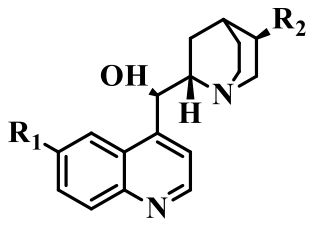

Name	R_1	R_2
Cinchonidine (Cdn)	-H	$-CH=CH_2$
Quinine (Qn)	$-OCH_3$	$-CH=CH_2$
Dihydrocinchonidine (DCdn)	-H	$-CH_2CH_3$
Dihydroquinine (DQn)	$-OCH_3$	$-CH_2CH_3$

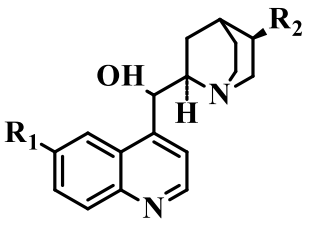

Name	R_1	R_2
Cinchonine (Cn)	-H	$-CH=CH_2$
Quinidine (Qdn)	$-OCH_3$	$-CH=CH_2$
Dihydrocinchonine (DCn)	-H	$-CH_2CH_3$
Dihydroquinidine (DQdn)	$-OCH_3$	$-CH_2CH_3$

Figure 3.1: Chemical structure of some *Cinchona* alkaloids [6].

Mobile phase procedure involving the use of low pH and at low temperature is the most applied analytical procedure to obtained separation of the major *Cinchon*a alkaloids and their derivatives with minimal separation selectivity or tailing/broadening constrains. This is because at low pH, ionisation of residual silanols group (pKa ~ 7.1) [16] on silica surface is suppressed. Though separation at room temperature and low pH minimises peak tailing effect, it gives rise to the problem of low solute retention where by retention time (t_R) of the

analyte is usually longer especially for RP HPLC. However this constrain can be overcome if the separation is carried out at high temperatures [17].

HPLC at high temperatures (up to 250 °C) is known to have some advantages over HPLC at ambient temperature [18-22]. For instance the characteristic lower system backpressure accompanying decreased viscosity of mobile phase at high temperature, leads to reduction in separation time, reduced consumption of organic solvent and improvement in mass transfer. Also separation selectivity variation due to changing column temperature can lead to chromatographic baseline separation and even fluctuations in elution order [23]. In addition, when high-temperature HPLC (HT-HPLC) is coupled to a sensitive detector such as MS (HT-HPLC-MS), a heated mobile phase in principle can aid in the MS desolvation process than a mobile phase at lower temperatures. In this regard, the use of HPLC at high temperature would not only lead to the characteristic decrease in analysis time, but could also influence the ionisation efficiency in a way different from HPLC at lower temperatures.

McCalley investigated the effect of temperature and flow rate on the RP-HPLC analysis of basic compounds including Qn [9]. The investigation, which was conducted using column temperature range, 20 to 60 °C, and a UV/Vis detector, reported an increase in column efficiency at elevated temperature. In the publication by Albert M. *et al.* [24], HT-HPLC at high pH (pH 10.4) was coupled to MS via electrospray ionisation (ESI) for the analysis of five basic pharmaceutical compounds including Qn, they highlighted the positive effect of temperature on the ESI-MS sensitivity. They attributed the positive effect on an increase in organic modifier (10 to 100% acetonitrile (ACN) under gradient flow) at the high temperature and pH used in the HPLC analysis. Also Gagliardi *et al*. [25] studied the retention behaviour of ionizable compounds made up of the four major Qn and derivatives upon simultaneous changes in mobile phase pH and column temperature (20, 30, 40, 50 and 60 °C). In their study, a mobile phase content of ACN/water (25 /85) and UV/Vis detector were applied to obtain an equation for predicting the retention factors.

In this chapter, potential advantages of HT-HPLC and the mass selectivity/ specificity of Quattro LC mass spectrometer are exploited for the analysis of *Cinchona* alkaloids. For the study, a temperature range from 25 to 90 °C and limited amount of organic modifier (10 % of methanol (MeOH) or ACN) are used. According to literature, *Cinchona* alkaloids separation have been accomplished using variety of columns [3, 6, 12], but to the best of our knowledge, none made use of Waters XBridge C_{18} column operated at elevated temperatures. The

XBridge C_{18} column has the following characteristics: 18% carbon load, low pH temperature limit of 80 °C, pH range of 1-12, low silanol activity, and thermally stable at low pH. Due to such characteristics, it has been used in the past for HT-HPLC analysis of basic compounds [26, 27]. After developing a HT-HPLC-MS method for the separation and detection of *Cinchona* alkaloids, the influence of temperature on separation and detection, as well as the effects of ACN and MeOH at the respective temperatures are compared. Before the HT-HPLC analysis, the mobile phase buffers (0.1% formic acid and 10 mM ammonium formate (AF), pH 3.0) were tested at room temperature for their influence on chromatographic parameters. The Quadrupole mass analyser is operated simultaneously in the MS ion scan and selected ion recording (SIR) modes (SIR-scan mode). The SIR-scan mode is advantageous as the SIR portion of the SIR-scan acquisition gives better reproducibility, accuracy, and better detection limits, etc., and the scan portion give the mass spectra of the compound of interest. Due to the better ionisation efficiency of ESI source compared to atmospheric pressure chemical ionisation (APCI) source for *Cinchona* alkaloids, the former is used in the HT-HPLC-MS analysis. The developed and optimised method is later applied in the analysis of commercial sample containing *Cinchona* alkaloids.

3.3 Experimental

3.3.1 Chemicals and materials

Analytical standard of Qn (99%), Qdn (>98.0%), and Cn (>98.0%) were purchased from Alfa Aesar GmbH (Karlsruhe, Germany) and Cdn (≥99.0%) was from Merck Schuchardt OHG (Hohenbrunn, Germany). According to the manufacturer the Qn standard contain up to 5% DQn, Cn contain up to 3% Qdn/DQdn. Ammonium formate (≥99.0%, Fluka, Steinheim, Germany) was used as chromatographic buffer. Formic acid (≥99.0%, Th.Geyer GmbH & Co.KG, Renningen, Germany) was added to the mobile phase for pH adjustment. MeOH (99.99%) and ACN (99.9%) were from Fisher Scientific (Loughborough, UK). Bi-distilled deionized water was prepared using a distillation apparatus from Heraeus-Quarzschmelze GmbH (Hanau, Germany). A Whatmann polyamide membrane filter, 0.22-µm pore size (Sigma-Aldrich Chemie GmbH, Schnelldorf, Germany) was employed to filter the aqueous solvent. Calibrated pH meter (Xylem Analytics Germany Sales GmbH & Co. KG, WTW, Weilheim, Germany) was applied for the pH measurement and adjustment. The mobile phase used consisted of MeOH/water (10/90) or ACN/water (10/90) with 10 mM AF (pH 3.0) in water.

3.3.2 HT-HPLC-MS instrumentation and analysis

An Acela HPLC system (Thermo Fisher Scientific, Bremen, Germany) consisting of a quaternary pump with built-in solvent degassing system and an autosampler with a 25-µL sample loop was used. The analytical column was a Waters XBridge C_{18} (150 x 4.6 mm, pore size 130 Å, particle size 3.5 µm; Waters, Dublin, Ireland). Mobile phase from the LC was transferred to an external heating system (*cf* Figure 2.1) via an inline filter with pore size 0.2 µm (VICI Valco Instruments Co. Inc., Schenkon, Switzerland). The Accela system was controlled with ChromQuest software (version ChromQuest 5.0, Thermo Fisher Scientific).

The heating system that was used for HT-HPLC analysis has been described in Chapter 2. For the experiments, the temperature of the eluent preheater unit was set five degrees higher than the one of the column heater unit. For this experiment, a temperature range from 25 to 90 °C was applied to investigate the effect of temperature on separation and ionisation efficiency.

A triple quadrupole mass spectrometer (model Quattro LC, Micromass, Wilmslow UK) with ESI and APCI sources was used for this experiment. The mass spectrometer was operated in

the SIR-scan mode of detection. After testing the ionisation efficiency of both ESI and APCI, the former, due to its better ionisation efficiency for *Cinchona* alkaloids, was used for further HT-HPLC-MS analysis. After tuning and optimisation of the ESI source, the following settings were used: 100 °C source temperature, 35 V sample cone voltage, 3.0 kV capillary voltage, 66 L h^{-1} N_2 nebulizer gas flow, 550 L h^{-1} desolvation gas, 400 °C desolvation temperature and 0.2 V radiofrequency (RF) lens. A scan function comprising both an MS scan (*m/z* 100 – 800) and SIR of *m/z* 295.4, 297.4, 325.4, and 327.4 corresponding to Cn/Cdn, DCn/DCdn, Qn/Qdn and DQn/DQdn respectively were used for the MS detection. MassLynx 3.5 software (Micromass, UK) was used to control the triple quadrupole mass spectrometer.

For HT-HPLC-ESI-MS analysis, the effluent from the heated column was forwarded to the inlet of the MS after a post-column splitting using a stainless steel T-connector (0.25 mm bore, VICI Valco Instruments Co. Inc., Schenkon, Switzerland.). The split ratio for the T-connector ratio was approximated by manually measuring the solvent volume from both the UV/Vis detector outlet and the solvent volume just before the ESI probe. The measurement was done at room temperature using MeOH/water (50/50) as mobile phase with a flow rate of 500 µL min^{-1}. In this case, the desired split ratio of 1:1 was obtained with an RSD of 0.6%. After the T-connector, the capillary leading to the mass spectrometer was connected directly to either the ESI probe without any prior cooling. For this chapter, the temperature of the preheating unit was 5 °C higher than the temperature of the column-heating unit. The polyether ether ketone (PEEK) capillary from the T-connector to the MS was maintained at 15 cm in order to minimize post-column cooling effect and thus benefit from potential advantages of hot solvent entering the ionisation source. The dead time for the HT-HPLC-MS system was approximated at room temperature to be 2.5 minutes.

3.3.3 Sample preparation

Four separate stock standard solutions (each 1000 µg mL^{-1}) of Qn, Qdn, Cn and Cdn were prepared by dissolving appropriate amounts in organic solvent. After dissolution in in ultrasonic bath for 10 minutes, each stock standard was filtered with a 0.2 µm membrane filter into separate amber sample vials. For the test mixture, the stock was diluted 150 times with the mobile phase to a concentration of 6.7 µg mL^{-1} for each compound (16.75 ng on column for 5-µL injection volume).

3.3.4 Data acquisition and processing

Signals from the mass spectrometer were processed using the MassLynx software. To obtain a mass spectrum after HT-HPLC separation, the average background scan around a detected peak had to be subtracted from the average scan around the peak top. For comparable mass spectrum, the peak t_R has to be the same from one measurement to the next. Further data analysis was done using OriginLab 2015 (OriginLab, Northampton, MU, USA).

3.4 Results and Discussion

3.4.1 Mobile phase optimisation

As stated in the introductory section, the four major *Cinchona* alkaloids are a set of basic chiral organic compounds with similar physicochemical properties. Each of the major *Cinchona* alkaloids has two basic nitrogen atoms with different pKa values. For instance, Qn has pKas of 4.3 and 8.6 with the quinoline nitrogen having the lower basicity (*cf* Table A 3.1 in the appendix section). As a result, their RP separation is usually accompanied by peak tailing and broadening. As mentioned in the introduction section, one strategy to overcome such tailing was to perform the RP separation at room temperatures and at low eluent pH where ionisation of residual silanol groups (pKa ~ 7.1) [16] on silica surface is suppressed. However, such a method results to low solute retention, which as have been postulated can be overcome when the separation is carried out at elevated temperatures. Before evaluating and applying elevated temperatures in RP-HPLC-MS analysis of *Cinchona* alkaloids, the mobile phase was pre-optimised with respect to buffer type and pH range.

FA and AF buffers, characterised by their lower pKa and LC-MS interface friendly nature [28] were evaluated for their effect on the retention and separation selectivity of *Cinchona* alkaloids. For this evaluation and the rest of the work, 10% organic modifier (MeOH and/or ACN) and mobile phase pH 3 were used.

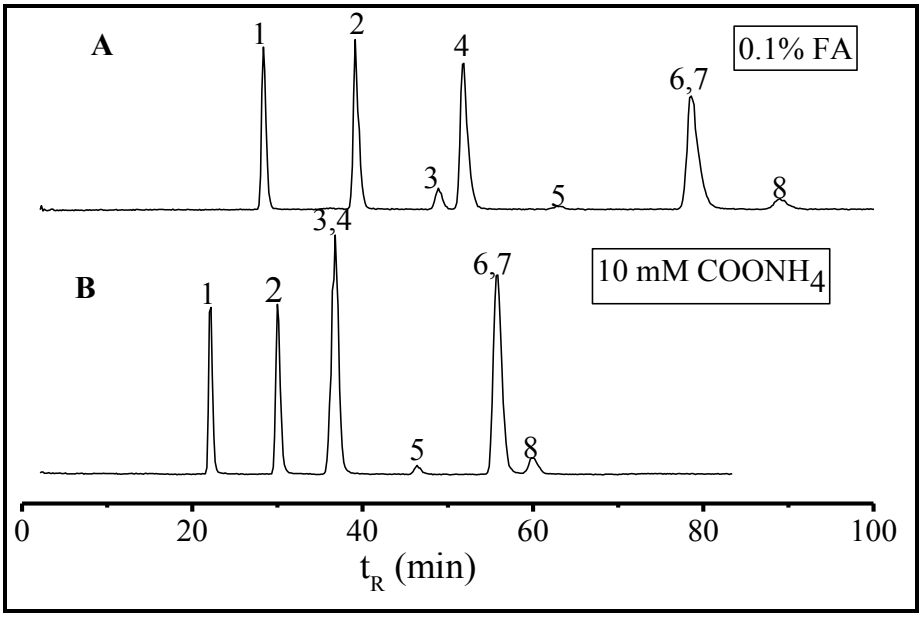

Figure 3.2: Effect of buffer on the separation of *Cinchona* alkaloids. Chromatographic conditions: Waters XBridge C_{18} (150 x 4.6 mm, 3.5 µm) stationary phase; mobile phase: MeOH/water (10/90) with 0.1% FA (A) and 10 mM AF (B) in water; flow rate: 1.0 ml min^{-1}; injection volume: 5 µL; column temperature: 25°C. Detection: Quattro LC in SIR mode; cone voltage: 35 V; capillary voltage: 3.0 eV. Analyte: 1) Cn (*m/z* 295.4), 2) Cdn (*m/z* 295.4), 3) DCn (*m/z* 297.4, 4) Qdn (*m/z* 325.4), 5) DCdn (*m/z* 297.4), 6) Qn (*m/z* 325.4), 7) DQdn (*m/z* 327.4) and 8) DQdn (*m/z* 327.4).

Figure 3.2 shows the effect of buffer on the separation of *Cinchona* alkaloids at room temperature HPLC on the XBridge C_{18} column with mobile phase containing 10% MeOH. The mass chromatogram shows the four main *Cinchona* alkaloids (Cn, Cdn, Qn and Qdn) injected, as well as their dihydro-derivatives (DCn, DCdn, DQn, and DQdn). The presence of the dihydro-derivatives is in accordance with the manufacturer's specifications. From the elution order, Cn is least retained while DQn is most retained. The overall elution order for both mobile phase additives can be attributed to the hydrophobic mechanism. This is because at a mobile phase pH of three, the *Cinchona* derivatives (quinoline) are expected to be in the protonated form or the protonated form is expected to be more dominating and thus permitting the hydrophobic interaction to define the elution order. Working within the hydrophobic interaction mechanism, the elution of Cn/Cdn before Qdn/Qdn can be attributed to their mass difference as oppose to their stereochemistry. The longer t_R of Cdn over its diastereomeric pair Cn could be because, for the applied chromatographic condition, Cdn adopts an overall conformation with more accessible hydrophobic surface area compared to Cn [3]. Same explanation is valid for the elution of the other pseudo enantiomeric pairs:

DCn/DCdn, Qn/Qdn, and DQn/DQdn. Apart from the buffer effect on retention, the mass chromatogram also shows co-eluted peaks such as peak pairs 6/7 and 3/4 (Figure 3.2B). Since the co-eluted peak pairs are not diastereomers (i.e., they differ in their *m/z*), each peak can be qualitatively and quantitatively detected by MS. This is because MS detector in the SIR-scan mode helps to avoid the separation selectivity problem associated with co-elution.

The overall decrease in the t_R, tailing and shorter retention factor, k, (k=19.7, calculated for Qn) with the use of AF can be attributed to stronger ionic interaction between ammonium ion (NH_4^+) and residual silanols. In the presence of ionic interactions, the separation selectivity of the stationary phase towards the mostly protonated quinoline derivative changes such that the *Cinchona* alkaloids are less retained and thus elutes faster than when FA was used. From Figure 3.2A, the separation of DCn (peak 3) and Qdn (peak 4) with R_s 1.4, could be attributed to the longer t_R/hydrophobic interactions. It can concluded here that, provided the co-eluted *Cinchona* alkaloids are not diastereomeric pairs, both buffers within the experimental conditions are useful in method development and application for the analysis of *Cinchona* alkaloids. Because of the elution strength of AF relative to FA and coupled to its LC-MS interface friendly nature, it was used as the buffer of choice for the next sections.

3.4.2 Effect of temperature on separation and chromatographic parameters

Temperature is known to affect the retention of ionizable compounds in MeOH/water and ACN/water mobile phases in different ways [29-31]. Figure 3.3 and Table A 2 (appendix for Chapter 3) show the effect of column temperature on the separation and retention of the four main *Cinchona* alkaloids and their dihydro-derivatives while using MeOH and ACN as organic modifier in the mobile phase. The mass chromatogram shows an overall decrease in t_R and *k* for all compounds. The decrease in *k* is visualized in Figure 3.4, which shows the variation of *k* with respect to temperature. Also shown on Figure 3.3, Figure 3.4 and Table A 3.2 is the effect of organic modifiers on chromatographic parameters (k, α, A_s, R_s, and N) at the respective column temperatures. For instance, *k* for Qn decreased by 71.8% when ACN was used as organic modifier, while a 42.6% decrease was observed with MeOH as organic modifier.

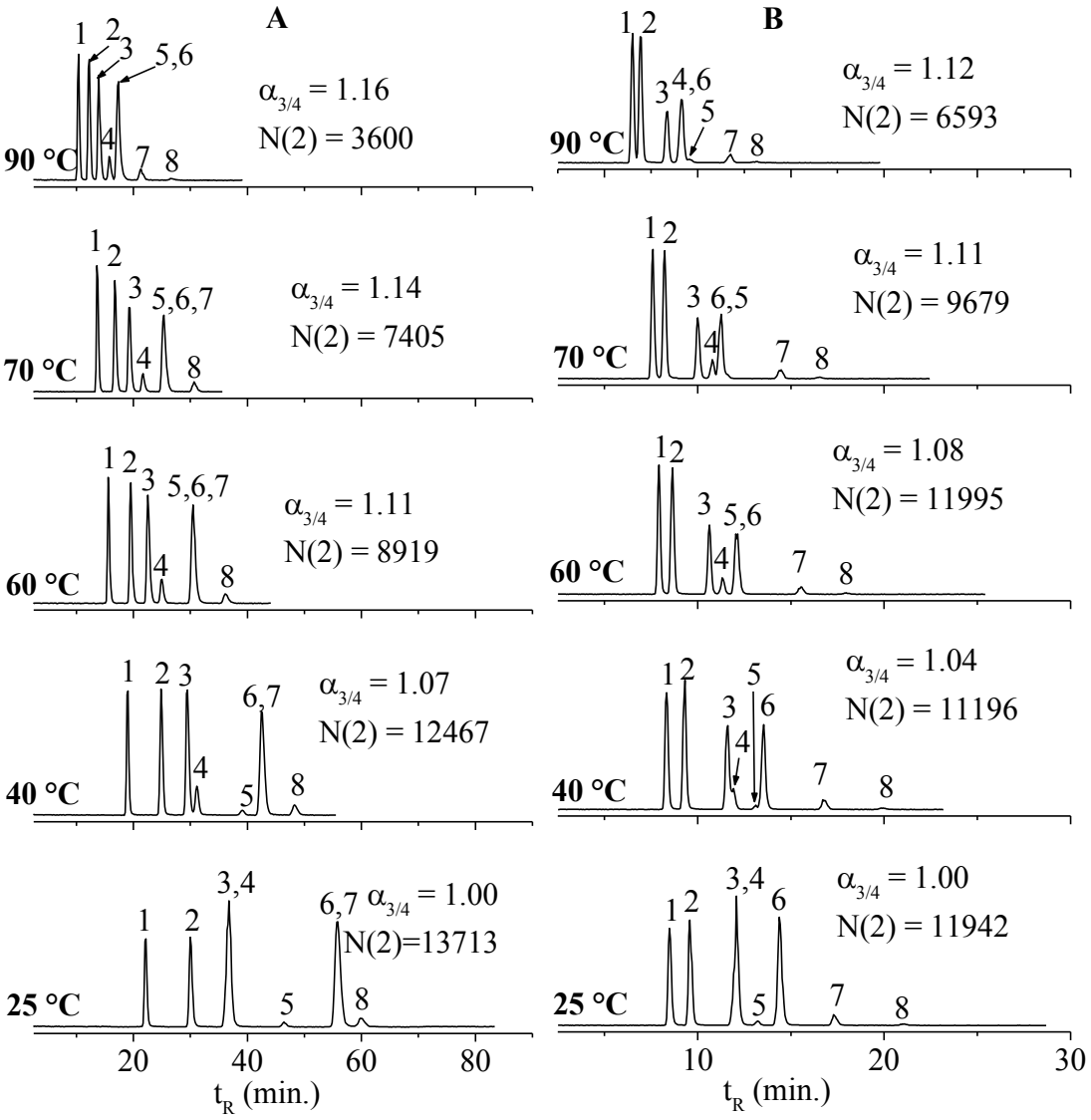

Figure 3.3: Isothermal separation of Qn and derivatives. Chromatographic conditions: Stationary phase: Waters XBridge C_{18} (4.6 x 150 mm, 3.5 µm); mobile phase: A) MeOH/water (10/90) with 10 mM AF in water, B) ACN/water (10/90) with 10 mM AF in water; flow rate: 1.0 mL min^{-1}; injection volume: 5 µL; detection: Quattro MS in selected ion recording (SIR) mode. Analyte: 1) Cn (*m/z* 295.4), 2) Cdn (*m/z* 295.4), 3) DCn (*m/z* 297.19, 4) Qdn (*m/z* 325.4), 5) DCdn (*m/z* 297.4), 6) Qn (*m/z* 325.4), 7) DQdn (*m/z* 327.4) and 8) DQn (*m/z* 327.4). (N (2) = number of plate for Cdn, $\alpha_{3/4}$ = selectivity between DCn and Qdn).

The high decrease *k* with ACN compared to MeOH is attributed to the low viscosity of the former over the latter. From Figure 3.3B, the elution order of peak 5&6 was swapped with peak 6 having a shorter t_R compared to peak 5 as the temperature was varied from 25 to 90 °C. It can also be seen that at the different column temperatures, the organic modifier also has an influence on the elution order. For instance, at a column temperature 70 °C, peak 6&7 co-eluted with MeOH but were separated with the use of ACN.

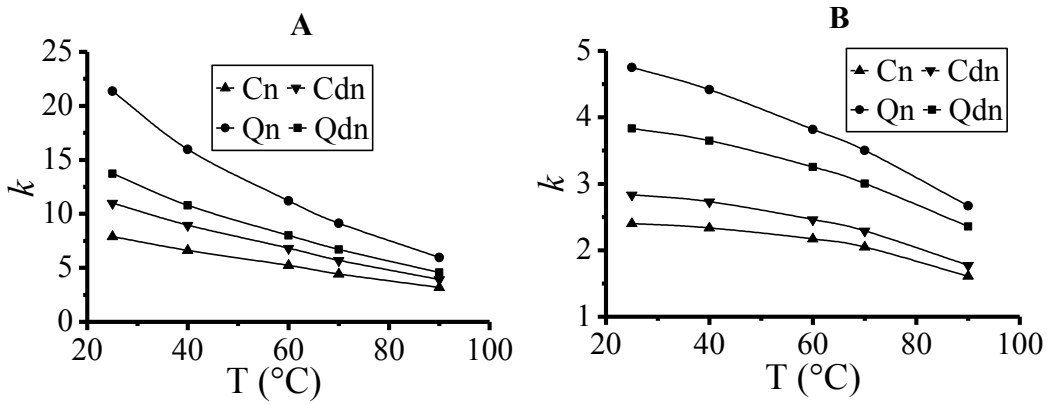

Figure 3.4: Effect of temperature on *k* obtained using HT-HPLC-MS analysis of *Cinchona* alkaloids. Chromatographic conditions: same as in Figure 3.3; mobile phase: A) MeOH/water (10/90) with 10 mM AF in water, B) ACN/water (10/90) with 10 mM AF in water. (*k* = retention factor).

This overall decrease in *k* with increasing column temperature is thermodynamically described using the van't Hoff equation given as

$$\ln k_i = -\frac{\Delta H}{RT} + \frac{\Delta S}{R} + \ln\beta \qquad 1$$

where k_i refers to the retention factor of the solute *i*, ΔH and ΔS are respectively the enthalpy and entropy of transfer of solute *i* from the mobile phase to the stationary phase, *T* is the column temperature in kelvin (K), *R* is the ideal gas constant and β is the volume phase ratio. Figure 3.5A&B show the van't Hoff plot based on Figure 3.3A&B respectively. For each of the *Cinchona* alkaloids, a curved van't Hoff plot was observed within the temperature range. This is contrary to the theoretically expected straight line proposed by the van't Hoff equation. The coefficient of variation (r^2) associated with this plot is shown at the bottom of the figure. Such curved van't Hoff plot complement the result of Wiese *et al.* [27], where a curved van't Hoff plot was observed for the HT-HPLC analysis of basic sulphonamide using a similar column (Waters XBridge C_{18} column) and column temperature interval of 60 to 180

°C. Based on the compound of interest, the decrease in t_R with increase in temperature is in contrast to the HT-HPLC analysis of basic compound including Qn by McCalley [8], where an increase in column temperature gave an anomalous increase in the retention of Qn.

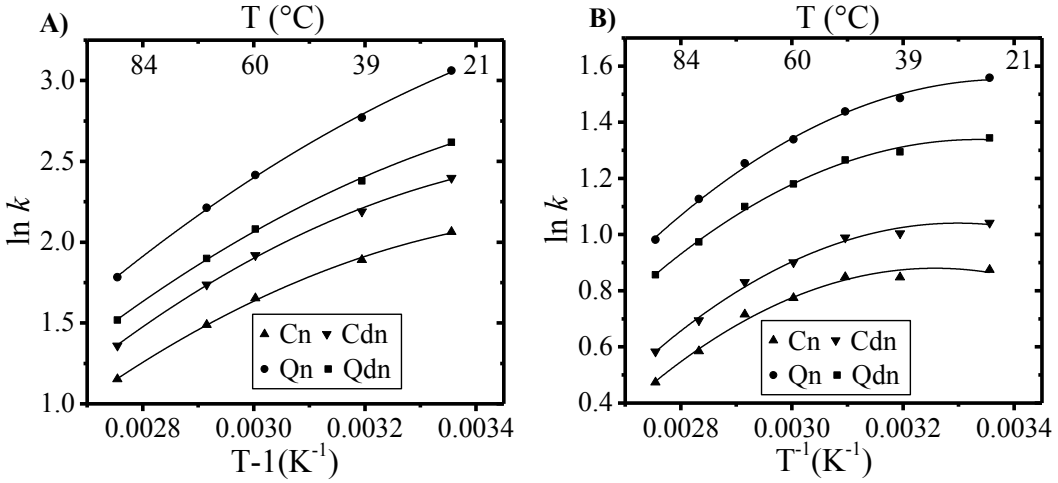

Figure 3.5: Van't Hoff plot of four major Qn and derivatives in a temperature interval from 25 to 90 °C. Chromatographic conditions and detection: same as in Figure 3.3. Mobile phase: MeOH/water (10/90) (A), ACN/water (10/90) (B) with 10 mM in water. Coefficient of variation (r^2) for Cn, Cdn, Qdn and Qn: 0.998, 0,998, 0.998 and 0.999 respectively for A and 0.984, 0.991, 0.996 and 0.996 for B.

According to scientific literature, the curved van't Hoff plot, though not fully understood, have been attributed in the case of silica column to several factors including dissimilarity in enthalpies associated with solvophobic and silanophilic interactions, high water content and possible phase transition phenomenon [32, 33].

In addition to the role played by stationary phases, mobile phase additives and organic modifier on separation selectivity, temperature also plays a centre role especially for ionizable compounds, since ionisation equilibria is temperature dependent. From Figure 3.3, at 25 °C, the main *Cinchona* alkaloids are separated but with no baseline resolution (co-elution) between peak 3 and 4. This is attributed to the lack of separation selectivity ($\alpha_{3/4} = 1$) between the peaks. However, increasing the temperature from 25 to 60 °C led to the separation of peak 3 and 4. This is because of an increase in the separation selectivity ($\alpha_{3/4} = 1.13$, Figure 3.3) with subsequent improvement in the baseline resolution ($R_{3/4}$=1.9). The values for chromatographic parameters including k, α, A_s and R_s for Cn, Cdn, Qn and Qdn at the different column temperatures are shown in Table A 3.2 in the appendix section.

The column efficiency decreases with increase in column temperature (*cf.* for peak 2 and 3 on Figure 3.3).This is also attributed to reduced peak width accompanying increasing column temperatures.

Also shown on Figure 3.3, Figure 3.4, and Table A 3.2 (see appendix section) is the effect of column temperatures and organic modifiers on column efficiency. The overall decrease in the efficiency with increasing column temperature (*cf.* for peak 2 on Figure 3.3) can also be attributed to reduced peak width with increasing column temperature.

3.4.3 Effect of temperature on MS detection

As stated above and based on principle, a hot eluent entering the MS ionisation source could facilitate the desolvation process and subsequently the ionisation process. To visualize this effect, the signal-to-noise (S/N) ratio and peak area percentage of the protonated molecular ion ($[M + H]^+$) for Cn ($C_{19}H_{22}N_2O$, *m/z* 295.4), Cdn ($C_{19}H_{22}N_2O$, *m/z* 295.4), Qdn ($C_{20}H_{25}N_2O_2$, *m/z* 325.4), and Qn ($C_{20}H_{25}N_2O_2$, *m/z* 325.4) were used. They were calculated from the extracted SIR mass chromatogram shown in Figure A 3.2 in the appendix section. It should be recalled that the extracted SIR mass chromatogram in Figure A 3.2 was obtained from Figure 3.3. Calculation from the extracted SIR mass chromatogram is advantageous because it is void of the separation selectivity constrain attached to co-elution as seen in Figure 3.3. In addition, it facilitates the integration of the peak area and S/N without interference. The percentage peak area was calculated by dividing each area with the total area of all four peaks and multiplied by 100%. Since the percentage area is concentration independent, the results using different organic modifier can be compared to see the effect of organic modifier at the different eluent temperatures. The S/N ratio was calculated from the ratio of the average peak height to the average baseline intensity. As can be seen from Figure 3.6, while there is an overall decrease in the percentage peak area for Qn & Qdn, there is an overall increase for Cn & Cdn. With MeOH as organic modifier, the ESI-MS response (column temperature 40-90 °C) was lower than with ACN organic modifier.

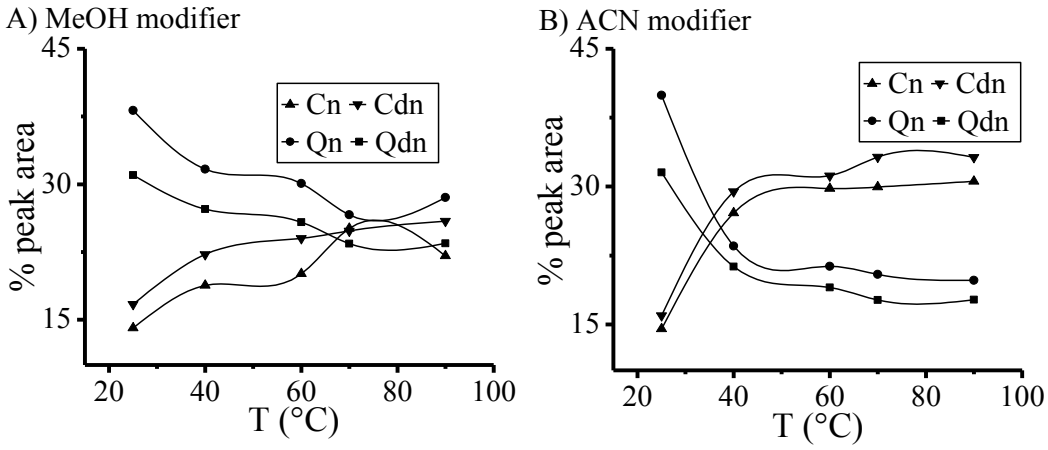

Figure 3.6: Influence of MeOH (A) vs. ACN (B) as mobile phase organic modifier on the variation of percentage peak area during HT-HPLC-ESI-MS analysis of *Cinchona* standard. Chromatographic conditions and detection: same as in Figure 3.3. Column temperature range: 25 - 90 °C.

From Figure 3.7, a non-uniform trend in S/N versus column temperature is observed. Despite the non-uniformity in the trend, it can be seen that with ACN as organic modifier, there is an overall decrease in the S/N ratio until 70 °C and then an increase until 90 °C. For MeOH as organic modifier, while the S/N ratio for Qn and Qdn showed an overall decrease until about 80 °C and the starts increasing, Cn and Cdn showed an increase until about 75 °C and then start decreasing.

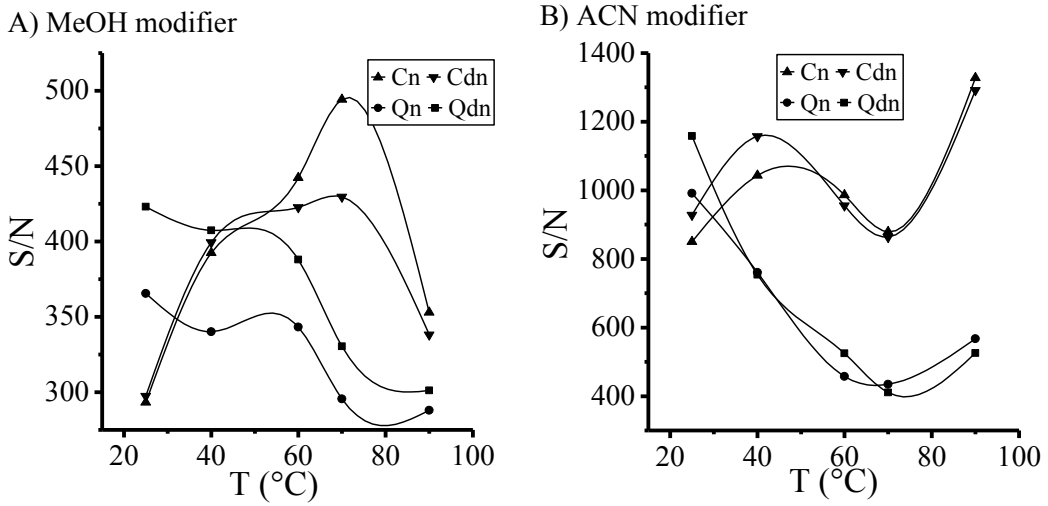

Figure 3.7: Influence of MeOH (A) vs. ACN (B) as mobile phase organic modifier on the variation of signal-to-noise ratio during HT-HPLC-ESI-MS analysis of *Cinchona* standard.

Chromatographic conditions and detection: same as in Figure 3.3. Column temperature range: 25 - 90 °C.

The overall increase and decrease in the signal portrays a difference in the ionisation efficiency, which could as well be linked to the physicochemical properties of the mobile phase contents. The non-uniformity in the trend could be attributed to some instability in the nebulisation process.

It is worth stating that, a similar trend was obtained when extracted mass chromatograms (XIC) from the MS scan function were evaluated. Since there were no standard for the dihydro-derivatives, the effect of temperature on their ionisation could not be evaluated. Nevertheless, based on their physicochemical properties including their stereochemistry, it could be said that the effect on DQn, DQn, DCn and DCdn should be similar to that on Qn, Qdn, Cn and Cdn respectively. The similarity in trend observed between the diastereomeric pairs (Qn/Qdn and Cn/Cdn) could be attributed mainly to their similar physical and chemical properties. The difference in ionisation efficiency from both modifiers at the respective eluent temperature is attributed to the solvent strength that affects the diastereomeric pairs in different ways. With this MS result, it has been shown that, both the solvent and the eluent temperature affects the ionisation process of *Cinchona* alkaloids in different ways.

Table 3.1: Estimate of LODs and LOQs of *Cinchona* alkaloids during HT-HPLC-MS analysis at column temperature 90 °C.

	Conc. (g L^{-1})	**Calculated S/N**	**LOD[a] (µg L^{-1})**	**LOQ[b] (µg L^{-1})**
Cn	0.0067	1327	15.1	50.5
Cdn	0.0067	1292	15.6	51.9
Qdn	0.0067	525	38.3	127.5
Qn	0.0067	568	35.4	118.0

[a] estimated for S: N 3:1 [b] estimated for S: N 10:1

Though more experiments are needed to study what happens beyond 90 °C, based on theory, the ionisation efficiency, S/N, and the peak area could increase at higher than the studied temperature range. For this purpose, a similar column, with temperature stability higher than 90 °C would be needed. At the same time, the analyte stability within the working temperature has to be investigated. With respect to stability, the mass spectra in Figure 3.8 (for ACN at T 90 °C), shows the stability of the analytes within this working range. The mass

spectra were obtained from the extracted mass *m/z* 295-296 for Cn/Cdn, *m/z* 297-298 for DCn/DCdn, *m/z* 325-326 for Qn/Qdn, and 327-328 for DQn/DQdn. The mass spectra show that each of the derivatives was detected as $[M + H]^+$. The mass spectrum at t_R 9.1 min. shows peak for *m/z* 297.4 and 325.4 corresponding to DCn/DCdn and Qn respectively.

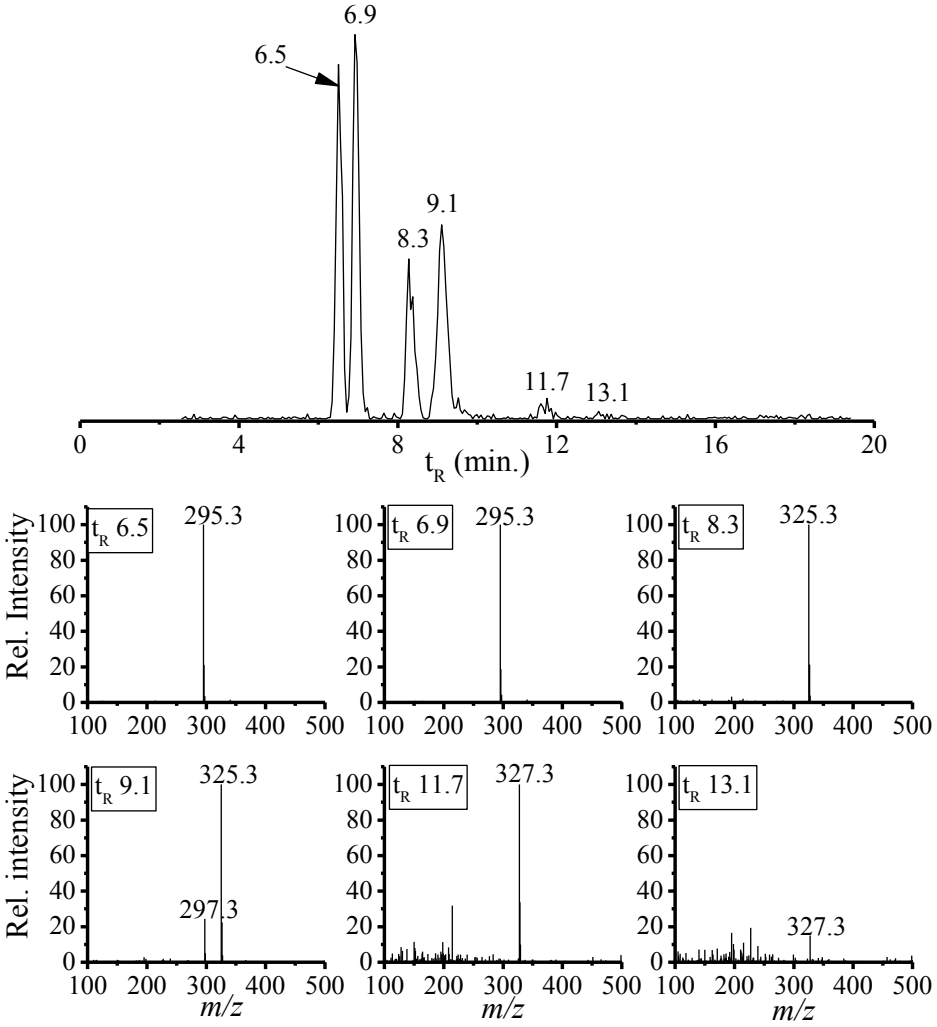

Figure 3.8: Extracted ion mass chromatogram (XIC) and mass spectra at respective t_R. Chromatographic condition and peak identity: same as in Figure 3.3B at T=90 °C. Detection: extracted mass: *m/z* 295-296 for Cn/Cdn, *m/z* 297-298 for DCn/DCdn, *m/z* 325-326 for Qn/Qdn, and 327-328 for DQn/DQdn.

This mass spectrum helps to confirm the co-elution shown in Figure 3.3. In a similar manner, when MeOH modifier was used at T 90 °C the mass spectrum (results not shown) also affirmed the co-elution of DCdn and Qn. The ability to identify the respective compounds via their t_R and mass fragment at T 90 °C shows on the one hand stability of the compounds and on the other, the applicability of the HT-HPLC-MS method in qualitative analysis. The S/N,

LOD and LOQ for the four main *Cinchona* alkaloids estimated at T 90 °C with ACN as modifier are shown in Table 3.1. For a 5-µL injection volume and a 1:1 post column splitting, the on-column LOD and LOQ were found to be in the picogram range.

3.4.4 Application of HT-HPLC-MS to commercial *Cinchona* extract

To test the feasibility of the developed method, it was applied to the analysis of *Cinchona* alkaloids in commercial *Cinchona* extract. The commercial extract was diluted 10 times with the mobile phase. For the analysis of the sample with ACN, T 80 °C was used. Figure 3.9 shows the extracted ion mass chromatograms (XICs) and the corresponding mass spectra of detected *Cinchona* alkaloids found in the commercial extract. From the figure, known *Cinchona* alkaloids as well as minor impurities were detected. The main *Cinchona* alkaloids were identified by their t_R and their mass to charge ratios (Figure 3.9 and Table 3.2). Hoffmann *et al*.[3], also reported such minor impurities but without identifying them via their *m/z*. From evaluating the *m/z* of the minor impurities at their respective t_R, their identities have been proposed in Table 3.2.

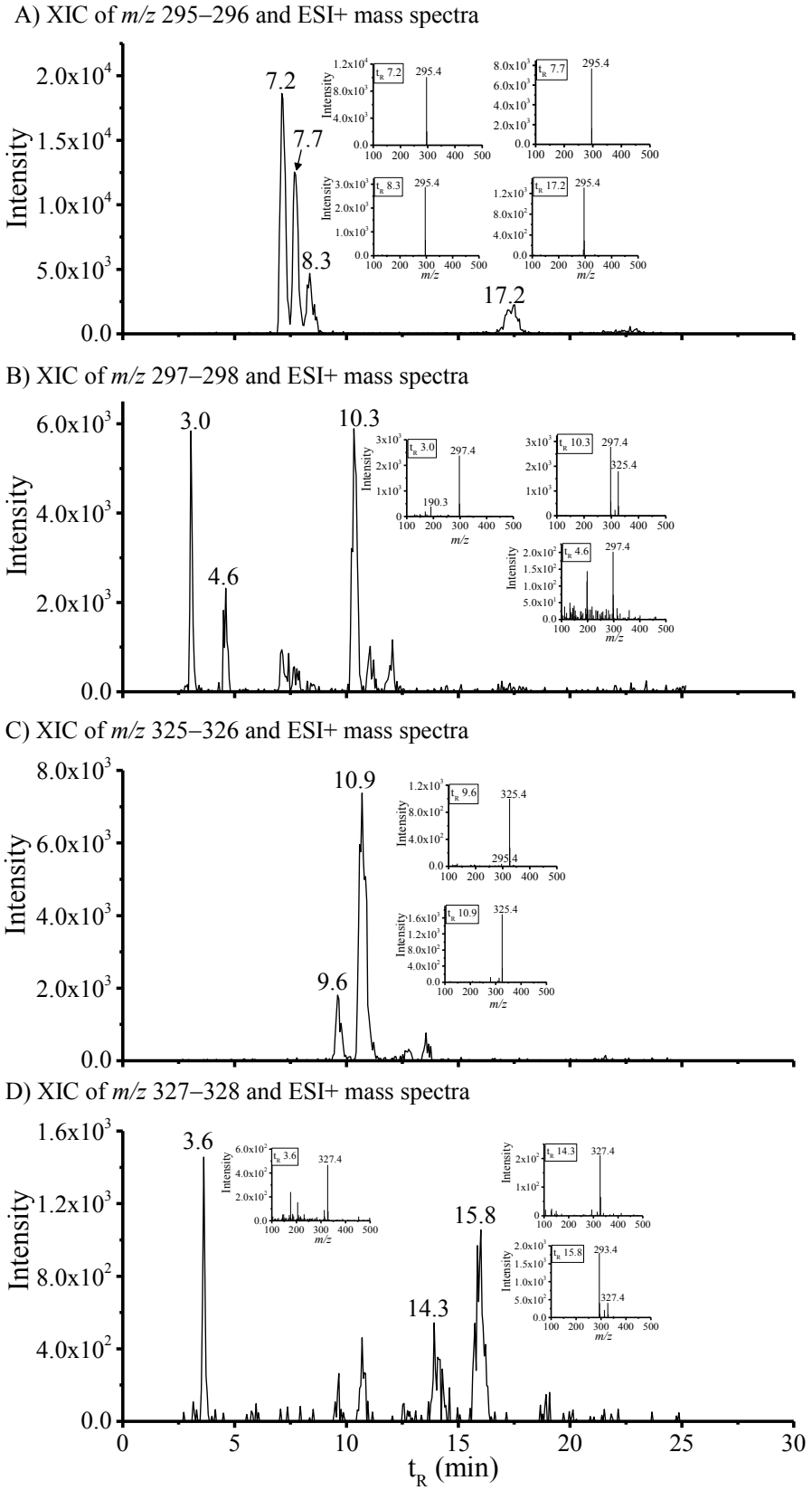

Figure 3.9: HT-HPLC-ESI(+)-MS extracted ion mass chromatogram and mass spectra (insets) of *Cinchona* alkaloids during analysis of commercial *Cinchona* extract. Chromatographic conditions: see Figure 3.3B.

Table 3.2: Detected peak and their identity from HT-HPLC-MS analysis of commercial *Cinchona* alkaloids.

t_R (min)	Detected *m/z*	Identity
3.0	297.4	DCn derivative
3.6	327.4	DQn derivative
4.6	297.4	DCdn derivative
7.2	295.4	Cn
7.7	295.4	Cdn
8.3	295.4	-
9.6	325.4	Qdn
10.3	297.4	DCn
10.9	325.4	Qn
14.3	327.4	DQdn
15.8	327.4, 293.4	DQn, unknown
17.2	295.4	-

3.5 Conclusion

A high-temperature high performance liquid chromatography-mass spectrometry (HT-HPLC-MS) method with Waters XBridge C_{18} column was developed and optimised for the analysis of *Cinchona* alkaloids. The separation temperature significantly influenced chromatographic parameters (t_R, α, R, and N) for the analysis. At the respective temperatures, the buffer and type of organic modifier also significantly influenced the chromatographic parameters. The MS ionisation efficiency was significantly affected by the temperature and composition of the mobile phase entering the MS ionisation source. Despite co-elution at some column temperatures, high specificity and S/N of the developed SIR-scan mode facilitates quantifiable results, provided the co-eluted peaks were dissimilar in their mass-to-charge ratio. The developed method was successfully applied for the separation and detection of *Cinchona* alkaloids in a commercial *Cinchona* sample. With an LOD and LOQ in the μg L^{-1} range for *Cinchona* alkaloids, the method could be used as an excellent alternative not only in HT-HPLC-MS analysis of *Cinchona* alkaloids but also in the analysis of related compounds in biological sample and fluids.

Appendix for Chapter 3

Table A 3.1: Chemical structure and acid-base dissociation constants of quinine and derivatives in water ($^{w}_{w}$**pKa**) and 30% ACN/70% H_2O ($^{s}_{s}$**pKa**) mixtures at 25 °C.

Name	Structure /formula/mass	Acidic group	$^{w}_{w}$pKa (25°C)[a]	$^{s}_{s}$pKa (25°C)[b]
Quinine (Qn)	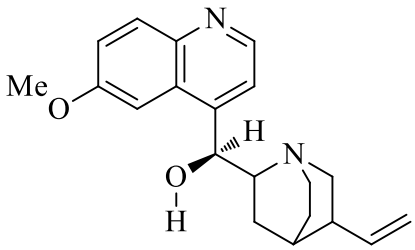 ($C_{20}H_{24}N_2O_2$, *m/z*: 324)	Quinolinic NH+	4.33	3.46
		$R_1R_2R_3NH+$	8.59	8.27
Quinidine (Qdn)	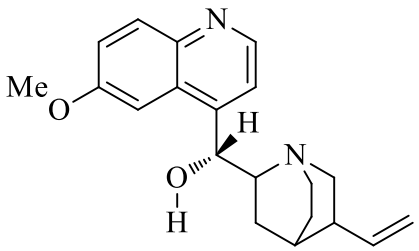 ($C_{20}H_{24}N_2O_2$, *m/z*: 324)	Quinolinic NH+	4.21	3.34
		$R_1R_2R_3NH+$	8.34	8.01
Cinchonine (Cn)	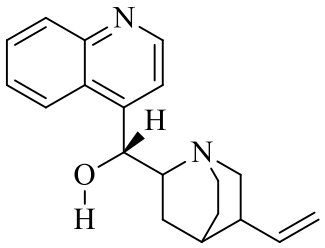 ($C_{19}H_{22}N_2O$, *m/z*: 294)	Quinolinic NH+	4.21	3.34
		$R_1R_2R_3NH+$	8.34	8.01
Cinchonidine (Cdn)	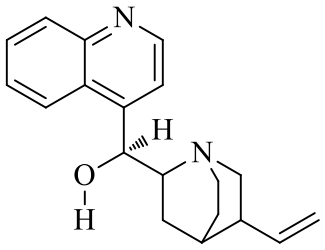 ($C_{19}H_{22}N_2O$, *m/z*: 294)	Quinolinic NH+	5.5	4.92
		$R_1R_2R_3NH+$	10.03	9.76

[a] pKa values taken from refs.[101] [102] [b] pKa values taken from ref [74]

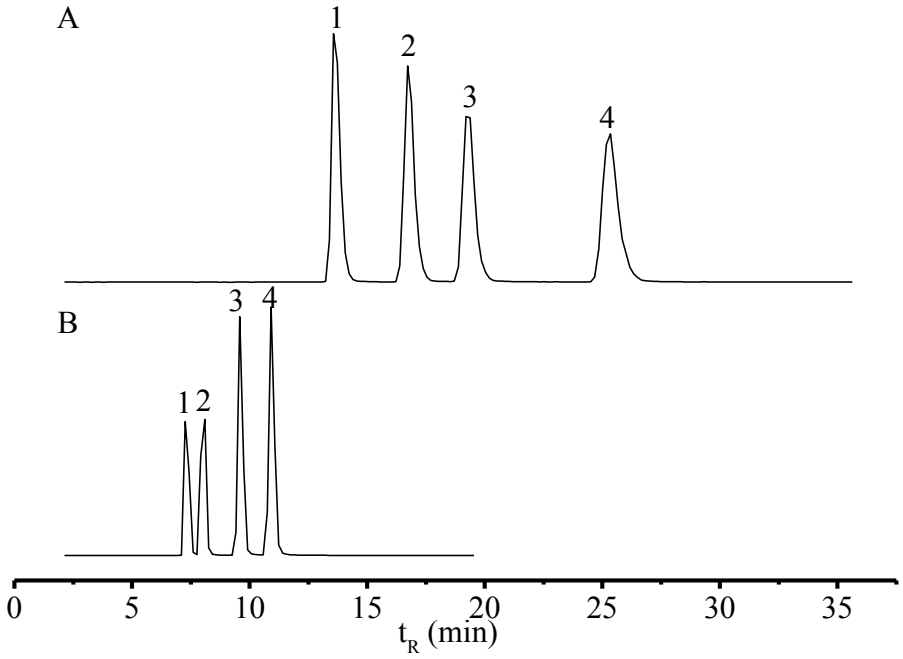

Figure A 3.1: Effect of organic modifier on retention time. Chromatographic condition: Waters XBridge C_{18} (150 x 4.6 mm, 3.5 µm) stationary phase; column temperature: 80 °C; mobile phase: MeOH/water (10/90) (A) and ACN/water (10/90) (B) (10% MeOH (A) with10 mM AF (pH 3.0) in water; flow rate: 1.0 ml/min; injection volume: 5 µl. Detection: Quattro LC in SIR mode; cone voltage: 35 V; capillary voltage: 3.0 eV. Analytes: 1) Cn (*m/z* 294.4), 2) Cdn (*m/z* 294.4), 3) Qdn (*m/z* 324.4), and 4) Qn (*m/z* 324.4).

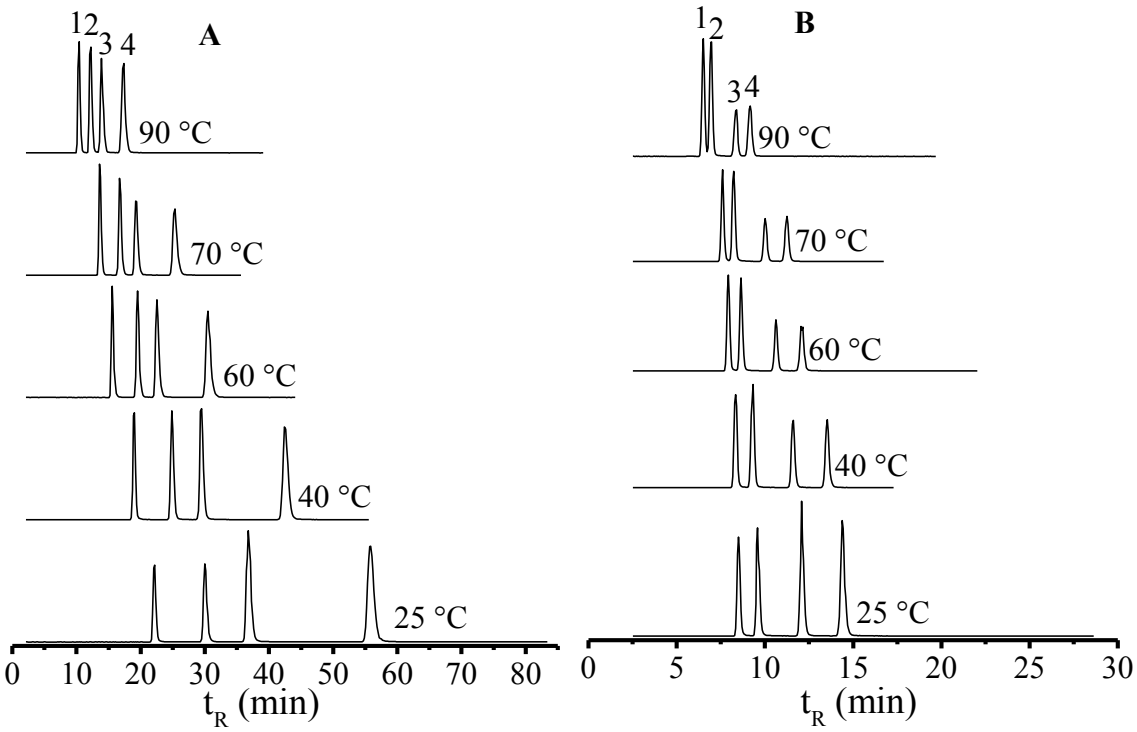

Figure A 3.2: Isothermal separation of *Cinchona* alkaloid. Chromatographic condition and detection: *cf* Figure A 3.1. Column temperature: 25-90 °C. Mobile phase: MeOH/water (10/90) (A) and ACN/water (10/90) (B) with 10 mM AF in water.

Table A 3.2: Influence of ACN vs. MeOH on chromatographic parameters during HT-HPLC-MS analysis of *Cinchona* alkaloids using Waters XBridge C_{18} column.

T(°C)	Retention factor				Peak symmetry				Resolution		Selectivity	
	Cn	Cdn	Qdn	Qn	Cn	Cdn	Qdn	Qn	Cdn/ Cn	Qdn/Qn	Cdn/Cn	Qdn/Qn
Mobile phase: ACN/ water (10/90) with 10 mM $COONH_4$ in water												
25	2.4	2.8	3.8	4.7	1.3	1.5	1.2	1.5	2.2	3.7	1.18	1.24
40	2.3	2.7	3.7	4.4	1.0	0.8	0.8	1.0	2.0	3.9	1.17	1.21
60	2.2	2.5	3.3	3.8	1.0	1.3	1.0	1.5	1.6	3.0	1.13	1.17
70	2.0	2.3	3.0	3.5	1.0	1.0	1.3	0.8	1.4	2.7	1.12	1.17
90	1.6	1.8	2.4	2.7	1.0	0.8	0.80	0.8	0.9	2.1	1.10	1.13
Mobile phase: MeOH/ water (10/90) with 10 mM $COONH_4$ in water												
25	7.9	11.0	13.7	21.3	2.0	1.3	1.8	1.3	5.9	11.5	1.40	1.77
40	6.6	8.9	10.8	16.0	1.0	1.3	1.3	1.7	5.4	7.9	1.35	1.37
60	5.2	6.8	8.0	11.2	2.0	1.3	1.7	1.5	3.7	5.3	1.30	1.05
70	4.4	5.7	6.7	9.1	2.0	2.0	2.5	1.3	3.2	4.6	1.28	0.91
90	3.2	3.9	4.6	6.0	1.5	1.0	1.3	1.0	1.8	2.8	1.23	0.71

Chapter 4

Analysis of Artemisinin-Based Antimalarial Pharmaceuticals by High-Temperature High Performance Liquid Chromatography Mass Spectrometry

Abstract

Artemisinin (ART) and a number of its derivatives are known to possess antimalarial properties. In this chapter, optimisation of a high temperature-high performance liquid chromatography (HT-HPLC) method on a zirconia-polybutadiene (Zr-PBD) column coupled to triple quadrupole mass spectrometer (MS) via electrospray ionisation (ESI) and atmospheric pressure chemical ionisation (APCI) is described for the analysis of ART, artesunate (AS), dihydroartemisinin (DHA), and artemether (AM). The use of temperature up to 90 °C permits the separation of ART and derivatives with a reduction in chemical waste, better chromatographic selectivity and enhanced desolvation process in the MS ionisation source compared to standard HPLC conditions. After optimisation of the HT-HPLC-MS method, DHA, ART, and AM were detected as their ammonium adduct ($[M + NH_4]^+$) at m/z 302, 300, and 316, while AS was detected as a characteristic fragment ion at m/z 272. Evaluation of ESI and APCI sources for best performance while using different organic modifier, showed that best detection sensitivity for ART and derivatives were obtained with ESI. Limits of detection (LOD) and limits of quantification (LOQ) for the ART and derivatives were found to be in the range from 0.52 to 1.12 µg mL^{-1} and 1.58 to 3.42 µg mL^{-1}, respectively with ESI. It was successfully used in the optimised HT-HPLC-ESI-MS and HT-HPLC-ESI-MS/MS screening of AM in commercial Coartem drug tablets.

Based on: D.N. Ateacha, C. Engelhard, submitted for publication.

4.1 Introduction

Artemisinin (ART), which is an endoperoxide compound isolated from *Artemisia annua,* is well known to possess antimalarial activity [103-105]. ART and its derivatives (*cf* Figure 4.1) are used in ART-based combination therapies (ACTs), which are presently the WHO first line of treatment against *Plasmodium falciparum* malaria and have made enormous contribution in reducing malaria-related death. In addition to their potency against *P. falciparum*, they are also known to possess anti-parasitic [106,107], anti-viral [108,109], and anti-cancer [110] effects. Despite these broad medicinal applications, one challenge associated to ART-based drugs, especially ACTs, is the fact that they are amongst the most counterfeited drugs in third-world countries, especially in sub-Saharan Africa [12-15].

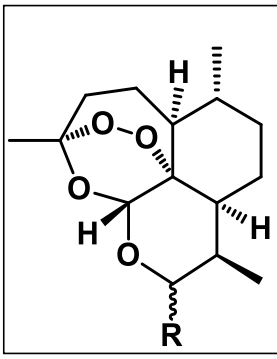

	R
Artemisinin (ART)	=O
Dihydroartemisin (DHA)	−OH
Artemether (AM)	$-OCH_3$
Artesunate (AS)	$-OCO(CH_2)_2COOH$

Figure 4.1 Chemical structure of ART and its derivatives (adapted from ref. [33]

Numerous techniques ranging from physical, chemical, or biological investigations have been employed to monitor the quality and efficacy of ACTs [111]. In physicochemical investigations, the active pharmaceutical ingredients were analysed using different techniques including derivatisation-based methods [112], immunological-based techniques [113,114], spectroscopic techniques [115] and separation-based methods, namely gas chromatography (GC), thin layer chromatography (TLC), supercritical fluid chromatography (SCFC), and liquid chromatography (LC) [116-118]. More recently, also ambient desorption/ionisation mass spectrometry (ADI-MS) methods were used for direct analysis. For example, direct analysis in real time (DART) and desorption electrospray ionisation (DESI) in both conventional and reactive mode were used to screen active ingredients in ART-based drugs [41,54]. Newton *et al.* [119] used X-ray diffractometry (XRD) and isotope ratio MS to determine the mineral composition of commercial ART-based drugs. The most used of the analytical techniques is based on reversed phase-high-performance liquid chromatography

(RP-HPLC) coupled to either ultraviolet/visible (UV/Vis), evaporative light scattering detector (ELSD), electron capture detector (ECD) or electrospray ionisation-mass spectrometry (ESI-MS) detection [37,35,36,120,121]. Because ART and derivatives are known not to absorb UV or display fluorescence, most of the reported HPLC-UV/Vs analytical procedure entailed derivatisation in acidic or basic solutions before analysis [122]. However, Ferreira *et al.* [120] later showed that the UV absorption of ART and derivatives is sufficiently high to permit quantification from crude plant samples and ART-based pharmaceutical formulations by UV/Vis detection without derivatization.

In an alternative method (*Cf.* Appendix 4.1 in the appendix section), a variant of the routine method: high temperature-HPLC (HT-HPLC) with zirconia-polybutadiene (Zr-PBD) column coupled to UV/Vis detector to analyse ART and its derivatives without any pre-derivatisation step. The method, which made use of 5 mM phosphate buffer in 15% aqueous acetonitrile (ACN), led to separation and detection of the four main ART derivatives. Despite the success of the method in separation and detection without any derivatization, the lack of specificity, especially in identifying the chemical identity of unknown peaks, necessitates the use of a sensitive, selective, and specific detection technique such as mass spectrometry (MS).

HPLC-MS with different ionisation sources was successfully used in the past to analyse this class of compounds. For example, Louw *et al.* [33] compared ESI, atmospheric pressure chemical ionisation (APCI), and atmospheric pressure photoionisation (APPI) for the identification of metabolites from labile ART based antimalarial drugs using a Q-Trap MS as a detector. After their method development and Optimisation procedure, the Q-Trap MS using ESI in combination with a first quadrupole (Q1) scan mode was capable of detecting the ammonium adduct ions of dihydroartemisin (DHA), ART, artemether (AM) and artesunic acid or artesunate (AS) as the base peaks. In addition, their optimised APCI and APPI MS source methods in combination with the Q1 MS scans could also detect the ammonium adduct ions of all four labile ART derivatives but not as base peaks. The preferential formation of the ammonium adduct instead of their protonated adduct for ART and derivatives is related to their thermodynamic stability. Also, it has been suggested in different publications that artemisinin and its derivatives tend to possess proton affinities (PAs) slightly above that of NH_3 (858 kJ mol^{-1}), thus favouring the formation of their NH_4 adducts rather than their protonated adducts [123-125,33].

Despite the use of HPLC-MS in the analysis of this class of basic compounds, there still challenges such as low solute retention resulting from the interaction of strong basic compounds with acidic unbonded site of a reversed phase (RP) stationary phase particles. HT-HPLC-MS could be more beneficial in the analysis of basic ART and derivatives than LC at ambient temperature. Some of those advantages include a decrease in the total analysis time, a reduction of chemical waste, and improved chromatographic selectivity [62,63,65,66]. With such advantages, coupling of HT-HPLC to MS would not only lead to the characteristic decrease in analysis time from the LC side, but could also affect the MS ionisation efficiency in a way different from LC at lower temperatures. It was postulated more than two decades ago that a hot eluent in HT-HPLC was likely to improve the desolvation process in the ionisation source (rather than an eluent at lower temperatures) [75].

In this chapter, a method based on HT-HPLC tandem mass spectrometry (HT-HPLC-MS/MS) was developed using zirconia-polybutadiene (Zr-PBD) column and a triple quadrupole mass spectrometer for the analysis of ART derivatives. For best performance, ESI and APCI sources were evaluated for best detection of ART and derivatives after HT-HPLC analysis. Simultaneously, the influence of the organic modifier on the HT-HPLC separation and the MS was studied. After Optimisation of HT-HPLC, fragmentation pathways of the compounds were investigated and collision energy settings in the MS were optimised. Finally, the developed method was applied to commercially available Coartem drug tablets.

4.2 Experimental

4.2.1 Chemicals and materials

Analytical standards of ART (97.0%), AM (98.0%), AS (98.0%) and DHA (98.0%) were purchased from Tokyo Chemical Industry (TCI), Belgium. Coartem tablets (Novartis, Basel Switzerland) containing 20 mg AM and 120 mg lumefantrine per tablet were acquired from a local pharmacy in Cameroon. HPLC grade methanol (MeOH) and acetonitrile (ACN) from Fisher Scientific (Loughborough, UK) were used. Ammonium formate (≥ 99.0%, Fluka, Steinheim, Germany) was used as chromatographic buffer. Formic acid (≥ 99.0%, Th.Geyer GmbH & Co.KG, Renningen, Germany) was added to the buffer for pH adjustment. Bi-distilled deionized water was prepared using a distillation apparatus from Heraeus-Quarzschmelze GmbH (Hanau, Germany). A Whatmann polyamide membrane filter, 0.22-µm pore size (Sigma-Aldrich Chemie GmbH, Schnelldorf, Germany) was used for filtration of the aqueous solvents. A calibrated pH meter (Xylem Analytics Germany Sales GmbH & Co. KG, WTW, Weilheim, Germany) was applied for pH measurement.

4.2.2 HT-HPLC-MS instrumentation and analysis

An Acela HPLC system (Thermo Fisher Scientific, Bremen, Germany) consisting of a quaternary pump with built-in solvent degassing system and an autosampler with a 25-µL sample loop was used. The analytical column was a Discovery zirconia polybutadiene (Zr-PBD) column (150 x 4.6 mm, pore size 300 Å, particle size 3 µm; SUPELCO, Bellefonte, PA, USA). Mobile phase from the LC was transferred to an external heating system via an inline filter with pore size of 0.2 µm (VICI Valco Instruments Co. Inc., Schenkon, Switzerland). The Accela system was controlled with ChromQuest software (ChromQuest 5.0, Thermo Fisher Scientific).

The heating system that was used for HT-HPLC analysis has been described in the experimental section in Chapter 2. Similar to the experiments in Chapter 2 and Chapter 3, the temperature of the eluent preheater unit was also set five degrees higher than the one of the column heater unit. The exact temperatures used for the analysis are stated in the results and discussion section.

A triple quadrupole mass spectrometer (model Quattro LC, Micromass, Wilmslow, UK) with ESI and APCI sources was used in this chapter. Both ionisation sources were optimised for detection of stable ammonium adducts of ART and derivatives. Unless otherwise stated, the

sources were operated in the positive ion mode and mass spectra were acquired in the mass range from mass-to-charge (*m/z)* 100 to 420. After pre-Optimisation of the ESI source temperature, the following settings were used: 100 °C source temperature, 3.0 kV capillary voltage, 5.0 V skimmer lens, 0.20 V radiofrequency (RF) lens, 67 L h^{-1} N_2 nebuliser gas flow, 550 L h^{-1} N_2 desolvation gas flow, 400 °C desolvation temperature, 6.5 x 10^{-6} mbar analyser vacuum, and 2.0 x 10^{-5} mbar gas cell vacuum. The sampling cone voltage was varied to monitor the effect on in-source fragmentation and to get the optimum sampling voltage for maximum sensitivity of the NH_4 adducts. The exact sample cone voltage values used are stated in the results and discussion section. For HT-HPLC-ESI-MS/MS analysis, the influence of collision-induced dissociation (CID) on the fragmentation of the NH_4 adducts of ART was evaluated by varying the collision energy in the range from 0 to 15 eV. For APCI evaluation, the optimised ESI settings were transferred and the following additional settings were used: 3.0 kV APCI pin voltage, and the nebuliser gas (N_2) flow was set to its maximum setting.

For HT-HPLC-MS analysis, the effluent from the heated column was forwarded directly to the inlet of the MS via a polyether ether ketone (PEEK) capillary. The post-column capillary was only 15 cm in length to minimize a potential post-column cooling effect and to benefit from potential advantages of a hot solvent entering the ionisation source. HT-HPLC-MS linearity study was carried out using ESI compared to APCI source because of the lower average signal-to-noise ratio (S/N) of the latter in contrast to the former for ART and derivatives. The S/N was calculated as the ratio of the intensity of the chromatographic peak in the extracted ion chromatogram (XIC) and the average intensity of noise around the peak. For HT-HPLC-ESI-MS calibration, each standard was injected twice and the average area was used to construct the calibration curve. For the same aforementioned reason, the commercial sample was analysed using the ESI source compared to APCI source.

4.2.3 Sample preparation

For this experiment, four separate stock standard solutions (each 1000 µg mL^{-1}) of ART, AS, DHA, and AM were prepared by dissolving appropriate amounts in organic solvent. For HPLC analysis with MeOH as organic modifier, the separate standards were prepared with MeOH solvent and for HPLC analysis with ACN, the standards were prepared in ACN solvent. After dissolution in an ultrasonic bath (SONOREX Super 10P, BANDELIN electronic GmbH&Co.KG, Berlin, Germany) set at 40 °C for 10 minutes, each stock standard

solution was filtered with a 0.2 μm membrane filter into separate amber sample vials. For the test mixture, the stock standard solution was diluted 100 times with the mobile phase to a concentration of 10 μg mL^{-1} for each compound. For calibration, a mixed standard solution of the different ART and derivatives were prepared by dilution with the mobile phase. After dilution, the concentration was in the range 0.33 – 10.0 μg mL^{-1} i.e., in the picomole range (for 10-μL injection volume) on column. The standards were prepared taking into consideration the amount of ART and derivatives present in known commercial ART-based drug containing tablets.

Commercial sample analysis was performed with Coartem drug tablets containing AM. Four tablets (average weight per tablet = 242.95 ± 0.0003 mg, RSD = 0.13%) were grinded and subjected to liquid extraction using 24.6 mg of material in 20 mL MeOH with the aid of an ultrasonic bath operated at 40 °C for 10 minutes. After filtration with a 0.2 μm PFTE syringe filter, the extracted sample was diluted 100 times before HT-HPLC-MS/MS analysis.

4.2.4 Data acquisition and processing

The MassLynx 3.5 software (Micromass, Wilmslow, UK) was used to control the mass spectrometer, and to perform data acquisition and signal processing. To obtain a mass spectrum after chromatographic separation, the instrument software is used to subtract the average background around a total ion chromatogram (TIC) peak from the average scan around the TIC peak top. Further data analysis was done using OriginLab 2015 (OriginLab, Northampton, MU, USA).

4.3 Results and Discussion

4.3.1 Optimisation of HT-HPLC-MS method for analysis of ART-based antimalarials

Apart from their notable ability to withstand extreme pH (1-14) and temperature (up to 200 °C), zirconia (ZrO_2)-based columns possess unique selectivity and retention capacity for different classes of compounds. These features stem from the surface chemistry, which is based on Lewis theory of acids and bases [126]. The free d-orbitals of Zr atoms on the surface of the carrier act as Lewis acid sites with strong affinity towards Lewis base components of the mobile phase (e.g. phosphate, hydroxyl, carboxyl, formate and fluoride groups). The Lewis bases are adsorbed on the surface by ligand exchange interactions and they interact with analyte ions via an ion-exchange mechanism (*cf* Figure 4.2).

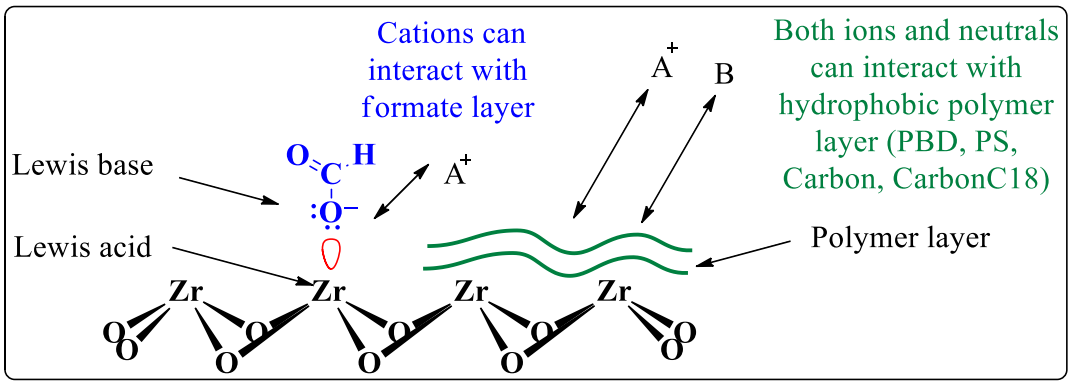

Figure 4.2: Acid base chemistry on Zr-based column. Adapted from ref.[127].

This mixed-mode mechanism can be exploited for the separation of basic and acidic analytes such as ART and derivatives, which are known to possess different pKa values (e.g. AS: pKa 4.6; DHA: pKa 12.6). In a previous study with HT-HPLC and UV/Vis detection (data not shown) and a Zr-PBD column, baseline separation of DHA, AS, ART and AM was achieved with a mobile phase containing phosphate buffer (pH 3.0). Despite the baseline separation, the method could not be applied directly for HT-HPLC-MS analysis of the same compounds. This was primarily due to the non-volatile buffer. In this work, the HT-HPLC separation was carefully optimised, taking into consideration the physicochemical properties of the investigated compounds, the surface chemistry of the ZrO_2-based column, the composition of the mobile phase, and the vaporization process of the LC-ESI-MS interface. As a result, ammonium formate (AF, 2.7<pH<3.7), was finally selected for the optimised HT-HPLC-MS method. This buffer is advantageous because the formate anion ($HCOO^-$) acts as Lewis base,

while the ammonium cation (NH_4^+) serves as a precursor for analyte ammonium adduct ion formation. As mentioned in the introductory section, formation of NH_4 adducts ($[M + NH_4]^+$) of ART and derivatives is thermodynamically preferred over protonated adducts ($[M + H]^+$). Therefore, the Quattro LC ionisation sources (ESI and APCI) were optimised for maximum intensity of $[M + NH_4]^+$ ions, relative to other analyte (fragment) ions. The detection of $[M + NH_4]^+$ ions as the most abundant peak in the in-source mass spectra are necessary for best MS/MS performance. The absolute abundance was assessed by taking the ratio between $[M + NH_4]^+$ ions and the most prominent in-source analyte fragments (e.g. *m/z* 267 for DHA in ESI(+) mode). Contrary to the method optimisation by Louw *et al.* [33], where flow injection was used, here the optimisation was carried out directly with the HT-HPLC system (at T = 90 °C) coupled to the ESI/APCI interface of the mass spectrometer.

4.3.2 ESI optimisation

With the exception of the sampling cone voltage, other source parameters in Quattro LC mass spectrometer vary little from one analyte to another. Source parameters such as the desolvation gas flow rate and temperature are depending on the mobile phase composition and the flow rate and were optimised accordingly. Dihydroartemisinin ($C_{15}H_{24}O_5$, *m/z* 284.16), an active metabolite for both AM and AS, was used as a reporter ion during ESI tuning. Figure 4.3, shows the effect of sample cone voltage settings on the fragmentation of DHA. DHA was detected as ammonium adduct (*m/z* 302, $[C_{15}H_{24}O_5 + NH_4]^+$). In addition, other characteristic adducts and fragments thereof were observed with *m/z* 284, 307, and 323 corresponding to dehydrated ammonium adduct ion $[C_{15}H_{24}O_5 + NH_4 - H_2O]^+$, sodium adduct ion $[C_{15}H_{24}O_5 + Na]^+$ and potassium adduct ion $[C_{15}H_{24}O_5 + K]^+$, respectively. Louw *et al*. [33] obtained identical mass fragments using a QTRAP® mass spectrometer for analysis.

It can be observed from Figure 4.3 that the S/N increases with increase in the cone voltage from 10 to 20 V and then decreases as the cone voltage was increased from 20 to 40 V.

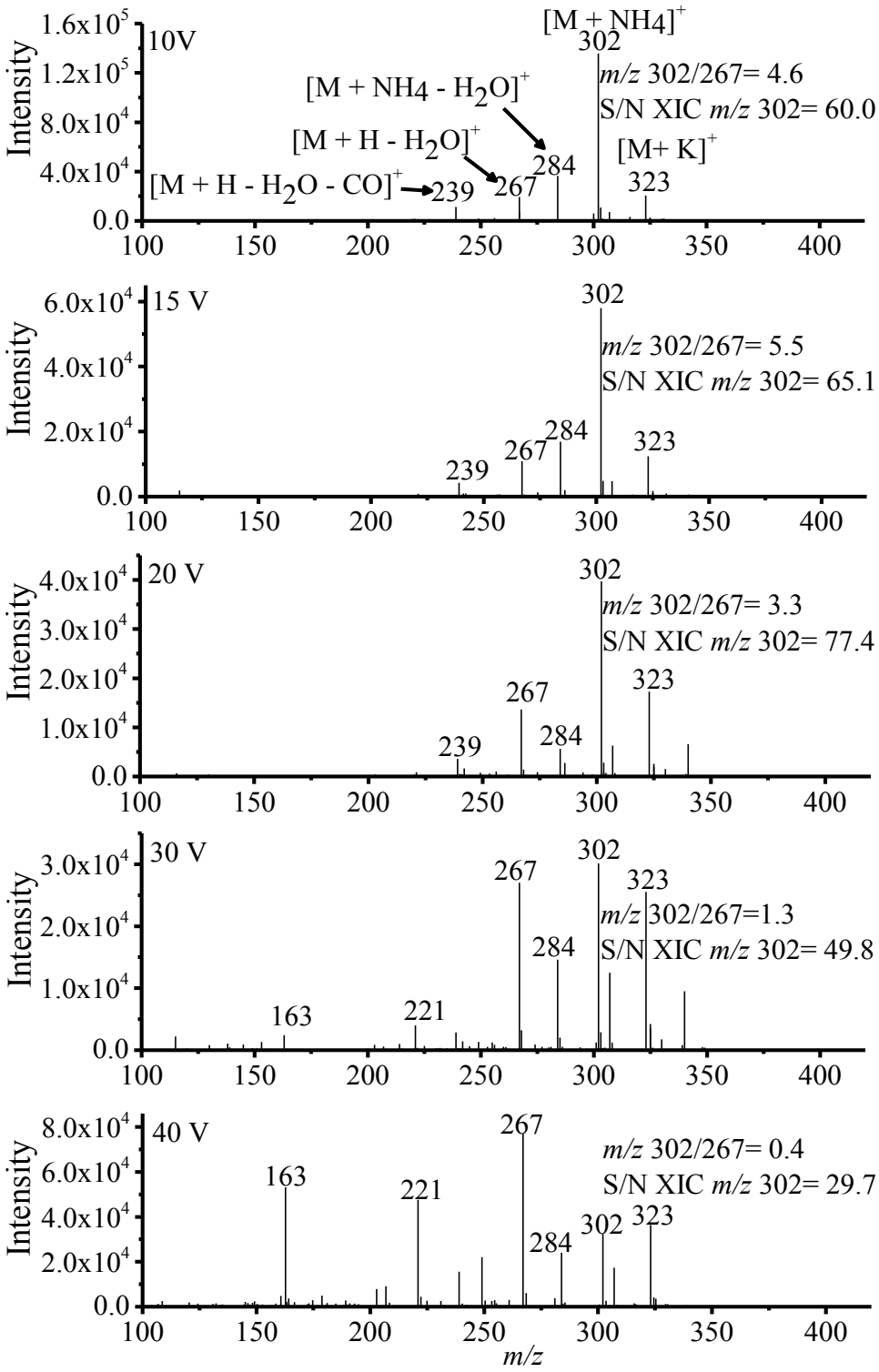

Figure 4.3: Influence of ESI cone voltage on in-source fragmentation of DHA (10 µg mL^{-1}) during HT-HPLC-ESI(+)-MS analysis. Mobile phase: MeOH/water (15/85) with 10 mM AF in water. ESI parameters: source temperature 100 °C, cone voltage +10 - +40 V.

The *m/z* 302 vs *m/z* 267 intensity ratio (*m/z* 302/267) increases with increasing cone voltage from 10 to 15 V and then steadily decreases towards higher voltages due to more severe in-source fragmentation. Therefore, despite the fact that with 20 V, relative abundance was highest, 15 V was selected and employed for further analysis and optimisation. This is because, with 15 V the intensity ratio of *m/z* 302/267 was highest and vital for best MS/MS analysis.

4.3.3 HT-HPLC-ESI-MS of ART and derivatives

Figure 4.4 shows extracted ion chromatograms (XICs) and mass spectra of ART and derivatives, which were obtained with the optimised HT-HPLC-ESI-MS method with a Zr-PBD column and mobile phase containing AF buffer. After separation of the standard mixture, the respective compounds were identified by their retention time and *m/z*. Apart from AS ($C_{19}H_{28}O_8$, *m/z* 384.18), which was detected with its base peak at *m/z* 272, the other derivatives DHA ($C_{15}H_{24}O_5$, *m/z* 284.16), ART ($C_{15}H_{22}O_5$, *m/z* 282.15), and AM ($C_{16}H_{26}O_5$, *m/z* 298.18) were detected as their ammonium adduct as base peak at *m/z* 302 ($[C_{15}H_{24}O_5 + NH_4]^+$), 300 ($[C_{15}H_{22}O_5 + NH_4]^+$), and 316 ($[C_{16}H_{26}O_5 + NH_4]^+$), respectively. The detection of AS with *m/z* 272 as the base peak is contrary to the expected $[M + NH_4]^+$ at *m/z* 402. The origin of *m/z* 272 and 286 could be attributed to in-source fragmentation of the ions $[M + H]^+$ or $[M + NH_4]^+$ of AS. As shown in the HT-HPLC-APCI-MS section below, a similar mass spectrum with the same *m/z* was found, indicating that this fragment ion was not inherent to ESI alone. Further optimisation of the ionisation source parameters may be needed to achieve a more stable formation of the AS ammonium adduct. However, this was not investigated further in this chapter and the peak at *m/z* 272 was used below as a representative ion from AS.

In Figure 4.4C, it can be seen that the presence of ART was ascertained by *m/z* 300($[C_{15}H_{22}O_5 + NH_4]^+$) and *m/z* 283($[C_{15}H_{22}O_5 + H]^+$) corresponding to the ammonium and protonated adduct ions respectively. The formation of the $[M + H]^+$ of ART is contrary to observations for DHA and AM (*cf* Figure 4.4B&D), which did not show significant peaks for their protonated molecular ions at *m/z* 285 ($[C_{15}H_{24}O_5 + H]^+$) and *m/z* 299 ($[C_{16}H_{26}O_5 + H]^+$). Such effect has been attributed to the stability of the $[M + H]^+$ of ART over those of DHA and AM [123]. The presence of characteristic fragments at *m/z* 239, 267, and 284 for the mass spectrum of AM (*cf* Figure 4.4D) is because DHA is a mass fragment from in-source fragmentation of AM.

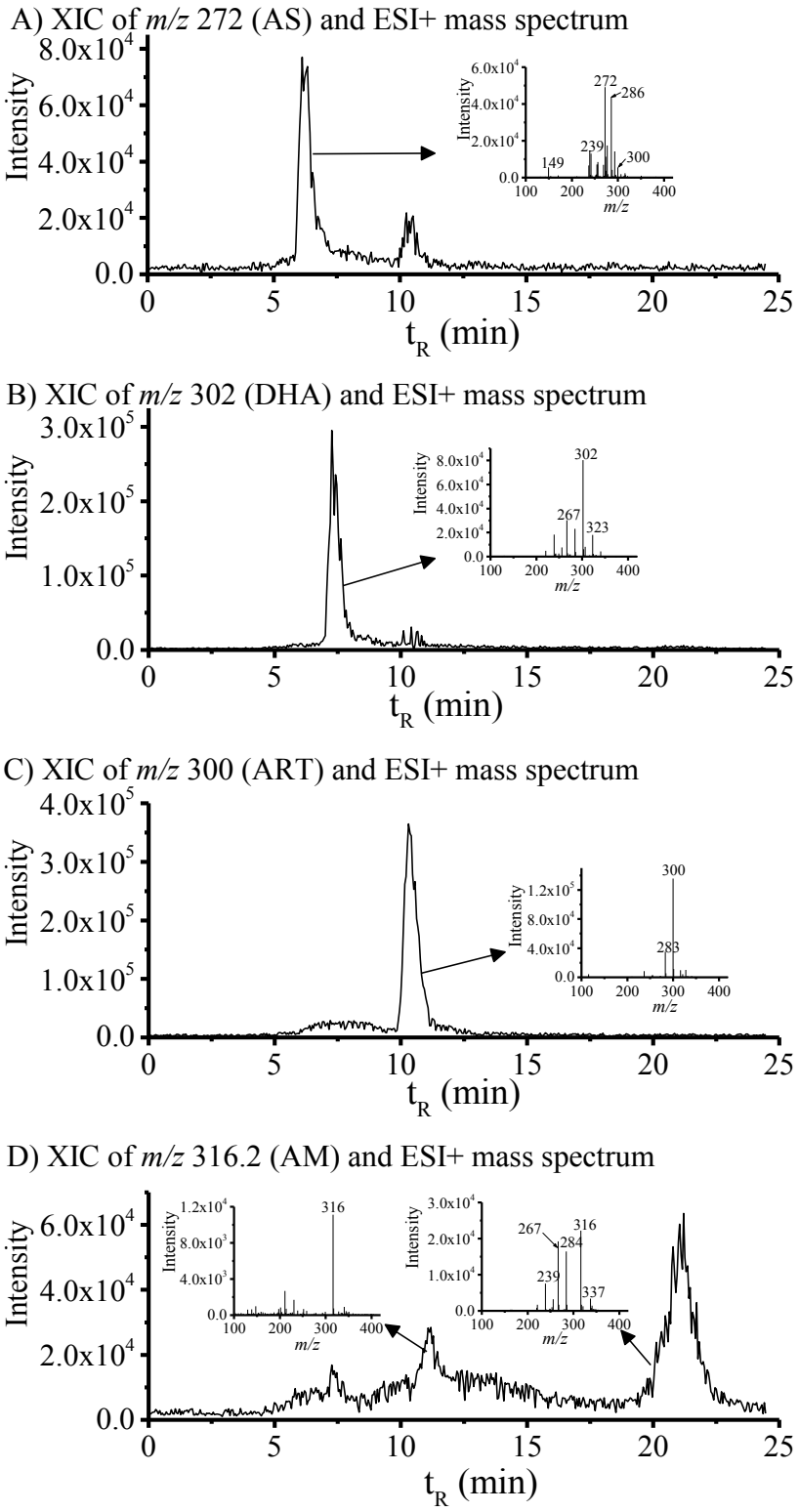

Figure 4.4: HT-HPLC-ESI(+)-MS extracted-ion chromatograms (XIC) and mass spectra (insets) during analysis of a standard mixture of ART and derivatives. Chromatographic conditions: Discovery Zr-PBD (150 x 4.6 mm, 3.0 µm) stationary phase; mobile phase: MeOH/water (15/85) with 10 mM AF in water; flow rate: 0.4 mL min^{-1}; injection volume: 10 µL; column temperature: 90 °C. Analytes: A) *m/z* 272.0 for AS, B) *m/z* 302.0 for DHA, C) *m/z* 300.0 for ART and D) 316.2 for AM.

From the extracted-ion mass chromatogram in Figure 4.4, AM was the most retained compound with t_R 21.2 min. and AS was the least retained with t_R 6.1 min. The additional peak at t_R 10.3 (*cf* Figure 4.4A) was identified to be a fragment of ART. From Figure 4.4D, it was surprising to see that XIC *m/z* 316.2 gave rise to several peaks instead of one expected from the standard beta-AM (CAS: 71963-77-4) analysed. The additional peak at t_R 11.2 min could be coming from alpha-AM (CAS: 71939-51-10). Though not specified by the manufacturer, the ß-artemether (98% purity) used in the standard mixture could contain some amount alpha-artemether. A similar additional peak was observed when methanol was replaced with acetonitrile as the organic modifier (*cf* Figure A 4.8 in the appendix section). As shown in Figure 4.7D, the additional peak was not observed when the ionisation source was replaced with APCI. This was attributed to the relatively low signal intensity during APCI ionisation as compared to ESI (*cf* mass spectra in Figure 4.8).

The observed elution order of AS<DHA<ART<AM is contrary to the elution order DHA<ART<AS<AM previously obtained with phosphate buffer. Based on the mixed mechanism on the Zr-PBD column, this difference could be attributed to an additional ionic interaction due to the presence of NH_4^+ in the mobile phase. The NH_4^+ ion may interact more with the formate layer on the zirconia surface (*cf* Figure 4.2) and as a result reduce analyte interaction with the formate layer. For analyte elution driven by ionic interaction, the retention time would presumably decrease in a reversed-phase mode separation. On the other hand, analyte retention governed by hydrophobic interactions with the stationary phase, the influence would be relatively insignificant. It can concluded here that the presence of formate and ammonium counter ions in the mobile phase have been influential in both optimising the separation selectivity and formation of stable ammonium adducts of ART and derivatives.

4.3.4 HT-HPLC-ESI-MS quantitative analysis

In order to assess the analytical performance of the optimised HT-HPLC-MS method for simultaneous determination and quantification of DHA, ART, and AM, analytical parameters such as the square of the correlation coefficient (r^2) and sensitivity (LOD and LOQ) were evaluated. The optimised MS scan method was further optimised to include selected ion recording (SIR) scan mode, known for higher S/N. The SIR scan was performed for *m/z* 302, 300, and 316.2 corresponding to the ammonium adduct ion for DHA, ART and AM respectively. Because the stable standard of AS capable of forming the $[M + NH_4]^+$ was not available, it was not possible to perform its quantification. To construct a calibration plot for

each standard, the mean area from the SIR scan mode was used. The identities of the peaks were confirmed by retention time matching and the mass spectra resulting from the MS scan mode. The LOD and the LOQ were calculated according to the following formulae: LOD = $3.3(S_y/b)$ and LOQ = $10(S_y/b)$, where S_y represents the standard deviation of the response and b stands for the slope of the calibration curve. The characteristics of the calibration plots, LOD, and LOQ of the method are shown in Table 4.1. The concentration range in Table 4.1 was prepared taking into consideration the typical concentration of ART and derivatives in commercial drug tablets. From the analysis, LOD and LOQ for the method were estimated to be in the range 0.52 – 1.12 μg mL^{-1} and 1.58 – 3.42 μg mL^{-1}, respectively.

Table 4.1: Calibration range, linearity, LOD and LOQ:

Sample	Conc. range[a]	Slope	Intercept	r^2	LOD[a]	LOQ[a]
DHA	0.33 - 10	175206.1	26618.0	0.999	0.52	1.58
ART	0.33 - 10	461316.4	-57548.6	0.999	0.55	1.68
AM	0.33 - 10	125233.4	-34958.5	0.997	1.12	3.42

[a] [μg mL^{-1}] injection volume: 10 μL

4.3.5 HT-HPLC-ESI-MS/MS optimisation and analysis of ART and derivatives

Prior to the application of the optimised HT-HPLC-MS method for HT-HPLC-MS/MS analysis, the method was further optimised with respect to the collision-induced dissociation (CID) energy. The CID optimisation experiment was performed by monitoring the dissociation of the peak at *m/z* 300 corresponding to the ammonium adduct ion of ART ($[C_{15}H_{22}O_5 + NH_4]^+$). As shown in Figure 4.5, the CID fragmentation of the ammonium adduct ion formed characteristic product ion at *m/z* 283, 265 and 209 corresponding to $[C_{15}H_{22}O_5 + H]^+$, $[C_{15}H_{22}O_5 + H - H_2O]^+$, and $[C_{15}H_{22}O_5 + H - H_2O - CO - C_2H_4]^+$ respectively. As can be seen from Figure 4.5, CID of 10 eV was optimum because the $[M + NH_4]^+$ and the main product ion has high abundances, thus aiding in structural clarification. In the course of optimisation of the CID energy for the ammonium adduct ion for DHA and AM, CID 10 eV was found to be best overall setting. For the HT-HPLC-MS-MS method optimisation and application 10 mM AF buffer in 20% MeOH was used. The increase in volume of organic modifier from 15 to 20% was aimed to reduce the elution times without hampering the peak resolution.

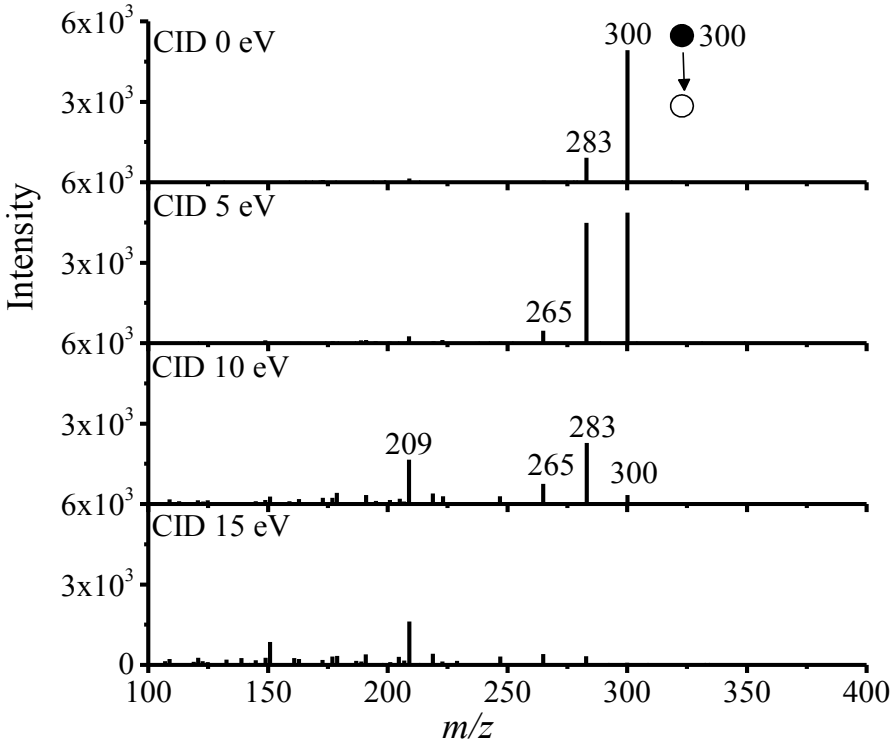

Figure 4.5: Influence of collision induced dissociation (CID) energy on fragmentation of ART (*m/z* 300) during HT-HPLC-ESI(+)-MS/MS analysis Mobile phase: MeOH/water (20/80) with 10 mM AF in water; flow rate: 0.4 mL min^{-1}; injection volume: 10 µL; column temperature: 90 °C. MS/MS parameters: argon collision gas, CID energy 0 – 15 eV.

For HT-HPLC-MS/MS analysis, a standard mixture of DHA, ART and AM was used. Figure 4.6 shows the product ion mass chromatogram and spectra after applying the optimised CID collision energy.

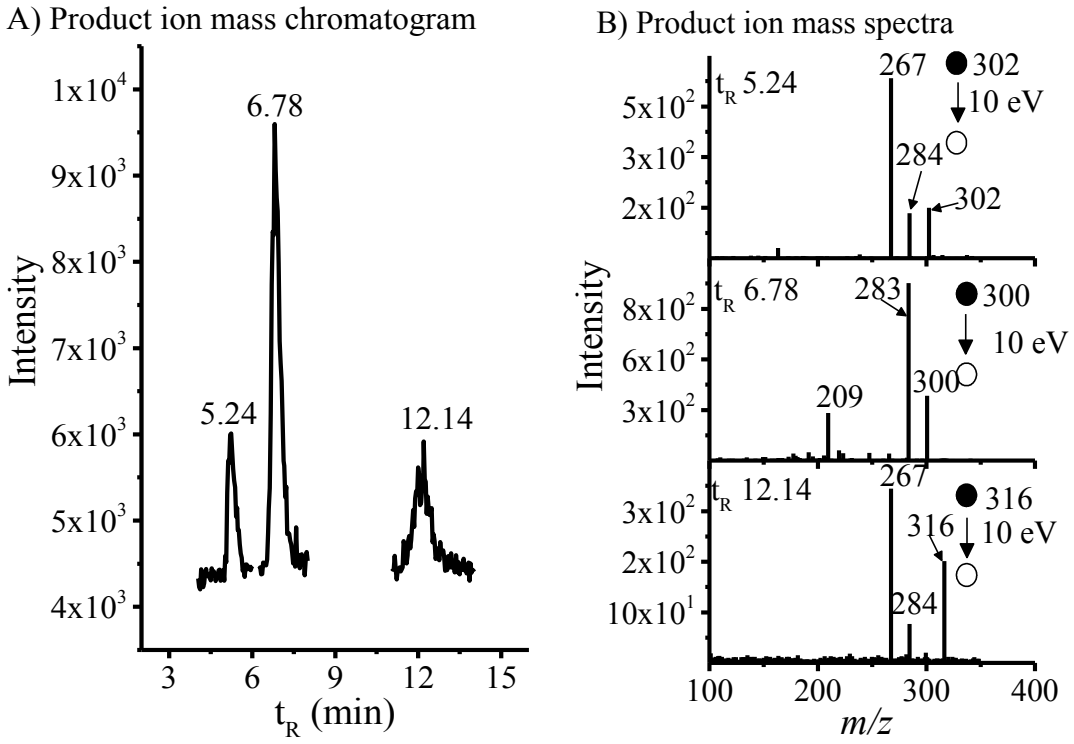

Figure 4.6: Product ion mass chromatogram (A) and spectra (B) of ammonium adduct of DHA (*m/z* 302, t_R 5.24 min), ART (*m/z* 300, t_R 6.78 min) and AM (*m/z* 316, t_R 12.24 min) during HT-HPLC-ESI(+)-MS/MS analysis. Chromatographic conditions: stationary phase: Discovery Zr-PBD (150 x 4.6 mm, 3.0 µm): mobile phase: MeOH/water (**20/80**) with 10 mM AF in water. Flow rate: 0.4 mL min^{-1}: injection volume: 10 µL: Column temperature: 90 °C.

4.3.6 HT-HPLC-APCI-MS optimisation and analysis of ART and derivatives

For the APCI source optimisation, all previously optimised ESI and chromatographic conditions, including test compound (DHA) were used. The APCI probe temperature was varied from 200 to 500 °C to visualise the effect on the detection sensitivity and in-source fragmentation of the ammonium adduct ion of DHA. As represented in Table 4.2, the signal intensity of *m/z* 302 ($[M + NH_4]^+$) increases with increase in APCI probe temperature from 200 to 400 °C and then decreases as the probe temperature was increased from 400 to 500 °C. On the other hand, the S/N decreases as the probe temperature was increased. The increase in the peak intensity, up till the probe temperature was 400 °C could be attributed to increase in the vaporization process of the LC solvent and the analyte ion within this temperature range. The subsequent decrease in the peak intensity beyond probe temperature of 400 °C could be attributed to thermal degradation of the $[M + NH_4]^+$ peak at the high probe temperature. The decrease in S/N is attributed to an increase in the background noise that is known to accompany high APCI probe temperature. Despite the lower S/N at probe temperature of 400

°C, it was selected for HT-HPLC-APCI-MS analysis and for comparative study based on the higher intensity ratio of *m/z* 302 versus 267 and signal intensity compared to the other tested probe temperatures. The corresponding mass spectra for the data in Table 4.2 are shown in Figure A 4.10 in the appendix section.

Table 4.2: Summary of APCI probe temperature effect on MS signal for $[M + NH_4]^+$ at *m/z* 302.

Probe temperature (°C)	**Intensity x 10^5**	**S/N ratio XIC**	**Ratio of *m/z* 302/ 267**
200	2.38 ± 0.02	21.88 ± 3.37	3.39 ± 0.24
300	8.92 ± 0.04	21.54 ± 1.17	3.53 ± 0.90
400	16.05 ± 0.11	18.42 ± 0.74	3.61 ± 0.05
500	10.61 ± 0.03	13.00 ± 0.00	2.66 ± 0.01

The mean ±standard deviation is reported for n = 3. DHA concentration: 100 μg mL^{-1}

For comparative purpose, same standard mixture (10 μg mL^{-1} of each compound) as in ESI was used for the HT-HPLC-APCI analysis of ART and derivatives. Similar to Figure 4.4 above, Figure 4.7 shows the extracted ion chromatogram (XIC) and mass spectra of the ART and derivatives obtained using the optimised HT-HPLC-APCI-MS with Zr-PBD column and AF containing buffer. Figure 4.7 shows the mass chromatogram of ART and derivative obtained using the optimised APCI source parameters.

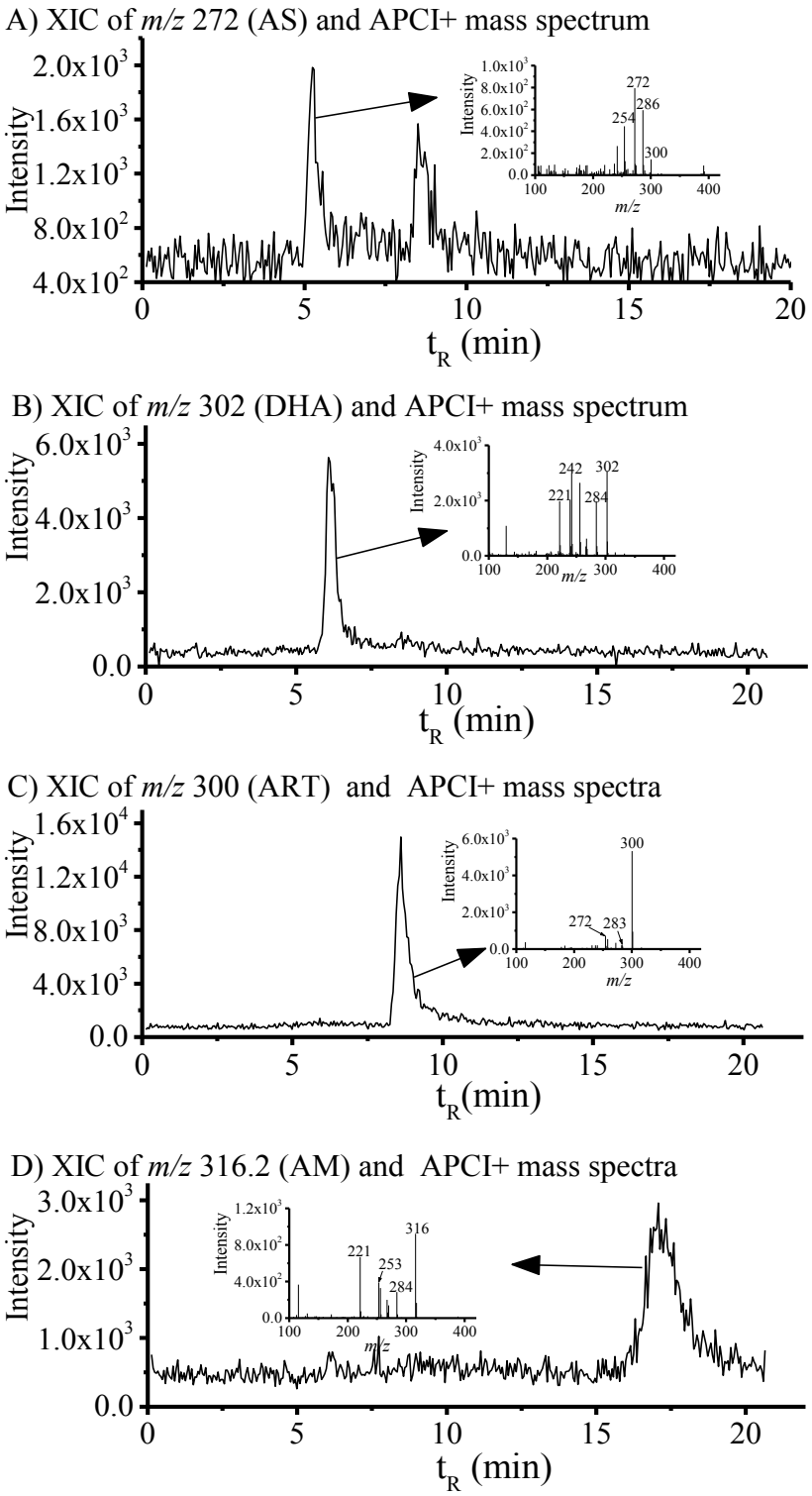

Figure 4.7: HT-HPLC-APCI(+)-MS extracted ion chromatogram (XICs) and mass spectra (insets) during analysis of a standard mixture of ART and derivatives. Chromatographic conditions: Discovery Zr-PBD (150 x 4.6 mm, 3.0 µm) stationary phase; mobile phase: MeOH/water (15/85) with 10 mM AF in water; flow rate: 0.4 mL min^{-1}; injection volume: 10 µL; column temperature: 90 °C. Analytes: A) *m/z* 272.0 for AS, B) *m/z* 302.0 for DHA, C) *m/z* 300.0 for ART and D) *m/z* 316.2 for AM.

Similar to the results in ESI-MS, the all compounds but for AS were detected as their ammonium adduct ion and characteristic fragments.

4.3.7 HT-HPLC-ESI- vs -APCI-MS of ART and derivatives

As shown in the above sections, both sources work efficiently for qualitative analysis of ART and derivatives. The extracted ion chromatograms and the mass spectra differ not only in the fragmentation pattern but also in the degree of fragmentation. Figure 4.8 shows a rough comparison of both ionisation sources for this chapter. In addition, it can be seen that MeOH and ACN affect the ionisation efficiency of the different sources for the different compounds in different ways. It is clear that irrespective of the organic modifier used, signal intensities for all tested compounds were higher with ESI than with APCI source. From Figure 4.9A, ACN as modifier showed higher response compared to MeOH for all tested compounds except for AM. This phenomenon may occur because for AM, the higher proton affinity of ACN (779.2 kJ mol^{-1}) compared to methanol (754 kJ mol^{-1}) [128], can lead to a decrease in the amount of protons in the mobile phase available for the formation of ammonium ions (NH_4^+).

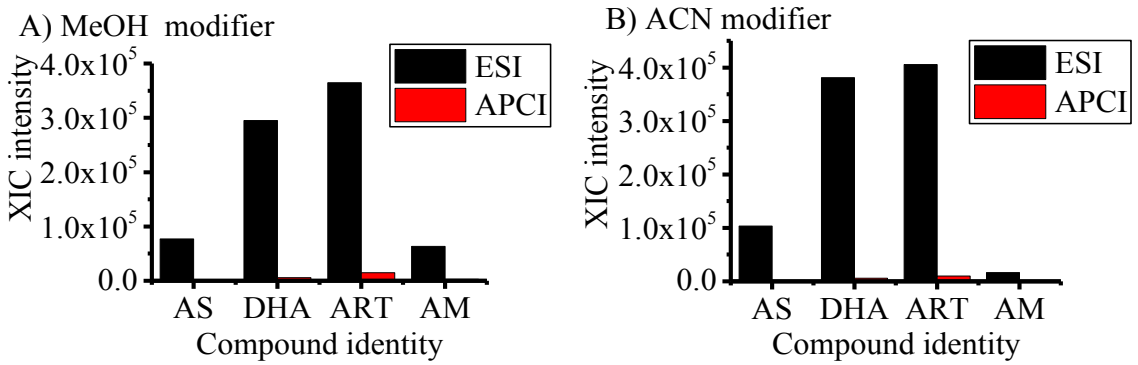

Figure 4.8: Comparison of ESI and APCI sources fragmentation after HT-HPLC-MS analysis of ART and derivatives with MeOH (A) and ACN (B) as organic modifier. Compound identity: XIC *m/z* 272 (AS), *m/z* 302 (DHA), *m/z* 300 (ART), *m/z* 316 (AM).

This subsequently decreases the quantity of $[M + NH_4]^+$ in the presence of ACN. This effect is even more pronounced in APCI ionisation (*cf* Figure 4.9B), where MeOH resulted in higher peak areas compared to ACN for all four compounds except for DHA, where ACN resulted in slightly higher signal intensity than MeOH.

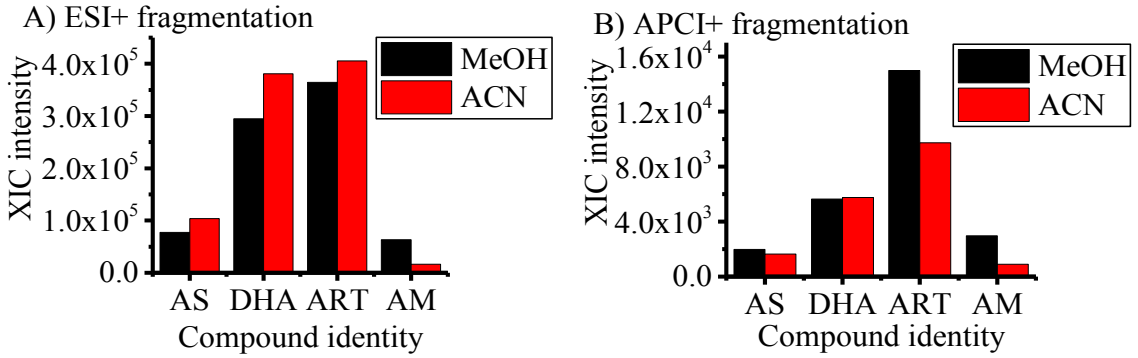

Figure 4.9: Influence of MeOH vs. ACN on ESI (A) and APCI (B) in-source fragmentation during HT-HPL-MS analysis of ART and derivatives. Compound identity: XIC *m/z* 272 (AS), *m/z*302 (DHA), *m/z* 300 (ART), *m/z* 316 (AM)

Because of the higher signal intensity obtained from the use of MeOH compared to the signal intensity from the use of ACN, MeOH containing mobile phase was used for the analysis of AM in commercial Coartem drug tablet. Also, considering the better signal response of ESI source compared to APCI for the detection of ammonium adduct ion of AM, ESI source was applied in the HT-HPLC-MS and HT-HPLC-MS/MS analysis of AM in commercial Coartem drug tablet.

4.3.8 Applications to the analysis of AM in Coartem drug tablet

To evaluate the optimised HT-HPLC-MS and HT-HPLC-MS/MS methods, they were applied in the analysis of AM in commercial Coartem drug tablet. As stated in the experimental section, commercial Coartem tablet contains 20 mg of AM per tablet (average weight per tablet = 242.95 ± 0.0003 mg) which is ≈ 0.0823 mass fraction. As can be seen in Figure 4.10A, the HT-HPLC-MS method with Zr-PBD column was capable of detecting the AM in Coartem tablet as $[M + NH_4]^+$ at *m/z* 316.2. The S/N for the XIC of *m/z* 316.2 was estimated to be 15.6 ± 1.07 with an RSD of 6.8% for the 10 µL injected sample. From the S/N, the LOD and LOQ for AM in the tablet were approximated to be 0.016 ± 0.001 and 0.053 ± 0.004 µg respectively on column concentration. The approximated LOD and LOQ correspond to 1.93 ± 0.13 % and 6.42 ± 0.43% of AM in Coartem tablet. The actual content of AM in the tablet was not quantified. The characteristic MS/MS spectra shown in Figure 4.10B helped to confirm the identity of AM in the commercial drug tablet.

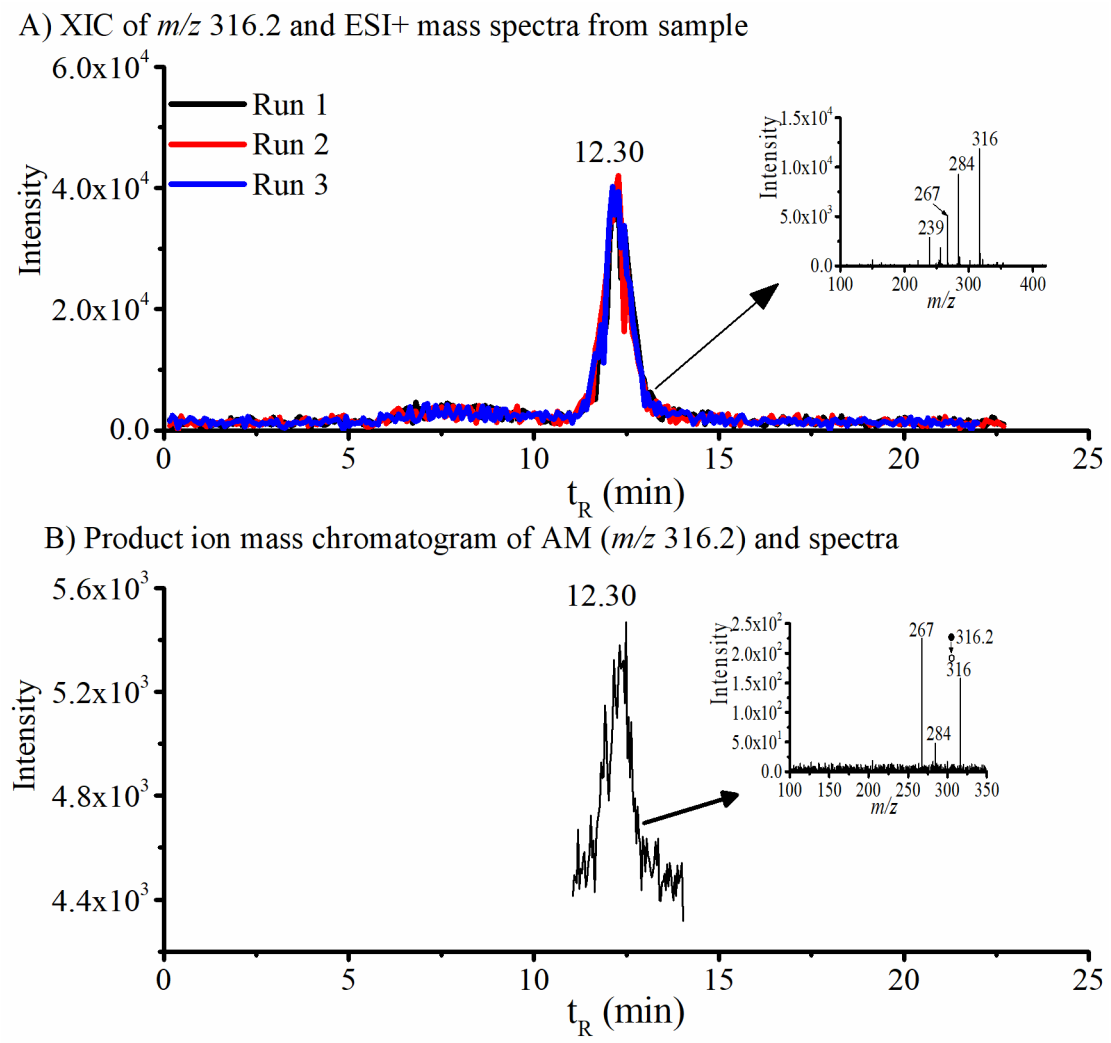

Figure 4.10: Extracted ion mass chromatogram and mass spectrum (inset) and B) Product ion mass chromatogram and mass spectrum (inset) of ammonium adduct ion of AM (*m/z* 316.2) during analysis of Coartem tablet with HT-HPLC-ESI(+)-MS and HT-HPLC-ESI(+)-MS/MS respectively. Chromatographic conditions: Discovery Zr-PBD (150 x 4.6 mm, 3.0 µm) stationary phase; mobile phase: MeOH/water (**20/80**) with 10 mM AF in water; flow rate: 0.4 mL min^{-1}; injection volume: 10 µL; column temperature: 90 °C. MS detection: Argon collision gas; collision energy: 10 eV; analyte: *m/z* 316.2 for AM.

4.4 Conclusion

In this chapter, the coupling of HT-HPLC to triple quadrupole MS via ESI and APCI ionisation sources for the analysis of ART and derivatives is described. Optimised ESI and APCI source parameters for maximum detection sensitivity of ART, DHA and AM and AS during HT-HPLC-MS analysis were obtained. After optimisation, ART, DHA and AM were detected as their ammonium adduct ions ($[M+NH_4]^+$) at *m/z* 300, 302 and 316, while AS was detected as a characteristic ion at *m/z* 272. The optimised HT-HPLC-MS method using Zr-PBD column was capable of separating and detecting ART and derivatives with good chromatographic selectivity and MS sensitivity. Based on the MS detection sensitivity for ART and derivatives using ESI and APCI sources with different organic modifiers, best sensitivity was obtained with the ESI during the HT-HPLC-MS analysis. With the ESI and APCI sources, MeOH organic modifier resulted to better signal intensity compared to the use of ACN as organic modifier.

Consequently, HT-HPLC-ESI-MS was applied to screen for AM in a Coartem drug tablet. LOD and LOQ in the range from 0.52 to 1.12 µg mL^{-1} and 1.58 to 3.42 µg mL^{-1} respectively were obtained for DHA, ART and AM. The optimised HT-HPLC-ESI-MS and HT-HPLC-ESI-MS/MS were successful in the screening and confirming the presence of AM in a MeOH extract of Coartem drug tablet. The advantages of HT-HPLC including faster analysis, less use of chemicals, ease of coupling to MS and MS/MS analyser with potential improve in the desolvation process in MS ionisation source, makes HT-HPLC-MS and HT.HPLC-MS/MS a with Zr-PBD column a good alternative for the analysis of ART and derivatives.

Appendix for Chapter 4

Abstract

The appendix for Chapter 4 is divided into two sections. The first section presents a work on the analysis of artemisinin-based antimalarial pharmaceuticals using high-temperature high performance liquid chromatography ultraviolet-visible spectroscopy (HT-HPLC-UV/Vis). For this section, the same column used in Chapter 4 was applied for the analysis. As opposed to Chapter 4 where an LC-MS interface friendly buffer (ammonium formate) was used, phosphate buffer was used in the HT-HPLC-UV/Vis analysis. The second section of this appendix contains additional Figures and Tables to support the results and discussion in Chapter 4.

Table of contents

Abstract

Appendix 4.1 Analysis of Artemisinin-Based Antimalarial Pharmaceuticals by HT-HPLC-UV/Vis Spectroscopy

Appendix 4.1.1 Introduction

Appendix 4.1.2 Experimental

Appendix 4.1.2.1 Chemicals and materials

Appendix 4.1.2.2 Mobile phase and sample preparation

Appendix 4.1.2.3 HT-HPLC-UV/Vis instrumentation and analysis

Appendix 4.1.2.4 Data acquisition and processing

Appendix 4.1.3 Results and Discussion

Appendix 4.1.3.1 UV absorption

Appendix 4.1.3.2 Wavelength optimisation for HT-HPLC-UV/Vis analysis

Appendix 4.1.3.3 Optimisation of phosphate buffer concentration

Appendix 4.1.3.4 HT-HPLC using Zr-PBD column

Appendix 4.1.3.5 HT-HPLC-UV/Vis calibration

Appendix 4.1.3.6 Application to real tablet

Appendix 4.1.4 Conclusion

Appendix 4.2 Additional Information to Analysis of Artemisinin-Based Antimalarial Pharmaceuticals by High-Temperature High Performance Liquid Chromatography Mass Spectrometry

Appendix 4.2.1 Optimising ESI parameters

Appendix 4.2.1.2 HT-HPLC-ESI-MS artemisinin and derivatives

Appendix 4.2.1.3 HT-HPLC-ESI-MS calibration curve

Appendix 4.2.2 Optimising APCI parameters

Appendix 4.2.2.1 HT-HPLC-APCI-MS artemisinin and derivatives

Appendix 4.1 Analysis of Artemisinin-Based Antimalarial Pharmaceuticals by HT-HPLC-UV/Vis Spectroscopy

Appendix 4.1.1 Introduction

Artemisinin (ART) and derivatives, their role as antimalarial agents, and the analytical techniques used for their analysis have been described in Chapter 4.1. As stated in Chapter 4.1, the high sensitivity and selectivity of mass spectrometer, HPLC-MS and HPLC-MS/MS have increasing become the choice of analytical technique in the analysis of pharmaceuticals including ACTs. However, because mass spectrometer is too expensive for institutions in resource-limited areas and the need for skilful personnells, UV/Vis detector which is easy to use and cheap is still been used in the analysis of ACTs. Because ART and derivatives are known not to absorb UV or display fluorescence, most of the reported HPLC-UV/Vis analytical procedure entailed derivatisation in acidic or basic solutions before analysis [122]. However, Ferreira *et al.* [120] later showed that the UV absorption of ART and derivatives is sufficiently high to permit quantification from crude plant samples and ART-based pharmaceutical formulations by UV detection without derivatization.

In this chapter, a variant of the mainstream method, called high temperature high performance liquid chromatography (HT-HPLC) coupled to UV/Vis detector is exploited in the analysis of ART and its derivatives without any pre-derivatisation step. The advantages of HT-HPLC analysis have been described in Chapter 4.1

The objective of this chapter is to exploit the advantages of HT-HPLC in the analysis of ART and derivatives. Two different columns: Discovery zirconia polybutadiene (Discovery Zr-PBD) and Waters XBridge BEH C_{18} column are evaluated. The method is applied for the analysis of AM in Coartem antimalarial drug.

Appendix 4.1.1 Experimental

Appendix 4.1.1.1 Chemicals and materials

Analytical standards of ART (97.0%), AM (98.0%), AS (98.0%) and DHA (98.0%) were purchased from Tokyo Chemical Industry (TCI), Belgium. Coartem tablets (Novartis, Switzerland) containing 20 mg AM and 120 mg lumefantrine per tablet were acquired from a local pharmacy in Cameroon. HPLC grade methanol (MeOH), acetonitrile (ACN) was from Fisher Scientific (Loughborough, UK). Potassium dihydrogen phosphate (99.5%, Merck, Darmstadt, Germany) was applied as the chromatographic buffer. Orthophosphoric acid 85 % Ph. Eur. (Carl Roth GmbH + Co. KG, Karlsruhe, Germany) was added to the buffer for pH adjustment. Bi-distilled deionised water was prepared using a distillation apparatus from Heraeus-Quarzschmelze GmbH (Hanau, Germany). A Whatmann polyamide membrane filter, 0.22-µm pore size (Sigma-Aldrich Chemie GmbH, Schnelldorf, Germany) was used for filtration of the aqueous solvents. Calibrated pH meter (Xylem Analytics Germany Sales GmbH & Co. KG, WTW, Weilheim, Germany) was applied for the pH measurement and adjustment. Ultrasonic bath (SONOREX Super 10P, BANDELIN electronic GmbH&Co.KG, Berlin, Germany) was used in solvent degassing and to increase dissolution of analytes.

Appendix 4.1.1.2 Mobile phase and sample preparation

Unless otherwise stated, the mobile phase for HPLC analysis consisted of 5.0 mM phosphate buffer (pH 3.0) in ACN. The exact volumetric ratio of the organic modifier used in the mobile phases is stated in the respective chromatograms in the results and discussion section. The phosphate buffer used for this experiment was prepared by dissolving the appropriate amount of KH_2PO_4 in bi-distilled water. After filtration with a membrane filter, the pH meter helped in adjusting the pH to 3.0 while adding drops of phosphoric acid. The pH 3 is lower than the pKas of the ART and derivatives and thus facilitates RP-HPLC separation. After degassing in an ultrasonic bath, appropriate volume of organic modifier was added to make up the final mobile phase for isocratic elution. The exact volumetric ratio of the phosphate buffer and the organic modifier are stated in the results and discussion section.

A stock standard of 3.76 mg mL^{-1} ART, 4.42 mg mL^{-1} AS, 4.94 mg mL^{-1} DHA and 5.4 mg mL^{-1} AM were prepared by separately dissolving appropriate amount in ACN. To increase dissolution of the standards in ACN, an ultrasonic bath set at 40 °C was used for 40 minutes. After filtration with a 0.2 µm Polytetrafluoroethylene (PTFE) syringe filter, the stock standards were kept in amber glassware. AM calibration standards (0.04, 0.08, 0.42, 1.05 and

1.41 mg mL^{-1}) for HT-HPLC-UV/Vis calibration were prepared by dilution with the mobile phase. The standards were prepared taking into consideration the amount of ART and derivative present in known commercial ART-based drug containing tablets.

For application of HT-HPLC-UV/Vis method to commercial sample, Coartem tablet containing AM was used. With the aid of the ultrasonic bath, 22.4 mg of grinded Coartem tablet was extracted in 5 mL ACN. After filtration with a 0.2 µm PFTE syringe filter, the sample was spiked with standard AM before injection into the LC system. The spiking was done because of lack of signal for AM from the extracted sample.

Appendix 4.1.1.3 HT-HPLC-UV/Vis instrumentation and analysis

The HPLC instrument used for this experiment was from Gilson (Villers Le Bel, France). The system comprises of Gilson 307 pump, Gilson 402 syringe pump, Gilson 231 XL sampling injector with a 20 µL sample loop and Gilson 118 ultraviolet/visible (UV/Vis) detector. For this chapter, a Discovery zirconia polybutadiene (Discovery Zr-PBD) column from SUPELCO (Bellefonte, PA, USA) with a dimension of 150 x 4.6 mm and zirconia particle size 3.0 µm was used. A calibrated WTW pH meter (Weilheim, Germany) was applied for pH adjustment and measurement. A Bandelin Sonorex Supper Ultrasonic bath (BANDELIN electronic GmbH & Co. KG, Berlin, Germany) was used to degas the mobile phase and to sonicate the sample. A Cenco Mixer (Cenco Instrumenten b.V Netherland) was utilized for sample homogenization before LC injection.

The heating system for HT-HPLC analysis was a prototype oven developed by German Institute of food technologies (DIL) (Quakenbrück, Germany). The system consisted of three units: the eluent preheater, column heater and post-column cooler units. Aluminium block was used in the construction of each unit where it helps to enhance heat transfer from the unit to the capillaries and column. The capillary in the eluent preheater unit is coiled such that the eluent entering the column unit has more or less the same temperature as eluent in the column heater unit, thus avoiding temperature gradient [66]. For the column heater unit, an additional aluminium column jacket, adapted to the dimensions of the column was used. The HPLC instrument used for this experiment was from Gilson (Villers Le Bel, France).

For HT-HPLC analysis, the effluent from the heated column was forwarded to the UV/Vis detector via the post-column cooler that was set at 25 °C eluent-preheater unit was fixed at 5 °C higher than the column-heating unit. For LC injection, each standard as well as a mix

standard was prepared by appropriate dilution with the mobile phase. Because of the light sensitive nature of these compounds, amber glassware and vials were used throughout the experiment. Prior to HT-HPLC-UV/Vis analysis, the wavelength for maximum UV/Vis absorbance for the ART and derivatives was investigated using Variant Cary 50 UV-visible spectrophotometer (Varian Australia PTY LTD, Australia). From the investigation, wavelength (λ) of 205 and/or 210 nm were applied for the HT-HPLC-UV/Vis analysis of ART and derivatives.

Appendix 4.1.1.4 Data acquisition and processing

The signal from the Cary 50 spectrophotometer was processed using the Cary WinUV software (Varian Australia PTY LTD, Australia). Gilson 402 syringe pump, Gilson 231 XL sampling injector was controlled by 735 Sampler Software (Gilson, France). Data acquisition for the UV/Vis detector was carried out with McDAcq Integrator version 1.5 (BISCHOFF Chromatography GmbH, Leonberg, Germany). Further data processing was done using OriginLab 2015 (OriginLab, Northampton, MU, USA).

Appendix 4.1.2 Results and Discussion

Appendix 4.1.2.1 UV absorption

As stated above, most HPLC-UV/Vis method for the analysis of ART and derivatives have been made possible only after derivatisation. This has been on the one hand due to the lack of chromophore by this class of compound and on the other hand, the UV absorption maxima for ART (usually λ = 205 nm) could be interfered by absorption from solvents such as MeOH (UV cutoff 200 nm) and ACN (UV cutoff 190 nm). With the aid of a UV/Vis spectrophotometer, the absorbance of ART and derivatives was evaluated. Figure A 4.1 shows the slight difference in the absorbance maxima for AM dissolved in MeOH and ACN. With ACN, a displayed instrumental reading of 200 nm was obtained as opposed to 207 nm for MeOH. The additional absorbance (at λ = 310 nm) for AM dissolved in MeOH could be attributed to some chemical transformation or polymorphism originating from exposure to light. The absorbance at 310 nm was eradicated when freshly prepared ART and derivatives were analysed without long exposure to light. The observed discrepancy in the absorption maxima originating from the AM in MeOH and ACN can also be attributed to the solvent polarity, which affects the solubility and absorbance of the analyte. To ensure that the observed absorbance was from the ART, solvent background was subtracted before any measurements. The absorbance from the from the other ART derivatives, were similar as shown in Figure A 4.1B.

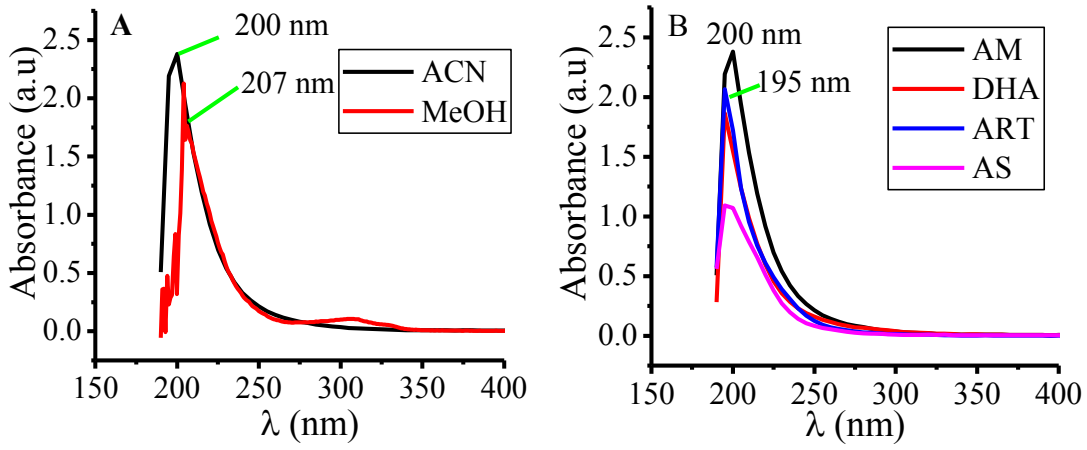

Figure A 4.1: UV absorption spectrum of ART and derivatives. A) Effect of organic modifier on UV absorption of 2.07 mg mL^{-1} AM. (B) Absorbance of AM (2.07 mg mL^{-1}), DHA (1.08 mg mL^{-1}), ART (1.28 mg mL^{-1}) and AS (1.03 mg mL^{-1}). Solvent: ACN. Optical path length: 1 cm.

It is worth stating here that, the absorbance for this class of compound depends on how the sample was prepared and kept. For instance, it was observed for ART and derivatives that, the absorbance maxima shifted from 205 to 270 nm when the standard solution was kept expose to light for a long (five days in this case) period of time (results not shown). The change in the absorbance was attributed to chemical transformation or polymorphism that originated from the exposure to light. For a sample prepared and kept in amber glassware, such transformation was not seen. Though the aim of this study was not to investigate the identity of the transformed product or the transformation process, the results helps to give a guideline on sample preparation and preservation.

Because of the low UV cutoff wavelength of ACN over MeOH, it was chosen as the organic modifier of interest for the HT-HPLC-UV/Vis analysis. The absorption maximum of λ = 200 nm for ART (*cf*. Figure A 4.1) was used as guide in setting the detector wavelength of the UV/Vis detector used in the HT-HPLC-UV/Vis analysis.

Appendix 4.1.2.2 Wavelength optimisation for HT-HPLC-UV/Vis analysis

Prior, to the HT-HPLC-UV/Vis analysis of ART and derivatives, the UV-absorption spectrum in Figure A 4.1A was used as a guide to choose the wavelength of the UV detector. A mobile phase of ACN/water (15/85), flow rate 1.2 mL min^{-1} and column temperature (T) 50 °C were used to investigate the detector response at λ = 205 and 210 nm. Table A 4.1 shows the effect of the wavelength on the UV detector signal response (peak area and height) for ART.

Table A 4.1: Effect of wavelength on signal response for ART.

N = 3	**λ = 210 nm**	**λ = 205 nm**
Area (mV.sec)	329.20 ± 4.77	555.72 ± 1.87
Height (mV)	7.07 ± 0.01	10.93 ± 0.18
Asymmetry	1.09 ± 0.00	1.06 ± 0.06
Number of plate	544 ± 1	587 ± 13

The mean ± standard deviation of the peak parameters are reported (n = 3)

From Table A 4.1, the highest signal response (peak area and height) was obtained at λ = 205 nm. With the use of phosphate buffer (pH 3.0), the signal response from λ = 205 nm was still higher than at λ = 210 nm. Because of the higher signal response, λ = 205 nm was applied throughout the HTLC-UV/Vis analysis.

Appendix 4.1.2.3 Optimisation of phosphate buffer concentration

To minimise possible peak tailing on RP-HPLC of ART and derivatives, the mobile phase pH had to be optimised such that the pH was lower than the pKas of the ART and derivatives. The buffer capacity of phosphate buffer (three pKa values: $1.1<pK_1<3.1$, $6.2<pK_2<8.2$ and $11.3<pK_3<13.3$) and it ability to be useful at wavelength lower than 220 nm, made it an optimum buffer for this HT-HPLC-UV/Vis analysis. The signal response (peak area, height), number of plate was shown to increase slightly with increase concentration of phosphate buffer. This can be attributed to the increase in the phosphate layer responsible for ionic interaction between the analyte and phosphate ion as depicted in Figure A 4.2. While the 20 mM phosphate buffer resulted to increase column efficiency (plate number 617 ± 1), peak corresponding to ART and AS co-eluted and as a result, the 5 mM phosphate buffer was used for further analysis. Similar effect on efficiency was observed for AM, AS and DHA.

Table A 4.2: Effect of phosphate concentration on signal response for ART.

Peak parameters	Conc. = 5 mM	Conc.= 20 mM
Area (mV.sec)	555.72 ± 1.87	589.24 ± 12.45
Height (mV)	10 ± 0.18	11.27 ± 0.12
Asymmetry	1.06 ± 0.05	1.00 ± 0.00
Number of plate	589 ± 13	617 ± 1

The mean ± standard deviation of the peak parameters are reported (n = 3)

Appendix 4.1.2.4 HT-HPLC using Zr-PBD column

Reversed phase separation on Zr-PBD column is driven by the surface chemistry that is based on Lewis theory of acids and bases [126]. The free d-orbitals of Zr atom on the surface of the carrier act as Lewis acid sites with strong affinity for Lewis bases components of the mobile phase (e.g. phosphate, hydroxylic, carboxylic, formate and fluoride). The Lewis bases are adsorbed on the surface by specific ligand exchange interactions and by interacting with

analyte ions, via ion-exchange interactions (*cf.* Figure A 4.2). This mixed-mode mechanism can be exploited for the separation of basic and acidic analyte such as ART and derivatives. Figure A 4.3 shows a chromatogram of ART and derivatives obtained after HT-HPLC on Zr-PBD column at T= 50&70 °C. In addition to the known ART derivative, was an unknown peak 2, which can be attributed to a soluble bi-product coming from the buffer or the ART derivatives. The fact that this unknown peak was present after injecting DHA, AS, ART and AM separately can portray the mobile phase buffer as the origin of the unknown. A similar unknown peak was noticed for HT-HPLC-UV/Vis analysis on XBridge C_{18} (results not shown) with phosphate buffer in the mobile phase. From the chromatogram, AM, the most retained compound had a retention factor (k) of 5.95, while DHA, the least retained had a k = 0.84. To relate the observed elution order and the chemistry of the stationary phase, its needs to be recalled that ART and derivatives have different pKa values (e.g., AS has a pKa of 4.6 and DHA has a pKa of 12.6) and thus different retention mechanism can be responsible for their separation.

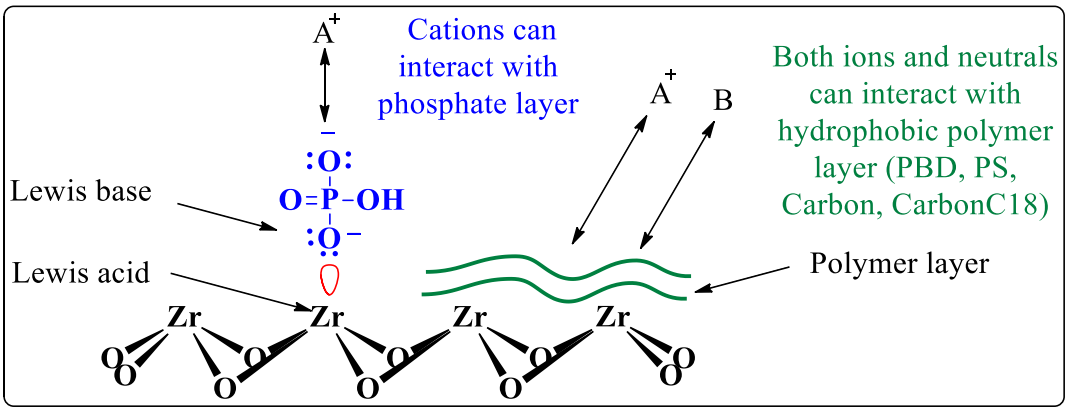

Figure A 4.2: Acid base chemistry on Zr-PBD column. Adapted from ref.[127]

For instance for a mobile phase pH 3.0, the non-ionized species of AS (pKa = 4.6) will predominate and as a result, the separation will be driven by hydrophobic interactions between the non-ionized AS and the polymer layer (PBD) on the surface of zirconia support. On the other hand, at mobile phase pH 3.0, DHA (pKa = 12.6), will tend to have more ionized species and thus the retention mechanism could be driven by both ion exchange and hydrophobic mechanism. Based on the mixed mode mechanism on Zr-PBD column, ART and derivatives have been separated at T 50&70 °C.

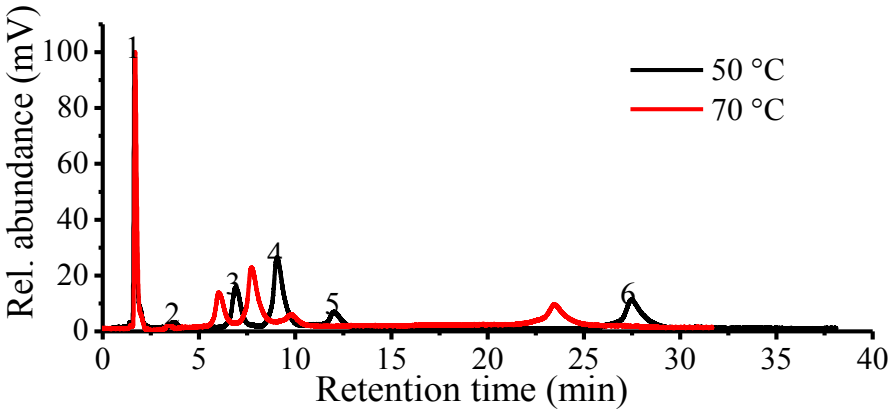

Figure A 4.3: HT-HPLC separation of ART and derivatives. Chromatographic conditions: stationary phase: Discovery Zr-PBD (150 x 4.6 mm, 3.0 µm): mobile phase: ACN/water (15/85) with 5 mM phosphate buffer. Flow rate: 1.2 mL min^{-1}: injection volume: 25 µL: column temperature: 50&70 °C. Detection: λ = 205 nm. Analytes: 1) mobile phase, 2) unknown, 3) DHA, 4) ART, 5) AS, 6) AM.

As expected, an increase in temperature, led to an overall decrease in retention factor. Such trend is thermodynamically described using the van't Hoff equation given as

$$\ln K_i = -\frac{\Delta H}{RT} + \frac{\Delta S}{R} + \ln\beta$$

where k_i refers to the retention factor of the solute i, ΔH and ΔS are respectively the enthalpy and entropy of transfer of solute i from the mobile phase to the stationary phase, T is the column temperature in kelvin, R is the ideal gas constant and β is the volume phase ratio.

Figure A 4.4 shows the van't Hoff plot for separation of ART and derivatives on Zr-PBD column. A linear van't Hoff plot was observed within the tested temperature range (30 - 110 °C). The correlation coefficient (r^2) associated with this plot is shown at the bottom.

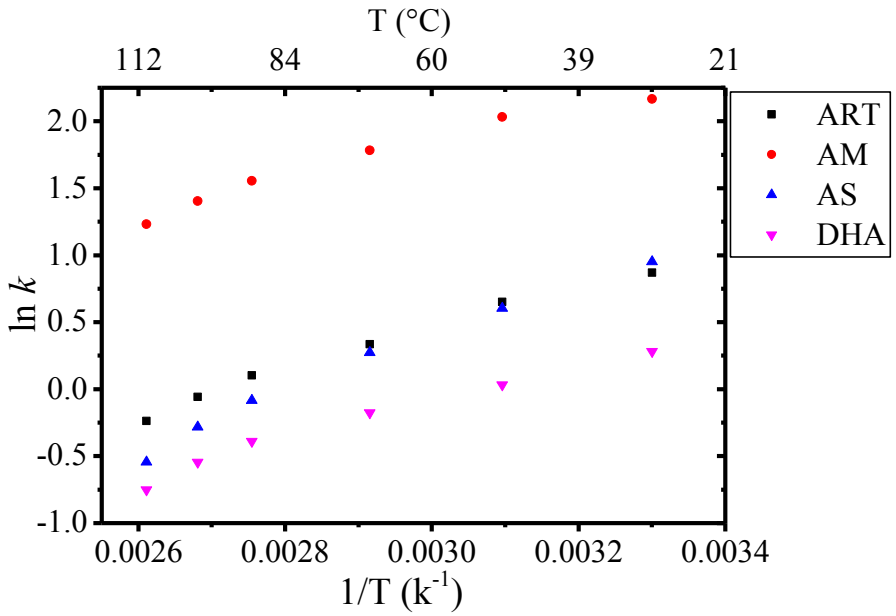

Figure A 4.4: Van't Hoff plot for ART and derivatives. Chromatographic conditions: same as in Figure A 4.3. Correlation coefficient (r^2) for DHA, AS, ART and AM: 0.992, 0.988, 0.998 and 0.997 respectively.

Increase in the percentage of ACN within the tested temperature range was found to be beneficial for the elution of AM but not for DHA and AS which eluted without any peak resolution.

Appendix 4.1.2.5 HT-HPLC-UV/Vis calibration

To assess the applicability of the HT-HPLC method with Zr-PBD for the analysis of AS in Coartem tablet, a calibration curve for AM was constructed as shown in Figure A 4.5B. For the calibration and linearity study, a mobile phase consisting of 35% ACN and 65% phosphate buffer (5 mM, pH 3.0) and column temperature of 80 °C was applied. The UV detector wavelength was adjusted to 203 nm. Figure A 4.5A shows the chromatogram at different concentrations and the calibration curve for AS. The calibration curve showed good linearity with an r^2 of 1.00. The calibration curve was constructed by plotting the average response (peak area) for two measurements against the concentration of the standards. For a 20-µL injection, an LOD and LOQ of 0.136 and 0.247 mg mL^{-1} respectively were obtained.

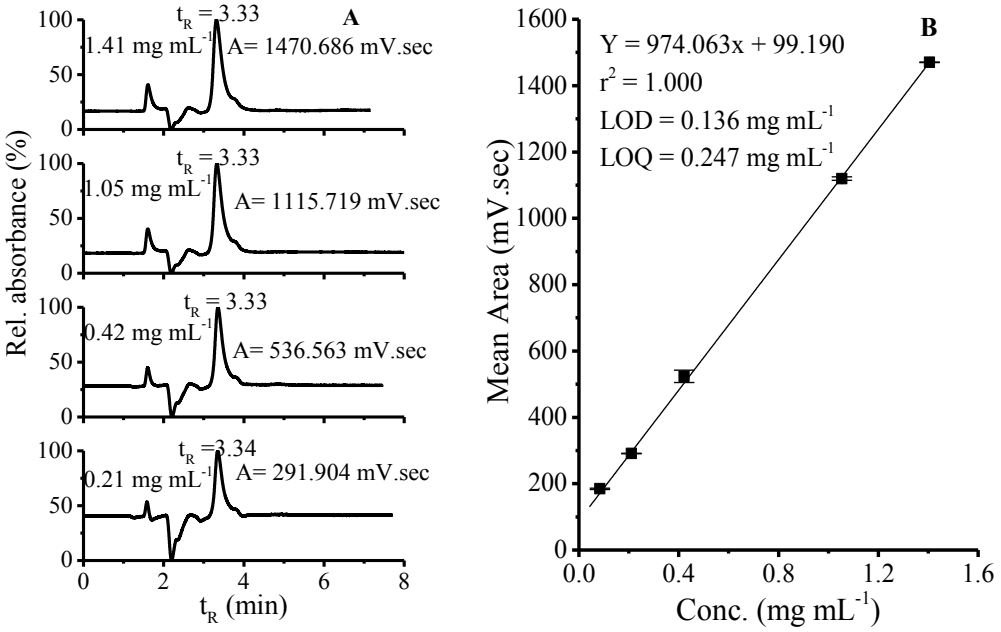

Figure A 4.5: Chromatogram of AS at different concentration levels (A) and calibration curve (B). Chromatographic conditions: stationary phase: Discovery Zr-PBD (150 x 4.6 mm, 3.0 µm): mobile phase: ACN/water (35/65) with 5 mM phosphate buffer. Flow rate: 1.2 mL min^{-1}: injection volume: 20 µL: CT: 80 °C. Detection: λ = 203 nm.

Appendix 4.1.2.6 Application to real tablet

After assessing the applicability of HT-HPLC-UV/Vis for quantitative analysis, the method was used for the analysis of AS in Coartem tablet. Coartem contains 20 mg of AS per tablet (242.95 mg average weight) which is a 0.0823 mass fraction. Analysis of the sample as prepared as stated in the experimental section, showed no peak for AS. For a 22.4 mg of Coartem in 5 mL ACN, an AS concentration of 0.37 mg mL^{-1} was expected which is higher than the LOD and LOQ determined above. However, HT-HPLC-UV/Vis analysis of the extract resulted to an unquantifiable peak. As a result, the extracted sample was analysed by adding 400 µL of sample and 100 µL of spike stock solution (4.22 mg mL^{-1}) to yield 0.84 mg mL^{-1} spike concentration. As can be seen in Table A 4.3, a concentration higher than the spiked concentration by 0.01 mg mL^{-1} was detected. The inability to detect AM, in the tablet could be attributed to different factors including quality of the tablet, solubility effect, sensitivity, and possible suppression or changing of the absorbance maxima.

Table A 4.3: Quantitative data for AM spiked in Coartem extract followed by HTLC-UV/Vis.

Spike sample	DF	Spike conc. (mg mL^{-1})	Observed area (mV.sec)	Observed conc. (mg mL^{-1})	Observed conc. x DF (mg mL^{-1})
Run 01	4:5	0.84	1192.6	1.06	0.85
Run 02	4:5	0.84	1178.9	1.05	0.84
Run 03	4:5	0.84	1178.3	1.07	0.85
Mean			1189.4	1.06	0.85
Std. dev.			9.3	0.010	0.007
CV (%)			0.8	0.71	0.57

Injection volume: 20 µL, DF= dilution factor

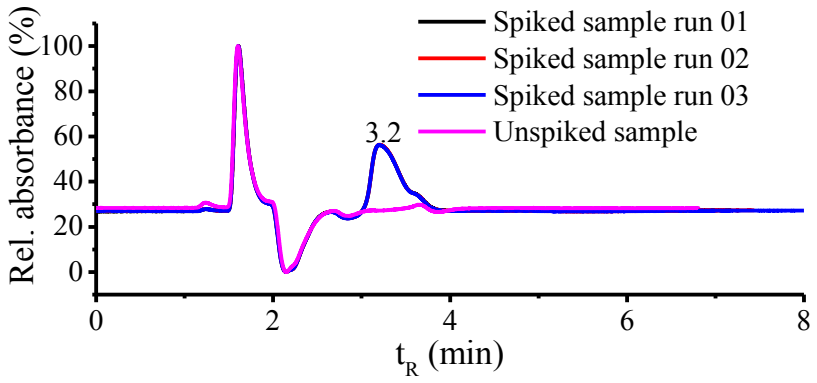

Figure A 4.6: Retention of spiked AM in Coartem extract. Chromatographic conditions: stationary phase: Discovery Zr-PBD (150 x 4.6 mm, 3.0 µm): mobile phase ACN/water (35/65) with 5 mM phosphate buffer. Flow rate: 1.2 mL min^{-1}: injection volume: 20 µL: column temperature: 80 °C. Detection: λ = 203 nm.

Since real tablet contains other components such cellulose, binders and other pharmaceutical ingredients (lumefantrine in this case). These components may not affect only the solubility, but also may suppress the absorbance or change the absorbance maxima. To improve the extraction process, another solvent with better solubility could be valuable. In the case where detector sensitivity was responsible for the poor sensitivity, other detectors such as such as MS, which is sensitive, selective, and specific, would be needed. MS detector would be advantageous in improving the sensitivity and the same time give information on the chemical identity of other components in the drug sample.

Appendix 4.1.3 Conclusion

The potential of HT-HPLC-UV/Vis in the analysis of ART and derivatives have been investigated with Discovery Zr-PBD column. The mixed mode chemistry of the column have been exploited for the separation of this class of compound. It has also been show that, without derivatisation, this class of compound, which have no chromophore, cannot only be detected, but also quantitative analysis is possible. The UV absorbance helped in choosing the right solvent for this class of compounds. Despite the lack of specificity, in terms of the chemical structure, HT-HPLC, with its reduced organic consumption and speed of analysis, is also a vital tool in the analysis of this class of compound. While selective and specific detectors, such as MS, will be very valuable, especially to know the chemical identity of the unknown peaks, the use of UV/Vis detector, a main stream detector, makes the method simple and straight forward.

Appendix 4.2 Additional Information to Analysis of Artemisinin-Based Antimalarial Pharmaceuticals by High-Temperature High Performance Liquid Chromatography Mass Spectrometry

Appendix 4.2.1 Optimising ESI parameters

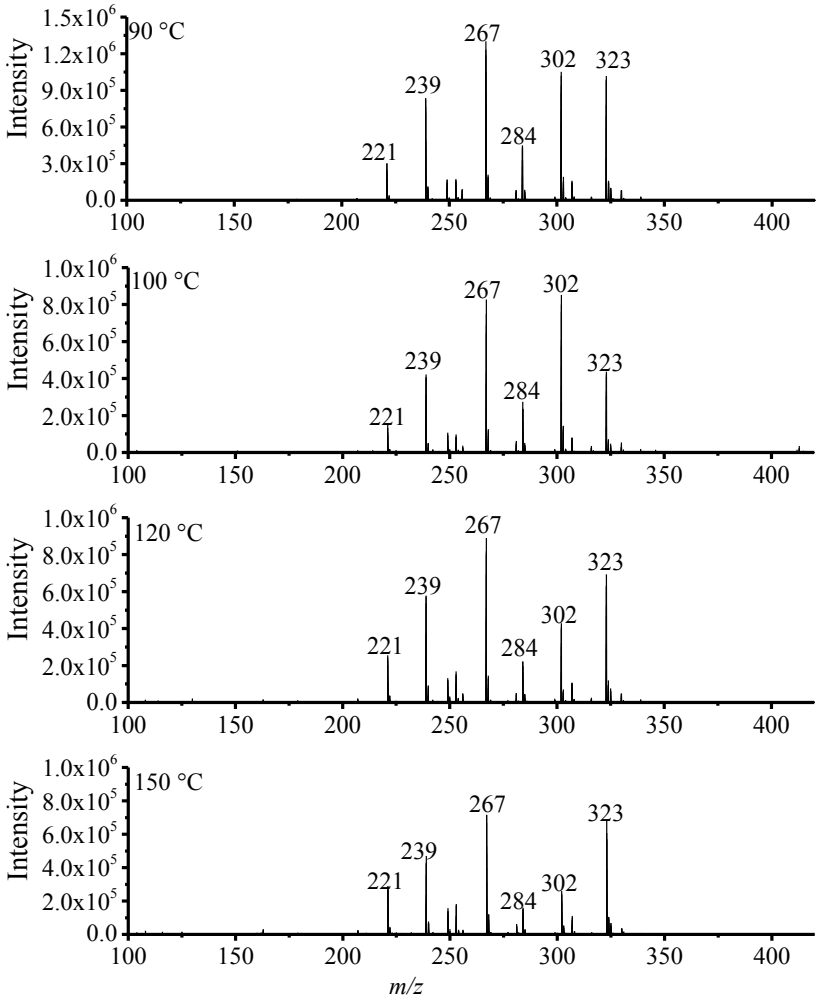

Figure A 4.7: Effect of source temperature on in-source fragmentation of DHA (10 µg mL^{-1}) after reversed-phase HT-HPLC-ESI(+)-MS. Mobile phase consisted of 10 mM AF (pH 3) in a **50% MeOH**. ESI parameters: cone voltage: 15 V. Source temperatures: 90-150 °C.

Table A 4.4: Summary of source temperature effect on MS signal for DHA ammonium adduct at *m/z* 302.

Source temperature (°C)	Intensity x 10^6	S/N ratio XIC	Ratio of *m/z* 302:267
90	0.96 ± 0.13	61.58 ± 3.0	0.8 ± 0.01
100	1.61 ± 0.44	51.13 ± 7.0	1.92 ± 0.57
120	0.45 ± 0.02	36.53 ± 3.03	0.52 ± 0.05
150	0.30 ± 0.06	24.63 ± 1.8	0.35 ± 0.05

The mean ±standard deviation is reported for n = 3.

Appendix 4.2.1.1 HT-HPLC-ESI-MS artemisinin and derivatives

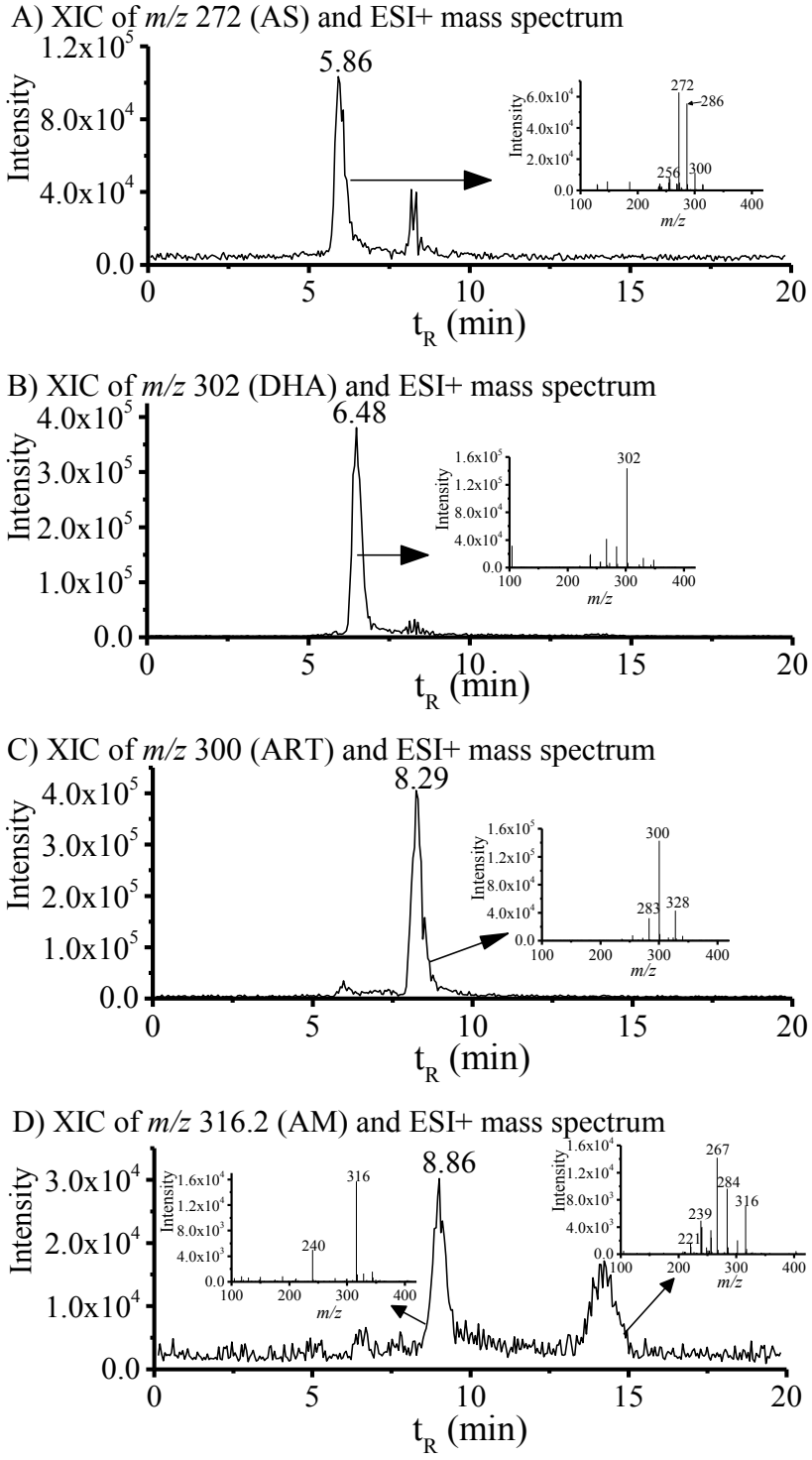

Figure A 4.8: HT-HPLC-ESI(+)-MS extracted-ion chromatograms (XIC) and mass spectra (insets) after analysis of a standard mixture of ART and derivatives. Chromatographic conditions: Discovery Zr-PBD (150 x 4.6 mm, 3.0 µm) stationary phase; mobile phase: **ACN/water** (15/85) with 10 mM AF in water; flow rate: 0.4 mL min^{-1}; injection volume: 10 µL; column temperature: 90 °C. Analytes: A) *m/z* 272.0 for AS, B) *m/z* 302.0 for DHA, C) *m/z* 300.0 for ART and D) 316.2 for AM.

Appendix 4.2.1.2 HT-HPLC-ESI-MS calibration curve

The calibration plot is a construction of the peak area of the extracted-ion chromatogram for the ammonium adduct of DHA, ART and AM against their on-column amount. The on-column amount was calculated for a 10-µL injection volume of the standard mixture.

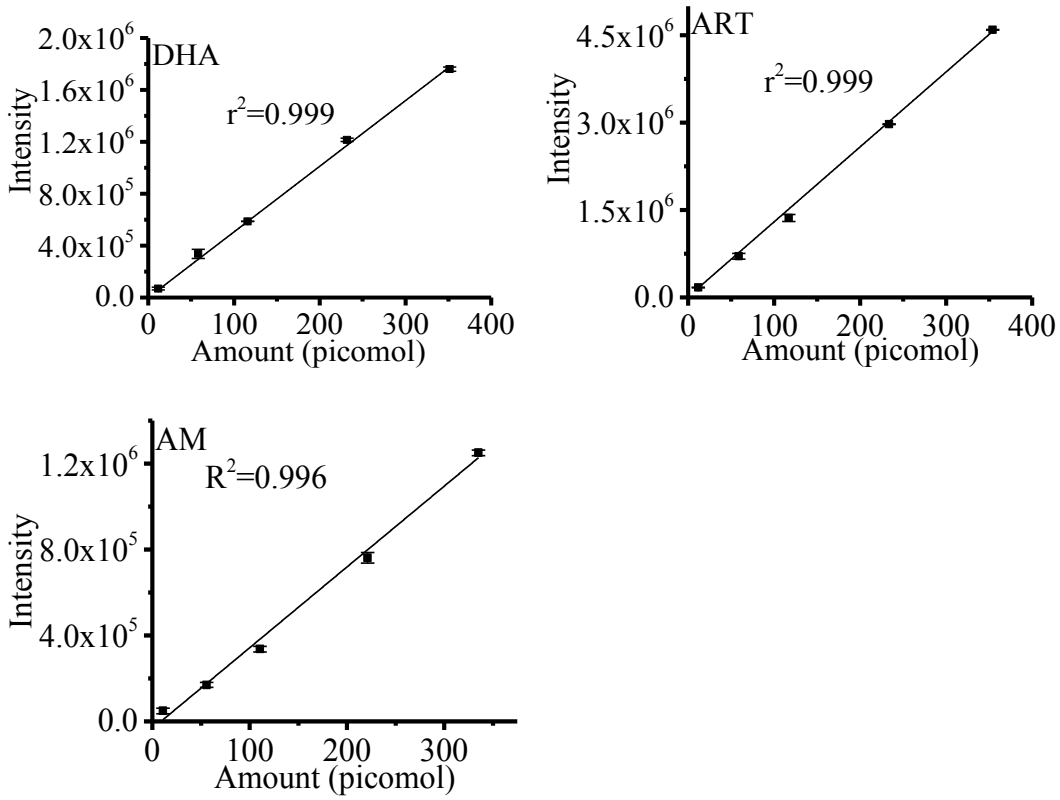

Figure A 4.9: HT-HPLC-ESI(+)-MS calibration curve for DHA, ART and AM with Zr-PBD column.

Appendix 4.2.2 Optimising APCI parameters

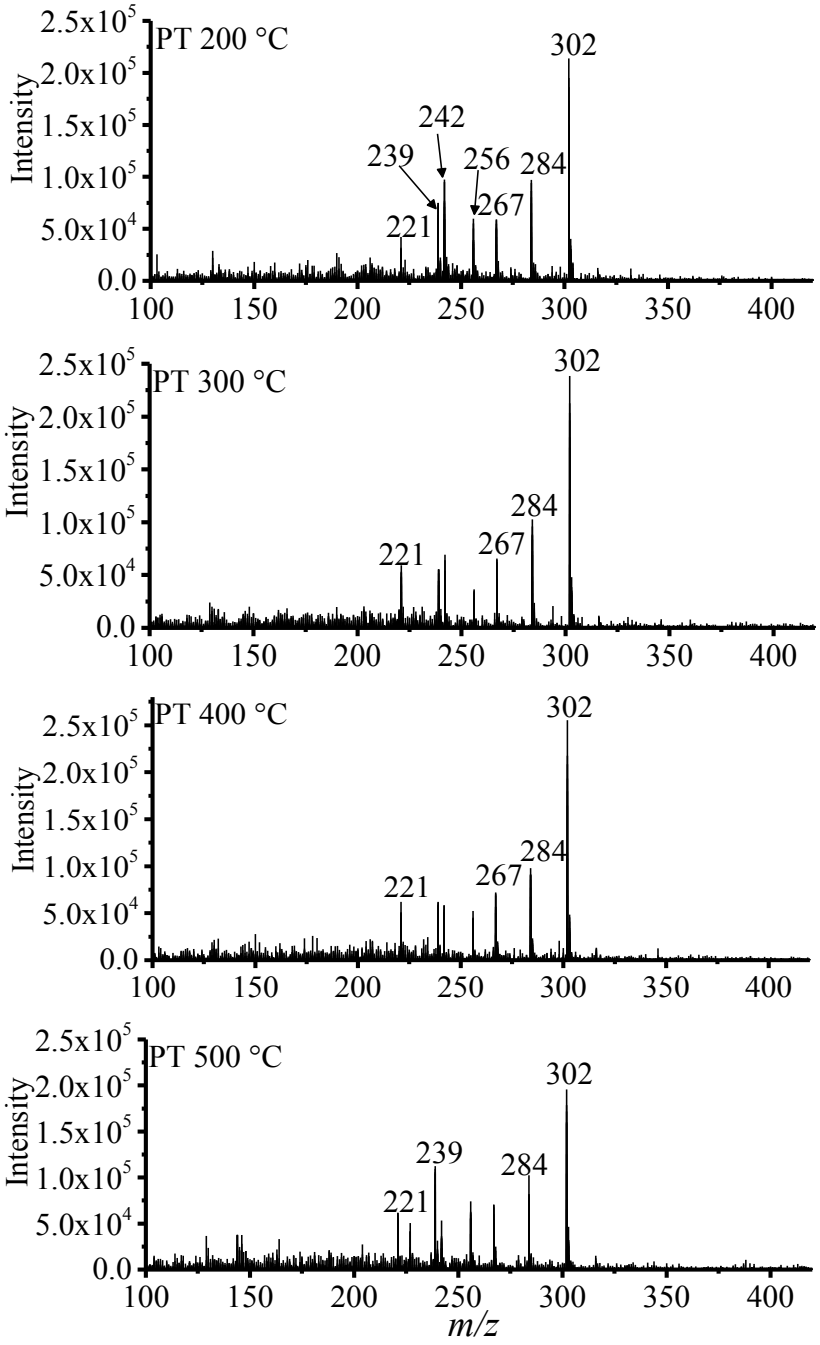

Figure A 4.10: Influence of APCI probe temperature (PT) on in-source fragmentation of DHA (100 µg mL^{-1}) during HT-HPLC-APCI(+)-MS. Mobile phase: MeOH/water (15/85) with 10 mM AF in water. APCI parameters: Corona pin voltage 3 kV, PT: 200-500 °C.

Appendix 4.2.2.1 HT-HPLC-APCI-MS artemisinin and derivatives

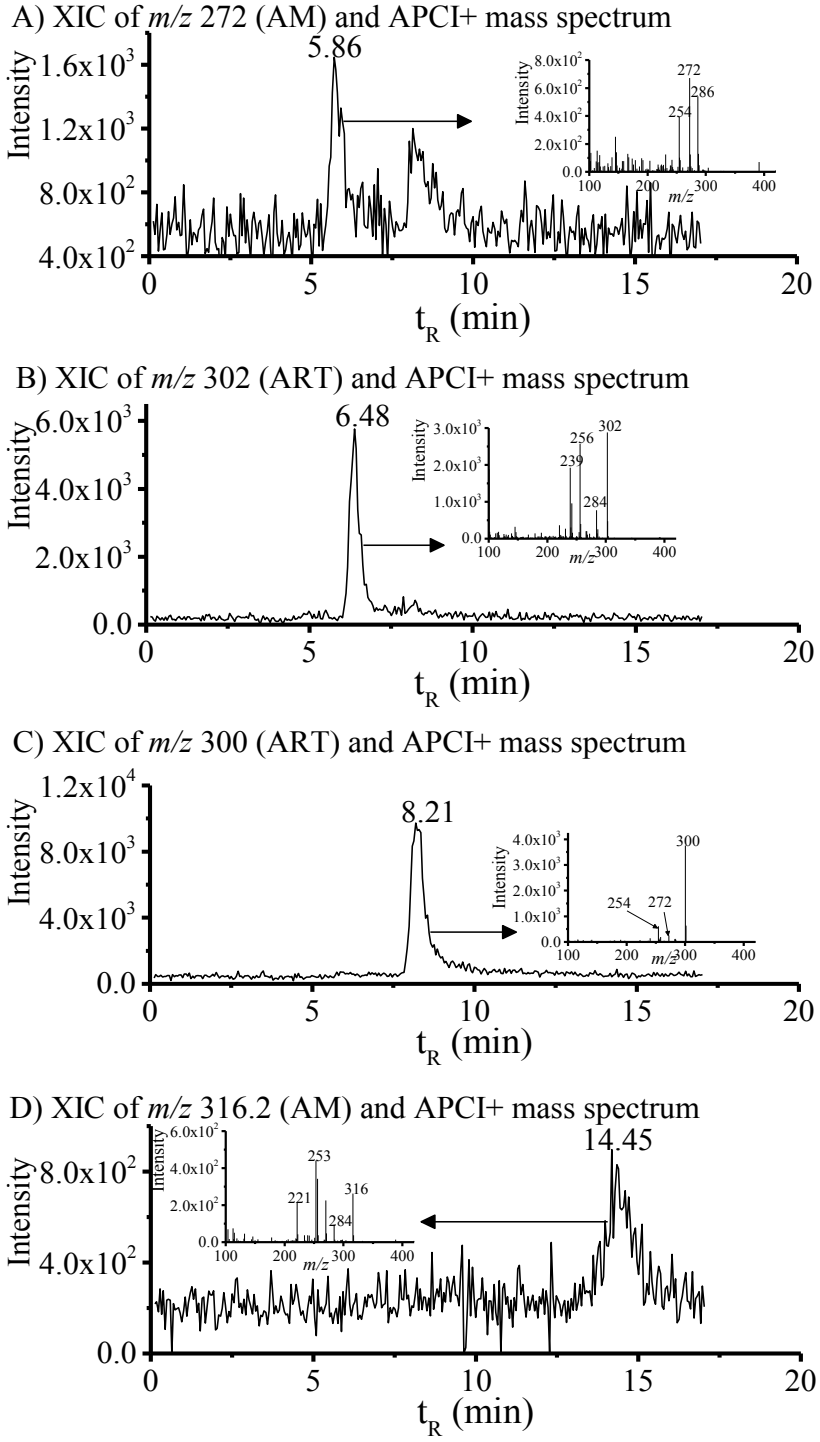

Figure A 4.11: HT-HPLC-APCI(+)-MS extracted ion chromatogram (XICs) and mass spectra (insets) after analysis of a standard mixture of ART and derivatives. Chromatographic conditions: Discovery Zr-PBD (150 x 4.6 mm, 3.0 µm) stationary phase; mobile phase: **ACN/water** (15/85) with 10 mM AF in water; flow rate: 0.4 mL min^{-1}; injection volume: 10 µL; column temperature: 90 °C. Analytes: A) *m/z* 272.0 for AS, B) *m/z* 302.0 for DHA, C) *m/z* 300.0 for ART and D) *m/z* 316.2 for AM.

Chapter 5

Direct Analysis of Alkaloids in Natural *Cinchona* Bark and Commercial Extracts using Time-of-Flight Secondary Ion Mass Spectrometry

Abstract

Time-of-flight secondary ion mass spectrometry (ToF-SIMS) is used for the first time to characterize Cinchona alkaloids in natural Cinchona bark and commercial Cinchona extracts. ToF-SIMS analysis of quinine (Qn), a major Cinchona alkaloid, provides significant molecular fragments, which can be used in the fast qualitative screening of Qn and related compounds in small amounts of Cinchona bark and extract. Conventional approaches for natural product analysis such as bark are time-consuming and typically require large amounts of sample, significant amounts of organic solvents for extensive liquid extraction as well as liquid chromatography for analyte separation from the matrix before detection. In this chapter, it is demonstrated that ToF-SIMS can be used for the direct analysis and fast qualitative screening (less than 10 minutes analysis time) of Cinchona alkaloids. It is also a greener approach over chromatography-based approaches because it uses less sample material and no organic solvents. Before ToF-SIMS analysis, the bark surface topography and roughness was analyzed using 3D laser microscopy. ToF-SIMS results in this chapter were validated by complementary high performance liquid chromatography - MS results. This work shows the potential of ToF-SIMS in screening of pharmaceutical relevant compounds that are present in natural samples such as bark and extracts.

Based on: *D.N. Ateacha, U. Koch, C. Engelhard, Analytical Methods, 2018, **10**, 950 - 958*, DOI: (10.1039/C7AY02822A).

5.1 Introduction

Natural products are and will continue to be a prolific source for new chemical compounds and pharmaceutical drugs in the chemical and pharmaceutical industries. For instance, the *Cinchona* bark is the natural source of *Cinchona* alkaloids, a group of approximately 35 basic organic molecules. The main *Cinchona* alkaloids are the quinolines; quinine (Qn), quinidine (Qdn), cinchonine (Cn) and cinchonidine (Cdn) (*cf*. Figure 3.1). An ‘‘average’’ bark contains 7–12% total alkaloids of which Qn accounts for 70–90%, Cdn 1–3%, and Qdn up to 1% [129]. The most important component, Qn is used in the treatment of malaria. The pseudo enantiomer of Qn, known as Qdn, functions as a cardiac depressant (antiarrhythmic)[130]. The first application of Qn as a drug to treat malaria dates back to the 17th century [131] and it holds a record as the first chemical compound successfully used to treat an infectious disease [132].

Another group of chemical compounds used for the treatment of malaria is artemisinin and derivatives (*Cf.* Chapter 4.1)., which is currently the World Health Organization (WHO) recommended first line of treatment against uncomplicated malaria [133]. Despite the successes recorded in the use of artemisinin and derivatives, limited availability and increasing wide spread resistance, especially in resource-limited areas, has led to resurgence and increased demand of Qn in recent times [134]. In a recent publication, Hrycyna *et al.* [135] found that Qn dimers are potent inhibitors of *plasmodium falciparum* chloroquine transporter (PfCRT) and are active against the quinoline-resistant *p. falciparum*.

Due to the expensive synthetic procedure to obtain Qn, *Cinchona* bark remains its primary source especially in resource-limited settings. The usefulness of the bark depends on its alkaloids profile and chemical content [83]. Different analytical procedures for the analysis of *Cinchona* alkaloids have been described in Chapter 3.1. On the one hand, the procedures tend to ascertain the chemical content of the bark and thus its usefulness. On the other hand, these procedures aim at assessing the chemical content of Qn, Qdn and their metabolites in human biological fluid, considering the fact that these drugs have narrow therapeutic limits, being toxic in high dose and ineffective at low dose [136,137]. Amongst the analytical procedures, the most important used up till date is high performance liquid chromatography (HPLC) in the reversed-phased (RP) mode coupled to different detection set-ups such as ultraviolet/visible (UV/Vis), fluorescence and mass spectrometry (MS).[89,34,80]. However, the RP-HPLC procedure is characterised by long sample preparation and analysis time, large

sample amount and the use of relatively large amount of organic solvents. Therefore, a method that requires minimal or no sample preparation and uses relatively minimal amount of sample while providing good detection sensitivity would be highly desirable. With focus on these needs, direct analysis method such as matrix-assisted laser desorption ionisation (MALDI) [138] and secondary ion mass spectrometry (SIMS) [139], known for their high mass resolution and small sample consumption, have been used in the past to examine plant tissues. The characteristic features of MALDI and SIMS are somewhat different in that, while SIMS does not require chemical pre-treatment of the sample surface and gives good spatial resolution in the low nanometer range, MALDI requires pre-treatment with a matrix material and the resolution is in the micron range. In a recent study, Kudina *et al.* [44], analysed Qn in a 2, 5-dihydroxybenzoic acid (DHB) matrix by the use of electrowetting-MALDI (e-MALDI). They achieved signal intensities increased by a factor of 10 compared to regular MALDI.

ToF-SIMS is a surface sensitive technique with information depth of only a few nanometers. It makes use of a pulsed primary ion beam to desorb and ionise species from the sample surface. In SIMS as opposed to other ionisation sources, the chemical composition of the sample is obtained from the secondary ions that are generated by bombardment of the sample surface with a beam of primary ions. The high spatial resolution of ToF-SIMS images is obtained by rastering a focused primary ion beam over the sample surface, providing information on the spatial distribution of secondary ions. Usually, the primary ion beam induces fragmentation especially in large molecules, thus the molecular ion often is only detectable in low intensity in the mass spectra. Fingerprint spectra, which show the required and characteristic signals, are used for the identification of organic substances of higher mass. In a study by Aoyagi *et al.* [139], the high sensitivity and spatial resolution of ToF-SIMS was utilized to study the distribution of singrin (a glucosinolate with antibacterial and anticancer effect) in Wasabi plant tissue. Although, *Cinchona* bark is physicochemically different from the Wasabi plant, it is very likely that ToF-SIMS with its high spatial and mass resolution can be applied in the analysis of *Cinchona* bark and its extract. To the best of our knowledge, this is the first attempt to study the chemical composition of *Cinchona* bark and its extract using ToF-SIMS.

5.2 Experimental Section

5.2.1 Chemicals and reagents

Analytical standard of Qn anhydrous, 99% (total base), Cn (98%), Qn (> 99%) were purchased from Alfa Aesar GmbH (Karlsruhe, Germany), while Cn was purchased from Merck Schuchardt OHG (Hohenbrunn, Germany). A commercial composited *Cinchona* bark tincture, Tinctura Chinae nomata (70 %) containing Qn and derivatives was purchased from Caesa & Loretzt GmbH (Hilden, Germany). The tincture or aqueous extract of *Cinchona* was contained in 70% of ethanol. The dried *Cinchona* bark was imported from Cameroon.

5.2.2 Standard and sample preparation

A stock solution of Qn was prepared in ethanol to a concentration of 1000 ng μL^{-1}. After ultrasonic dissolution and homogenisation, the standard was filtered using a 0.22 µm Whatmann polyamide membrane filter (Sigma-Aldrich Chemie GmbH, Schnelldorf, Germany) into a light sensitive sample container, because of its sensitivity to light. Different diluted standards with concentrations 100, 10, 1 and 0.1 ng μL^{-1} were prepared and used as test solutions for the ToF-SIMS study. The *Cinchona* bark used in this study was initially sun-dried to prevent the loss of alkaloids. For preservation of the bark for long-term use, further drying was carried out for 1 hour in an 80 °C laboratory oven. This was done to remove water molecules which can cause degradation of the bark sample. Since *Cinchona* alkaloids are known to have low volatility, drying at 80 °C has no effect on the active *Cinchona* alkaloids. For ToF-SIMS analysis of the bark sample, thin sections of dimension ca. 3 x 3 x 1 mm^3 using an acetone-cleaned Xacto knife. The thin sections were placed on the sample holder using carbon conductive adhesive tape (from Agar scientific, Stansted Essex, UK). The natural extract (Tinctura Chinae nomata) containing a mixture of *Cinchona* alkaloid was diluted 100 times with ethanol before analysis. One microliter each of the standard and the extract was pipetted onto respective pre-cleaned silicon wafers, blow dried with nitrogen, and kept in petri dishes to avoid any surface contamination until needed for ToF-SIMS measurements. The surface of the Si wafers was cleaned by placing the wafers in warm acetone (ca. 15 minutes) followed by immersion in methanol (ca. 3 minutes), rinsing with deionised water, and blow drying with nitrogen.

5.2.3 High-performance liquid chromatography mass spectrometry

To support results from ToF-SIMS analysis of Cinchona bark and extract, HPLC-MS analysis was carried out. Details with respect to the HPLC-MS system, chromatographic conditions, instrumental control/setup, and data acquisition can be obtained from the experimental section in Chapter 3. A mixed standard consisting of 6.7 mg L^{-1} of Cn, Cdn, Qn and Qdn each was prepared by dilution with the eluent. The commercial composited *Cinchona* bark tincture and an extract of *Cinchona* bark (100 mg in 100 ml ethanol) were diluted with the mobile phase before the LC-MS analysis.

5.2.4 ToF-SIMS measurements

The measurements were done with a TOF-SIMS IV instrument (ION-TOF GmbH, Münster, Germany), equipped with a bismuth metal ion source as the primary ion gun. The sample to be analysed was mounted on a sample holder and introduced into the vacuum system via the load lock. The analysis position was chosen by the integrated video camera image. The bombardment of the surface was done with a 25 keV Bi^+ primary ion beam on a raster area of 500 x 500 μm^2 with a 128 x 128 pixel and 20 scans per measurement. For analysis of the bark sample, charge compensation was used as opposed to when analysis was done on a wafer. Using the positive mode, a cycle time of 100 µs was used. Secondary ions were acquired over a mass range of *m/z* 1-890. For a 1 µL of 0.1 ng μL^{-1} Qn on silicon wafer, mass resolution m/Δm of 9321 and 10872 (at 50% intensity) was obtained for a *m/z* of 160.08 ($C_{10}H_{10}NO^+$) and 325.19 ($C_{20}H_{25}N_2O_2^+$) respectively. To obtain statistically relevant data, each measurement was done thrice. Instrumental control, data acquisition, mass scale calibration and data processing were achieved with the SurfaceLab 6 (version 6.5.) software (Ion-ToF GmbH, Münster, Germany). Prior to data processing the mass spectra of the secondary ions, positive ion spectra were calibrated using H_2^+, CH_3^+, $C_2H_5^+$, $C_3H_5^+$, $C_3H_7^+$, and $C_5H_9^+$ with a maximum deviation between -37.6 ppm for CH_3^+ and +22.0 for $C_3H_7^+$. Further data processing was done using OriginLab 2015 (OriginLab, Northampton, MU, USA).

5.2.5 Laser Microscopy

To evaluate the surface roughness and other surface qualities that may have significant effect on the ToF-SIMS measurement of the bark sample, a LEXT OLS4000 3D Laser Measuring Microscope (OLYMPUS) employing a 20X objective was used. For this measurement, a thin section of same sample used in ToF-SIMS analysis was used.

5.3 Results and Discussion

Despite the advancements made in ToF-SIMS, the application of the technique in the analysis of organic compounds in environmental and natural samples is still a challenge. This is primarily due to the huge and complicated mass spectra data produced. ToF-SIMS produces both molecular species and fragments, with a mass resolution often better than 0.05 amu, given the analyst a "veritable forest of peaks" to interpret [140]. To facilitate the identification and interpretation of organic molecule in a real sample, it is necessary to analyse a reference compound in order to identify characteristic peaks expected from the analyte of interest. Prior to a ToF-SIMS measurement, initial analysis by liquid chromatography-mass spectrometry (LC/MS) with electrospray ionisation (ESI) was used here to establish a prior knowledge on e.g. the Qn molecular ion and pertinent fragments found in the *Cinchona* bark and extract. Clearly, because of the differences in the ionisation mechanisms between ToF-SIMS and ESI, the results obtained from the two techniques cannot be directly compared, but in tandem they provide useful chemical information, which further facilitates data interpretation.

The goal of this work was to exploit the advantages of ToF-SIMS in the analysis of Qn and derivatives in *Cinchona* bark and commercial *Cinchona* extract. Firstly, 1-µL droplet of 0.1 ng μL^{-1} Qn on a silicon wafer was analysed by ToF-SIMS in the positive mode, for possible characteristic secondary ions fragments from quinine and related compounds. Second, the characteristic secondary ion fragments are grouped into a peak list that is later applied for identification and interpretation of quinine and related compound in a natural sample.

5.3.1 Ionisation and fragmentation of Qn standard

Figure 5.1 shows the positive ion ToF-SIMS mass spectrum of Qn (analysed on a silicon wafer). The mass spectrum is characterised by the most intense peak at *m/z* 325 ($C_{20}H_{25}N_2O_2^+$), which is attributed to the protonated molecular ion ($[M + H]^+$) of Qn (M = $C_{20}H_{24}N_2O_2$). Despite the difference in the ionisation and fragmentation mechanism between SIMS and ESI, the $[M + H]^+$ obtained is similar to that obtained from LC/MS analysis of Qn with ESI source (*cf*. Figure A 5.1, in the appendix section). The peaks below *m/z* 325 are a result of Qn fragmentation and reorganization and, thus, could be used as a SIMS fingerprint for Qn. The most intense SIMS fragment in the lower mass region (*m/z* 1-200) is *m/z* 136 ($C_9H_{14}N^+$), which supposedly stems from the fragmentation of the C_8C_9 bond linking the quinuclidine and quinoline part of the main molecule (*cf*. Figure 5.1). The presence of *m/z*

189 ($C_{11}H_{11}NO_2^+$), attributed to the loss of $C_9H_{14}N^+$, after C_8C_9 bond (see molecular structure in Figure 5.1 for details) fragmentation, goes further to confirm the presence of *m/z* 136. At the lower mass range (*m/z* 1-100), the ions at *m/z* 27 ($C_2H_3^+$), 41 ($C_3H_5^+$), and 55 ($C_4H_7^+$) are stemming from simple hydrocarbons typically present as background in ToF-SIMS mass spectra. Here, *m/z* 73 ($C_3H_7NO^+$) and *m/z* 82 ($C_5H_8N^+$), with a relative mass accuracy of -22 and -23 ppm respectively, are considered unspecific fragments related to the molecule. As shown in Table 5.1, other specific fragments related to the Qn molecule fragments are *m/z* 160 ($C_{10}H_{10}NO^+$), 166 ($C_{11}H_{11}NO_2^+$), 309 ($C_{20}H_{24}N_2O^+$), 337 ($[C_{20}H_{24}N_2O_2 + CH]^+$), and 341 ($C_{20}H_{24}N_2O_3^+$).

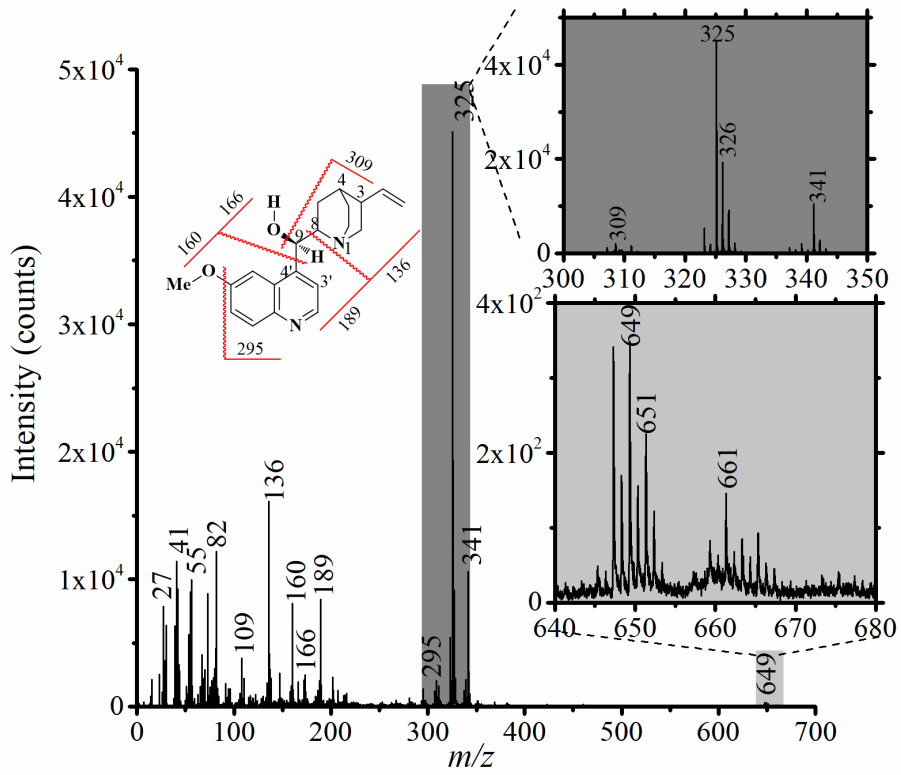

Figure 5.1: Positive time-of-flight secondary ion mass spectrometry (ToF-SIMS) spectrum of Qn standard with an interpretation of the fragmentation.

The higher relative abundance of the $[M + H]^+$ ion relative to the fragment ions in the lower mass region shows characteristics of gentle SIMS [141] in which most structurally significant ions are prominent, while degraded and rearranged fragment ions can be suppressed. Such an approach can be used to screen for Qn and derivatives in an unknown sample. In the higher mass range (*m/z* > 500), the most significant secondary ion is *m/z* 649 (m/Δm 5782) with a

proposed composition of $C_{40}H_{49}N_4O_4^+$, which is attributed to the dimer ion of Qn, $[2M + H]^+$, where M is $C_{20}H_{24}N_2O_2$.

Though the exact mechanism for the formation of the dimer ion $[2M + H]^+$ is not well understood here, dimers have been observed in SIMS mass spectra of organic compounds, especially when a neat compound present in bulk is analysed by ToF-SIMS. In the publication by Spool *et al.* [140], the SIMS spectrum of stearic acid (*m/z* 284.27) showed peak at *m/z* 569.55 (2M + H) which was attributed to dimerization of the stearic acid. In addition Bittencourt *et al.* [142] found in their ToF-SIMS characterisation of the carotenoid Bixin that dimerization commences after a temperature of 70 °C.

In this work, detailed study on some factors influencing the dimerization process was not investigated. However from analysis of the SIMS fragments of different quinine concentrations on silicon wafer, it can be postulated based on the ion counts that, at lower concentrations (< 0.1 ng μL^{-1} on silicon wafer), the dimerization of Qn that tend to bring two Qn molecules into close proximity is less probable. It is worth stating that the necessary close proximity of several Qn molecules depends on the concentration of the solution and the drying behaviour of the spotted droplet.

In addition to the dimer peak, another pertinent peak is that at *m/z* 661 that can be ascribed to ion of the form 2M + CH, which in this case is. $C_{41}H_{50}N_4O_4^+$. This methylation process of the dimer is similar to that seen at *m/z* 337 $(C_{20}H_{24}N_2O_2+CH)^+$.Though a direct explanation to its formation is not understood, it can be because of methylation of the dimerized molecule. The source of the methyl group can be from hydrocarbons in the SIMS system, contaminant on the wafer, fragments from the molecule, joined effect of these or other sources. Considering the methoxy (CH_3 - O) functional group of Qn, fragmentation of the group from the molecule will make the analyte surface rich in methyl ion. Subsequently, there is a possibility that the dimerized ion picks up a CH group after collision with a methyl ion rich surface. Actually this possibility, though not with a similar molecule, has been suggested by Cooks *et al.* [143], in a study where a benzene ion picked up CH after collision with a hydrocarbon-rich surface. A summary of the distinctive SIMS fragments that resulted from the bombardment of a Qn standard on a silicon wafer are listed on Table 5.1.

Table 5.1: Characteristic positive secondary ion mass spectrometry (SIMS) fragment peaks for quinine standard

Nominal mass (*m/z*)	Exact mass (*m/z*)	Relative mass accuracy (ppm)	Fragments ions	Source
82	82.0657	21	C_5H_8N+	[M + H-$C_{15}H_{17}NO_2$]+
109	109.0891	-4	$C_7H_{11}N$+	[M + H-$C_{11}H_{11}NO_2$-C_2H_3]+
136	136.1121	15	$C_9H_{14}N$+	[M-$C_{11}H_{11}NO_2$]+
166	166.1232	20	$C_{10}H_{16}NO$+	[M + H-$C_{10}H_9NO$]+
189	189.0790	-3	$C_{11}H_{11}NO_2$+	[M-$C_9H_{14}N$]+
309	309.1967	13	$C_{20}H_{25}N_2O$+	[M + H-O]+
325	325.1916	6	$C_{20}H_{25}N_2O_2$+	[M + H]+
341	341.1865	7	$C_{20}H_{25}N_2O_3$+	[M+O]+
649	649.3754	-18	$C_{40}H_{49}N_4O_4$+	[2M + H]+

M = $C_{20}H_{24}N_2O_2$

The relative mass accuracy and the source of the different fragments are a challenging task because the intensity (total ion counts, TIC) of the signal in the mass spectrum depends on different factors such as the actual surface concentration of the species, the primary ion flux, and the transformation probability of the species, which also depend on the matrix in which the species is found [144,145]. Figure 5.2 shows mass signal intensity for protonated molecular ion of Qn (*m/z* 325.19) after ToF-SIMS analysis of Qn standards on a silicon wafer. The expected overall linearity between mass signal and the effective surface concentration was not achieved. The signal response for a standard on the wafer varies from one spot to another leading to an overall large standard deviation in the signal response. The varying signal resulted from the heterogeneity of the deposit formed after drop-drying 1 µL of standard on the wafer. The heterogeneous deposits implies that the monolayer distribution of the analyte was inhomogeneous at different spots and the ion counts obtained after bombardment depend on the thickness of the monolayer, the distribution of the molecule on the spot and the precision in analysing the spot.

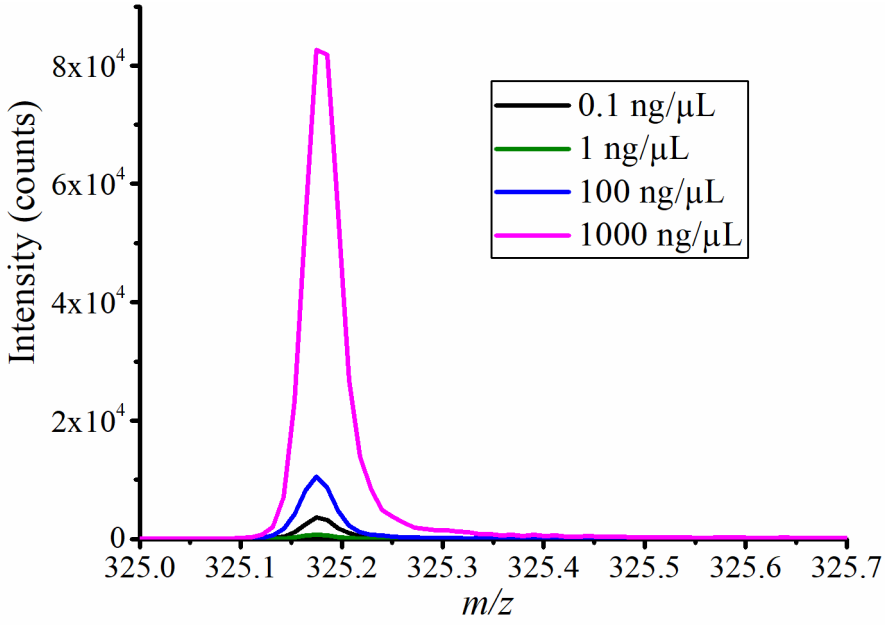

Figure 5.2: ToF-SIMS signal intensity for protonated molecular ion of Qn (*m/z* 325.19, $C_{20}H_{25}N_2O_2^+$, total counts (TIC) in a 500 x 500 µm image) from different Qn standards drop-dried on silicon wafer.

In physical chemistry and wetting science, such effect is referred to as "coffee stain effect" where heterogeneous deposits are formed upon evaporation of drops of complex fluids, solutions and suspension [146]. As a result of the heterogeneity the ion count especially from the protonated molecular ion did not vary proportionally with the concentration of the analyte, thus hampering quantitative analysis (*cf.* Figure A 5.2 in the appendix section).

5.3.2 Characterisation of *Cinchona* bark

Generally, ToF-SIMS analysis of standards gives characteristic peaks or fingerprints, which are useful in spectroscopy to identify the molecule especially when it is present in a sample mixture containing other chemical species. In addition, if the sample does not contain chemical species that generate the same molecular ion or characteristic secondary ion fragments similar to the standard molecule, then the characteristic peaks of the standard molecule can be used to map the distribution of the molecule in a sample. Usually, the fact that a pure and neat molecule is detected with ToF-SIMS does not necessary guarantee its detection in a real world sample. This is true primarily because a real world sample is usually characterised with co-existing organic molecules in the sample matrix, sample topographical variation or a combine effect of these. These characteristic affects the sensitivity, signal-to-noise and mass resolution for ejected ions from a real world sample. Figure 5.3 shows a 3D

laser microscope image (top row) and a secondary ion image of *Cinchona* bark (bottom row). As can be seen from the microscopic image, the bark surface shows varying topography at different spots on the surface. The blue colour of the bark corresponds to the lowest measured height in the image whereas the red colour represents the highest measured height. In addition, the images show a "ridge-like" structure with different heights on the surface. As stated in Table 5.1 in the Appendix Section, a root mean square roughness (Sq.) of 7.66 µm ± 1.4 nm was measured for the *Cinchona* bark.

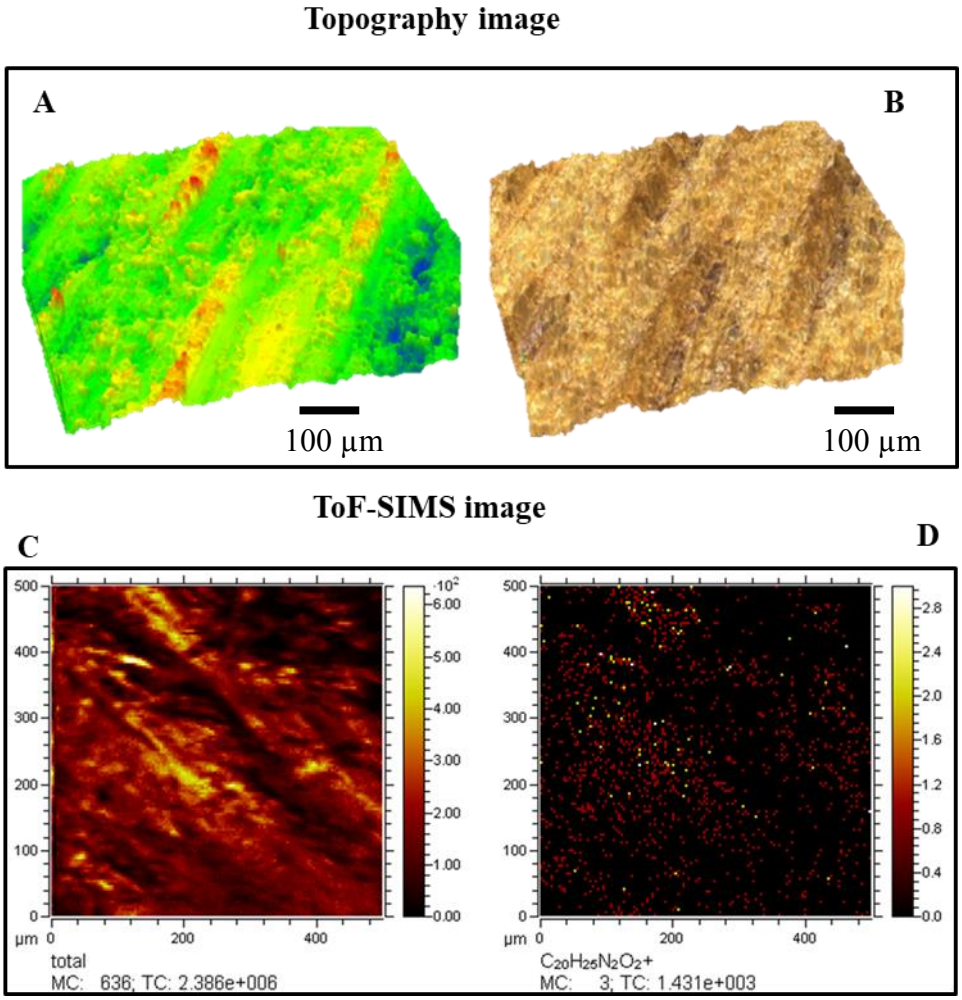

Figure 5.3: A 3D laser microscope image (top column) and secondary ion images (bottom column) of *Cinchona* bark showing topographical effect and ion distribution respectively. Top column: (a) Enhanced image, (b) real image of sample; bottom column: (c) total ion and (d) Qn (*m/z* 325.19, $C_{20}H_{25}N_2O_2^+$) image.

ToF-SIMS, which is a surface analysis technique capable of an average analysis depth of less than 2 nm, analysis of such a sample with topographical effects is challenging. From the ToF-SIMS total ion image acquired in the positive mode shown in Figure 5.3 (bottom left); the

contrast is distinctive with maximum ion counts found at the uppermost and minimum ion counts at the lowest part of the "ridge-like" structure.

The SIMS ion image of *m/z* 325 ($C_{20}H_{25}N_2O_2^+$) in Figure 5.3 (bottom right) also shows similar contrast with the ions found mainly at the upper part of the "ridge-like" structure. Figure 5.4 shows the corresponding mass spectrum from the SIMS images shown in Figure 5.3. At the lower mass region (*m/z* 1-100), the mass spectrum is characterised by *m/z* 27, 41, 55 and 69 which as stated in the ionisation of quinine standard above, could be attributed to $C_2H_3^+$, $C_3H_5^+$, $C_4H_7^+$, and $C_5H_9^+$ respectively. Other peaks at *m/z* 81, 91, 95 and 105 are characteristic peaks for polysaccharides and lignin usually on the cell walls of plants [147]. In addition to the masses at the lower mass region, the intense peak at *m/z* 39 can be attributed to K^+, an essential nutrient needed in plant growth processes. The intense peak at *m/z* 147 ($C_9H_7O_2^+$), is a characteristic positive ion peak that is descriptive of polydimethylsiloxane (PDMS) [147,148].

Before interpreting the *m/z* > 270 it is worth recalling that *Cinchona* bark contains *Cinchona* alkaloids as diastereomers. The main component, Qn and its pseudo-enantiomer, Qdn have same chemical formula ($C_{20}H_{24}N_2O_2$, mass = 324.18), while Cn and its pseudo-enantiomer, Cdn have same chemical formula ($C_{19}H_{22}N_2O$, mass = 294.17). Since ToF-SIMS is (until now) unable to separate enantiomers by their mass, the signal and ion image at *m/z* 325 ($C_{20}H_{24}N_2O_2^+$) should be interpreted as coming possibly from Qn and/or Qdn and at *m/z* 295 ($C_{19}H_{23}N_2O^+$) coming from Cn and /or Cdn.

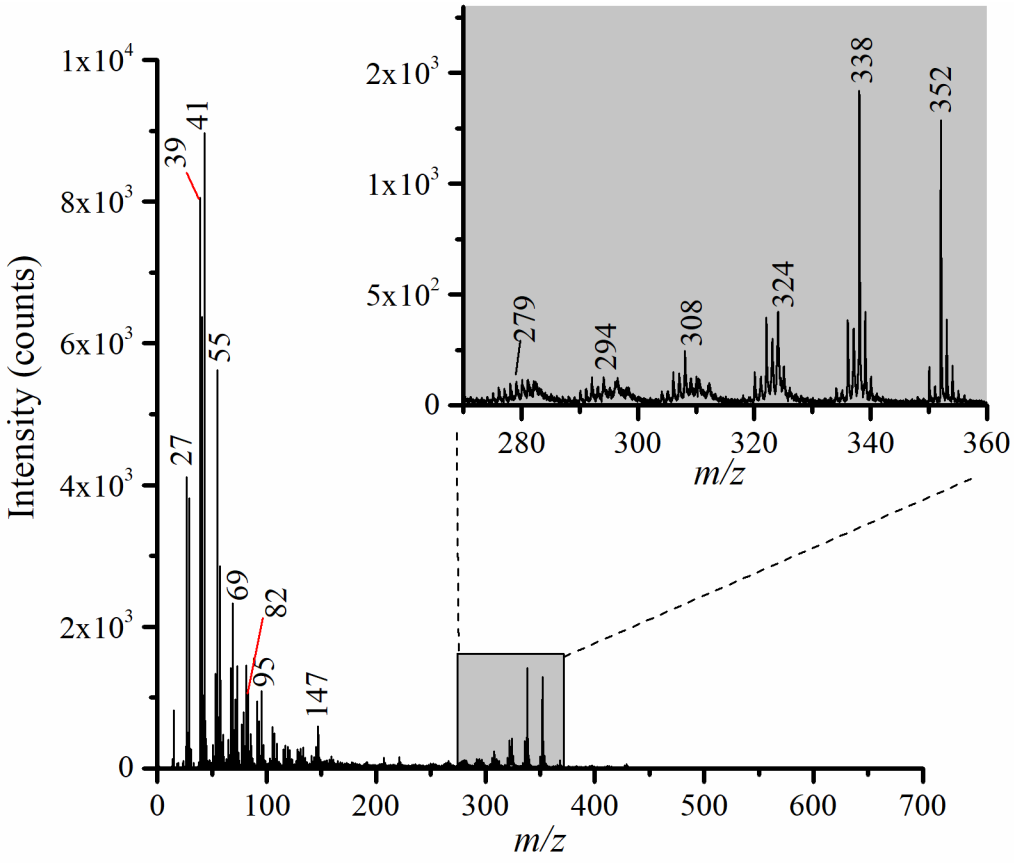

Figure 5.4: Positive SIMS spectrum of *Cinchona* bark, showing sparsely presence of Qn.

Considering the peaks > *m/z* 270, some characteristic fragments related to Qn derivatives are *m/z* 294 ($C_{19}H_{22}N_2O^+$), 324 ($C_{20}H_{24}N_2O_2^+$), 338 ($C_{21}H_{26}N_2O_2^+$) and 352 ($C_{22}H_{28}N_2O_2^+$). In the mass spectrum at Figure 5.4, the peaks at *m/z* 295 ($C_{19}H_{23}N_2O^+$) and 325 ($C_{20}H_{25}N_2O_2^+$), attributed to the protonated molecular ion of Cn/Cdn and Qn/Qdn respectively, portrays poor signal-to-noise ratio and mass resolution. Table 5.2 summarizes the characteristic peaks found in the analysis of *Cinchona* bark. These were obtained by applying the generated secondary ion peak list for Qn standard to the mass calibrated mass spectra from bark analysis. Also stated in Table 5.2 are two most intense secondary ions at *m/z* 338 ($[C_{20}H_{24}N_2O_2 + CH]^+$) and 352 ($[C_{20}H_{24}N_2O_2 + C_2H_4]^+$), which are alkaloids coming from possible molecular transformation of molecular Qn or Qdn during the drying or storage process. In a similar manner, the *m/z* 307 ($[C_{19}H_{22}N_2O + CH]^+$) and 322 ($[C_{19}H_{22}N_2O + C_2H_4]^+$) are secondary ions coming from a possible transformation of Cn or Cdn.

Table 5.2: Positive SIMS fragments from ToF-SIMS analysis of *Cinchona* bark (From mass spectrum in Figure 5.4).

Nominal mass (*m/z*)	Exact mass (*m/z*)	Relative mass accuracy (ppm)	Fragment ions	Possible source
82	82.0657	41	$C_5H_8N^+$	Qn derivative
109	109.0891	52	$C_7H_{11}N^+$	〃
136	136.1121	96	$C_9H_{14}N^+$	〃
147	147.0446	4	$C_9H_7O_2^+$	PDMS
160	160.0762	-84	$C_{10}H_{10}NO^+$	Qn derivative
166	166.1232	-19	$C_{10}H_{16}NO^+$	〃
189	189.0790	2	$C_{11}H_{11}NO_2^+$	〃
295	295.1810	-86	$C_{19}H_{23}N_2O^+$	〃
309	309.1967	-1	$C_{20}H_{25}N_2O^+$	〃
325	325.1916	-35	$C_{20}H_{25}N_2O_2^+$	〃
338	338.1994	>100	$C_{21}H_{26}N_2O_2^+$	Qn derivatives
352	352.2151	>100	$C_{22}H_{28}N_2O_2^+$	〃

In addition to the aforementioned factors affecting ToF-SIMS analysis for real world samples with topography, a limited signal-to-noise ratio and mass resolution can be attributed to artefacts during ion extraction and detection. Such variation in the mass spectra and ion image has been studied in detail for an insulating sample by Lee *et al.* [149]. In their study (fibre mounted on a conducting surface), they showed that secondary ions emitted from the site of the fibre are accelerated by a larger potential difference than ions emitted from the top. In the same study, it was stated that because of the potential difference, the same ion from different locations on the sample surface would arrive at the time-of-flight detector at different times resulting in limited mass resolution in the overall mass spectra. In addition, it was proposed that the varying surface potential goes further to influence the instrumental setting that determines the energy of acceptance of the reflectron mass analyser. In this analysis, it can be said that secondary ions from different locations on the sample surface

migrated with different kinetic energy to the time-of-flight detector. In addition, possible interference with other co-existing molecular ions affect the overall signal-to-noise ratio and mass resolution of the detection. Such topographical effects mentioned above can be reduced through the use of extraction delay in SIMS, which allows extraction voltage to be switch on several microseconds after primary ion impact, allowing secondary ions to be less distorted by topographical sample [149]. Unfortunately this feature is not available on the ToF-SIMS model IV used here.

In Figure A 5.3 in the appendix section, the LC-MS results for the analysis of 100 mg bark powder in 100 mL ethanol, shows the presence of the protonated molecular ion at *m/z* 338 ($C_{21}H_{26}N_2O_2^+$) and 352 ($C_{22}H_{28}N_2O_2^+$) which goes further to supports the ToF-SIMS results. Based on the assumption that *m/z* 338 and 352 are from possible transformation of quinine molecule, one can say the *Cinchona* bark was richer in Qn/Qdn than in Cn/Cdn. A detailed study on the reason for this possible transformation or if these peaks were inherent to this sample was not conducted. Despite the poor S/N and the mass resolution, ToF-SIMS proof to be a useful tool for direct analysis of quinine and related derivatives in *Cinchona* bark via their protonated molecular ion. The S/N for the measurements can be increased via sputtering the surface.

5.3.3 Characterisation of *Cinchona* extract

As stated above, ToF-SIMS analysis of standard gives characteristic peaks or fingerprint which is useful in spectroscopy to identify the molecule especially when it is present in a sample mixture containing other chemical species.

The mass spectrum in Figure 5.5 is Characterised by *m/z* 295 ($C_{19}H_{23}N_2O^+$) and 325 ($C_{20}H_{25}N_2O_2^+$) that correspond to the protonated molecular ions of Cn/Cdn and Qn/Qdn respectively. The characteristic SIMS fragments (*m/z* 109, 136, 160, 166, 189 and 325) that define the ToF-SIMS mass spectra in Figure 5.1 are also seen in the mass spectrum for the commercial *Cinchona* extract shown in Figure 5.5. This shows that the mass spectra for the Qn standard can be used to map the presence of Qn in this sample. The peak appearing at *m/z* 297 and 327 can be attributed to the protonated molecular ion of DCn/DCdn ($C_{19}H_{25}N_2O^+$) and DQn/DQdn ($C_{20}H_{27}N_2O_2^+$) respectively. The attribution of the mass to charge to the respective quinine derivative is supported by the LC-MS results from the analysis of the commercial extract (*cf.* Figure A 5.5 in the appendix section). Fragments at the lower mass range are associated with molecular fragmentation due to impact of emitted ion with primary

ions. Figure 5.6 shows a suggested fragmentation pattern of Cn/Cdn and Qn/Qdn based on the positive SIMS spectra shown in Figure 5.6. As stated above, Cn and Qn cannot be differentiated from Cdn and Qdn respectively, due to their similarity in chemical formula and mass. Nevertheless, as shown in Figure 5.5 and Table 5.3, in addition to their protonated molecular ions, Cn/Cdn can be differentiated from Qn/Qdn by their characteristic secondary ion at *m/z* .130, 159, and 279 for Cn/Cdn and 160, 189, and 309 for Qn/Qdn. That is to say in ToF-SIMS analysis of Cinchona alkaloids, *m/z* 130, 159 and 279 can be used as finger print fragment for Cn or Cdn, and *m/z* 160, 189 and 309 for Qn or Qdn. Also shown in Table 5.3 is the fact that secondary ions at *m/z* 82, 109, 136 and 166 are characteristic to both Cn/Cdn and Qn/Qdn.

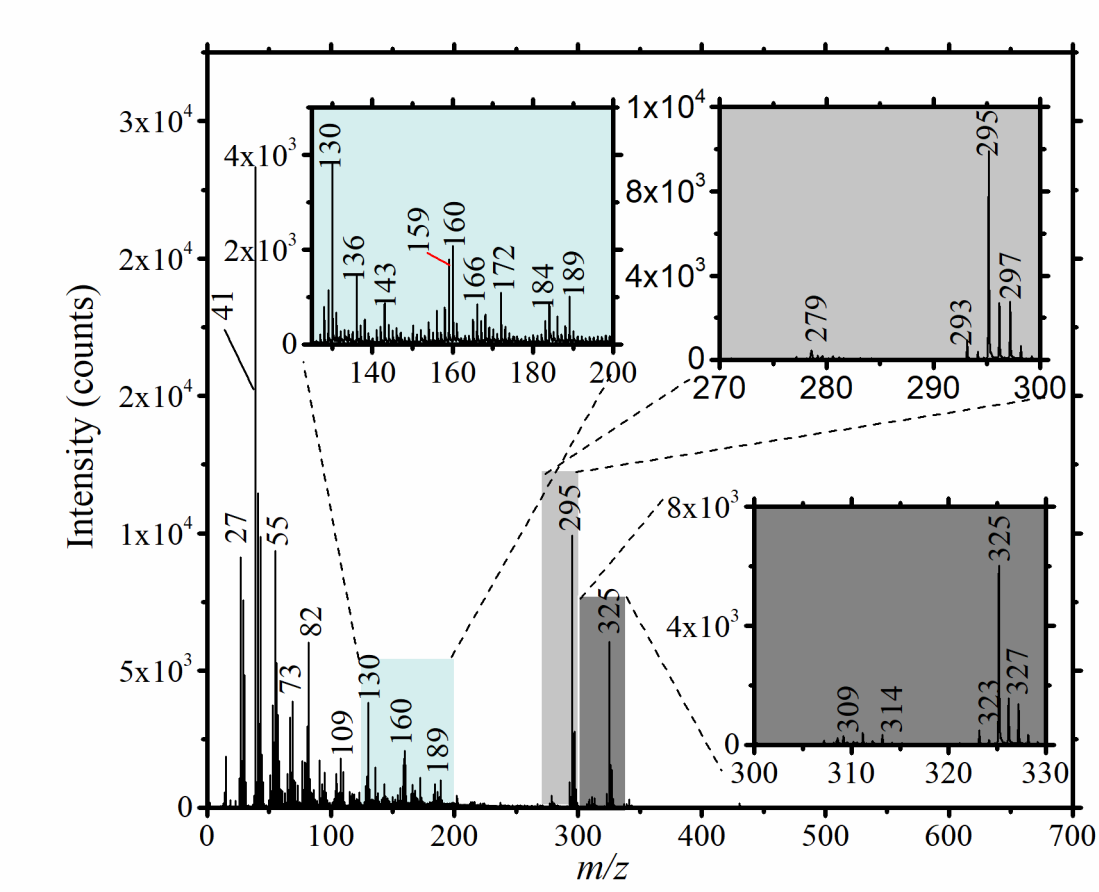

Figure 5.5: Positive ToF-SIMS spectrum of *Cinchona* bark extract showing protonated molecular ion of Cn/Cdn (*m/z* 295), DCn/DCdn (297), Qn/Qdn (*m/z* 325), and DQn/DQdn (327).

Table 5.3: Characteristic positive secondary ion mass spectrometry (SIMS) fragment peaks for quinine derivatives in *Cinchona* extract.

Nominal mass (*m/z*)	Exact mass (*m/z*)	Relative mass accuracy (ppm)	Fragments	Source
15	15.0235	-22	CH_3+	Qn/hydrocarbon
31	31.0184	-13	CH_3O+	Qn
42	42.0344	-2	C_2H_4N+	Qn/Cn
55	55.0548	27	C_4H_7+	Hydrocarbon
82	82.0657	5	C_5H_8N+	[M + H - $C_{15}H_{17}NO_2$]+ [M′ + H - $C_{15}H_{15}NO$]+
109	109.0891	52	$C_7H_{11}N$+	[M + H - $C_{11}H_{11}NO_2$ - C_2H_3]+ [M′ + H- $C_{10}H_9NO$- C_2H_3]+
130	130.0657	-14	C_9H_8N+	[M′+H - $C_{10}H_9NO$]+
136	136.1126	22	$C_9H_{14}N$+	[M + H - $C_{11}H_{11}NO_2$]+ [M′+H - $C_{10}H_9NO$]+
159	159.0684	-0.3	$C_{10}H_9NO$+	[M′+H - $C_9H_{14}N$]+
160	160.0762	28	$C_{10}H_{10}NO$+	[M + H - $C_{10}H_{16}NO$]+
166	166.1232	-19	$C_{10}H_{16}NO$+	[M + H - $C_{10}H_{16}NO$]+ [M′+H - $C_{10}H_9NO$]+
189	189.0790	-13	$C_{11}H_{11}NO_2$+	[M + H - $C_9H_{14}N$]+
279	279.1861	-49	$C_{19}H_{23}N_2$ +	[M′+H - O]+
295	295.1810	-41	$C_{19}H_{23}N_2O$+	Cn/Cdn
297	297.1967	-59	$C_{19}H_{25}N_2O$+	HCn/HCdn
309	309.1967	-38	$C_{20}H_{25}N_2O$+	[M + H - O]+
325	325.1916	-36	$C_{20}H_{25}N_2O_2$+	Qn/Qdn
327	327.2073	-80	$C_{20}H_{27}N_2O_2$+	HQn/HQdn

M = $C_{20}H_{24}N_2O_2$, M′ = $C_{19}H_{22}N_2O$

The dimerization of Qn noticed in the SIMS spectra of the Qn standard was not visible in either the analysis of *Cinchona* bark or the extract. Firstly this could be because the alkaloids in the natural samples are not pure and it is known that dimerization in ToF-SIMS readily occurs when pure compounds are available. Secondly, assuming dimerization is still possible for a compound found in natural sample, the dimer signal intensity could be much lower than the detection limit of the instrument. The second possibility could be ruled out because, while the SIMS spectrum of the sample shows a Qn signal with higher intensity relative to Qn in the standard, it felt short of showing Qn dimer, which characterise the SIMS spectrum of Qn standard.

Though ToF-SIMS did not differentiate the enantiomers, it has proven to be valuable technique in direct analysis of *Cinchona* alkaloids, providing information on the presence of *Cinchona* alkaloids in the extract.

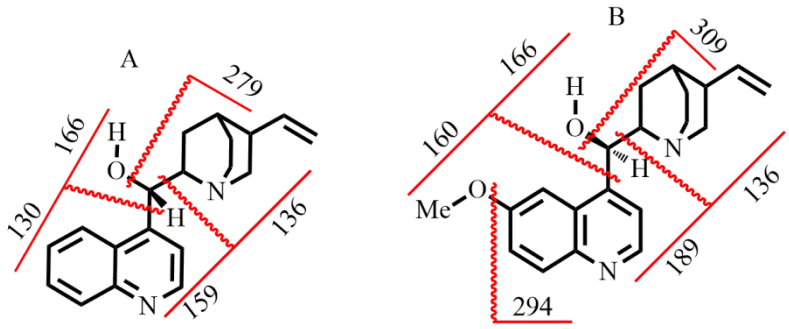

Figure 5.6: Suggested fragmentation pattern of A) Cn/Cdn and B) Qn/Qdn according to ToF-SIMS spectra in Figure 5.5.

5.3.4 Detectability of quinine from bark vs. extract

The ToF-SIMS mass spectra in Figure 5.8 shows protonated molecular ion of Qn (*m/z* 325.17, $C_{20}H_{25}N_2O_2^+$) from Qn standard, Cinchona bark and extract. As can be seen in Figure 5.8, while the peak width for Qn in the extract is comparable to that from the Cinchona extract, that for the Cinchona bark is characterise by a broader peak width. As can be obtained from Figure 5.7, Table 5.2 and Table 5.3 above, the mass deviation for *m/z* 325 is highest for the bark sample. The better peak shape for the extract is on the one hand due to lesser topographical effect as the analysis was done on a silicon wafer. On the other hand, there are limited co-existing organic molecules such as lignin and cellulose, which must have been removed during the extraction process. It is worth noting that same effect was noticed for other secondary ions from the three different matrices. The fact that quinine is detected as

protonated molecular ion from both *Cinchona* bark and *Cinchona* extract, shows that a large fragment of the quinine molecule is preserved after TOF-SIMS analysis and thus can be applied for quality control and degradation studies. Despite the matrix effect and topographical effect, TOF-SIMS under the right instrumental condition has proven to be capable of detecting quinine and derivatives.

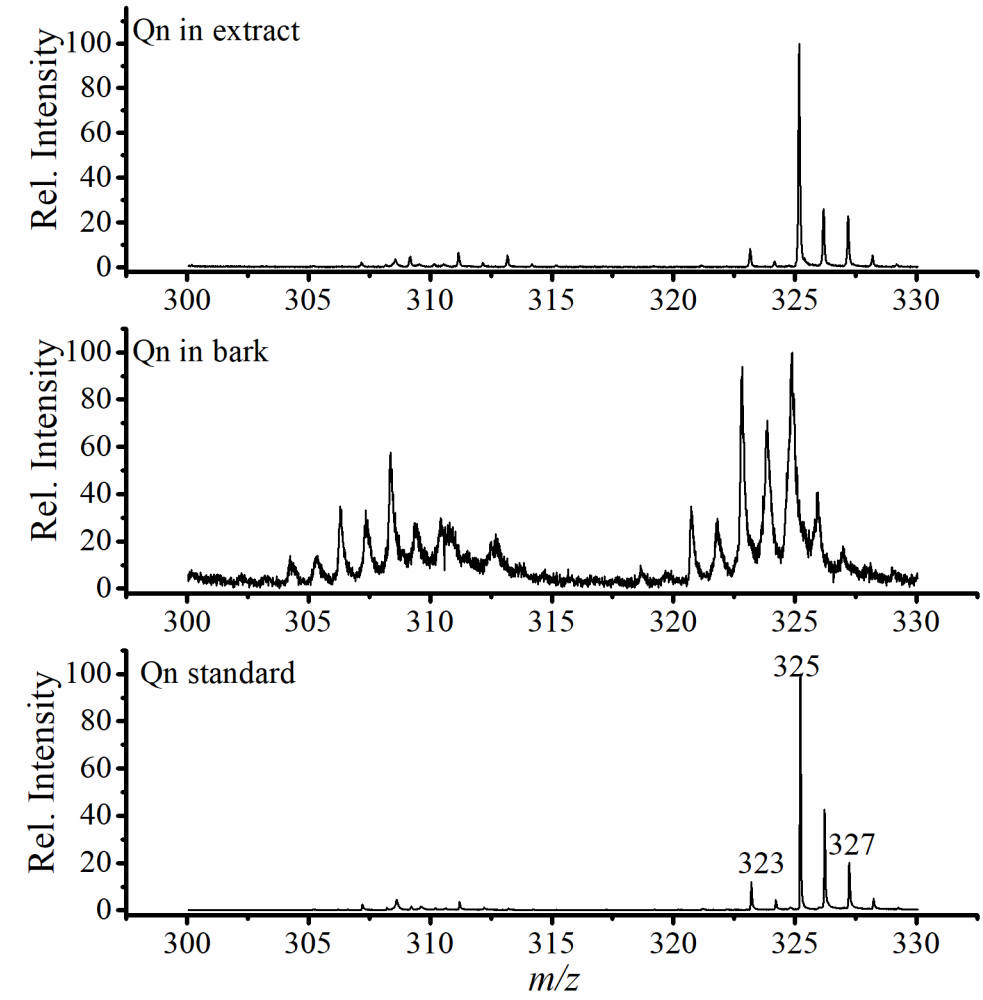

Figure 5.7: Positive ToF-SIMS spectra showing protonated molecular ion of Qn from quinine standard, *Cinchona* bark and extract.

5.4 Conclusion and Future Perspectives

In this chapter, a fast and direct qualitative screening analysis method for *Cinchona* alkaloids in *Cinchona* bark and *Cinchona* extracts using ToF-SIMS is presented. Compared to standard protocols that would include e.g. time-consuming soxhlet extraction and chromatography of natural bark extracts, ToF-SIMS provides direct surface analysis capabilities, works with small sample sizes, and does not require extensive sample preparation or the use of chemicals. After careful characterization, ToF-SIMS was successfully used in identifying Qn and derivatives present in *Cinchona* bark. In addition, commercially available *Cinchona* extract were probed and characteristic fingerprints of fragment ions were used to identify Cn and Cdn (*m/z* 130, 159, and 295) as well as Qn and Qdn (*m/z* 160, 189, 309, and 325). The results were validated with HPLC-ESI/MS. While HPLC-ESI/MS can be used for quantitative analysis, ToF-SIMS is typically not able to provide quantitative results for a large variety of compounds and in complex samples. This is also valid in this chapter, where matrix effects in solid samples and the formation of coffee-ring effects for dried liquid samples were observed. Further, mass resolution was negatively affected by the bark surface roughness. In the future, this could be improved by e.g. the use of delayed extraction in the mass spectrometer (not available on the ToF-SIMS model used) and by preparation of flat surface pellets of the *Cinchona* bark. Also, a detailed optimisation of instrumental parameters (see Lee *et al*.[149]) might help to improve the ToF-SIMS performance when samples with significant topography are to be analysed. As a general trend, signal-to-background ratios and relative mass accuracy values were better in the analysis of *Cinchona* extract compared to *Cinchona* bark.

In conclusion, ToF-SIMS is considered to be an attractive tool for fast screening of pharmaceuticals ingredient in natural samples. In the future, improved semi-quantitative results could be obtained in dried liquid samples by the use of e.g. internal deuterated standards and dedicated wafer substrates that prevent coffee-ring effects. Clearly, due to the inability of ToF-SIMS to differentiate enantiomers and to perform quantitative analysis, complementary techniques such as HPLC-MS are of added value in natural product research.

Appendix for Chapter 5

Bark sample preparation. *Cinchona* bark with a dimension of ca 40 x 10 cm^2 was obtained from a forest region, Southwest of Cameroon. The bark was sun dried to enhance preservation. The bark was further dried at 80 °C to a constant weight using laboratory oven set at 80 °C. The dried sample was milled using a milling pot. The powder was passed through a mesh sieve to remove ungrounded fibres and larger particles.

A 100 mg of the powder was extracted with 100 mL ethanol in the ultrasonic bath at 60 °C for 30 minutes. After sedimentation, a clear supernatant was filtered with a syringe filter (pore size 0.2 μm) and kept for analysis.

Table A 5.1: Surface roughness parameters for *Cinchona* bark obtained from 3D laser microscope.

	Roughness parameters	**Values**
Sa	Average roughness	5.78 μm ± 1.0 nm
Sq.	Root mean square roughness	7.66 μm ± 1.4 nm
Ssk	Skewness	0.41 ± 0.1
Sku	kurtosis	4.68 ± 1.2
Sv	Maximum profile valley depth	96.09 μm ± 2.6 nm
Sp	Maximum profile peak height	97.70 μm ± 4.2 nm
Sz	Ten-spot average roughness	193.79 μm ± 6.8 nm

Uncertainty measured according to NIST measurements of roughness height parameters

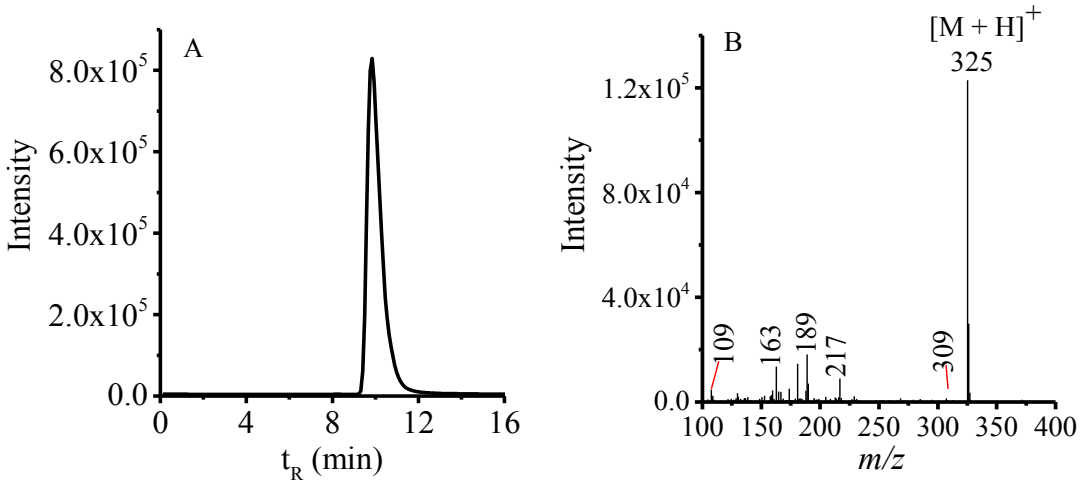

Figure A 5.1: Liquid chromatography-mass spectrometry of Qn. A) Mass chromatogram, B) mass spectra. Column: XBridge C_{18}, 3.5 µm, 150 x 4.6 mm Mobile phase: MeOH/water (50/50) with 0.1% FA in water, pH= 3.0, column temperature = 80 °C, flow rate: 1.0 mL min^{-1} with post-column splitting. Injection volume: 20-µL. Detection: Micromass Quattro LC MS in positive electrospray (ESI+) mode; capillary voltage: 3.5 kV; cone voltage: 50 V.

Heterogenous deposit. As can be seen from Figure A 5.2, the ion image of protonated molecular ion that results from different concentrations of Qn on silicon wafer shows variability in the spot size, shape and homogeneity.

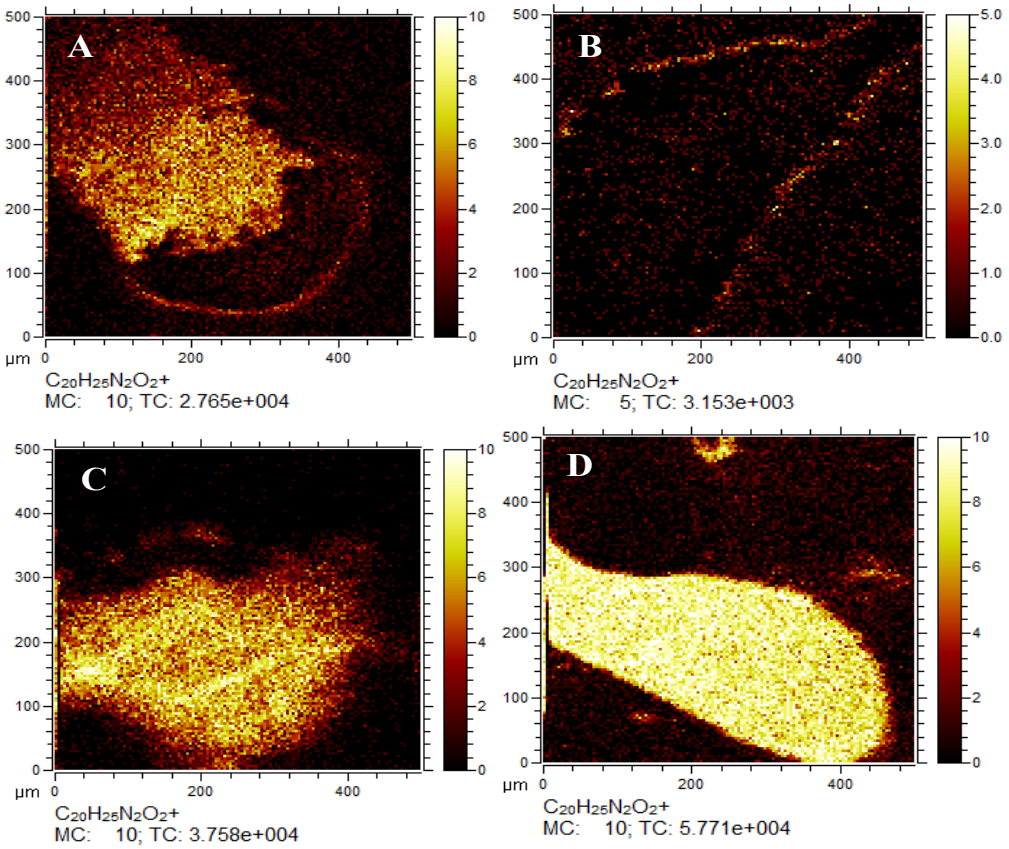

Figure A 5.2: Coffee-stain effect seen on the SIMS image of protonated molecular ion of Qn. A = 0.1 ng μL^{-1}, B = 1 ng μL^{-1}, C = 100 ng μL^{-1} and D = 1000 ng μL^{-1} of Qn standard on silicon wafer.

This is as a result of the nature of the deposit formed after blow-drying the solution on the silicon wafer. As is evident from Figure A 5.2, the protonated molecular ion of Qn is found at the edges of the "coffee stain ring". This is because in the course of blow-drying with nitrogen, the solution was pushed towards the edge. The coffee stain artefact does not only affect the ion image and the signal intensity from the spot but also goes further to pose challenges in quantification and data interpretation. The coffee stain effect can be minimised by controlling the solution deposition and the drying process. Even then, the nature of the monolayer bonding will still have an effect on the intensity of the ejected secondary ions.

LC-MS of extracted bark powder. To elucidate the intense peak at *m/z* 338 and 352, seen in the ToF-SIMS spectra, 100 mg bark powder was extracted in a 100 mL ethanol. Soxhlet extraction, a reference method for extraction of quinoline alkaloids from *Cinchona* bark powder after treatment with alkali could not be used because large sample amount and long operation time required.

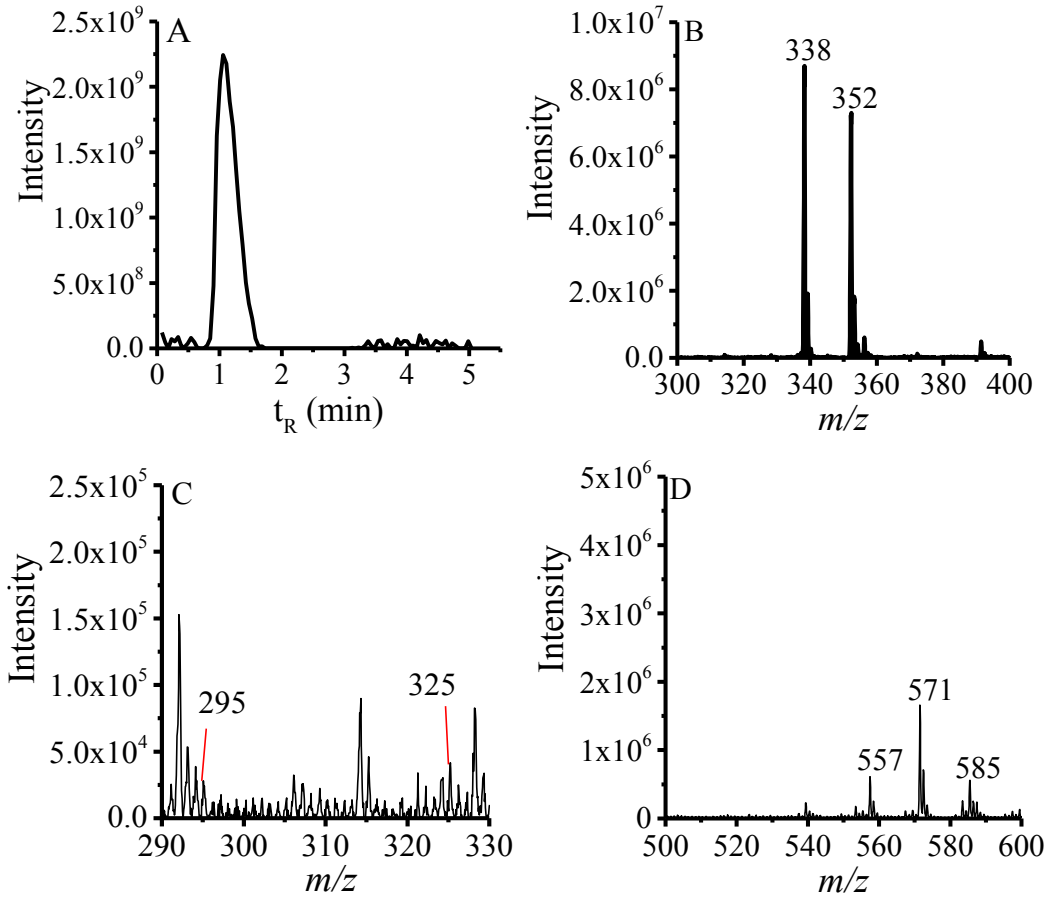

Figure A 5.3: LC-MS analysis of ethanol extract of *Cinchona* barks powder. A) Mass chromatogram, B-D) Mass spectra at different *m/z* intervals. LC condition: Instrument: Accela LC system; flow injection: 150 µl min^{-1}; mobile phase: MeOH/water (50/50) with 0.1% FA in water. Detector: Quattro LC mass spectrometer operated in positive ESI mode.

HPLC-MS analysis of *Cinchona* extract. The mass chromatogram shows the separation of quinine and derivatives after a high temperature liquid chromatography on an XBridge C_{18} column. The standard mixture used in the analysis contains 6.7 mg L^{-1} each of Cn, Cdn, Qdn and Qn. The broader nature of peak 6 in the mass chromatogram is due to co-elution of hydrocinchonidine and quinine. Selected ion recording (SIR) chromatogram for *m/z* 297.4 shows a peak at same retention time as quinine. The *Cinchona* extract shows peak of the *Cinchona* alkaloid standards. In addition to the known peaks, there are other minor peaks before the retention time, 8 minutes and after the elution of Qdn, which can probably be attributed to some other impurities with same mass-to-charge as those in the SIR scan mode.

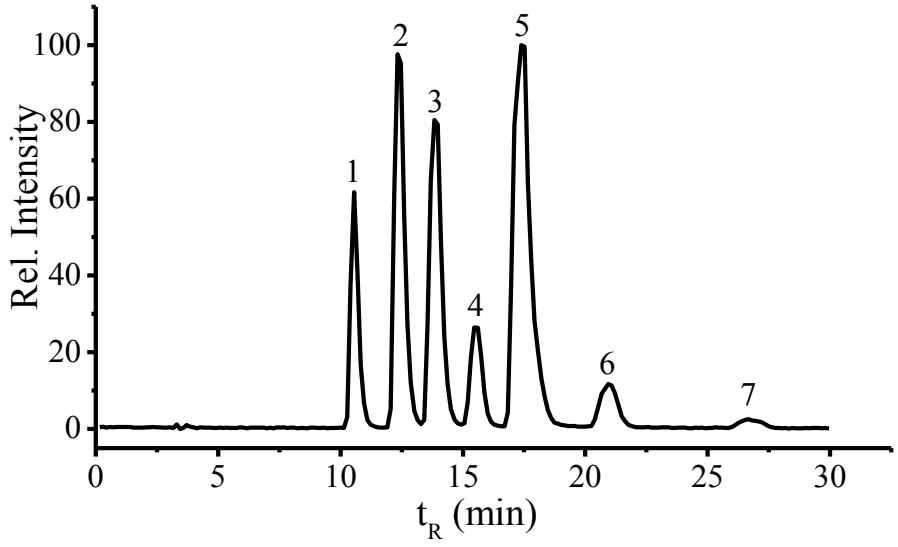

Figure A 5.4: SIR mass chromatogram of protonated molecular ion of Qn and derivatives standard: 1) Cn (*m/z* 295.14), 2) Cdn (*m/z* 295.14), 3) Qdn (*m/z* 325.18), 4) DCn (*m/z* 297.14), 5) DCdn (*m/z* 297.18)/Qn (*m/z* 325.18), 6) DQdn (*m/z* 327.18), 7) DQn (*m/z* 327.18). Column: XBridge C_{18}, 150 x 4.6 mm, 3 µm particles; Column temperature 80 °C. Mobile phase: MeOH/water (10/90) with 0.1% FA in water, pH 3.0). Detector: Quattro LC mass spectrometer.

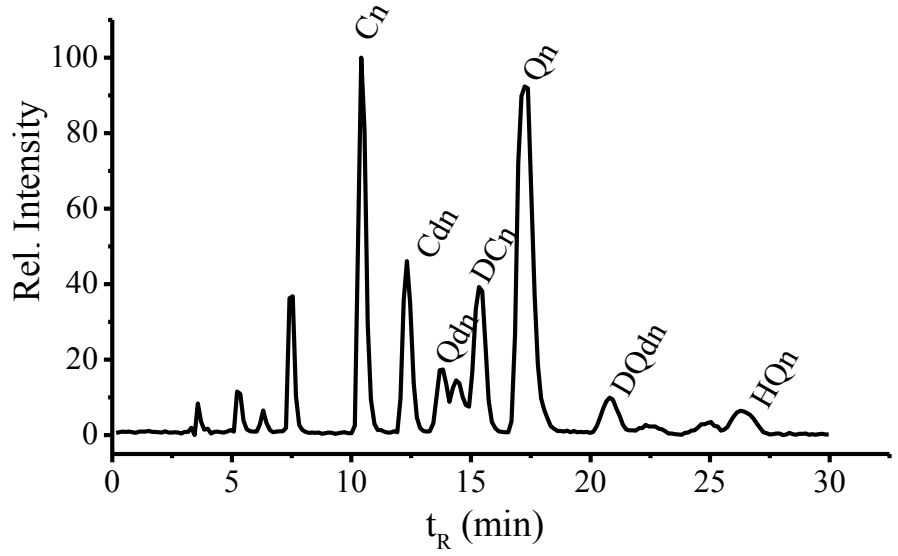

Figure A 5.5: SIR mass chromatogram of protonated molecular ion of Qn and derivatives in *Cinchona* extract. The peak identities are shown on the chromatogram. The LC and MS conditions are same as in Figure A 5.4.

Chapter 6

Rapid Qualitative Screening of Antimalarials Using Low-Temperature Plasma Desorption/Ionisation Orbitrap Mass Spectrometry

Abstract

Antimalarial drugs for the treatment of malaria are amongst the most counterfeit drugs in third world countries. An analytical technique capable of rapid determination of active pharmaceutical agents in real drug samples with minimal sample preparation is a useful tool for quality control in the pharmaceutical industry, in the search for illicit drugs, and consumer safety. Low-temperature plasma mass spectrometry (LTP-MS) has the ability to carry out rapid analysis of samples in their native form with minimal sample preparation and is a promising tool for qualitative screening. In this chapter, a direct analysis method for the characterization of active ingredients in Coartem (artemether, lumefantrine) and Malarone (atovaquone, proguanil hydrochloride) tablets using a high-resolution mass spectrometer (HR-MS) and a home-built LTP desorption/ionisation source was developed and optimised. Direct tablet analysis is completed in less than three minutes and does not require extensive sample preparation or the use of solvents. This is considered a significant benefit compared to spray-based ambient desorption/ionisation methods or even a conventional high performance liquid chromatography (HPLC) approach. Artemether and lumefantrine in Coartem were detected directly both as their protonated molecular ions in LTP-HRMS. Atovaquone was detected after solvent extraction of Malarone. In addition, LTP-HRMS provided characteristic fragment ions of the target molecules that aided in their structural identification even in the presence of a tablet matrix. LTP-HRMS results were validated by HPLC-MS analysis of the samples under investigation.

Based on: D.N. Ateacha, C. Kuhlmann, C. Engelhard, submitted for publication

6.1 Introduction

State-of-the-art analytical techniques to control the quality of antimalarial drugs include calorimetry,[7,8] gas chromatography (GC),[9,10] thin layer chromatography (TLC),[11,12] supercritical fluid chromatography (SCFC),[13] spectroscopy[14-18] and high-performance liquid chromatography (HPLC) either coupled to electrochemical detection (EC)[19] or electrospray ionisation (ESI) mass spectrometry (MS) detection systems.[20-23] Mass spectrometry is advantageous over other detection approaches because of its high sensitivity, specificity, and ability to elucidate chemical structures via controlled fragmentation experiments (MS/MS). It is, therefore, an indispensable instrument in the analysis of complex antimalarial pharmaceuticals.

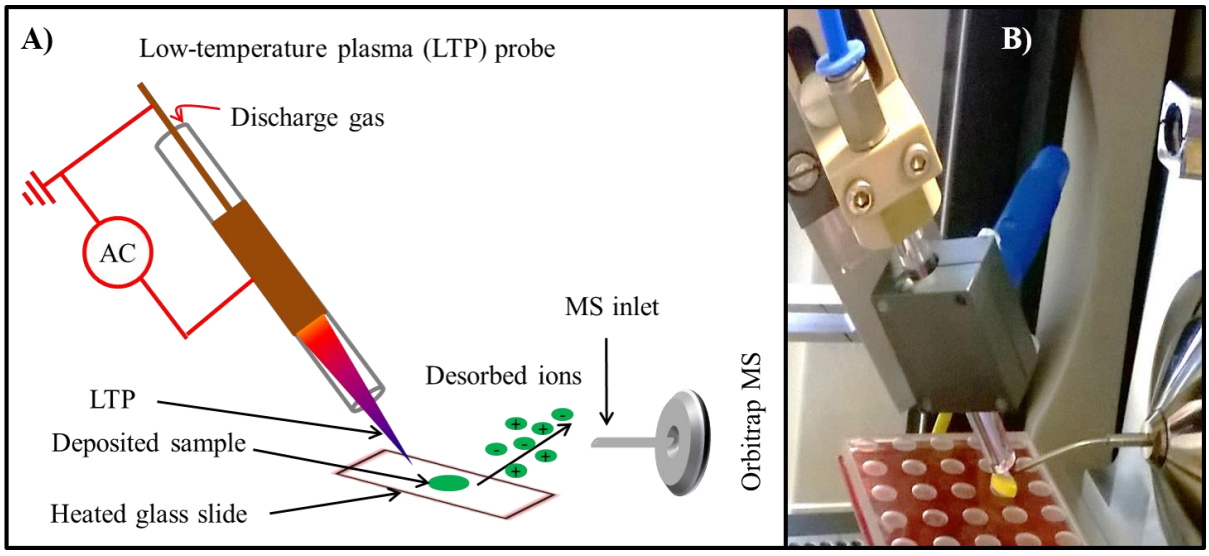

Figure 6.1: A) Schematic of the LTP probe positioned in front of a mass spectrometer for direct ambient desorption ionisation mass spectrometry (ADI-MS). B) Photograph of LTP probing a Coartem drug tablet during an ADI-MS experiment.

Despite the fact that HPLC-MS is widely used, it typically requires extensive sample preparation, large amounts of organic solvents, and long analysis times. Therefore, a faster analytical technique is needed, which requires minimal or no sample preparation, and uses relatively small sample volumes. At the same time, good detection sensitivity is highly desirable, especially, when fast screening is needed to ascertain product quality and the presence of active pharmaceutical ingredients. The growing area of ambient desorption/ionisation mass spectrometry (ADI-MS) is an analytical technique that can potentially fulfil these requirements. In principle, in ADI-MS, samples are desorbed/ionized

in open air and transferred via an inlet capillary into the mass spectrometer.[24] The first two published ADI techniques, namely direct analysis in real time (DART)[25,26] and desorption electrospray ionisation (DESI),[27,28] coupled to MS have been used in screening of antimalarial agents. Both techniques have demonstrated their usefulness in the direct screening of widely counterfeit antimalarial drugs containing artesunate. In a recent publication by Bernier *et al.* [16], a portable DART-single quadrupole (QDa) mass analyser was used efficiently for rapid fingerprinting of a set of ACTs antimalarial tablets. The instrument used, though not handheld, was capable of sorting falsified antimalarial drugs and identify wrong ingredients with potential health implications. Another portable ADI-MS technique capable of direct analysis of gaseous, liquid and/or solid samples is low-temperature plasma MS (LTP-MS).[29,30] The ability of LTP-MS to carry out direct analysis of samples under ambient conditions permits its use in a number of applications including polycyclic aromatic hydrocarbons (PAHs),[31] drugs of abuse in biofluids,[32] explosives,[33] and toxic compounds in complex biological samples.[34] With the goals of having a portable handheld instrument capable of direct analysis, a handheld and wireless LTP source with benchtop and miniature mass spectrometers was developed for point-and-shoot analysis.[35] The developed source, including consumables, such as helium, and power supply was enclosed in a handheld device weighing approx. 0.9 kg. The system was found to be effective in the analysis of, e.g., pesticides and explosives, and provided limits of detection (LODs) within an order of magnitude of a few nanograms (absolute quantities). The ability of such a portable and handheld device to perform direct analysis of complex mixtures could facilitate the fulfilment of the above-mentioned WHO strategy of eliminating malaria by 2030 by being applied in rapid qualitative analysis of commercial antimalarial drugs. Because handheld ADI-MS instruments are not commercialized yet and prototypes were not available to us at the time of this study, a home-built LTP probe coupled to a benchtop high-resolution orbitrap mass spectrometer was used. The system was applied in fast qualitative screening of active pharmaceutical ingredients in Coartem and Malarone antimalarial tablets. High-energy collision induced dissociation (HCD)-fragmentation is used to elucidate the structure via characteristic fragments generated. The data generated on a high-resolution mass spectrometer could then be used as reference spectra for these types of compounds and samples when data acquired with portable mass spectrometers with lower mass resolution are obtained.

6.2 Experimental Section

6.2.1 Chemicals and Sample

Artemether (98.0%) was purchased from Tokyo Chemical industry (TCI, Zwijndrecht, Belgium). Quinine (99% total base) was bought from Alfa Aesar GmbH (Karlsruhe, Germany). Ammonium formate (≥99.0%, Fluka, Steinheim, Germany) was used as buffer for LC-MS reference method. Formic acid (≥99.0%, Th.Geyer GmbH & Co.KG, Renningen, Germany) was added to the LC mobile phase for pH adjustment. Coartem tablet (Novartis, Switzerland) was acquired from a local pharmacy in Cameroon and Malarone (GlaxoSmithKline, Brentford, UK) was from a local pharmacy in Germany. Each Coartem tablet contained 20 mg artemether and 120 mg lumefantrine as active ingredients with celluloses and magnesium stearate as inactive ingredients. Malarone tablet contained 250 mg of atovaquone and 100 mg of proguanil hydrochloride as active ingredients with magnesium stearate core and hypromellose coating. HPLC-grade methanol (MeOH) was obtained from Fisher Scientific (Loughborough, UK). Bi-distilled deionized water was prepared using a distillation apparatus from Heraeus-Quarzschmelze GmbH (Hanau, Germany).

6.2.2 Standard and sample preparation

Quinine (Qn) standard solutions (1, 10 and 100 μg mL^{-1}) were prepared by dilution with a MeOH/H_2O 50:50 (*v/v*) solvent containing 0.1% formic acid. Working standards of artemether were prepared by appropriate dilution with a MeOH/H_2O 50:50 (*v/v*) solvent containing 5 mM ammonium formate (pH 3). Prior to LTP-MS analysis of solid drug tablets, the surfaces of the tablets were smoothed with sandpaper (Grade P600) to remove the coating, and later cleaned with nitrogen stream to eliminate any particles that may clog or contaminate the MS inlet capillary. Tablets for LC-MS analysis were grinded into powder and extracted with methanol. The extract, along with the other liquid analytes were filtered with a 0.2 μm pore size syringe filter (Carl Roth GmbH+Co.KG, Karlsruhe, Germany), diluted appropriately with the mobile phase before subjected to analysis.

6.2.3 LTP-MS analysis

The home-built LTP probe used in this chapter is related to the design described by Harper *et al.* [34] The probe consisted of a glass tube (outer diameter (OD) 6.0 mm and inner diameter (ID) 2.0 mm) surrounded by an outer electrode of copper tape (20.0 mm axial width). An inner stainless-steel pin electrode (diameter 0.5 mm), was positioned axially in the centre of

the glass tube. An alternating current voltage of 13 kVpp (peak-to-peak voltage) at 31 kHz was supplied to the inner pin electrode by a DC-AC high-voltage transformer (HVGEN10AC v3.1, Voltagezone Electronics e.U., Graz, Austria). Helium (He) discharge gas was fed via a T-piece (Swagelok Company, Solon, OH, USA) into the glass capillary at a flow rate of 0.3 L min^{-1}. A gas flow controller (EL-FLOW® *Select* mass flow meters/ mass controllers, Bronkhorst Mättig GmbH, Kamen, Germany), calibrated for He gas was employed to set and adjust the flow rate of He. The LTP probe was aligned at an angle of 60° with respect to the sample surface. A movable sample stage was used to bring the sample at the aligned probe and MS inlet capillary position, such that the final distance between the probe to the sample and MS inlet capillary were approx. 6 and 3 mm, respectively. The LTP probe was operated continuously permitting direct probing of solid sample and pipetting of liquid sample for in-situ analysis. For the liquid samples, 1 µL was dropped on a glass sample holder with supplementary heat (~65 °C) applied to the back of the sample well plate to aid in the thermal desorption process. The supplementary heat was achieved via a rubber heating matt Peltier heating device. For solid samples, the analysis was done by placing the sample directly under the plasma at the above-mentioned adjusted probe angle. The movable stage was used to adjust the vertical position of the sample with respect to constant LTP probe angle to the MS inlet capillary.

The experiments were performed on a high-resolution Exactive mass spectrometer (Thermo Fisher Scientific, Bremen, Germany). The LTP-MS was performed in either positive or negative ion mode, depending on the compound of interest. Details regarding Optimisation of the LTP setup and operating parameters when coupled to the high-resolution orbitrap mass spectrometer for organic mass spectrometry were published previously by Albert *et al.*[36] Unless otherwise stated, the MS operating parameters used in this experiment are shown in Table A 6.1 (see appendix section). Data collection was achieved with the Xcalibur software (version 2.0, Thermo Fisher Scientific, Bremen, Germany). Further data processing was done with OriginLab 2015 (OriginLab, Northampton, MU, USA).

6.2.4 LC-MS reference method analysis

The LTP-HRMS results were compared to a LC-ESI-MS/MS screening of the tablets. An Accela HPLC system (Thermo Fisher Scientific, Bremen, Germany) was coupled to a triple quadrupole mass spectrometer (Quattro LC, Micromass, UK), via ESI source, for the MS/MS analysis. No chromatographic separation was carried out in order to get the results in the

shortest possible time. For LC-MS/MS analysis, 10 µL sample volume was injected for analysis. The LC was operated isocratically at a flow rate of 0.3 mL min^{-1} using a mobile phase consisting of MeOH/H_2O 50:50 (*v/v*) with 5 mM ammonium formate. Nitrogen gas was used as desolvation and nebulisation gas. Argon gas was used for collision induced dissociation (CID).

6.3 Results and Discussions

6.3.1 Ambient ionisation mass spectrometry

Low-temperature plasma (LTP) desorption/ionisation is known to typically form protonated molecular ions ($[M + H]^+$) or deprotonated molecular ions ($[M - H]^-$) via proton transfer reactions between atmospheric water clusters and the analyte molecules (note that other ionisation pathways exist as well, see ref. 29 for details). Initial LTP-MS analysis of 1 µL droplets of 1 and 10 µg mL^{-1} of Qn, an antimalarial agent,[37] resulted in neither a peak for $[M + H]^+$ of Qn at *m/z* 325.1916 ($C_{20}H_{25}N_2O_2^+$), nor any key fragment ion peaks from Qn. However, by applying supplementary heating (65 °C) to the glass sample holder, a $[M + H]^+$ peak at *m/z* 325.1916 was observed for a 10 µg mL^{-1} standard (*cf* Figure A 6.1 in the appendix section). The supplementary heat aided in the thermal desorption of the Qn in the matrix (ethanol in this case). This is in accordance to results from earlier studies, in which heating of the sample was found to be beneficial, especially during the analysis of non-volatile compounds.[29]

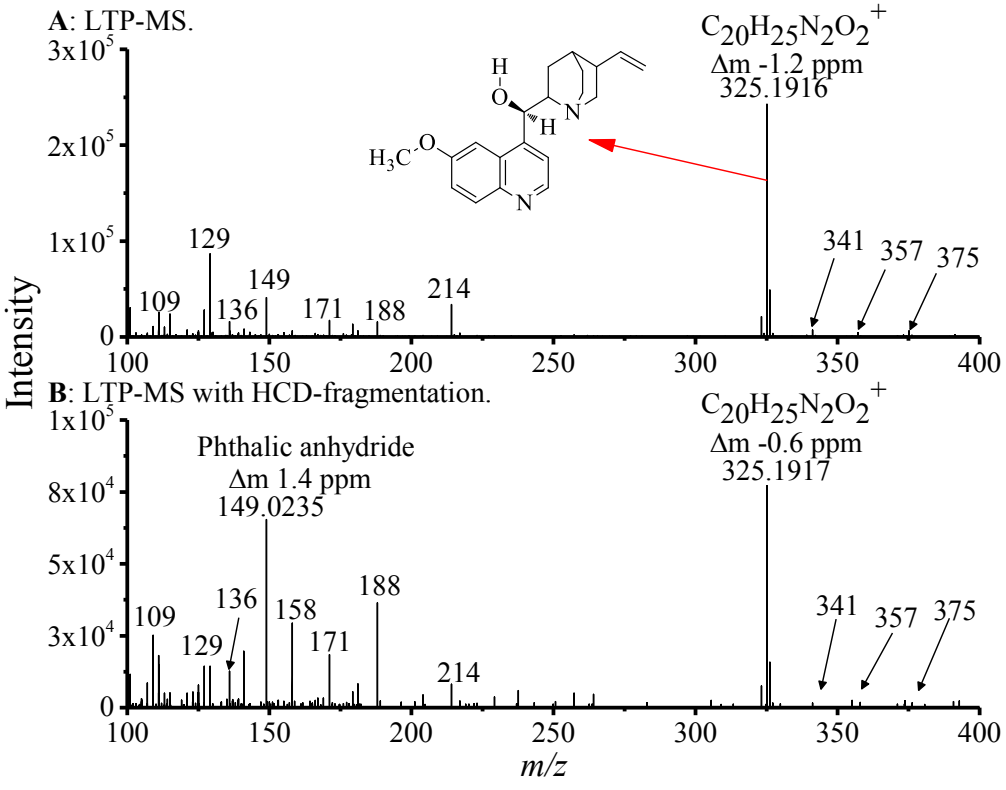

Figure 6.2: LTP (+)-HRMS mass spectra of quinine obtained by (A) LTP-MS and (B) LTP-MS with HCD fragmentation.

The mass spectrum in Figure 6.2A shows a LTP (+)-HRMS spectrum after direct analysis of a Qn standard (100 µg mL^{-1}) on a heated (65 °C) sample well plate. The target Qn was detected as $[M + H]^+$ at *m/z* 325 with a mass accuracy of -1.2 ppm and mass resolution of 81000. The spectrum shows characteristic fragments of Qn at *m/z* 109 and 136, which can be attributed to $[M + H\text{-}C_{11}H_{11}NO_2\text{-}C_2H_3]^{\bullet+}$ and $[M + H\text{-}C_{11}H_{10}NO_2]^+$, respectively, and are considered a result of plasma source ionisation and fragmentation. In addition, other relevant fragment ions include at *m/z* 129, 171, and 188, which are suggested to be $[M + H\text{-}C_{10}H_{16}NO\text{-}OCH_3]^{\bullet+}$, $[M + H\text{-}C_9H_{14}N\text{-}OH]^{\bullet+}$ and $[M + H\text{-}C_9H_{14}N]^+$ respectively. A possible fragmentation pattern of the free radical ion peaks at *m/z* 129, 171, and 188 is shown in Figure A 6.2 in the appendix section. In addition to the identified fragments, there were also fragments at *m/z* 341 ($C_{20}H_{25}O_3N_2^+$), 357 ($C_{20}H_{25}O_4N_2^+$) and 375 ($C_{20}H_{25}O_5N_2^+$), which correspond to oxidation products of the protonated molecular ion of Qn ($C_{20}H_{25}N_2O_2^+$). The intense peak at *m/z* 149 corresponds to the plasticizer, phthalic anhydride, originating from the Teflon T-piece used in the LTP setup. Table A 6.2 in the appendix section contains other known characteristic fragments of Qn such as *m/z* 160 ($C_{10}H_{10}ON^+$) and 166 ($C_{10}H_{16}ON^+$), which were detected but at relatively low abundance. The fragmentation pattern leading to known Qn fragments including *m/z* 109 ($C_7H_{11}N^+$), 136 ($C_9H_{14}N^+$), 160 ($C_{10}H_{10}ON^+$), 166 ($C_{10}H_{16}ON^+$), and 189 ($C_{11}H_{11}O_2N^+$) is shown in Figure A 6.3 in the appendix section. For clarity, the relative mass accuracies of the detected peaks are shown in Table A 6.2 in the appendix section. Figure 6.2B shows a LTP (+)-HRMS spectrum of Qn obtained with all-ion HCD-type fragmentation (the model Exactive used in this chapter did not feature an additional quadrupole in the front). Compared to Figure 6.2A, Figure 6.2B shows a Qn fragmentation pattern with an additional peak at *m/z* 158 corresponding to $C_{10}H_8NO^+$ (*cf* fragmentation pattern in Figure A 6.2 in the appendix section).

To further study applicability of LTP in analysis of antimalarial agent, the setup was applied in the analysis of artemether ($C_{16}H_{26}O_5$), an antimalarial agent used in the commercial drug Coartem. Figure 6.3 shows a LTP (+)-HRMS spectrum of artemether after direct liquid analysis (1 µL droplet, 100 µg mL^{-1}) on the heated sample holder (surface temperature of 65°C) and HCD-type fragmentation was used. Artemether was detected as ammonium adduct ion ($[M + NH_4]^+$) at *m/z* 316 and protonated molecular ion ($[M + H]^+$) at *m/z* 299 with Δm values of -2.54 and -2.42 ppm, respectively. Other characteristic fragments derived from the LTP ionisation of the artemether include *m/z* 267 ($[M + H - OHCH_3]^+$), 249 ($[M + H - OHCH_3\text{-}H_2O]^+$), 239 ($[M + H - OHCH_3 - CO]^+$), 221 ($[M + H - OHCH_3 – CO - H_2O]^+$), and

163 ([M + H - $OHCH_3C_4H_8O_3$ - H_2O]$^+$). The LTP-HRMS fragments from artemether are the same to those obtained using other MS ionisation sources and mass analysers.[38,23,39,16]. The formation of ammonium adducts by LTP shows its similarity to other ambient ionisation sources, such as dielectric-barrier discharge ionisation (DBDI) and plasma assisted desorption/ionisation (PADI) sources, which are known to form ammonium adducts in addition to protonated or deprotonated species.[40,41]

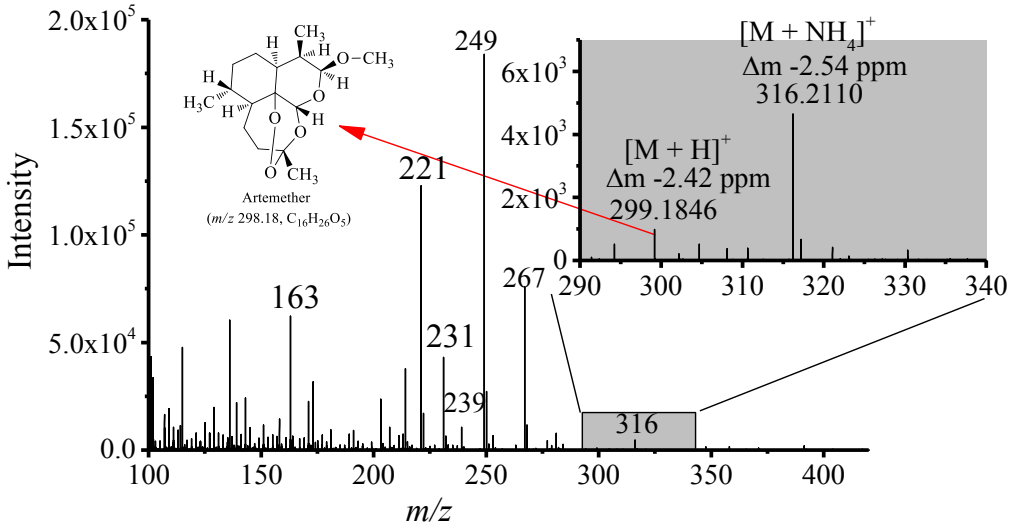

Figure 6.3: LTP (+)-HRMS mass spectra of artemether with HCD-type fragmentation.

For another ambient ionisation technique, DART-MS, it has also been reported that if both the protonated and ammonium adduct are present, the ion signal for the latter is higher than for the former.[42-45] The source of ammonium in this experiment is likely to be the ammonium formate solvent used in the dilution of the artemether standard solution. While the ionisation mechanism responsible for the formation of [M + H]$^+$ has been suggested to occur via penning ionisation where a proton is transferred from a water cluster to the molecule M: [H_2O] $_nH^+$ + M → [M + H]$^+$ + nH_2O,[46-48] that for the ammonium adduct formation, could occur via interaction of NH_4^+ with the substrate molecule M in the gas phase: M + NH_4^+ → [M + NH_4]$^+$.[49,50] The higher signal abundance of *m/z* 316 ([$C_{16}H_{26}O_5$ + NH_4]$^+$) over *m/z* 299 ([$C_{16}H_{26}O_5$ + H]$^+$) can be attributed to thermodynamic favourability for the formation of [$C_{16}H_{26}O_5$ + NH_4]$^+$ compared to [$C_{16}H_{26}O_5$ + H]$^+$. Similarly to other basic compounds, artemisinin and derivatives (including artemether) have been proposed to possess proton affinities (PAs) slightly above the PA of NH_3 (858 kJ mol^{-1}), favouring the formation of their [M + NH_4]$^+$ rather than their [M + H]$^+$ adducts. [39,51,52]

6.3.2 Analysis of real drug sample

One of the advantages of LTP-MS analysis is the rapid screening ability to determine the chemical composition of a sample. The ability was tested by screening two antimalarial drugs: Coartem and Malarone tablets. Coartem contains 20 mg of artemether (MW 298.37 g mol^{-1}, $C_{16}H_{26}O_5$) and 120 mg lumefantrine (MW 528.94 g mol^{-1}, $C_{30}H_{33}Cl_3NO$) per tablet while Malarone consist of 250 mg atovaquone (MW 366.84 g mol^{-1}, $C_{22}H_{17}ClO_3$) and 100 mg proguanil hydrochloride (MW 253.73 g mol^{-1}, $C_{11}H_{16}ClN_5$) as their active pharmaceutical ingredients.

Figure 6.4 shows the LTP (+)-HRMS spectrum from LTP-MS analysis of a Coartem drug tablet. The presence of artemether was ascertained by the $[M + H]^+$ peak at *m/z* 316 and unique characteristic fragments at *m/z* 163 ($C_{11}H_{15}O^+$), 221 ($C_{14}H_{21}O_2^+$), 249 ($C_{15}H_{21}O_3^+$) and 267 ($C_{15}H_{23}O_4^+$). The observed characteristic *m/z* values are explained via the fragmentation patterns shown in Figure 6.5, and are the same to those already shown in Figure 6.3 and reported in literature.[23,38,16] The fragmentation pattern in Figure 6.5 is modelled after the fragmentation proposed by Verbeken *et al.,*[53,23] with the addition of *m/z* 145 ($C_{11}H_{13}^+$) which is likely to be due to a loss of a water molecule from *m/z* 163. The characteristic fragment ions and the mass accuracies shown in Table 6.2 further help to ascertain the presence of artemether in the Coartem tablet. Contrary to the mass spectra in Figure 6.3, where *m/z* 316 was attributed to ammonium adduct of artemether, the *m/z* 316 (exact mass 316.7381) in Figure 6.4 could not be attributed to the ammonium adduct of artemether. Based on the exact mass it could be attributed to some compound in the matrix of the tablet that was co-desorbed and ionized under the experimental conditions. Without any $[M + NH_4]^+$ from artemether, the characteristic fragments could only be coming from the $[M + H]^+$ (*m/z* 299.1853).

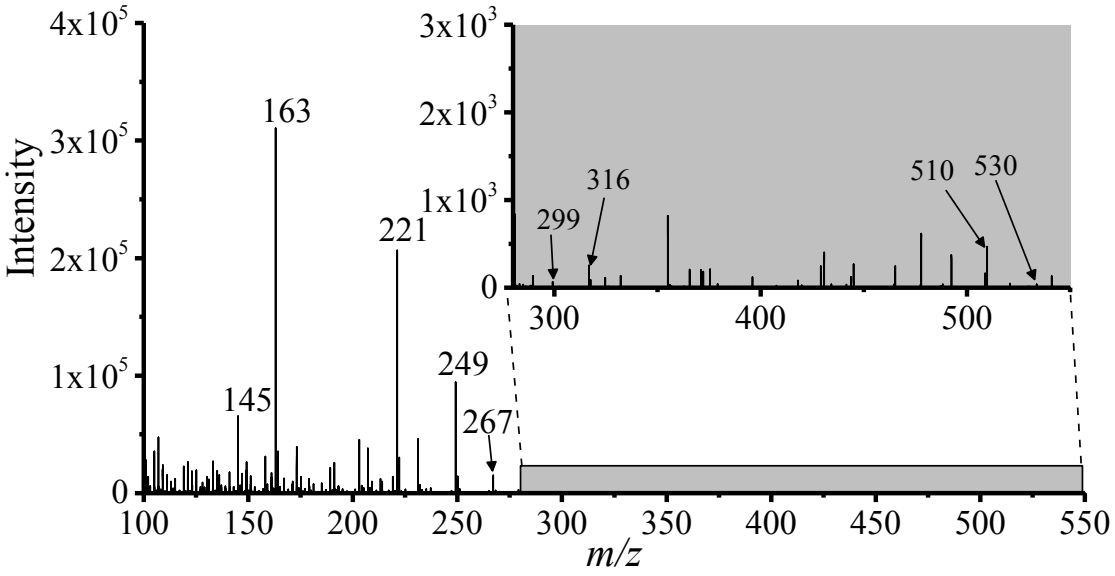

Figure 6.4: LTP (+)-HRMS spectrum of artemether (*m/z* 299) and lumefantrine (*m/z* 530) in Coartem drug tablet.

While the results in Figure 6.4 ascertains the presence of artemether in Coartem drug tablet, the presence of lumefantrine ($C_{30}H_{33}Cl_3NO$, *cf.* Figure 6.7 for molecular structure), the second active pharmaceutical ingredient could not be detected with certainty. Characteristic peaks were detected at *m/z* 530 ($C_{30}H_{32}{}^{35}Cl_2{}^{37}ClNO^+$) (mass accuracy of +0.27 ppm) corresponding to the $[M + H]^+$ ion and the *m/z* 510 ($C_{30}H_{30}{}^{35}Cl_3N^+$) corresponding to [M + H - H_2O, from *m/z* 528]$^+$ ion but with relatively low signal intensity. In addition, the mass spectra is somewhat contrary to that published by Bernier *et al.,*[16] where another plasma-based ADI-MS technique, DART, was applied in the screening of a Coartem drug tablet. In the latter experiment, lumefantrine was observed at *m/z* 528 as the major protonated molecular ion with the identity confirmed by the characteristic isotopic pattern from three chlorine atoms present in the molecule.[16,53] Here, the absence of *m/z* 528 and the characteristic isotopic pattern is very likely due to the low signal intensity. In fact, later analysis of the drug tablet with LC-MS and LC-MS/MS (results discussed below) of a methanol extract confirmed the presence of lumefantrine and also showed the characteristic isotopic peak pattern.

In general, the higher LTP-MS signals for fragments unique to artemether compared to lumefantrine can be related to their difference in vapour pressure (*cf.* Table A 6.4 in the appendix section).

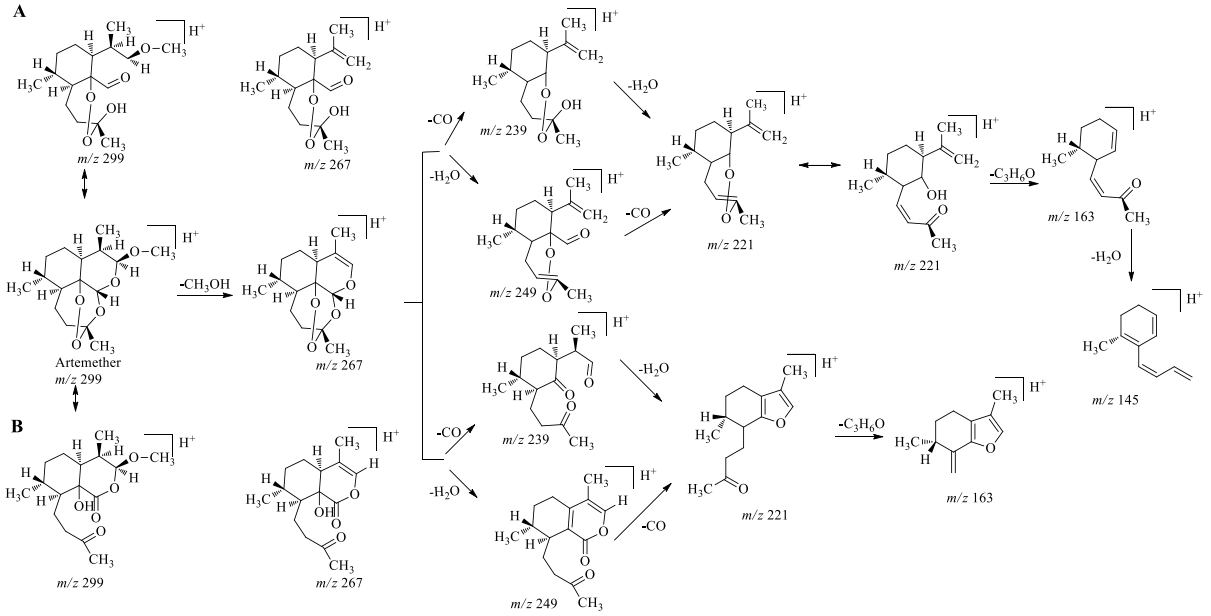

Figure 6.5: Proposed fragmentation pattern of artemether after LTP-MS, with rupture of peroxide bridge , modelled from ref.[53]A,[23] B.

The higher vapour pressure of artemether (7.48 x 10^{-5} mBar) compared to lumefantrine (2.93 x 10^{-17} mBar) is one important reason for the observed differences in signal abundance when a low-temperature desorption/ionisation source such as the LTP probe is applied. Also, the proton affinities of the molecules and the specific sample matrix could play a major role in enhancing/reducing the gas-phase ionisation of one species over the other. A relevant study on the severity of matrix effects on analyte desorption/ionisation, ion suppression, and quantification in plasma-based ADI-MS was published by Shelley *et al*.[54]

Quantitative analysis could not be carried out because of the lack of a matrix-matched sample to use as background. However, to carry out quantitative analysis some sample pre-treatment (e.g. extraction with organic solvents) and matrix/analyte separation via TLC can be possible sample preparation steps prior to the LTP-MS.

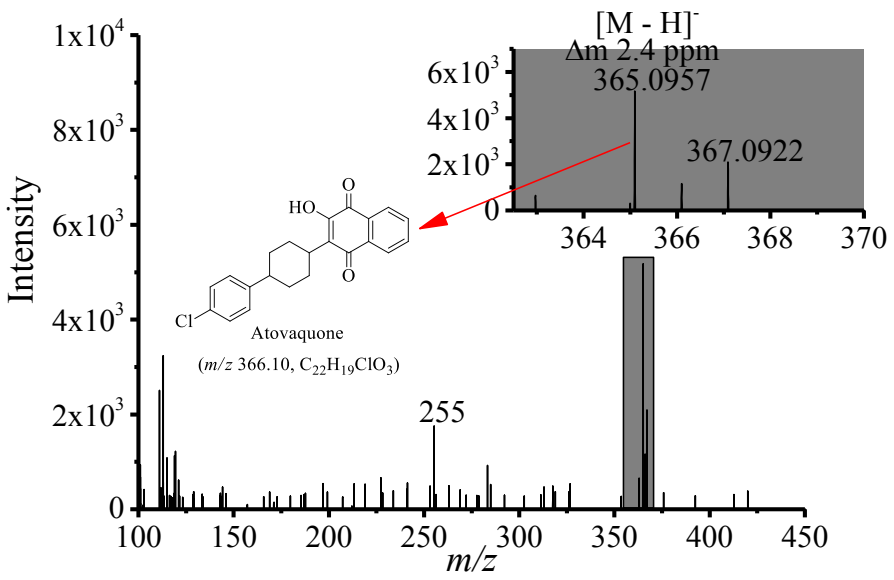

Figure 6.6: LTP (-)-HRMS spectra of atovaquone obtained from analysis of a methanol extract of Malarone drug tablet.

Using similar sample preparation procedure and LTP-MS conditions as in the analysis of Coartem drug tablet, LTP-MS analysis of an uncrushed Malarone drug tablet, was not capable of detecting any of the active pharmaceutical ingredients (proguanil and atovaquone) in either positive or negative ion mode. The lack of signal for proguanil (with a higher vapour pressure than artemether, *cf.* Table A 6.4 in the appendix section) shows that another factor other than vapour pressure could be a limiting factor. A possible reason could be related to the sample matrix effect, low proton affinities, and competitive ionisation process whereby matrix components with the same or higher proton affinities than the active molecule could lead to suppression of the ion signal. However, with the aid of supplementary heat, LTP (-)-HRMS analysis of a filtered methanol extract of a grinded Malarone tablet led to the successful detection of atovaquone at *m/z* 365.0956, corresponding to the deprotonated molecular ion ($[M - H]^-$) (*cf* Figure 6.6). The mass accuracy of detected fragments from LTP-MS analysis of Coartem and Malarone drug tablets are shown in Table 6.1.

LTP-MS analysis of the methanol extract of Malarone was unsuccessful in detecting proguanil. This could be a result of the low gas-phase proton affinity of the compound or competitive ionisation process taking place in the gas phase. For instance, quantum chemical analysis by Abbat *et al.*[55] reveal that cycloguanil, the cyclized and active form of proguanil is characterized by low proton affinity (509.2 kJ mol^{-1}).

Table 6.1: List of *m/z* fragments detected from LTP-MS of Coartem and Malarone tablets.

Nominal mass (*m/z*)	Exact mass (*m/z*)	Relative mass accuracy (ppm)	Fragment ions	Source
Coartem tablet				
145	145.1006	-3.8	$C_{11}H_{13}^+$	Artemether
163	163.1117	-4.2	$C_{11}H_{15}O^+$	Artemether
221	221.1536	-4.1	$C_{14}H_{21}O_2^+$	Artemether
231	231.1380	-3.9	$C_{15}H_{19}O_2^+$	Artemether
249	249.1485	-4.0	$C_{15}H_{21}O_3^+$	Artemether
267	267.1591	-3.9	$C_{15}H_{23}O_4^+$	Artemether
299	299.1853	-2.2	$C_{16}H_{27}O_5^+$	Artemether
510	510.1522	>10	$C_{30}H_{30}Cl_3N^+$	Lumefantrine
530	530.1628	+0.27	$C_{30}H_{32}Cl_3NO^+$	Lumefantrine
Malarone tablet				
365	365.0938	2.4	$C_{22}H_{18}ClO_3^-$	Atovaquone

Despite the ability of LTP to analyse and detect artemether, lumefantrine in Coartem and atovaquone in methanol extract of Malarone, it can be seen based on the above presented results that analysis of composite tablets such as Coartem (artemether + lumefantrine) and Malarone (proguanil + atovaquone) is challenging. In addition to aforementioned explanations, this could also be because the LTP-MS experimental setup can favour the desorption/ionisation of one component compared to the other. For instance, using the LTP-MS experimental setup above, signal intensity of artemether was higher than for lumefantrine present in the Coartem drug tablet. Similarly, atovaquone was detected compared to proguanil from a methanol extract of Malarone. In the future, such effects could be minimized, for example, by performing a simple sample extraction protocol followed by TLC before LTP-MS analysis. In such a scenario, compounds of interest would be separated in space and desorbed/ionized without competitive ionisation processes taking place in the gas phase.

6.3.3 LC-QQQ-MS screening

To support and clarify the results from LTP-MS analysis, liquid chromatography coupled to triple quadrupole mass analyser was used. An initial flow injection LC-MS screening of a methanol extract of Coartem drug tablet showed characteristic ion fragments for artemether and lumefantrine. Figure 6.7A shows *m/z* 163, 221, 239, 267, 284 and 316 which as described above and also reported in literature are unique to artemether.[39] In addition lumefantrine was readily detected as *m/z* 528 (*cf* Figure 6.7B) corresponding to the protonated molecular ion.

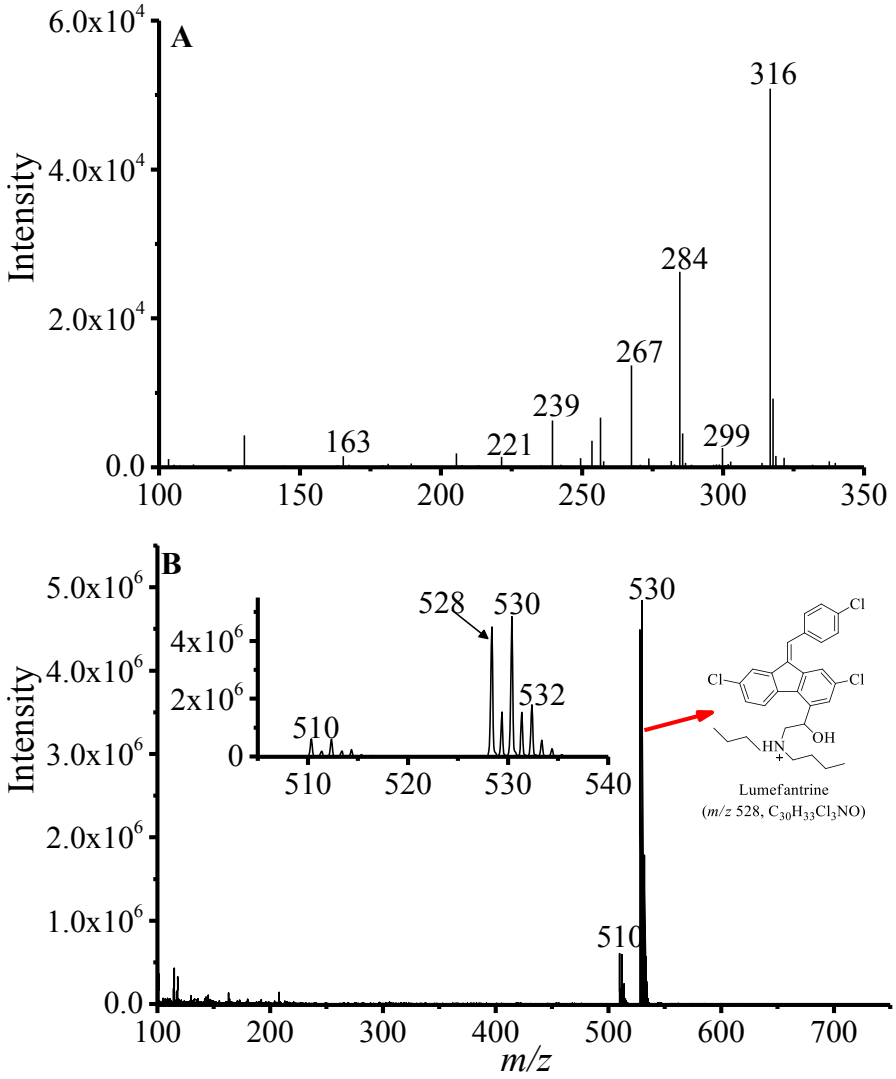

Figure 6.7: ESI (+)-MS of methanol extract of Coartem drug tablet diluted MeOH/H_2O 50:50 (*v/v*) solvent containing 5 mM ammonium formate. A) Artemether and B) Lumefantrine.

The mass spectra also shows the unique M + 2 isotopic pattern due to the presence of three chlorine atoms with ^{35}Cl and ^{37}Cl isotopes.[38] LC-MS/MS analysis of the ammonium adduct of artemether (Figure A 4A in the appendix section) and the protonated molecular ion of lumefantrine, *m/z* 528 ($^{35}Cl_3$), 530 ($^{35}Cl_2{}^{37}Cl$) (Figure A 4A&B in the appendix section) further confirms the presence of lumefantrine.[38] The pre-optimised MS parameters used for the MS/MS analysis are shown in Table A 6.5 and Table A 6.6 in the appendix section.

Similar to the LTP-MS results, artemether was detected as ammonium adduct $[M + NH_4]^+$ at *m/z* 316. The presence of artemether was ascertain by the ammoniated adduct and characteristic product ions. In contrast to the LTP-MS results, lumefantrine was also detected as the protonated molecular ion at *m/z* 528 and 530.

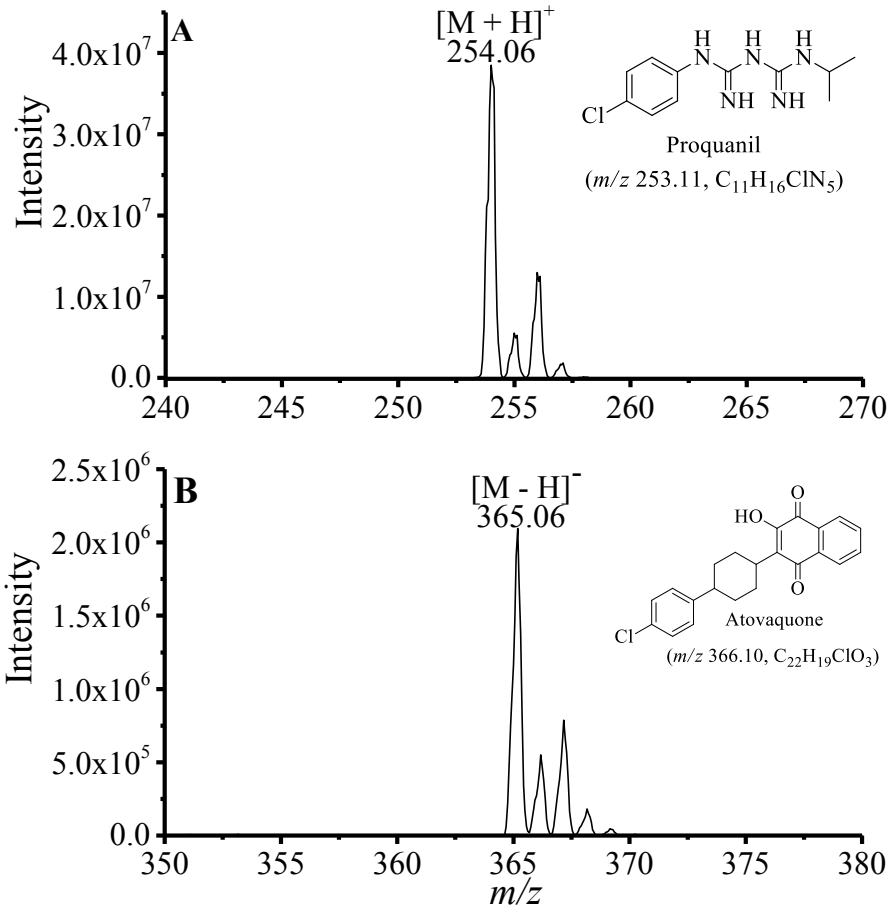

Figure 6.8: Mass spectra, chemical structure and molecular weight of proguanil (A) and atovaquone (B) from LC-MS analysis of methanol extract of Malarone drug tablet.

Furthermore, the mass spectrum in Figure 6.8A shows the detection of proguanil at *m/z* 244.06 corresponding to the protonated molecular ion. Contrary to the detection of proguanil, the mass spectrum in Figure 6.8B displays the detection of atovaquone as deprotonated molecular ion at *m/z* 365.06.

6.4 Conclusion

A fast screening method for antimalarial agents was developed using a home-built LTP probe for direct sample desorption/ionisation coupled to a high-resolution Orbitrap mass spectrometer. The antimalarial agents were detected via their protonated molecular ions and unique fingerprint fragments. Supplementary heat applied to the bottom of a glass sample holder was found to increase the analyte signal intensity for liquid samples. Application of the developed method in the screening of Coartem revealed the presence of artemether and lumefantrine. While the direct LTP-HRMS analysis of Malarone was not successful, LTP-HRMS analysis after simple liquid extraction of Malarone with methanol readily identified the presence of atovaquone in the tablet. The LTP-HRMS results were supported by results from LC-QQQ-MS analysis of the same samples.

The results demonstrate the ability of LTP-HRMS to be used as a fast screening tool for antimalarials and related pharmaceuticals. In the future, the sensitivity can be further optimised and potential matrix effects should be investigated in detail. Further, the high-resolution data of these compounds with LTP ionisation could potentially serve as a reference, when portable mass spectrometers with lower resolution are used in the field in combination with a handheld plasma-based desorption/ionisation. Portable mass spectrometers could then be used as quality assurance tools, to detect counterfeits, and to help achieve the WHO goal of eradicating malaria by 2030.

Appendix for Chapter 6

Table A 6.1: LTP-Orbitrap-MS parameters used fort the LTP-MS analysis

MS scan parameters	
Scan range	50-550
HCD gas	ON
Resolution	High
Polarity	Positive/Negative
Lock masses	Off
Automatic gain control (AGC)	On
Maximum ion injection time	100 ms
MS source parameters	
Sheath gas flow rate (L h^{-1})	0
Aux. gas flow rate (L h^{-1})	0
Sweep gas flow rate (L h^{-1})	0
Spray voltage (V)	0
Capillary voltage (V)	35
Capillary temperature (°C)	300
Tube lens voltage (V)	100
Skimmer voltage (V)	20

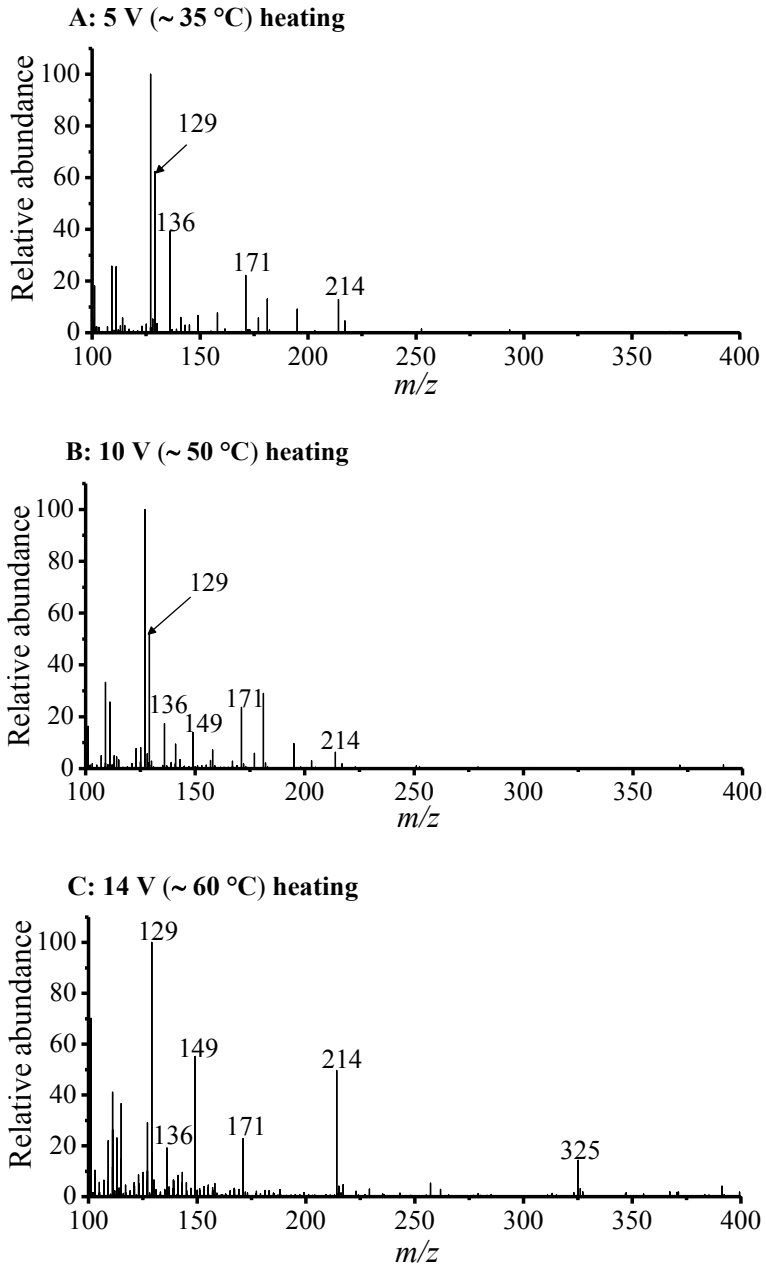

Figure A 6.1: Positive ion mode low temperature plasma-high resolution mass spectrometry (LTP (+)-HRMS) spectra of quinine with additional heating: A) 5.0 V (~35 °C) heating, B) 10.0 V (~50 °C) heating, and C) 14 V (~65 °C) heating Analyte: 10 µg mL^{-1} (30 ng absolute) of quinine (*m/z* 325.1916, $C_{20}H_{25}N_2O_2^+$).

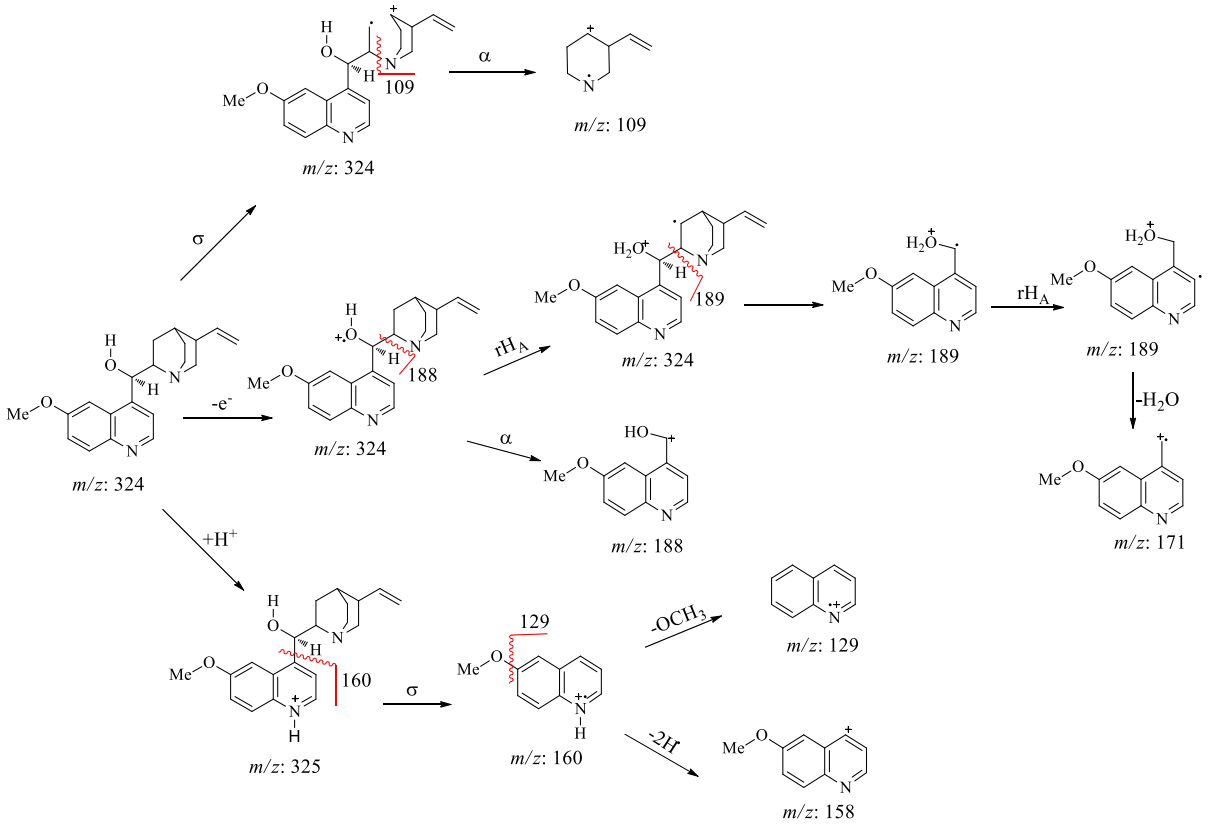

Figure A 6.2: Proposed fragmentation pathway of quinine showing the formation of free radical cations during LTP (+)-HRMS analysis.

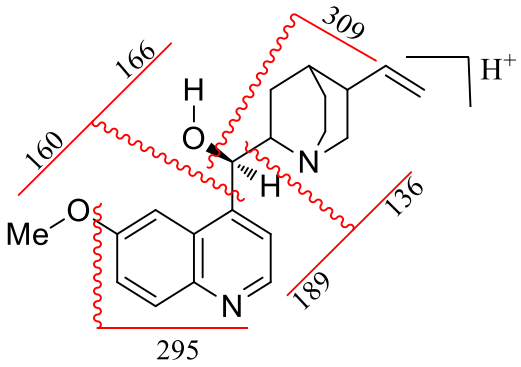

Figure A 6.3: Fragmentation pattern of the protonated molecular ion of quinine with known characteristics fragments as reported in literature.

Table A 6.2: Proposed fragment ions of quinine obtained with LTP (+)-HRMS.

Nominal mass (*m/z*)	Exact mass (*m/z*)	Relative mass accuracy (ppm)	Fragment ions	Source
109	109.0891	-	$C_7H_{11}N^{\bullet+}$	Quinine
129	129.0578	-	$C_9H_7N^{\bullet+}$	eniuiuQ
136	136.1124	2.3	$C_9H_{14}N^{+}$	eniuiuQ
149	149.0239	1.4	$C_8H_5O_3^{+}$	Phthalic anhydride
160	160.0760	2.2	$C_{10}H_{10}ON^{+}$	Quinine
166	166.1231	3.0	$C_{10}H_{16}ON^{+}$	eniuiuQ
171	171.0268	-3.9	$C_{11}H_9NO^{\bullet+}$	eniuiuQ
188	188.0712	-3.2	$C_{11}H_{10}O_2N^{+}$	eniuiuQ
325	325.1914	-1.2	$C_{20}H_{25}O_2N_2^{+}$	eniuiuQ
341	341.1863	1.0	$C_{20}H_{25}O_3N_2^{+}$	Quinine oxide
357	357.1812	1.0	$C_{20}H_{25}O_4N_2^{+}$	Quinine dioxide
375	375.1920	1.5	$C_{20}H_{25}O_5N_2^{+}$	Quinine trioxide

Table A 6.3: Proposed fragment ions of quinine obtained with LTP (+)-HRMS with high-energy collision-induced dissociation (HCD) fragmentation.

Nominal mass (*m/z*)	Exact mass (*m/z*)	Relative mass accuracy (ppm)	Fragment ions	Source
109	109.0891	-	$C_7H_{11}N^{\bullet+}$	Quinine
129	129.0578	-	$C_9H_7N^{\bullet+}$	Quinine
136	136.1124	2.6	$C_9H_{14}N^{+}$	Quinine
149	149.0239	1.7	$C_8H_5O_3^{+}$	lilahihP aul r nyinQ
160	160.0760	1.2	$C_{10}H_{10}ON^{+}$	Quinine
166	166.1231	2.5	$C_{10}H_{16}ON^{+}$	Quinine
171	171.0268	-3.9	$C_{11}H_9NO^{\bullet+}$	Quinine
188	188.0712	-2.7	$C_{11}H_{10}O_2N^{+}$	Quinine
325	325.1914	-0.6	$C_{20}H_{25}O_2N_2^{+}$	Quinine
341	341.1863	0.65	$C_{20}H_{25}O_3N_2^{+}$	Quinine oxide
357	357.1812	0.75	$C_{20}H_{25}O_4N_2^{+}$	Quinine dioxide
375	375.1920	0.88	$C_{20}H_{25}O_5N_2^{+}$	Quinine trioxide

Table A 6.4: Compounds screened from drug tablet, with their boiling point and vapour pressure.

Compound	Boiling point (°C) [a]	Vapour pressure (mBar) [b]
Artemether	357.5 ± 42.0	7.48×10^{-5}
Lumefantrine	642.0 ± 55.0	2.93×10^{-17}
Atovaquone	535.0 ± 50.0	3.76×10^{-12}
Proguanil	325.1 ± 44.0	3.15×10^{-4}

[a] Values calculated at 760 Torr (1013.24 mBar), [b] Calculated at 25 ° C

The values were obtained from https://scifinder.cas.org/scifinder, and were calculated using Advanced Chemistry Development (ACD/Labs) Software V11.02 (© 1994-2017 ACD/Labs).

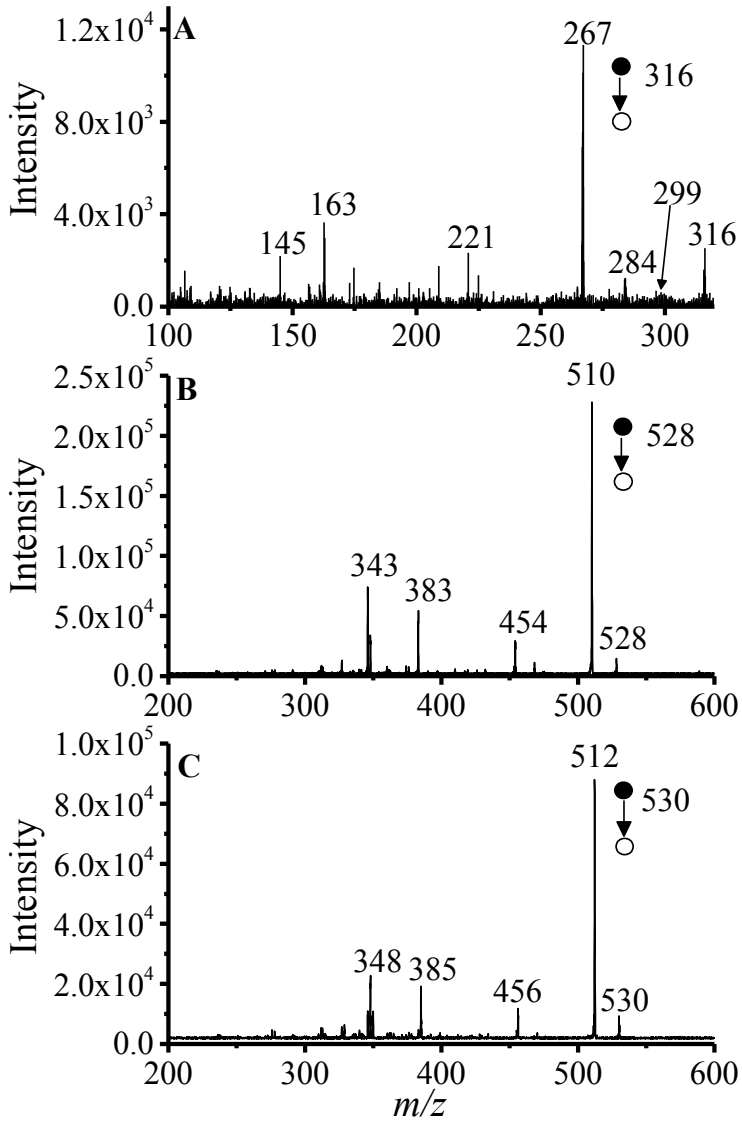

Figure A 6.4: ESI(+)-MS/MS spectra of the ammonium adduct of artemether ($C_{16}H_{26}O_5$) (A) at *m/z* 316, and the protonated molecular ion of lumefantrine ($C_{30}H_{32}Cl_3NO$) (B) at *m/z* 528 with, $^{35}Cl_3$ and (C) at *m/z* 530, with $^{35}Cl_2$ ^{37}Cl.

Table A 6.5: Liquid chromatography triple quadrupole mass spectrometry (LC-QQQ-MS) parameters applied for the screening of artemether from Coartem drug tablet.

Scan Parameters	
Mass range	100 - 420
Scan duration (sec)	3.00
Inter scan delay (sec)	0.15
Ionisation mode	ESI+
Data type	Accurate mass
ESI Source	
Capillary voltage (V)	3.00
Cone voltage (V)	15.0
Extractor voltage (V)	5.0
RF lens voltage (V)	5.0
Source block temp. (°C)	100
Desolvation temp (°C)	400
Analyser vacuum (mBar)	6.8 x 10-6
Gas cell vacuum (mBar)	2.0 x 10-5
Nebuliser gas flow (L h^{-1})	68.0
Desolvation gas flow (L h^{-1})	636.0

Table A 6.6: LC-QQQ-MS parameters used for the screening of lumefantrine from Coartem drug tablet.

Scan Parameters	
Mass range	200 - 600
Scan duration (sec)	3.00
Inter scan delay (sec)	0.15
Ionisation mode	ESI+
Data type	Accurate mass
ESI Source	
Capillary voltage (V)	3.00
Cone voltage (V)	60.0
Extractor voltage (V)	5.0
RF lens voltage (V)	5.0
Source block temp. (°C)	100
Desolvation temp (°C)	400
Analyser vacuum (mBar)	6.8 x 10-6
Gas cell vacuum (mBar)	2.0 x 10-5
Nebuliser gas flow (L h^{-1})	68.0
Desolvation gas flow (L h^{-1})	636.0

Chapter 7

Concluding Remarks and Future Perspectives

7.1 Summary and Conclusions

The quality of antimalarials currently in use continues to play a major role in the eradication of malaria parasites. The capacity of mass spectrometry to provide good detection sensitivity, selectivity, and specificity for ionisable organic molecules, makes it indispensable analytical technique for qualitative analysis of antimalarial pharmaceuticals. In this thesis, different mass spectrometric-based techniques including high-temperature high performance liquid chromatography mass spectrometry (HT-HPLC-MS)-based techniques and direct MS-based methods have been developed and optimised for the analysis of antimalarials

In Chapter 2, a HT-HPLC heating system, a prototype developed by German Institute of Food Technologies was optimised and evaluated with respect to chromatographic parameters. The repeatability in peak retention, height, area, and asymmetry showed the efficiency of the heating system for HT-HPLC-MS analysis.

In Chapter 3, a HT-HPLC method with an XBridge C_{18} column coupled to a triple quadrupole mass spectrometer via ESI was developed and used in the analysis of *Cinchona* alkaloids. Separation and detection of the four major chiral alkaloids: cinchonine, cinchonidine, quinine, and quinidine and their dihydro-derivatives: dihydrocinchonine, dihydrocinchonidine, dihydroquinine, and dihydroquinidine were achieved. The method developed here showed faster analysis, minimal solvent consumption, better chromatographic selectivity, and enhanced MS ionisation compared to standard HPLC-MS method. The method could be used as an excellent alternative not only in HT-HPLC-MS analysis of *Cinchona* alkaloids but also in the analysis of related compounds in biological sample and fluids.

In Chapter 4 the optimised HT-HPLC method with zirconia-polybutadiene (Zr-PBD) column coupled to a triple quadrupole mass spectrometer was capable of separating and detecting ART and derivatives with good chromatographic selectivity and MS sensitivity. The ability of the method to perform HT-HPLC-MS and HT-HPLC-MS/MS makes it an alternative technique in the analysis of ART and derivatives.

In Chapter 5, a ToF-SIMS method for the direct analysis of *Cinchona* alkaloids present in *Cinchona* bark and commercial *Cinchona* extracts is developed and optimised. The method demonstrates that ToF-SIMS is an attractive tool for fast screening of pharmaceuticals ingredient in natural plant samples. ToF-SIMS results were supported by 3D laser

microscopy and HPLC-MS analysis. Due to the inability of ToF-SIMS to differentiate enantiomers, perform quantitative analysis, and relatively high instrumental cost, it is valuable to use it in tandem with other techniques such as HPLC-MS or MS/MS.

In Chapter 6, a direct analysis method involving the use of a home-built LTP probe coupled to high-resolution Orbitrap mass spectrometer is developed and optimised for the fast screening of active antimalarial agents in antimalarial drugs. Active antimalarial agents were detected as their protonated molecular ions and unique fingerprint fragments. For liquid samples, supplementary heat applied to the bottom of a glass sample holder was found to increase the analyte signal intensity. The ability of the method to provide information on active pharmaceutical ingredients with minimal sample preparation procedure makes it a valuable tool for fast screening of antimalarial drugs.

Comparing the different mass spectrometric techniques used in this thesis, it can be concluded that each of the technique is characterised by some unique identity that makes it advantageous than the other for a particular type of analysis. For instance, taking the results from the analysis of *Cinchona* alkaloids from *Cinchona* bark, the application of HT-HPLC-MS necessitates extraction of the sample which is time-consuming and costly. However, amongst the presented methods, it is capable of providing chemical identity of all chemical components while using less organic modifier and shorter analysis time. The use of smaller amount of organic modifier makes the technique very suitable for resource-limited areas. ToF-SIMS analysis shows good detection sensitivity and uses very small sample size. However, for the analysis of pseudo-enantiomers such Cn/Cdn and Qn/Qdn, ToF-SIMS cannot differentiate the compounds. In addition, the lack of application of ToF-SIMS in the analysis of this class of compounds could be attributed to the cost of the instrument and the need of skilled personnel, making it rarely applied in resource limited settings. Similar to ToF-SIMS analysis, LTP-ADI-MS cannot differentiate pseudo-enantiomers and the cost of a high-resolution Orbitrap mass analyser could limit its application. However, with advancement of portable hand-held LTP-ADI-MS, the cost of LTP-ADI-MS instrument could be affordable and thus could help in rapid qualitative screening of active pharmaceuticals even in resource limited areas.

Comparatively, HT-HPLC-MS method with its advantages still remains a promising technique in the analysis of this class of compounds. But with improvement in sample preparation and handheld instrumentation development/availability, LTP along with other

ambient ionisation sources would lead the way for rapid screening of the active pharmaceutical ingredients in commercial drugs.

7.2 Future Perspectives

In this thesis, different MS-based methods development and optimisation tailored for the analysis of antimalarial pharmaceuticals have been presented. For the preliminary section of the HT-HPLC-MS based methods, a prototype, high-temperature HPLC heating system developed by German Institute for Food Technologies have been used. In the HT-HPLC-MS method development and optimisation for the analysis of *Cinchona* alkaloids, temperature was found to influence both separation and the MS ionisation. The applicability of the method was tested in the analysis of *Cinchona* alkaloids in commercial *Cinchona* extract. In future, this method could be used in qualitative and quantitative analysis of *Cinchona* alkaloids in biological fluids such as blood and urine. Similarly, the developed HT-HPLC-MS method for the analysis of ART and derivatives could be applied in qualitative and quantitative analysis of similar compounds in biological fluids.

Furthermore, based on the results obtained from ToF-SIMS method in the analysis of *Cinchona* alkaloids from *Cinchona* bark and commercial extract, future research should focus on improving detection sensitivity for such natural samples with rough surfaces and at the same time enhancing the mass resolution. This can be approached from sample preparation point of view and instrumental setups. On the former, preparation of pellets of the *Cinchona* bark with relatively uniform and flat surfaces could help overcome some of the challenges faced in the interpretation of the sample with rough surfaces. On the latter, the use of delayed extraction in the mass spectrometer could help improve the mass resolution. In addition, depth profiling can be carried out to study the variation of the active pharmaceutical ingredients at different depths of the *Cinchona* bark. For future application of ToF-SIMS in the analysis of the different components of *Cinchona* extract including Cn, Cdn, Qn, and Qdn, there is a need of pre-separation using TLC, followed by ToF-SIMS analysis of the TLC plates.

The results presented from LTP-ADI-MS demonstrated its ability to be used for future rapid qualitative analysis of antimalarial and related compounds. Similar to ToF-SIMS analysis, for future application of LTP-ADI-MS in the analysis of the different components of *Cinchona* extract including Cn, Cdn, Qn, and Qdn, a pre-separation using TLC, followed by LTP-MS

analysis of the TLC plates would be needed. In addition, future work should focus on optimising and understanding the ionisation mechanism of different antimalarial compounds and related species. With improvement in the technique, LTP-MS, especially handheld LTP-MS can also be used in to study metabolism of antimalarials and related compounds in blood samples.

Overall, future applications of the MS-based methods should centre on measuring the concentration of antimalarials and similar drugs in biological fluids such as blood, plasma and urine. For such applications, sample preparation procedures would be needed to minimise effects of the sample matrices.

References

1. WHO (2015) World Malaria Report 2015. World Health Organization

2. Kantele A, Jokiranta TS (2011) Review of cases with the emerging fifth human malaria parasite, Plasmodium knowlesi. Clin Infect Dis 52 (11):1356-1362. doi:10.1093/cid/cir180

3. Franco-Paredes C, Santos-Preciado JI (2006) Problem pathogens: prevention of malaria in travellers. The Lancet Infectious Diseases 6 (3):139-149. doi:10.1016/s1473-3099(06)70410-8

4. Timmerman P, Lausecker B, Barosso B, van Amsterdam P, Luedtke S, Dijksman J (2012) 'Large Meets Small': connecting the bioanalytical community around peptide and protein bioanalysis with LC-MS(/MS). Bioanalysis 4 (6):627-631. doi:10.4155/bio.12.37

5. Eisenstein M (2012) Drug development: Holding out for reinforcements. Nature 484 (7395):S16-18. doi:10.1038/484S16a

6. Dronamraju KR, Arese P (2010) Malaria: Genetic and Evolutionary Aspects. In: Dronamraju KR, Arese P (eds) Malaria: Genetic and Evolutionary Aspects. Emerging Infectious Diseases of the 21st Century. Springer Science+Business Media, Inc.,

7. Biot C, Castro W, Botte CY, Navarro M (2012) The therapeutic potential of metal-based antimalarial agents: implications for the mechanism of action. Dalton Trans 41 (21):6335-6349. doi:10.1039/c2dt12247b

8. Rosenthal PJ, Miller LH (2001) Antimalarial Chemotherapy: Mechanisms of Action, Resistance, and New Directions in Drug Discovery. Infectious Disease, 1 edn. Springer-Science+Business Media, LLC, New Jersey doi:10.1007/978-1-59259-111-4

9. Noedl H, Se Y, Schaecher K, Smith BL, Socheat D, Fukuda MM (2008) Evidence of artemisinin-resistant malaria in western Cambodia. N Engl J Med 359 (24):2619-2620. doi:10.1056/NEJMc0805011

10. Dondorp AM, Nosten F, Yi P, Das D, Phyo AP, Tarning J, Lwin KM, Ariey F, Hanpithakpong W, Lee SJ, Ringwald P, Silamut K, Imwong M, Chotivanich K, Lim P, Herdman T, An SS, Yeung S, Singhasivanon P, Day NP, Lindegardh N, Socheat D, White NJ (2009) Artemisinin resistance in Plasmodium falciparum malaria. N Engl J Med 361 (5):455-467. doi:10.1056/NEJMoa0808859

11. Choi SR, Mukherjee P, Avery MA (2008) The fight against drug-resistant malaria: novel plasmodial targets and antimalarial drugs. Curr Med Chem 15 (2):161-171

12. Nayyar GM, Breman JG, Herrington JE (2015) The global pandemic of falsified medicines: laboratory and field innovations and policy perspectives. Am J Trop Med Hyg 92 (6 Suppl):2-7. doi:10.4269/ajtmh.15-0221

13. Kelesidis T, Falagas ME (2015) Substandard/counterfeit antimicrobial drugs. Clin Microbiol Rev 28 (2):443-464. doi:10.1128/CMR.00072-14

14. Moreira AS, Coimbra MA, Nunes FM, Passos CP, Santos SA, Silvestre AJ, Silva AM, Rangel M, Domingues MR (2015) Chlorogenic acid-arabinose hybrid domains in coffee melanoidins: Evidences from a model system. Food Chem 185:135-144. doi:10.1016/j.foodchem.2015.03.086

15. Kaur H, Green MD, Hostetler DM, Fernández FM, Newton PN (2010) Antimalarial drug quality: methods to detect suspect drugs. Therapy 7 (1):49-57. doi:10.2217/thy.09.84

16. WHO (1999) Counterfeit Drugs. Guidelines for the Development of Measures to Combat Counterfeit Drugs. World Health Organization 99.1

17. Hajjou M, Krech L, Lane-Barlow C, Roth L, Pribluda VS, Phanouvong S, El-Hadri L, Evans L, 3rd, Raymond C, Yuan E, Siv L, Vuong TA, Boateng KP, Okafor R, Chibwe KM, Lukulay PH (2015) Monitoring the quality of medicines: results from Africa, Asia, and South America. Am J Trop Med Hyg 92 (6 Suppl):68-74. doi:10.4269/ajtmh.14-0535

18. Hajjou M, Qin Y, Bradby S, Bempong D, Lukulay P (2013) Assessment of the performance of a handheld Raman device for potential use as a screening tool in evaluating medicines quality. J Pharm Biomed Anal 74:47-55. doi:10.1016/j.jpba.2012.09.016

19. Ricci C, Nyadong L, Yang F, Fernandez FM, Brown CD, Newton PN, Kazarian SG (2008) Assessment of hand-held Raman instrumentation for in situ screening for potentially counterfeit artesunate antimalarial tablets by FT-Raman spectroscopy and direct ionization mass spectrometry. Analytica Chimica Acta 623 (2):178-186. doi:10.1016/j.aca.2008.06.007

20. Loethen YL, Kauffman JF, Buhse LF, Rodriguez JD (2015) Rapid screening of anti-infective drug products for counterfeits using Raman spectral library-based correlation methods. Analyst 140 (21):7225-7233. doi:10.1039/c5an01679g

21. de Veij M, Vandenabeele P, Hall KA, Fernandez FM, Green MD, White NJ, Dondorp AM, Newton PN, Moens L (2007) Fast detection and identification of counterfeit antimalarial tablets by Raman spectroscopy. J Raman Spectrosc 38 (2):181-187. doi:10.1002/jrs.1621

22. Green MD, Hostetler DM, Nettey H, Swamidoss I, Ranieri N, Newton PN (2015) Integration of novel low-cost colorimetric, laser photometric, and visual fluorescent techniques for rapid identification of falsified medicines in resource-poor areas: application to artemether-lumefantrine. Am J Trop Med Hyg 92 (6 Suppl):8-16. doi:10.4269/ajtmh.14-0832

23. Hall KA, Newton PN, Green MD, De Veij M, Vandenabeele P, Pizzanelli D, Mayxay M, Dondorp A, Fernandez FM (2006) Characterization of counterfeit artesunate antimalarial tablets from southeast Asia. Am J Trop Med Hyg 75 (5):804-811

24. Green MD, Mount DL, Wirtz RA, White NJ (2000) A colorimetric field method to assess the authenticity of drugs sold as the antimalarial artesunate. Journal of Pharmaceutical and Biomedical Analysis 24 (1):65-70. doi:10.1016/s0731-7085(00)00360-5

25. Khuluza F, Kigera S, Jahnke RW, Heide L (2016) Use of thin-layer chromatography to detect counterfeit sulfadoxine/pyrimethamine tablets with the wrong active ingredient in Malawi. Malar J 15:215. doi:10.1186/s12936-016-1259-9

26. Sitoe AR, Lopes F, Moreira R, Coelho A, Bronze MR (2013) Contribution of Mass Spectrometry to the Study of Antimalarial Agents. In: Coelho AV, Franco CdMF (eds) Tandem Mass Spectrometry - Molecular Characterization. InTech. doi:10.5772/56225

27. Pitt JJ (2009) Principles and applications of liquid chromatography-mass spectrometry in clinical biochemistry. Clin Biochem Rev 30 (1):19-34

28. Dongre VG, Karmuse PP, Nimbalkar MM, Singh D, Kumar A (2005) Application of GC-EI-MS for the identification and investigation of positional isomer in primaquine, an antimalarial drug. J Pharm Biomed Anal 39 (1-2):111-116. doi:10.1016/j.jpba.2005.03.019

29. ElSohly MA, Gul W, Feng S, Nanayakkara NPD, Clark AM, Khan S, Cogswell FB, Walker LA (2006) GC-MS analysis of the 8-aminoquinoline antimalarial NPC1161 and its carboxy metabolite in plasma and red blood cells of primates. Chromatographia 64 (3-4):199-205. doi:10.1365/s10337-006-0015-7

30. Nyunt M, Pisciotta J, Feldman AB, Thuma P, Scholl PF, Demirev PA, Lin JS, Shi L, Kumar N, Sullivan DJ (2005) Detection of Plasmodium Falciparium in Pregnancy by Laser Desorption Mass Spectrometry The American Journal of Tropical Medicine and Hygiene 73 (3):485-490

31. Scholl PF, Kongkasuriyachai D, Demirev PA, Feldman AB, Lin JS, Sullivan DJ, Kumar N (2004) Rapid Detection of Malaria Infection in Vivo by Laser Desorption Mass Spectrometry. The American Journal of Tropical Medicine and Hygiene 71 (5):546-551

32. Demirev PA, Feldman AB, Kongkasuriyachai D, Scholl P, Sullivan D, Kumar N (2002) Detection of Malaria Parasites in Blood by Laser Desorption Mass Spectrometry. Analytical Chemistry 74 (14):3262-3266. doi:10.1021/ac025621k

33. Louw S, Njoroge M, Chigorimbo-Murefu N, Chibale K (2012) Comparison of electrospray ionisation, atmospheric pressure chemical ionisation and atmospheric pressure photoionisation for the identification of metabolites from labile artemisinin-based anti-malarial drugs using a QTRAP(R) mass spectrometer. Rapid Commun Mass Spectrom 26 (20):2431-2442. doi:10.1002/rcm.6359

34. Hoffmann CV, Lammerhofer M, Lindner W (2009) Separation of Cinchona alkaloids on a novel strong cation-exchange-type chiral stationary phase-comparison with commercially available strong cation exchanger and reversed-phase packing materials. Anal Bioanal Chem 393 (4):1257-1265. doi:10.1007/s00216-008-2557-z

35. Verbeken M, Suleman S, Baert B, Vangheluwe E, Van Dorpe S, Burvenich C, Duchateau L, Jansen FH, De Spiegeleer B (2011) Stability-indicating HPLC-DAD/UV-ESI/MS impurity profiling of the anti-malarial drug lumefantrine. Malar J 10:51. doi:10.1186/1475-2875-10-51

36. Vandercruyssen K, D'Hondt M, Vergote V, Jansen H, Burvenich C, De Spiegeleer B (2014) LC-UV/MS quality analytics of paediatric artemether formulations. J Pharm Anal 4 (1):37-52. doi:10.1016/j.jpha.2013.03.006

37. Wang M, Park C, Wu Q, Simon JE (2005) Analysis of artemisinin in Artemisia annua L. by LC-MS with selected ion monitoring. J Agric Food Chem 53 (18):7010-7013. doi:10.1021/jf051061p

38. Maraschiello C, Vilageliu J, Dorronsoro I, Martinez A, Floriano P, Gomez-Acebo E (2006) Enantioselective LC/MS method for the determination of an antimalarial agent fenozan B07 in dog plasma. Chirality 18 (5):297-305. doi:10.1002/chir.20253

39. Nyadong L, Harris GA, Balayssac S, Galhena AS, Malet-Martino M, Martino R, Parry RM, Wang MDM, Fernandez FM, Gilard V (2009) Combining Two-Dimensional Diffusion-Ordered Nuclear Magnetic Resonance Spectroscopy, Imaging Desorption Electrospray Ionization Mass Spectrometry, and Direct Analysis in Real-Time Mass Spectrometry for the Integral Investigation of Counterfeit Pharmaceuticals. Analytical Chemistry 81 (12):4803-4812. doi:10.1021/ac900384j

40. Ricci C, Nyadong L, Fernandez FM, Newton PN, Kazarian SG (2007) Combined Fourier-transform infrared imaging and desorption electrospray-ionization linear ion-trap mass spectrometry for analysis of counterfeit antimalarial tablets. Anal Bioanal Chem 387 (2):551-559. doi:10.1007/s00216-006-0950-z

41. Nyadong L, Green MD, De Jesus VR, Newton PN, Fernandez FM (2007) Reactive desorption electrospray ionization linear ion trap mass spectrometry of latest-generation counterfeit antimalarials via noncovalent complex formation. Analytical Chemistry 79 (5):2150-2157. doi:10.1021/ac062205h

42. Bernier MC, Li F, Musselman B, Newton PN, Fernández FM (2016) Fingerprinting of falsified artemisinin combination therapies via direct analysis in real time coupled to a compact single quadrupole mass spectrometer. Anal Methods 8 (36):6616-6624. doi:10.1039/c6ay01418f

43. Shrivas K, Wu HF (2007) Quantitative bioanalysis of quinine by atmospheric pressure-matrix assisted laser desorption/ionization mass spectrometry combined with dynamic drop-to-drop solvent microextraction. Anal Chim Acta 605 (2):153-158. doi:10.1016/j.aca.2007.10.032

44. Kudina O, Eral B, Mugele F (2016) e-MALDI: An Electrowetting-Enhanced Drop Drying Method for MALDI Mass Spectrometry. Anal Chem 88 (9):4669-4675. doi:10.1021/acs.analchem.5b04283

45. Fenn JB (2003) Electrospray Wings for Molecular Elephants (Nobel Lecture). Angewandte Chemie International Edition 42 (33):3871-3894. doi:10.1002/anie.200300605

46. Fenn JB, Mann M, Meng CK, Wong SF, Whitehouse CM (1989) Electrospray ionization for mass spectrometry of large biomolecules. Science 246 (4926):64-71

47. Banerjee S, Mazumdar S (2012) Electrospray ionization mass spectrometry: a technique to access the information beyond the molecular weight of the analyte. Int J Anal Chem 2012:282574. doi:10.1155/2012/282574

48. Covey TR, Thomson BA, Schneider BB (2009) Atmospheric pressure ion sources. Mass Spectrom Rev 28 (6):870-897. doi:10.1002/mas.20246

49. French JB, Thomson BA, Davidson WR, Reid NM, Buckley JA (1985) Atmospheric Pressure Chemical Ionization Mass Spectrometry. In: Karasek FW, Hutzinger O, Safe S (eds) Mass Spectrometry in Environmental Sciences. Springer US, Boston, MA, pp 101-121. doi:10.1007/978-1-4613-2361-7_6

50. Robb DB, Blades MW (2008) State-of-the-art in atmospheric pressure photoionization for LC/MS. Anal Chim Acta 627 (1):34-49. doi:10.1016/j.aca.2008.05.077

51. Marchi I, Rudaz S, Veuthey JL (2009) Atmospheric pressure photoionization for coupling liquid-chromatography to mass spectrometry: a review. Talanta 78 (1):1-18. doi:10.1016/j.talanta.2008.11.031

52. Hodel EM, Zanolari B, Mercier T, Biollaz J, Keiser J, Olliaro P, Genton B, Decosterd LA (2009) A single LC-tandem mass spectrometry method for the simultaneous determination of 14 antimalarial drugs and their metabolites in human plasma. J Chromatogr B Analyt Technol Biomed Life Sci 877 (10):867-886. doi:10.1016/j.jchromb.2009.02.006

53. Monge ME, Harris GA, Dwivedi P, Fernandez FM (2013) Mass spectrometry: recent advances in direct open air surface sampling/ionization. Chem Rev 113 (4):2269-2308. doi:10.1021/cr300309q

54. Fernandez FM, Cody RB, Green MD, Hampton CY, McGready R, Sengaloundeth S, White NJ, Newton PN (2006) Characterization of solid counterfeit drug samples by

desorption electrospray ionization and direct-analysis-in-real-time coupled to time-of-flight mass spectrometry. ChemMedChem 1 (7):702-705. doi:10.1002/cmdc.200600041

55. Nyadong L, Late S, Green MD, Banga A, Fernandez FM (2008) Direct quantitation of active ingredients in solid artesunate antimalarials by noncovalent complex forming reactive desorption electrospray ionization mass spectrometry. J Am Soc Mass Spectrom 19 (3):380-388. doi:10.1016/j.jasms.2007.11.016

56. Albert A, Shelley JT, Engelhard C (2014) Plasma-based ambient desorption/ionization mass spectrometry: state-of-the-art in qualitative and quantitative analysis. Anal Bioanal Chem 406 (25):6111-6127. doi:10.1007/s00216-014-7989-z

57. Zenobi R, Knochenmuss R (1998) Ion formation in MALDI mass spectrometry. Mass Spectrom Rev 17 (5):337-366

58. Marvin LF, Roberts MA, Fay LB (2003) Matrix-assisted laser desorption/ionization time-of-flight mass spectrometry in clinical chemistry. Clinica Chimica Acta 337 (1-2):11-21. doi:10.1016/j.cccn.2003.08.008

59. Duncan MW, Roder H, Hunsucker SW (2008) Quantitative matrix-assisted laser desorption/ionization mass spectrometry. Brief Funct Genomic Proteomic 7 (5):355-370. doi:10.1093/bfgp/eln041

60. Thiel V, Sjövall P (2011) Using Time-of-Flight Secondary Ion Mass Spectrometry to Study Biomarkers. Annual Review of Earth and Planetary Sciences 39 (1):125-156. doi:10.1146/annurev-earth-040610-133525

61. Benninghoven A (1994) Chemical Analysis of Inorganic and Organic Surfaces and Thin Films

by Static Time-of-Flight Secondary Ion Mass Spectrometry (TOF-SIMS. Angew Chem Int Ed Engl 33:20

62. Greibrokk T, Andersen T (2003) High-temperature liquid chromatography. J Chromatogr A 1000 (1-2):743-755. doi:10.1016/s0021-9673(02)01963-5

63. Vanhoenacker G, Sandra P (2005) High temperature liquid chromatography and liquid chromatography-mass spectroscopy analysis of octylphenol ethoxylates on different stationary phases. J Chromatogr A 1082 (2):193-202. doi:10.1016/j.chroma.2005.05.050

64. Lestremau F, Cooper A, Szucs R, David F, Sandra P (2006) High-efficiency liquid chromatography on conventional columns and instrumentation by using temperature as a variable I. Experiments with 25 cm x 4.6 mm I.D., 5 microm ODS columns. J Chromatogr A 1109 (2):191-196. doi:10.1016/j.chroma.2005.12.112

65. Yang Y (2007) Subcritical water chromatography: A green approach to high-temperature liquid chromatography. J Sep Sci 30 (8):1131-1140. doi:10.1002/jssc.200700008

66. Teutenberg T (2010) High-Temperature Liquid Chromatography: A User's Guide for Method Development. Royal Society of Chemistry, Cambridge, UK

67. Teutenberg T, Wagner P, Gmehling J (2009) High-temperature liquid chromatography. Part I. Determination of the vapour pressures of binary solvent mixtures--implications for liquid chromatographic separations. J Chromatogr A 1216 (37):6471-6480. doi:10.1016/j.chroma.2009.07.035

68. Teutenberg T, Wiese S, Wagner P, Gmehling J (2009) High-temperature liquid chromatography. Part II: Determination of the viscosities of binary solvent mixtures--implications for liquid chromatographic separations. J Chromatogr A 1216 (48):8470-8479. doi:10.1016/j.chroma.2009.09.075

69. Teutenberg T, Wiese S, Wagner P, Gmehling J (2009) High-temperature liquid chromatography. Part III: Determination of the static permittivities of pure solvents and binary solvent mixtures--implications for liquid chromatographic separations. J Chromatogr A 1216 (48):8480-8487. doi:10.1016/j.chroma.2009.09.076

70. Yang Y, Belghazi M, Lagadec A, Miller DJ, Hawthorne SB (1998) Elution of organic solutes from different polarity sorbents using subcritical water. Journal of Chromatography A 810 (1-2):149-159. doi:10.1016/s0021-9673(98)00222-2

71. Guillarme D, Heinisch S, Gauvrit JY, Lanteri P, Rocca JL (2005) Optimization of the coupling of high-temperature liquid chromatography and flame ionization detection. Journal of Chromatography A 1078 (1-2):22-27. doi:10.1016/j.chroma.2005.04.092

72. Vanhoenacker G, Sandra P (2006) Elevated temperature and temperature programming in conventional liquid chromatography – fundamentals and applications. Journal of Separation Science 29 (12):1822-1835. doi:10.1002/jssc.200600160

73. Teutenberg T (2009) Potential of high temperature liquid chromatography for the improvement of separation efficiency--a review. Anal Chim Acta 643 (1-2):1-12. doi:10.1016/j.aca.2009.04.008

74. Gagliardi LG, Castells CB, Rafols C, Roses M, Bosch E (2008) Effect of temperature on the chromatographic retention of ionizable compounds. III. Modeling retention of pharmaceuticals as a function of eluent pH and column temperature in RPLC. J Sep Sci 31 (6-7):969-980. doi:10.1002/jssc.200700491

75. Albert M, Cretier G, Guillarme D, Heinisch S, Rocca J-L (2005) Some advantages of high temperature for the separation of pharmaceutical compounds with mass spectrometry detection. Journal of Separation Science 28 (14):1803-1811. doi:10.1002/jssc.200500145

76. de Vlieger JS, Giezen MJ, Falck D, Tump C, van Heuveln F, Giera M, Kool J, Lingeman H, Wieling J, Honing M, Irth H, Niessen WM (2011) High temperature liquid chromatography hyphenated with ESI-MS and ICP-MS detection for the structural characterization and quantification of halogen containing drug metabolites. Anal Chim Acta 698 (1-2):69-76. doi:10.1016/j.aca.2011.04.053

77. Zhang L, Thevis M, Piper T, Jochmann MA, Wolbert JB, Kujawinski DM, Wiese S, Teutenberg T, Schmidt TC (2014) Carbon isotope ratio analysis of steroids by high-temperature liquid chromatography-isotope ratio mass spectrometry. Anal Chem 86 (5):2297-2302. doi:10.1021/ac403353x

78. Zhang L, Kujawinski DM, Jochmann MA, Schmidt TC (2011) High-temperature reversed-phase liquid chromatography coupled to isotope ratio mass spectrometry. Rapid Commun Mass Spectrom 25 (20):2971-2980. doi:10.1002/rcm.5069

79. Pereira L, Aspey S, Ritchie H (2007) High temperature to increase throughput in liquid chromatography and liquid chromatography-mass spectrometry with a porous graphitic carbon stationary phase. Journal of Separation Science 30 (8):1115-1124. doi:10.1002/jssc.200600521

80. McCalley DV (2002) Analysis of the Cinchona alkaloids by high-performance liquid chromatography and other separation techniques. Journal of Chromatography A 967 (1):1-19. doi:10.1016/s0021-9673(01)01557-6

81. Lammerhofer M, Lindner W (2008) Liquid Chromatographic Enantiomer Separation and Chiral Recognition by Cinchona Alkaloid-Derived Enantioselective Separation Materials. Advances in Chromatography, Vol 46 46:1-107

82. Lammerhofer ML, W. (1996) Quinine and quinidine derivatives as chiral selectors. I. Brush type chiral stationary phases for high-performance liquid chromatography based on cinchonan carbamates and their application as chiral anion exchangers. J Chromatogr A 741 (1):33-48

83. McCalley DV (2002) Analysis of the Cinchona alkaloids by high-performance liquid chromatography and other separation techniques. J Chromatogr A 967 (1):1-19. doi:10.1016/s0021-9673(01)01557-6

84. Bürgi T, Baiker A (2004) Heterogeneous Enantioselective Hydrogenation over Cinchona Alkaloid Modified Platinum: Mechanistic Insights into a Complex Reaction. Accounts of Chemical Research 37 (11):909-917. doi:10.1021/ar040072l

85. McCalley DV (2000) Effect of temperature and flow-rate on analysis of basic compounds in high-performance liquid chromatography using a reversed-phase column. J Chromatogr A 902 (2):311-321

86. McCalley DV (1990) Quantitative analysis of alkaloids from Cinchona bark by high-performance liquid chromatography. Analyst 115 (10):1355-1358. doi:10.1039/AN9901501355

87. McCalley DV (1983) Analysis of the cinchona alkaloids by liquid chromatography. Reversed-phase chromatography on octadecylsilyl columns. Chromatographia 17 (5):264-266. doi:10.1007/bf02263037

88. Verpoorte ABSaR Chromatography of Alkaloids. Part A: Thin-Layer Chromatography and Part B: Gas and Liquid Chromatography. Journal of Chromatography Library 23 A and 23 B

89. Hoffmann CV, Laemmerhofer M, Lindner W (2007) Novel strong cation-exchange type chiral stationary phase for the enantiomer separation of chiral amines by high-performance liquid chromatography. J Chromatogr A 1161 (1-2):242-251. doi:10.1016/j.chroma.2007.05.092

90. Fornstedt T, Zhong G, Guiochon G (1996) Peak tailing and slow mass transfer kinetics in nonlinear chromatography. Journal of Chromatography A 742 (1-2):55-68. doi:10.1016/0021-9673(96)00323-8

91. Mccalley DV (1990) Quantitative-Analysis of Alkaloids from Cinchona Bark by High-Performance Liquid-Chromatography. Analyst 115 (10):1355-1358. doi:DOI 10.1039/an9901501355

92. McCalley DV (1999) Comparison of the performance of conventional C18 phases with others of alternative functionality for the analysis of basic compounds by reversed-phase high-performance liquid chromatography. Journal of Chromatography A 844 (1-2):23-38. doi:10.1016/s0021-9673(99)00250-2

93. Nawrocki J (1997) the silanol group and its role in liquid chromatography. journal of chromatography a 779:29-71

94. Heinisch S, Rocca JL (2009) Sense and nonsense of high-temperature liquid chromatography. J Chromatogr A 1216 (4):642-658. doi:10.1016/j.chroma.2008.11.079

95. Wiese S, Teutenberg T, Schmidt TC (2012) A general strategy for performing temperature-programming in high performance liquid chromatography--further improvements in the accuracy of retention time predictions of segmented temperature gradients. J Chromatogr A 1222:71-80. doi:10.1016/j.chroma.2011.12.018

96. Wiese S, Teutenberg T, Schmidt TC (2011) A general strategy for performing temperature-programming in high performance liquid chromatography--prediction of segmented temperature gradients. J Chromatogr A 1218 (39):6898-6906. doi:10.1016/j.chroma.2011.08.022

97. Dolan J A Guide to HPLC and LC-MS Buffer Selection. In, Aberdeen, Scotland, 2006. ACE HPLC Columns,

98. Wiese S, Teutenberg T, Schmidt TC (2011) General strategy for performing temperature programming in high performance liquid chromatography: prediction of linear temperature gradients. Anal Chem 83 (6):2227-2233. doi:10.1021/ac103113m

99. Coym JW, Dorsey JG (2004) Reversed-phase retention thermodynamics of pure-water mobile phases at ambient and elevated temperature. J Chromatogr A 1035 (1):23-29

100. Nahum A, Horváth C (1981) Surface silanols in silica-bonded hydrocarbonaceous stationary phases. Journal of Chromatography A 203:53-63. doi:10.1016/s0021-9673(00)80281-2

101. Ishihama Y, Nakamura M, Miwa T, Kajima T, Asakawa N (2002) A rapid method for pKa determination of drugs using pressure-assisted capillary electrophoresis with photodiode array detection in drug discovery. J Pharm Sci 91 (4):933-942

102. Bernard Testa SDK, Heidi Wunderli-Allenspach, Gerd Folkers (Eds.) (2001) Pharmacokinetic Profiling in Drug Research. Willey, Zurich. doi:10.1002/9783906390468

103. Klayman DL (1985) Qinghaosu (artemisinin): an antimalarial drug from China. Science 228 (4703):1049-1055

104. Eckstein-Ludwig U, Webb RJ, Van Goethem ID, East JM, Lee AG, Kimura M, O'Neill PM, Bray PG, Ward SA, Krishna S (2003) Artemisinins target the SERCA of Plasmodium falciparum. Nature 424 (6951):957-961. doi:10.1038/nature01813

105. Miller LH, Su X (2011) Artemisinin: discovery from the Chinese herbal garden. Cell 146 (6):855-858. doi:10.1016/j.cell.2011.08.024

106. Liu R, Dong HF, Jiang MS (2012) Artemisinin: the gifts from traditional Chinese medicine not only for malaria control but also for schistosomiasis control. Parasitol Res 110 (5):2071-2074. doi:10.1007/s00436-011-2707-7

107. Li HJ, Wang W, Li YZ, Qu GL, Xing YT, Tao YH, Wei JY, Dai JR, Liang YS (2011) Effects of artemether, artesunate and dihydroartemisinin administered orally at multiple doses or combination in treatment of mice infected with Schistosoma japonicum. Parasitol Res 109 (2):515-519. doi:10.1007/s00436-011-2474-5

108. Efferth T, Romero MR, Wolf DG, Stamminger T, Marin JJ, Marschall M (2008) The antiviral activities of artemisinin and artesunate. Clin Infect Dis 47 (6):804-811. doi:10.1086/591195

109. Chou S, Marousek G, Auerochs S, Stamminger T, Milbradt J, Marschall M (2011) The unique antiviral activity of artesunate is broadly effective against human cytomegaloviruses including therapy-resistant mutants. Antiviral Res 92 (2):364-368. doi:10.1016/j.antiviral.2011.07.018

110. Crespo-Ortiz MP, Wei MQ (2012) Antitumor activity of artemisinin and its derivatives: from a well-known antimalarial agent to a potential anticancer drug. J Biomed Biotechnol 2012:247597. doi:10.1155/2012/247597

111. Newton PN, Green MD, Mildenhall DC, Plancon A, Nettey H, Nyadong L, Hostetler DM, Swamidoss I, Harris GA, Powell K, Timmermans AE, Amin AA, Opuni SK, Barbereau S, Faurant C, Soong RC, Faure K, Thevanayagam J, Fernandes P, Kaur H, Angus B, Stepniewska K, Guerin PJ, Fernandez FM (2011) Poor quality vital anti-malarials in Africa - an urgent neglected public health priority. Malar J 10:352. doi:10.1186/1475-2875-10-352

112. Liu H, Li Q, Li S, Zou Y, Gu A (2008) The rapid determination of artemisinin by post-column derivatization high-performance liquid chromatography using matrix solid-phase dispersion method. J Chromatogr Sci 46 (2):122-126

113. Paudel MK, Takei A, Sakoda J, Juengwatanatrakul T, Sasaki-Tabata K, Putalun W, Shoyama Y, Tanaka H, Morimoto S (2012) Preparation of a single-chain variable fragment and a recombinant antigen-binding fragment against the anti-malarial drugs, artemisinin and artesunate, and their application in an ELISA. Anal Chem 84 (4):2002-2008. doi:10.1021/ac203131f

114. He SP, Tan GY, Li G, Tan WM, Nan TG, Wang BM, Li ZH, Li QX (2009) Development of a sensitive monoclonal antibody-based enzyme-linked immunosorbent assay for the antimalaria active ingredient artemisinin in the Chinese herb Artemisia annua L. Anal Bioanal Chem 393 (4):1297-1303. doi:10.1007/s00216-008-2527-5

115. Camps C, Toussirot M, Quennoz M, Simonnet X (2011) Determination of artemisinin and moisture content of Artemisia annua L. dry powder using a hand-held near infrared spectroscopy device. J Near Infrared Spectrosc 19 (3):191-198. doi:10.1255/jnirs.927

116. Liu S, Tian N, Li J, Huang J, Liu Z (2009) Simple and rapid micro-scale quantification of artemisinin in living Artemisia annua L. by improved gas chromatography with electron-capture detection. Biomed Chromatogr 23 (10):1101-1107. doi:10.1002/bmc.1230

117. Quennoz M, Bastian C, Simonnet X, Grogg AF (2010) Quantification of the total amount of artemisinin in leaf samples by thin layer chromatography. Chimia (Aarau) 64 (10):755-757. doi:10.2533/chimia.2010.755

118. Dost K, Davidson G (2003) Analysis of artemisinin by a packed-column supercritical fluid chromatography-atmospheric pressure chemical ionisation mass spectrometry technique. Analyst 128 (8):1037-1042. doi:10.1039/b301342a

119. Newton PN, Fernandez FM, Plancon A, Mildenhall DC, Green MD, Ziyong L, Christophel EM, Phanouvong S, Howells S, McIntosh E, Laurin P, Blum N, Hampton CY, Faure K, Nyadong L, Soong CW, Santoso B, Zhiguang W, Newton J, Palmer K (2008) A collaborative epidemiological investigation into the criminal fake artesunate trade in South East Asia. PLoS Med 5 (2):e32. doi:10.1371/journal.pmed.0050032

120. Ferreira JF, Gonzalez JM (2009) Analysis of underivatized artemisinin and related sesquiterpene lactones by high-performance liquid chromatography with ultraviolet detection. Phytochem Anal 20 (2):91-97. doi:10.1002/pca.1101

121. Gaudin K, Kauss T, Lagueny AM, Millet P, Fawaz F, Dubost JP (2009) Determination of artesunate using reversed-phase HPLC at increased temperature and ELSD detection. J Sep Sci 32 (2):231-237. doi:10.1002/jssc.200800437

122. Zhao S-S, Zeng M-Y (2007) Spektrometrische Hochdruck-Flüssigkeits-Chromatographische (HPLC) Untersuchungen zur Analytik von Qinghaosu. Planta Medica 51 (03):233-237. doi:10.1055/s-2007-969466

123. Nakata H, Konishi H, Takeda N, Tatematsu A, Suzuki M (1983) Ammonium adduct ion in ammonia chemical ionization mass spectrometry. Formation of adduct ion. J Mass Spectrom Soc Jpn 31 (4):275-279. doi:10.5702/massspec.31.275

124. Ranasinghe A, Sweatlock JD, Cooks RG (1993) A rapid screening method for artemisinin and its congeners using ms/ms: search for new analogues in Artemisia annua. J Nat Prod 56 (4):552-563

125. Kostiainen R, Kauppila TJ (2009) Effect of eluent on the ionization process in liquid chromatography-mass spectrometry. J Chromatogr A 1216 (4):685-699. doi:10.1016/j.chroma.2008.08.095

126. Janeckova L, Kalikova K, Bosakova Z, Tesarova E (2010) Study of interaction mechanisms on zirconia-based polystyrene HPLC column. J Sep Sci 33 (19):3043-3051. doi:10.1002/jssc.201000391

127. Bell DS, Shawn R. Wyatt, Santasania CT Comparison of Zirconia- and Silica-Based Stationary Phases for the Retention and Selectivity of Pharmaceutically Relevant Analytes. Supelco, Sigma-Aldrich, Bellefonte, PA, USA

128. Hunter EPL, Lias SG (1998) Evaluated gas phase basicities and proton affinities of molecules: An update. J Phys Chem Ref Data 27 (3):413-656. doi:Doi 10.1063/1.556018

129. Bajaj YPS (1988) Medicinal and Aromatic Plants I. Medicinal and Aromatic Plants I, vol 4, 1 edn. Springer-Verlag Berlin Heidelberg, Berlin. doi:10.1007/978-3-642-73026-9

130. Melchiorre P (2010) Cinchona Alkaloids in Synthesis & Catalysis. Ligands, Immobilization and Organocatalysis. Edited by Choong Eui Song. Angewandte Chemie International Edition 49 (19):3259-3260. doi:10.1002/anie.201000372

131. Kaufman TS, Ruveda EA (2005) The quest for quinine: those who won the battles and those who won the war. Angew Chem Int Ed Engl 44 (6):854-885. doi:10.1002/anie.200400663

132. David B J, Youngson RM (2005) Encyclopedia of Family Health, vol 14. 3rd edn. Marshall Cavendish, New York

133. Jessing KK, Juhler RK, Strobel BW (2011) Monitoring of artemisinin, dihydroartemisinin, and artemether in environmental matrices using high-performance liquid chromatography-tandem mass spectrometry (LC-MS/MS). J Agric Food Chem 59 (21):11735-11743. doi:10.1021/jf2027632

134. Yeka A, Achan J, D'Alessandro U, Talisuna AO (2009) Quinine monotherapy for treating uncomplicated malaria in the era of artemisinin-based combination therapy: an appropriate public health policy? The Lancet Infectious Diseases 9 (7):448-452. doi:10.1016/s1473-3099(09)70109-4

135. Hrycyna CA, Summers RL, Lehane AM, Pires MM, Namanja H, Bohn K, Kuriakose J, Ferdig M, Henrich PP, Fidock DA, Kirk K, Chmielewski J, Martin RE (2014) Quinine dimers are potent inhibitors of the Plasmodium falciparum chloroquine resistance transporter and are active against quinoline-resistant P. falciparum. ACS Chem Biol 9 (3):722-730. doi:10.1021/cb4008953

136. Pershing LK, Peat MA, Finkle BS (1982) An HPLC method for the quantitation of quinidine and its metabolites in plasma: an application to a quinidine-phenytoin drug interaction study. J Anal Toxicol 6 (3):153-156

137. Nielsen F, Nielsen KK, Brøsen K (1994) Determination of quinidine, dihydroquinidine, (3S)-3-hydroxyquinidine and quinidine N-oxide in plasma and urine by high-performance liquid chromatography. Journal of Chromatography B: Biomedical Sciences and Applications 660 (1):103-110. doi:10.1016/0378-4347(94)00259-2

138. Monagas M, Quintanilla-Lopez JE, Gomez-Cordoves C, Bartolome B, Lebron-Aguilar R (2010) MALDI-TOF MS analysis of plant proanthocyanidins. J Pharm Biomed Anal 51 (2):358-372. doi:10.1016/j.jpba.2009.03.035

139. Aoyagi S, Kodani N, Yano A, Asao T, Iwai H, Kudo M (2014) ToF-SIMS data analysis for complex plant tissue samples using multivariate analysis and G-SIMS. Surface and Interface Analysis 46 (S1):131-135. doi:10.1002/sia.5588

140. Spool AM (2004) Interpretation of static secondary ion spectra. Surface and Interface Analysis 36 (3):264-274. doi:10.1002/sia.1685

141. Gilmore IS, Seah MP (2000) Static SIMS: towards unfragmented mass spectra — the G-SIMS procedure. Applied Surface Science 161 (3-4):465-480. doi:10.1016/s0169-4332(00)00317-2

142. Bittencourt C, Felicissimo MP, Pireaux JJ, Houssiau L (2005) ToF-SIMS characterization of thermal modifications of bixin from Bixa orellana fruit. J Agric Food Chem 53 (16):6195-6200. doi:10.1021/jf0505271

143. Cooks RG, Ast T, Mabud MA (1990) Collisions of polyatomic ions with surfaces. International Journal of Mass Spectrometry and Ion Processes 100:209-265. doi:10.1016/0168-1176(90)85077-f

144. Vickerman JC, Brown AA, Reed NM (1989) Secondary ion mass spectrometry: principles and applications. Clarendon Press,

145. Reed NM, Vickerman JC (1993) The Application of Static Secondary Ion Mass Spectrometry (SIMS) to the Surface Analysis of Polymer Materials. . In Surface Characterization of Advanced Polymers. VCH, Weinheim, Germany

146. Brutin D (2015) Droplet Wetting and Evaporation, From Pure to

Complex Fluids. Academic Press, London

147. Goacher RE, Jeremic D, Master ER (2011) Expanding the library of secondary ions that distinguish lignin and polysaccharides in time-of-flight secondary ion mass spectrometry analysis of wood. Anal Chem 83 (3):804-812. doi:10.1021/ac1023028

148. Saito K, Watanabe Y, Shirakawa M, Matsushita Y, Imai T, Koike T, Sano Y, Funada R, Fukazawa K, Fukushima K (2012) Direct mapping of morphological distribution of syringyl and guaiacyl lignin in the xylem of maple by time-of-flight secondary ion mass spectrometry. Plant J 69 (3):542-552. doi:10.1111/j.1365-313X.2011.04811.x

149. Lee JLS, Gilmore IS, Seah MP, Levick AP, Shard AG (2012) Topography and field effects in secondary ion mass spectrometry Part II: insulating samples. Surface and Interface Analysis 44 (2):238-245. doi:10.1002/sia.3833

150. Suleman S, Verheust Y, Dumoulin A, Wynendaele E, D'Hondt M, Vandercruyssen K, Veryser L, Duchateau L, De Spiegeleer B (2015) Gas chromatographic method for the determination of lumefantrine in antimalarial finished pharmaceutical products. J Food Drug Anal 23 (3):552-559. doi:10.1016/j.jfda.2015.03.004

151. Sen A, Bouchet A, Lepere V, Le Barbu-Debus K, Scuderi D, Piuzzi F, Zehnacker-Rentien A (2012) Conformational analysis of quinine and its pseudo enantiomer quinidine: a combined jet-cooled spectroscopy and vibrational circular dichroism study. J Phys Chem A 116 (32):8334-8344. doi:10.1021/jp3047888

152. Lai CS, Nair NK, Muniandy A, Mansor SM, Olliaro PL, Navaratnam V (2009) Validation of high performance liquid chromatography-electrochemical detection methods with simultaneous extraction procedure for the determination of artesunate, dihydroartemisinin, amodiaquine and desethylamodiaquine in human plasma for application in clinical pharmacological studies of artesunate-amodiaquine drug combination. J Chromatogr B Analyt Technol Biomed Life Sci 877 (5-6):558-562. doi:10.1016/j.jchromb.2008.12.037

153. Gatti R, Gioia MG, Cavrini V (2004) Determination of Cinchona alkaloids and Vitamin B6 by high-performance liquid chromatography with fluorescence detection. Analytica Chimica Acta 512 (1):85-91. doi:10.1016/j.aca.2004.02.018

154. Shelley JT (2011) Development and characterization of plasma-based sources for ambient desorption/ionization mass spectrometry. Doctoral Dissertation, Indiana University.,

155. Albert A, Engelhard C (2012) Characteristics of low-temperature plasma ionization for ambient mass spectrometry compared to electrospray ionization and atmospheric pressure chemical ionization. Anal Chem 84 (24):10657-10664. doi:10.1021/ac302287x

156. Jackson AU, Garcia-Reyes JF, Harper JD, Wiley JS, Molina-Diaz A, Ouyang Z, Cooks RG (2010) Analysis of drugs of abuse in biofluids by low temperature plasma (LTP) ionization mass spectrometry. Analyst 135 (5):927-933. doi:10.1039/b920155f

157. Zhang Y, Ma X, Zhang S, Yang C, Ouyang Z, Zhang X (2009) Direct detection of explosives on solid surfaces by low temperature plasma desorption mass spectrometry. Analyst 134 (1):176-181. doi:10.1039/b816230a

158. Harper JD, Charipar NA, Mulligan CC, Zhang X, Cooks RG, Ouyang Z (2008) Low-temperature plasma probe for ambient desorption ionization. Anal Chem 80 (23):9097-9104. doi:10.1021/ac801641a

159. Wiley JS, Shelley JT, Cooks RG (2013) Handheld low-temperature plasma probe for portable "point-and-shoot" ambient ionization mass spectrometry. Anal Chem 85 (14):6545-6552. doi:10.1021/ac4013286

160. Albert A, Engelhard C (2015) Chemometric optimization of a low-temperature plasma source design for ambient desorption/ionization mass spectrometry. Spectrochim Acta, Part B 105:109-115. doi:10.1016/j.sab.2014.08.034

161. Huang G, Ouyang Z, Cooks RG (2009) High-throughput trace melamine analysis in complex mixtures. Chem Commun (Camb) (5):556-558. doi:10.1039/b818059h

162. Santos VGd, Alves RJ, Eberlin MN, Pianetti GA, César IC (2012) Electrospray ionization tandem mass spectrometry of the two main antimalarial drugs: artemether and lumefantrine. J Braz Chem Soc 23:65-71

163. Salter TL, Green FM, Faruqui N, Gilmore IS (2011) Analysis of personal care products on model skin surfaces using DESI and PADI ambient mass spectrometry. Analyst 136 (16):3274-3280. doi:10.1039/c1an15138j

164. Salter TL, Gilmore IS, Bowfield A, Olabanji OT, Bradley JW (2013) Ambient surface mass spectrometry using plasma-assisted desorption ionization: effects and optimization of analytical parameters for signal intensities of molecules and polymers. Anal Chem 85 (3):1675-1682. doi:10.1021/ac302677m

165. Shen Y, van Beek TA, Claassen FW, Zuilhof H, Chen B, Nielen MW (2012) Rapid control of Chinese star anise fruits and teas for neurotoxic anisatin by Direct Analysis in Real Time high resolution mass spectrometry. J Chromatogr A 1259:179-186. doi:10.1016/j.chroma.2012.03.058

166. Wang L, Zhao P, Zhang F, Li Y, Pan C (2012) Direct analysis in real time mass spectrometry for the rapid identification of four highly hazardous pesticides in agrochemicals. Rapid Commun Mass Spectrom 26 (16):1859-1867. doi:10.1002/rcm.6274

167. Vaclavik L, Mishra A, Mishra KB, Hajslova J (2013) Mass spectrometry-based metabolomic fingerprinting for screening cold tolerance in Arabidopsis thaliana accessions. Anal Bioanal Chem 405 (8):2671-2683. doi:10.1007/s00216-012-6692-1

168. Musah RA, Cody RB, Dane AJ, Vuong AL, Shepard JR (2012) Direct analysis in real time mass spectrometry for analysis of sexual assault evidence. Rapid Commun Mass Spectrom 26 (9):1039-1046. doi:10.1002/rcm.6198

169. Horning EC, Carroll DI, Dzidic I, Haegele KD, Horning MG, Stillwell RN (1974) Atmospheric pressure ionization (API) mass spectrometry. Solvent-mediated ionization of samples introduced in solution and in a liquid chromatograph effluent stream. J Chromatogr Sci 12 (11):725-729

170. Kambara H, Mitsui Y, Kanomata I (1979) Identification of clusters produced in an atmospheric pressure ionization process by a collisional dissociation method. Anal Chem 51 (9):1447-1452. doi:10.1021/ac50045a022

171. Dzidic I, Carroll DI, Stillwell RN, Horning EC (1976) Comparison of positive ions formed in nickel-63 and corona discharge ion sources using nitrogen, argon, isobutane, ammonia and nitric oxide as reagents in atmospheric pressure ionization mass spectrometry. Anal Chem 48 (12):1763-1768. doi:10.1021/ac50006a035

172. Kostiainen R, Kauppila TJ (2009) Effect of eluent on the ionization process in liquid chromatography-mass spectrometry. J Chromatogr A 1216 (4):685-699. doi:10.1016/j.chroma.2008.08.095

173. Shelley JT, Hieftje GM (2010) Ionization matrix effects in plasma-based ambient mass spectrometry sources. J Anal Atom Spectrom 25 (3):345-350. doi:10.1039/b923564g

List of Figures

Figure 1.1: Chemical structures and names of current antimalarial drug. 4

Figure 1.2: Schematic of different API probes and their ionisation mechanism. 9

Figure 1.3: Schematic of SIMS source and mechanism. 12

Figure 2.1: Schematic of HT-HPLC system coupled simultaneously to MS and UV/Vis detectors. 1) Eluent preheater, 2) column heater, 3) post-column cooler. 15

Figure 2.2: Effect of eluent temperature on positive ESI-MS response. A) Extracted ion mass chromatogram (XIC) of *m/z* 195 ($C_8H_{11}N_4O_2^+$), B) mass spectra of caffeine at the respective column temperatures. 22

Figure 2.3: Effect of eluent temperature on peak area (A) and S/N (B). The areas were calculated using the SIR mass chromatogram of *m/z* 195 and extracted ion chromatogram (XIC) of caffeine (scan range, *m/z* 195 - 196). 23

Figure 3.1: Chemical structure of some *Cinchona* alkaloids [6]. 28

Figure 3.2: Effect of buffer on the separation of *Cinchona* alkaloids. Chromatographic conditions: Waters XBridge C_{18} (150 x 4.6 mm, 3.5 µm) stationary phase; mobile phase: MeOH/water (10/90) with 0.1% FA (A) and 10 mM AF (B) in water; flow rate: 1.0 ml min^{-1}; injection volume: 5 µL; column temperature: 25°C. Detection: Quattro LC in SIR mode; cone voltage: 35 V; capillary voltage: 3.0 eV. Analyte: 1) Cn (*m/z* 295.4), 2) Cdn (*m/z* 295.4), 3) DCn (*m/z* 297.4, 4) Qdn (*m/z* 325.4), 5) DCdn (*m/z* 297.4), 6) Qn (*m/z* 325.4), 7) DQdn (*m/z* 327.4) and 8) DQdn (*m/z* 327.4). 34

Figure 3.3: Isothermal separation of Qn and derivatives. Chromatographic conditions: Stationary phase: Waters XBridge C_{18} (4.6 x 150 mm, 3.5 µm); mobile phase: A) MeOH/water (10/90) with 10 mM AF in water, B) ACN/water (10/90) with 10 mM AF in water; flow rate: 1.0 mL min^{-1}; injection volume: 5 µL; detection: Quattro MS in selected ion recording (SIR) mode. Analyte: 1) Cn (*m/z* 295.4), 2) Cdn (*m/z* 295.4), 3) DCn (*m/z* 297.19, 4) Qdn (*m/z* 325.4), 5) DCdn (*m/z* 297.4), 6) Qn (*m/z* 325.4), 7) DQdn (*m/z* 327.4) and 8) DQn (*m/z* 327.4). (N (2) = number of plate for Cdn, $\alpha_{3/4}$ = selectivity between DCn and Qdn). 36

Figure 3.4: Effect of temperature on *k* obtained using HT-HPLC-MS analysis of *Cinchona* alkaloids. Chromatographic conditions: same as in Figure 3.3; mobile phase: A) MeOH/water (10/90) with 10 mM AF in water, B) ACN/water (10/90) with 10 mM AF in water. (*k* = retention factor).....37

Figure 3.5: Van't Hoff plot of four major Qn and derivatives in a temperature interval from 25 to 90 °C. Chromatographic conditions and detection: same as in Figure 3.3. Mobile phase: MeOH/water (10/90) (A), ACN/water (10/90) (B) with 10 mM in water. Coefficient of variation (r^2) for Cn, Cdn, Qdn and Qn: 0.998, 0,998, 0.998 and 0.999 respectively for A and 0.984, 0.991, 0.996 and 0.996 for B. 38

Figure 3.6: Influence of MeOH (A) vs. ACN (B) as mobile phase organic modifier on the variation of percentage peak area during HT-HPLC-ESI-MS analysis of *Cinchona* standard. Chromatographic conditions and detection: same as in Figure 3.3. Column temperature range: 25 - 90 °C. 40

Figure 3.7: Influence of MeOH (A) vs. ACN (B) as mobile phase organic modifier on the variation of signal-to-noise ratio during HT-HPLC-ESI-MS analysis of *Cinchona* standard. Chromatographic conditions and detection: same as in Figure 3.3. Column temperature range: 25 - 90 °C. 40

Figure 3.8: Extracted ion mass chromatogram (XIC) and mass spectra at respective t_R. Chromatographic condition and peak identity: same as in Figure 3.3B at T=90 °C. Detection: extracted mass: *m/z* 295-296 for Cn/Cdn, *m/z* 297-298 for DCn/DCdn, *m/z* 325-326 for Qn/Qdn, and 327-328 for DQn/DQdn. 42

Figure 3.9: HT-HPLC-ESI(+)-MS extracted ion mass chromatogram and mass spectra (insets) of *Cinchona* alkaloids during analysis of commercial *Cinchona* extract. Chromatographic conditions: see Figure 3.3B. 44

Figure 4.1 Chemical structure of ART and its derivatives (adapted from ref. [33].....52

Figure 4.2: Acid base chemistry on Zr-based column. Adapted from ref.[127].....58

Figure 4.3: Influence of ESI cone voltage on in-source fragmentation of DHA (10 µg mL^{-1}) during HT-HPLC-ESI(+)-MS analysis. Mobile phase: MeOH/water (15/85) with 10 mM AF in water. ESI parameters: source temperature 100 °C, cone voltage +10 - +40 V. 60

Figure 4.4: HT-HPLC-ESI(+)-MS extracted-ion chromatograms (XIC) and mass spectra (insets) during analysis of a standard mixture of ART and derivatives. Chromatographic conditions: Discovery Zr-PBD (150 x 4.6 mm, 3.0 µm) stationary phase; mobile phase: MeOH/water (15/85) with 10 mM AF in water; flow rate: 0.4 mL min^{-1}; injection volume: 10 µL; column temperature: 90 °C. Analytes: A) *m/z* 272.0 for AS, B) *m/z* 302.0 for DHA, C) *m/z* 300.0 for ART and D) 316.2 for AM. 62

Figure 4.5: Influence of collision induced dissociation (CID) energy on fragmentation of ART (*m/z* 300) during HT-HPLC-ESI(+)-MS/MS analysis Mobile phase: MeOH/water (20/80) with 10 mM AF in water; flow rate: 0.4 mL min^{-1}; injection volume: 10 µL; column temperature: 90 °C. MS/MS parameters: argon collision gas, CID energy 0 – 15 eV. 65

Figure 4.6: Product ion mass chromatogram (A) and spectra (B) of ammonium adduct of DHA (*m/z* 302, t_R 5.24 min), ART (*m/z* 300, t_R 6.78 min) and AM (*m/z* 316, t_R 12.24 min) during HT-HPLC-ESI(+)-MS/MS analysis. Chromatographic conditions: stationary phase: Discovery Zr-PBD (150 x 4.6 mm, 3.0 µm): mobile phase: MeOH/water (**20/80**) with 10 mM AF in water. Flow rate: 0.4 mL min^{-1}: injection volume: 10 µL: Column temperature: 90 °C. 66

Figure 4.7: HT-HPLC-APCI(+)-MS extracted ion chromatogram (XICs) and mass spectra (insets) during analysis of a standard mixture of ART and derivatives. Chromatographic conditions: Discovery Zr-PBD (150 x 4.6 mm, 3.0 µm) stationary phase; mobile phase: MeOH/water (15/85) with 10 mM AF in water; flow rate: 0.4 mL min^{-1}; injection volume: 10 µL; column temperature: 90 °C. Analytes: A) *m/z* 272.0 for AS, B) *m/z* 302.0 for DHA, C) *m/z* 300.0 for ART and D) *m/z* 316.2 for AM. 68

Figure 4.8: Comparison of ESI and APCI sources fragmentation after HT-HPLC-MS analysis of ART and derivatives with MeOH (A) and ACN (B) as organic modifier. Compound identity: XIC *m/z* 272 (AS), *m/z* 302 (DHA), *m/z* 300 (ART), *m/z* 316 (AM).....69

Figure 4.9: Influence of MeOH vs. ACN on ESI (A) and APCI (B) in-source fragmentation during HT-HPL-MS analysis of ART and derivatives. Compound identity: XIC *m/z* 272 (AS), *m/z*302 (DHA), *m/z* 300 (ART), *m/z* 316 (AM).....70

Figure 4.10: Extracted ion mass chromatogram and mass spectrum (inset) and B) Product ion mass chromatogram and mass spectrum (inset) of ammonium adduct ion of AM (*m/z* 316.2) during analysis of Coartem tablet with HT-HPLC-ESI(+)-MS and HT-HPLC-ESI(+)-MS/MS respectively. Chromatographic conditions: Discovery Zr-PBD (150 x 4.6 mm, 3.0 µm) stationary phase; mobile phase: MeOH/water (**20/80**) with 10 mM AF in water; flow rate: 0.4 mL min^{-1}; injection volume: 10 µL; column temperature: 90 °C. MS detection: Argon collision gas; collision energy: 10 eV; analyte: *m/z* 316.2 for AM.....71

Figure 5.1: Positive time-of-flight secondary ion mass spectrometry (ToF-SIMS) spectrum of Qn standard with an interpretation of the fragmentation. 100

Figure 5.2: ToF-SIMS signal intensity for protonated molecular ion of Qn (*m/z* 325.19, $C_{20}H_{25}N_2O_2^+$, total counts (TIC) in a 500 x 500 µm image) from different Qn standards drop-dried on silicon wafer. 103

Figure 5.3: A 3D laser microscope image (top column) and secondary ion images (bottom column) of *Cinchona* bark showing topographical effect and ion distribution respectively. Top column: (a) Enhanced image, (b) real image of sample; bottom column: (c) total ion and (d) Qn (*m/z* 325.19, $C_{20}H_{25}N_2O_2^+$) image.....104

Figure 5.4: Positive SIMS spectrum of *Cinchona* bark, showing sparsely presence of Qn. .106

Figure 5.5: Positive ToF-SIMS spectrum of *Cinchona* bark extract showing protonated molecular ion of Cn/Cdn (*m/z* 295), DCn/DCdn (297), Qn/Qdn (*m/z* 325), and DQn/DQdn (327). 109

Figure 5.6: Suggested fragmentation pattern of A) Cn/Cdn and B) Qn/Qdn according to ToF-SIMS spectra in Figure 5.5. 111

Figure 5.7: Positive ToF-SIMS spectra showing protonated molecular ion of Qn from quinine standard, *Cinchona* bark and extract. 112

Figure 6.1: A) Schematic of the LTP probe positioned in front of a mass spectrometer for direct ambient desorption ionisation mass spectrometry (ADI-MS). B) Photograph of LTP probing a Coartem drug tablet during an ADI-MS experiment. 120

Figure 6.2: LTP (+)-HRMS mass spectra of quinine obtained by (A) LTP-MS and (B) LTP-MS with HCD fragmentation. 125

Figure 6.3: LTP (+)-HRMS mass spectra of artemether with HCD-type fragmentation. 127

Figure 6.4: LTP (+)-HRMS spectrum of artemether (*m/z* 299) and lumefantrine (*m/z* 530) in Coartem drug tablet. 129

Figure 6.5: Proposed fragmentation pattern of artemether after LTP-MS, with rupture of peroxide bridge , modelled from ref.[53]A,[23] B. 130

Figure 6.6: LTP (-)-HRMS spectra of atovaquone obtained from analysis of a methanol extract of Malarone drug tablet. 131

Figure 6.7: ESI (+)-MS of methanol extract of Coartem drug tablet diluted MeOH/H_2O 50:50 (*v/v*) solvent containing 5 mM ammonium formate. A) Artemether and B) Lumefantrine. 133

Figure 6.8: Mass spectra, chemical structure and molecular weight of proguanil (A) and atovaquone (B) from LC-MS analysis of methanol extract of Malarone drug tablet. 134

Figure A 3.1: Effect of organic modifier on retention time. Chromatographic condition: Waters XBridge C_{18} (150 x 4.6 mm, 3.5 µm) stationary phase; column temperature: 80 °C; mobile phase: MeOH/water (10/90) (A) and ACN/water (10/90) (B) (10% MeOH (A) with10 mM AF (pH 3.0) in water; flow rate: 1.0 ml/min; injection volume: 5 µl. Detection: Quattro LC in SIR mode; cone voltage: 35 V; capillary voltage: 3.0 eV. Analytes: 1) Cn (*m/z* 294.4), 2) Cdn (*m/z* 294.4), 3) Qdn (*m/z* 324.4), and 4) Qn (*m/z* 324.4). 48

Figure A 3.2: Isothermal separation of *Cinchona* alkaloid. Chromatographic condition and detection: *cf* Figure A 3.1. Column temperature: 25-90 °C. Mobile phase: MeOH/water (10/90) (A) and ACN/water (10/90) (B) with 10 mM AF in water. 49

Figure A 4.1: UV absorption spectrum of ART and derivatives. A) Effect of organic modifier on UV absorption of 2.07 mg mL^{-1} AM. (B) Absorbance of AM (2.07 mg mL^{-1}),

DHA (1.08 mg mL^{-1}), ART (1.28 mg mL^{-1}) and AS (1.03 mg mL^{-1}). Solvent: ACN. Optical path length: 1 cm.....79

Figure A 4.2: Acid base chemistry on Zr-PBD column. Adapted from ref.[127] 82

Figure A 4.3: HT-HPLC separation of ART and derivatives. Chromatographic conditions: stationary phase: Discovery Zr-PBD (150 x 4.6 mm, 3.0 µm): mobile phase: ACN/water (15/85) with 5 mM phosphate buffer. Flow rate: 1.2 mL min^{-1}: injection volume: 25 µL: column temperature: 50&70 °C. Detection: λ = 205 nm. Analytes: 1) mobile phase, 2) unknown, 3) DHA, 4) ART, 5) AS, 6) AM. 83

Figure A 4.4: Van't Hoff plot for ART and derivatives. Chromatographic conditions: same as in Figure A 4.3. Correlation coefficient (r^2) for DHA, AS, ART and AM: 0.992, 0.988, 0.998 and 0.997 respectively.....84

Figure A 4.5: Chromatogram of AS at different concentration levels (A) and calibration curve (B). Chromatographic conditions: stationary phase: Discovery Zr-PBD (150 x 4.6 mm, 3.0 µm): mobile phase: ACN/water (35/65) with 5 mM phosphate buffer. Flow rate: 1.2 mL min^{-1}: injection volume: 20 µL: CT: 80 °C. Detection: λ = 203 nm.....85

Figure A 4.6: Retention of spiked AM in Coartem extract. Chromatographic conditions: stationary phase: Discovery Zr-PBD (150 x 4.6 mm, 3.0 µm): mobile phase ACN/water (35/65) with 5 mM phosphate buffer. Flow rate: 1.2 mL min^{-1}: injection volume: 20 µL: column temperature: 80 °C. Detection: λ = 203 nm. ...86

Figure A 4.7: Effect of source temperature on in-source fragmentation of DHA (10 µg mL^{-1}) after reversed-phase HT-HPLC-ESI(+)-MS. Mobile phase consisted of 10 mM AF (pH 3) in a **50% MeOH**. ESI parameters: cone voltage: 15 V. Source temperatures: 90-150 °C. 88

Figure A 4.8: HT-HPLC-ESI(+)-MS extracted-ion chromatograms (XIC) and mass spectra (insets) after analysis of a standard mixture of ART and derivatives. Chromatographic conditions: Discovery Zr-PBD (150 x 4.6 mm, 3.0 µm) stationary phase; mobile phase: **ACN/water** (15/85) with 10 mM AF in water; flow rate: 0.4 mL min^{-1}; injection volume: 10 µL; column temperature: 90 °C. Analytes: A) *m/z* 272.0 for AS, B) *m/z* 302.0 for DHA, C) *m/z* 300.0 for ART and D) 316.2 for AM. 90

Figure A 4.9: HT-HPLC-ESI(+)-MS calibration curve for DHA, ART and AM with Zr-PBD column.....91

Figure A 4.10: Influence of APCI probe temperature (PT) on in-source fragmentation of DHA (100 µg mL^{-1}) during HT-HPLC-APCI(+)-MS. Mobile phase: MeOH/water **(**15/85) with 10 mM AF in water. APCI parameters: Corona pin voltage 3 kV, PT: 200-500 °C. 92

Figure A 4.11: HT-HPLC-APCI(+)-MS extracted ion chromatogram (XICs) and mass spectra (insets) after analysis of a standard mixture of ART and derivatives. Chromatographic conditions: Discovery Zr-PBD (150 x 4.6 mm, 3.0 µm) stationary phase; mobile phase: **ACN/water** (15/85) with 10 mM AF in water; flow rate: 0.4 mL min^{-1}; injection volume: 10 µL; column temperature: 90 °C. Analytes: A) *m/z* 272.0 for AS, B) *m/z* 302.0 for DHA, C) *m/z* 300.0 for ART and D) *m/z* 316.2 for AM.....93

Figure A 5.1: Liquid chromatography-mass spectrometry of Qn. A) Mass chromatogram, B) mass spectra. Column: XBridge C_{18}, 3.5 µm, 150 x 4.6 mm Mobile phase: MeOH/water (50/50) with 0.1% FA in water, pH= 3.0, column temperature = 80 °C, flow rate: 1.0 mL min^{-1} with post-column splitting. Injection volume: 20-µL. Detection: Micromass Quattro LC MS in positive electrospray (ESI+) mode; capillary voltage: 3.5 kV; cone voltage: 50 V. 115

Figure A 5.2: Coffee-stain effect seen on the SIMS image of protonated molecular ion of Qn. A = 0.1 ng $µL^{-1}$, B = 1 ng $µL^{-1}$, C = 100 ng $µL^{-1}$ and D = 1000 ng $µL^{-1}$ of Qn standard on silicon wafer. 116

Figure A 5.3: LC-MS analysis of ethanol extract of *Cinchona* barks powder. A) Mass chromatogram, B-D) Mass spectra at different *m/z* intervals. LC condition: Instrument: Accela LC system; flow injection: 150 µl min^{-1}; mobile phase: MeOH/water (50/50) with 0.1% FA in water. Detector: Quattro LC mass spectrometer operated in positive ESI mode.....117

Figure A 5.4: SIR mass chromatogram of protonated molecular ion of Qn and derivatives standard: 1) Cn (*m/z* 295.14), 2) Cdn (*m/z* 295.14), 3) Qdn (*m/z* 325.18), 4) DCn (*m/z* 297.14), 5) DCdn (*m/z* 297.18)/Qn (*m/z* 325.18), 6) DQdn (*m/z* 327.18), 7) DQn (*m/z* 327.18). Column: XBridge C_{18}, 150 x 4.6 mm, 3 µm particles; Column

temperature 80 °C. Mobile phase: MeOH/water (10/90) with 0.1% FA in water, pH 3.0). Detector: Quattro LC mass spectrometer.....118

Figure A 6.1: Positive ion mode low temperature plasma-high resolution mass spectrometry (LTP (+)-HRMS) spectra of quinine with additional heating: A) 5.0 V (~35 °C) heating, B) 10.0 V (~50 °C) heating, and C) 14 V (~65 °C) heating Analyte: 10 µg mL^{-1} (30 ng absolute) of quinine (*m/z* 325.1916, $C_{20}H_{25}N_2O_2^+$). 138

Figure A 6.2: Proposed fragmentation pathway of quinine showing the formation of free radical cations during LTP (+)-HRMS analysis. 139

Figure A 6.3: Fragmentation pattern of the protonated molecular ion of quinine with known characteristics fragments as reported in literature.....139

Figure A 6.4: ESI(+)-MS/MS spectra of the ammonium adduct of artemether ($C_{16}H_{26}O_5$) (A) at *m/z* 316, and the protonated molecular ion of lumefantrine ($C_{30}H_{32}Cl_3NO$) (B) at *m/z* 528 with, $^{35}Cl_3$ and (C) at *m/z* 530, with $^{35}Cl_2$ ^{37}Cl. 142

List of Tables

Table 2.1: HT-HPLC chromatographic parameters of benzene (B) and ethylbenzene (EB) used to evaluate the efficiency of the HTLC heating system. 20

Table 2.2: Effect of eluent temperature on MS response (peak area) for caffeine using HT-HPLC-MS. 23

Table 3.1: Estimate of LODs and LOQs of *Cinchona* alkaloids during HT-HPLC-MS analysis at column temperature 90 °C. 41

Table 3.2:Detected peak and their identity from HT-HPLC-MS analysis of commercial *Cinchona* alkaloids.....45

Table 4.1: Calibration range, linearity, LOD and LOQ:.....64

Table 4.2: Summary of APCI probe temperature effect on MS signal for $[M + NH_4]^+$ at *m/z* 302.....67

Table 5.1: Characteristic positive secondary ion mass spectrometry (SIMS) fragment peaks for quinine standard 102

Table 5.2: Positive SIMS fragments from ToF-SIMS analysis of *Cinchona* bark (From mass spectrum in Figure 5.4). 107

Table 5.3: Characteristic positive secondary ion mass spectrometry (SIMS) fragment peaks for quinine derivatives in *Cinchona* extract. 110

Table 6.1: List of *m/z* fragments detected from LTP-MS of Coartem and Malarone tablets.132

Table A 2.1: Mass spectrometric parameters used in fundamental HT-HPLC-MS of caffeine. 25

Table A 3.1: Chemical structure and acid-base dissociation constants of quinine and derivatives in water ($^{w}_{w}$pKa) and 30% ACN/70% H_2O mixtures ($^{s}_{s}$pKa) at 25 °C. 47

Table A 3.2: Influence of ACN vs. MeOH on chromatographic parameters during HT-HPLC-MS analysis of *Cinchona* alkaloids using Waters XBridge C_{18} column. 50

Table A 4.1: Effect of wavelength on signal response for ART. 80

Table A 4.2: Effect of phosphate concentration on signal response for ART. 81

Table A 4.3: Quantitative data for AM spiked in Coartem extract followed by HTLC-UV…86

Table A 4.4: Summary of source temperature effect on MS signal for DHA ammonium adduct at *m/z* 302.....89

Table A 5.1: Surface roughness parameters for *Cinchona* bark obtained from 3D laser microscope. 114

Table A 6.1: LTP-Orbitrap-MS parameters used fort the LTP-MS analysis.....137

Table A 6.2: Proposed fragment ions of quinine obtained with LTP (+)-HRMS. 140

Table A 6.3: Proposed fragment ions of quinine obtained with LTP (+)-HRMS with high-energy collision-induced dissociation (HCD) fragmentation. 141

Table A 6.4: Compounds screened from drug tablet, with their boiling point and vapour pressure. 141

Table A 6.5: Liquid chromatography triple quadrupole mass spectrometry (LC-QQQ-MS) parameters applied for the screening of artemether from Coartem drug tablet. .143

Table A 6.6: LC-QQQ-MS parameters used for the screening of lumefantrine from Coartem drug tablet. 144

List of Abbreviations and Symbols

ACN	Acetonitrile
AF	Ammonium formate
AGC	Automatic gain control
APCI	Atmospheric pressure chemical ionisation
APPI	Atmospheric pressure photoionisation
au	Absorbance unit
BEH	Ethylene bridged hybrid
BET	Brunauer Emmett Teller
C_{18}	Carbon 18
cSCX	Chiral strong cation exchanger
CID	Collision-induced dissociation
Cdn	Cinchonodone
Cn	Cinchonine
CT	Column temperature
DHB	Dihydrobenzoic acid
DHFR	dihydrofolate reductase
DHPS	dihydropteroate synthase
ELSD	Evaporative light scattering detector
ESI	Electrospray ionisation
ESI-MS	Electrospray ionisation mass spectrometry
e-MALDI	Electrowetting-enhanced matrix assisted laser desorption ionisation
FA	Formic acid
GC	Gas chromatography

GC-MS	Gas chromatography coupled to mass spectrometry
HPLC	High performance liquid chromatography
HTLC	High temperature liquid chromatography
ID	Inner diameter
LC	Liquid chromatography
LC-MS/MS	Liquid chromatography-tandem mass spectrometry
LDI	Laser desorption ionisation
$L\ h^{-1}$	Liter per hour
LTP	Low-temperature plasma
mAU	Milli absorbance unit
MeOH	Methanol
MS	Mass spectrometry
MS/MS	Tandem mass spectrometry
m/z	Mass to charge
ODS	Octadecylsilyl
OD	Outer diameter
PBD	Polybutadiene
PDMS	Polydimethylsiloxane
PEEK	Polyether ether ketone
pH	Potential hydrogenii
Ph. Eur	European Pharmacopoeia
pKa	Acid constant
PTFE	Polytetrafluoroethylene
Qdn	Quinine

Qn	Quinidine
RF	Radiofrequency
RPLC	Reversed-phase liquid chromatography
Rs	Baseline resolution
SIR	Selected ion recording
TLC	Thin layer chromatography
ToF-SIMS	Time of flight secondary ion mass spectrometry
t_R	Retention time
µl	Microliter
µm	Micrometer
UV-Vis	Ultraviolet-visible
v/v	Volume to volume
w/w	Weight to weight
ZrO_2-PBD	Zirconia-based polybutadiene
ΔH	Enthalpy of transfer of a solute from the mobile phase into the stationary phase
ΔS	Entropy of transfer of a solute from the mobile phase into the stationary phase
β	Volume phase ratio of the stationary and mobile phase in the column
k_i	Retention factor of solute i
R	Ideal gas constant

Acknowledgements

I would like to acknowledge the following people without whom the completion of this thesis would not have been possible. It was a great privilege to work in the Analytical Chemistry working group.

First and foremost, I will like to extend my deepest gratitude to my supervisor, Prof. Dr. Carsten Engelhard for accepting me into his working group, providing the instruments that kept my research focused, and for advising me through my research. His promotion of freedom to think on my own ideas and bring them to fruition, gave me mastery on my research, and this would not have been possible without his advice. I would also give a special appreciation to Prof. Bernd W. Wenclawiak for bringing me into the Analytical Chemistry group to start my research, and for being there even when it was hard for him to do so. From onset of my research, through the tough times of my research, Frau Ulrike Koch was not only a colleague who provided the scientific advice, and encouragements, but she was a mother. My appreciation to her is limitless. To my colleagues, Ingo Strenge, Christopher Kuhlmann, Darya Mozhayeva, Lothar Veith, Bastian Spelz, Danica Heller, Narmina Heupel, Sigrid Hübner and all other past members of the working group, I appreciate the courage, contributions, corrections and your open-mindedness. You all created an awesome working environment that became a family.

I am most grateful to my elder brother, Dr. Dominic Bequikeh and my elder sisters, Doris Nzogoa, and Caroline Nzogoa for their love and unending encouragement. To Canris Nzogoa, and Eric Cantona, you were there when I needed support. I am thankful. My special gratitude to my wife Honorine. Your patience and love especially in tough times, kept me going.

To my Parents, your love, advice and prayers kept me going despite all odds. I am indebted to you all.

Curriculum Vitae

PERSONAL DETAILS

Name	Derick Nzogoa Ateacha
Place of birth	Muyuka, Cameroon
Nationality	German

EDUCATION

09/1989 – 06/1996	Primary school, Munyenge-Muyuka, Cameroon
09/1996 – 06/2001	Secondary school, Saint Joseph's College, Sasse-Buea, Cameroon
09/2001 – 06/2003	High school, Saint Joseph's College, Sasse-Buea, Cameroon
10/2003 – 08/2007	Bachelor of Science in Chemistry with minor in Material Sciences, University Buea, Cameroon
10/2008 – 02/2011	Master of Science in Chemistry with thesis entitled "*Hot Water Reversed-Phase HPLC with Silica-C18 and Subsequent Coupling to ICP-OES"* in Analytical Chemistry, University of Siegen, Germany, with Prof. Dr. Bernd W. Wenclawiak
03/2011- 09/2013	Begin of Dissertation in Analytical Chemistry, University of Siegen, Germany, with Prof. Dr. Bernd W. Wenclawiak
10/2013 till present	Continuation of the Dissertation in Analytical Chemistry, University of Siegen, Germany with Prof. Dr. Carsten. Engelhard

List of Publications

Publications in Peer-Reviewed Journals

D. N. Ateacha, U. Koch, C. Engelhard, Direct Analysis of Alkaloids in Natural Cinchona Bark and Commercial Extracts using Time-of-Flight Secondary Ion Mass Spectrometry, *Analytical Methods, 2018, **10**, 950 - 958*, DOI: (10.1039/C7AY02822A).
Featured by Analytical Methods on the Inside Front Cover, of Issue 9.

D. N. Ateacha, C. Kuhlmann, C. Engelhard, Rapid Qualitative Screening of Antimalarial Using Low-Temperature Plasma Ionisation Orbitrap Mass Spectrometry, ***(Submitted for publication).***

D. N. Ateacha, C. Engelhard, Analysis of Artemisinin-Based Antimalarial Pharmaceuticals by High-Temperature High Performance Liquid Chromatography Mass Spectrometry ***(in preparation for submission).***

D. N. Ateacha, C. Engelhard, Optimisation and Application of High-Temperature High Performance Liquid Chromatography Mass Spectrometry for the Analysis of *Cinchona* Alkaloids ***(in preparation for submission).***

Oral presentations

D. N. Ateacha, C. Engelhard, *High Temperature RPLC/MS - Application to Pharmaceuticals,* Young chemist report-GDCh Kolloquien des Ortsverbandes Siegen, 16.12.2014, Siegen, Germany.

D. N. Ateacha, C. Engelhard, *Development and Optimisation of Analytical Methods for the Separation and Identification Antimalarial Agents*, 26. Doktorandenseminar des AK Separation Science, 10-12.01.2016, Hohenroda, Germany.

D.N. Ateacha, U. Koch, C. Kuhlmann, C. Engelhard, *Development and Optimization of Direct Mass Spectrometric-Based Approaches fort the Analysis of Antimalarials*, 12th interdisciplinary doctoral seminar, 25 – 27.03.2018, Berlin, Germany

Poster presentations

D. N. Ateacha, B. W. Wenclawiak, *Hot water reversed-phase HPLC with silica-C18 and subsequent coupling to ICP-OES*, 6th interdisciplinary doctoral seminar, 26-28.02.2012, Berlin, Germany.

D. N. Ateacha, C. Engelhard, *High temperature liquid chromatography-mass spectrometry (HTLC-MS) analysis of quinine and derivatives*, ANAKON 2015, 23-26.03.2015, Graz, Austria.